

Photocatalytic Transformation of Water Pollutants into Fuels

Von der Naturwissenschaftlichen Fakultät der
Gottfried Wilhelm Leibniz Universität Hannover

zur Erlangung des Grades

Doktor der Naturwissenschaften

(Dr. rer. nat.)

genehmigte Dissertation

von

Osama Youssef Jakob Al-Madanat

Master of Science (Jordanien)

2021

Referent: apl. Prof. Dr. rer. nat. Detlef W. Bahnemann

Korreferent: apl. Prof. Dr. rer. nat. habil. Armin Feldhoff

Tag der Promotion: 19.10.2021

For My Mother & My Father's Memory

For My Family

Printed with the support of the Katholischer Akademischer Ausländer-Dienst

Acknowledgments

I would like to sincerely express my utmost gratitude to all who had supported, encouraged, and accompanied me during my PhD research journey to completion. Without your wise assistance and help in each step of my study and stay in Germany, it would have been impossible for me to achieve my goal and cross the finish line!

To begin with, special and heartfelt thanks to my supervisor **Prof. Dr. Detlef W. Bahnemann** for giving me the honor to be a member of his research group. Your insightful guidance, advice, motivation, stimulating discussion, and the absolute scientific freedom you provided which developed my skills and competence are greatly acknowledged. I'm also grateful for supporting me to participate in many conferences and workshops to widen my research scope from various perspectives. I could not have imagined having a better advisor throughout my Ph.D. research.

I would also like to acknowledge **Dr. Ralf Dillert**, for his valuable feedback, beneficial discussion, and productive suggestions in each stage of this thesis. Thank you for being my co-advisor and sharing your valuable knowledge and enormous experience with me.

I am also thankful to **Prof. Dr. Thomas Scheper** for giving me the opportunity to do my doctorate study at the institute of technical chemistry, for supporting me in different occasions, and for accepting to be the head of my examination committee.

I am thankful to **Prof. Dr. Armin Feldhoff** at the Institut für Physikalische Chemie, Universität Hannover for accepting to be a co-referee of my thesis and for the time he has spent in the productive revision of my PhD thesis. I would like to acknowledge him also for his help in the HR-TEM measurements and analysis.

I would also like to thank **Dr. Mariano Curti** for his valuable input in terms of thoughtful scientific discussions, productive suggestions, and valuable advice, as well as his great help throughout our collaborated publications.

I express my warmest appreciation to the **Katholischer Akademischer Ausländer-Dienst (KAAD)**, Bonn, Germany, for the financial support through a full scholarship during my doctoral study here in Germany. Herein, I would like to thank the team of Middle East department at KAAD, the former head of the department **Dr. Nora Kalbarczyk** (currently, the General Secretary of KAAD), **Santra Sontowski**, and **Fernanda Hulverscheidt Fagundes**. A special thanks to **Santra Sontowski** for her cooperation, help and her quick response to my frequent inquiries from the first day in Germany.

My sincere appreciation also goes to the official representative of the KAAD in Jordan, **Prof. Dr. Farah Al-Rabadi** at Mutah University / Jordan, for his encourage and the weekly communications. I would also convey my great gratitude to him for supporting and recommending me during my application to the KAAD scholarship.

I wish to express my thanks to **Graduiertenakademie** at Leibniz Universität Hannover for the Completion scholarship, and the travel grants when participating in the conferences.

I also thank the **staff at the Institute of Technical Chemistry (TCI)** for their continuous help, support, and the comfortable environment in the TCI.

I want to extend my thanks to my current and previous colleagues in **AK Bahnemman's group** for the fruitful discussions in our weekly seminars and also for our pleasant conversations and the fun time we had together.

I would especially like to thank my colleague and brother **Dr. Yamen Alsalka** for his great friendship, support, and help from the first steps to the end of this research, as well as, for the scientific and non-scientific discussion with each cup of the morning coffee.

I would also like to thank my friend **Abdulrahim Alahmad** for his technical support in SEM measurements and also for his willingness to help every time I need especially in the translation issues. A special thanks to my colleague **Carsten Günnemann** for his help in the laser measurements, and translating the abstract of my thesis to German. My thank goes also to my colleague **Barbara nunes** for her help in the HR-TEM and XRD measurements.

I would also like to extend my sincere and special appreciation to **Bettina Wehr** in the KHG office, Braunschweig, for her generous help and care, especially in the Corona crisis since she offered me the KHG office to continue my papers writing.

A special thanks to **Dr. Nour Hafi** for his help during our first days in Germany especially in the formal procedures.

I would also like to acknowledge my **Professors and Colleagues in Mutah University**, for their encouragement and support.

Last but by no means the least:

I express my warmest appreciation to my close friends **Hesham & Suha Swaid** and **Bassam & Anni Baboujian** for the nice family environment they create for us in the different occasions to relief our homesickness.

No words can express how grateful I am to **my Mother** for her unconditional love, care and the sacrifices she offered at every stage of my life. To my sisters **Suhad, Sawsan, Odate** and their families, thanks for your love and unwavering belief in me. Without you, I would not be the person I am today.

Many thanks go to every person in my **big family**, especially my uncle and spiritual father **Adel** and uncle **Awni** for their support and care during my life.

A special thanks to my wife's family especially my **Mother-in-law** for their, trust, love, and encouragement all the time.

To my beloved Children, **Maria, Zeina, and Yousef** who are truly the driving force behind all this hard work and success. Although you did not offer me the quiet environment that I need in home to finish my work, however, I love you more than anything in this world.

Finally, I'm extremely indebted to thank my soul mate and wonderful wife **Tahani**, for her love and care, for all the late nights and early mornings, for all the sacrifices that she made during the past four years. But most of all, I am sorry for all the responsibilities that you held during our stay in Germany, especially taking care of our children. Without your constant support, I may never have completed this stage. I owe you everything.

Kurzzusammenfassung

Die Verwendung von Sonnenstrahlung für die Entfernung von organischen Schadstoffen aus Wässern hat das Potential, als erneuerbare Energiequelle fossile Brennstoffe zu ersetzen. Die Kopplung der H₂-Entwicklung und des Abbaus organischer Schadstoffe durch doppel funktionelle TiO₂-Photokatalyse wird häufig als eine der nachhaltigsten und umweltfreundlichsten Technologien angesehen. Die niedrigen Quanteneffizienzen, die bisher mit TiO₂-Photokatalysatoren erzielt wurden, und das Fehlen des grundlegenden Verständnisses des Reaktionsmechanismus stellen jedoch große Herausforderungen dar, die bewältigt werden müssen, bevor das Potential vollständig ausgeschöpft werden kann. Trotz der großen Anzahl von Studien jedes Jahr, die doppel funktionelle Photokatalyse-Prozesse für die H₂-Produktion aus einfachen Wasserschadstoffen, wie Methanol, Formaldehyd und Ameisensäure untersuchen, wurden aromatische Schadstoffe bislang nur selten betrachtet. Somit bestehen einige offene Fragen bezüglich der photokatalytischen Effizienzen und des Reaktionsmechanismus während der Photoreformierung von aromatischen Verbindungen.

In der vorliegenden Arbeit wurde die photokatalytische Reformierung von Naphthalin in Wasser unter Verwendung von Photokatalysatoren auf TiO₂-Basis unter solarer Bestrahlung untersucht. Der Effekt verschiedener kristalliner Phasen von TiO₂, nämlich Sachtleben Hombikat UV100 (reines Anatas) und Evonik Aeroxid P25 (Mischphase aus Anatas und Rutil), wurde unter den gleichen experimentellen Bedingungen bewertet.

Um den Effekt von Pt-Cokatalysatoren auf die H₂-Produktion zu verstehen, wurde Pt in unterschiedlichen Mengen auf P25 und UV100 abgeschieden. Beim optimalen Beladungsverhältnis von 0.5 Gew.-% zeigte Pt/UV100 im Vergleich zu sämtlichen Pt/P25-Proben eine höhere photokatalytische Aktivität für die H₂-Bildung und die Photooxidation von Naphthalin. Die beobachtete Abnahme der photokatalytischen Aktivität von P25 nach der Platinisierung zeigt, dass Pt-Nanopartikel als Rekombinationszentrum für die photogenerierten Ladungsträger fungieren, wie auch durch Elektronenspinresonanz-Techniken gezeigt wurde. Außerdem wurde beobachtet, dass die Platinisierungsmethode die H₂-Bildung während der Photoreformierung von Naphthalin über Pt/UV100 stark beeinflusst. Die Entwicklung von H₂ ist bei Verwendung von Pt/UV100, das durch Photoabscheidung hergestellt wurde, um 40 % höher als dasjenige, das durch physikalisches Mischen von TiO₂ mit Pt-Nanopartikeln hergestellt wurde. Die Analyse der Ladungsträgerdynamiken unter Verwendung verschiedener spektroskopischer Techniken ergab, dass die starke Metall-Halbleiter-Wechselwirkung, die aus der Photoabscheidung resultiert, zu einer Abnahme der Ladungsträgerrekombinationsraten führt, was die Geschwindigkeit von photokatalytischen Reaktionen erhöht und die H₂-Bildung verbessert.

Die Analyse der Reaktionszwischenprodukte unter Verwendung einer Kombination aus chromatographischen und massenspektroskopischen Techniken zeigt, dass 1- und 2-Naphthalinol neben anderen hydroxylierten Verbindungen die Hauptreaktionsprodukte der Photoreformierung von Naphthalin sind. Darüber hinaus wurde festgestellt, dass die Anreicherung dieser Zwischenprodukte im photokatalytischen System neben dem

ungleichen Massengleichgewicht zwischen den Halbreaktionen der Hauptgrund für die Hemmung der H₂-Bildung und der Photooxidation von Naphthalin ist.

Mehrere mögliche Wege für den Photoreformierungsmechanismus von Naphthalin, an dem verschiedene reaktive Spezies beteiligt sind, wurden getestet. Die Kombination der Spin-Trapping-Studien mit verschiedenen spektroskopischen Techniken legte nahe, dass die Löcher eine wichtige Rolle bei der Naphthalin-Oxidation spielen. Isotopenmarkierungsstudien zeigten, dass Gittersauerstoffatome nicht in die Photooxidationsprodukte eingebaut wurden und die photogenerierten Elektronen Protonen, die hauptsächlich aus Wasser stammen, zu molekularem Wasserstoff reduzieren, während Wasser (aber nicht Naphthalin) am geschwindigkeitsbestimmenden Schritt der Reaktion beteiligt zu sein scheint.

Stichworte: TiO₂-Photokatalyse, Naphthalin, H₂-Bildung, Wasserspaltung, Reaktionsmechanismus, solarer Brennstoff, Photoreformierung.

Abstract

The exploitation of solar radiation in the remediation of organic water pollutants has the potential to be a sustainable energy source to replace fossil fuel. Conceptually, coupling H₂ evolution and the degradation of organic pollutants through dual-functional TiO₂ photocatalysis has been frequently nominated as one of the most sustainable and environmentally friendly technologies. However, the low quantum efficiencies achieved so far by using TiO₂ photocatalysts, and the lack of a fundamental understanding of the reaction mechanism represent big challenges that need to be overcome before their potential can be fully realized. Despite the large number of studies every year that utilize the dual functional photocatalysis processes for the H₂ production from simple water pollutants such as methanol, formaldehyde, and formic acid, aromatic pollutants, however, have been rarely considered. Thus, several open questions regarding the photocatalytic efficiencies and the reaction mechanism during the photoreforming of aromatic compounds still exist. In the presented work, the photocatalytic reforming of naphthalene in water has been investigated employing TiO₂-based photocatalysts under solar irradiation. The effect of different crystalline phases of TiO₂, namely Sachtleben Hombikat UV100 (pure anatase) and Evonik Aeroxide P25 (mixed phase of anatase and rutile), were assessed under the same experimental conditions.

In order to understand the effect of Pt co-catalysts on H₂ production, different fraction ratios were deposited on P25 and UV100. At the optimum loading ratio, 0.5 wt.% Pt-UV100 exhibited the higher photocatalytic activity toward the H₂ formation and photooxidation of naphthalene comparing to all Pt-P25 samples. The observed decrease of the photocatalytic activity of the P25 after the platinization indicates that Pt nanoparticles act as a recombination center for the photogenerated charge carriers as revealed by electron paramagnetic spectroscopy techniques. Besides that, it has been found that the platinization method strongly affects the H₂ formation during the photoreforming of naphthalene over Pt-UV100. The evolution of H₂ is 40 % higher when using Pt-UV100 that was prepared by the photodeposition method than that prepared by the physical mixing of TiO₂ with Pt nanoparticles. The analysis of the charge carrier dynamics employing different spectroscopic techniques revealed that the strong metal-semiconductor interaction resulting from the photodeposition process leads to a significant decrease in the charge carrier recombination rates, which increases the rate of the photocatalytic reactions and enhances the H₂ formation.

The analysis of the reaction intermediates employing a combination of chromatographic, and mass spectroscopic techniques reveals that 1- and 2-naphthalenol, among other hydroxylated compounds, are the main reaction products during the photoreforming of naphthalene. Moreover, the accumulation of these intermediates in the photocatalytic system was found to be the main reason for the inhibition of the H₂ formation and the photooxidation of naphthalene, besides, the unequal mass balance between the half reactions.

Several possible pathways for the photoreforming mechanism of naphthalene involving different reactive species has been tested. Combining the spin trapping studies with

different spectroscopic techniques suggested that the holes play the significant role in naphthalene oxidation. Isotopic labeling studies showed that lattice oxygen atoms were not incorporated into the photooxidation products, and the photogenerated electrons reduced the proton originating mainly from water to molecular hydrogen, whereas, water (but not naphthalene) appears to be involved in the rate-determining step of the reaction.

Keywords: TiO₂ photocatalysis, naphthalene, H₂ formation, water splitting, reaction mechanism, solar fuel, photoreforming.

Table of Contents

Dedication	I
Acknowledgments	III
Kurzzusammenfassung.....	V
Abstract.....	VII
Chapter One: Introduction	1
1.1 Background	1
1.2 The Objectives of this Thesis	6
1.3 Thesis Structure.....	8
1.4 References	10
Chapter Two: TiO₂ Photocatalysis for the Transformation of Aromatic Water Pollutants into Fuels.....	15
2.1 Foreword	15
2.2 Abstract	15
2.3 Introduction	16
2.4 Aromatic Hydrocarbons as Water Pollutants	18
2.4.1 Phenols	19
2.4.2 Polyaromatic Hydrocarbons	20
2.4.3 Organic Dyes	22
2.5 Methods of Treatment	23
2.6 Semiconductor-Based Heterogeneous Photocatalysis	26
2.6.1 The Electronic Structure of a Semiconductor-Photocatalyst.....	27
2.6.2 Photocatalytic Water-Splitting vs. Photocatalytic Reforming.....	29
2.6.3 Titanium dioxide (TiO ₂) as a photocatalyst.....	31
2.6.4 Enhancing the Performance of Pristine TiO ₂	37
2.6.5 Effect of the Loading Method on H ₂ Production.....	41

2.7 Photocatalytic Reforming of Aromatic Compounds.....	43
2.7.1 Monoaromatic and Phenolic-Based Compounds	44
2.7.2 Dyes and Polyaromatic-Based Pollutants.....	51
2.8 Conclusions	58
2.9 Acknowledgments.....	59
2.10 Author Contributions	59
2.11 References.....	59
Chapter Three: Photocatalytic H₂ Production from Naphthalene by Various TiO₂ Photocatalysts: Impact of Pt Loading and Formation of Intermediates	79
3.1 Foreword	79
3.2 Abstract	79
3.3 Introduction.....	80
3.4 Results and Discussion.....	82
3.4.1 Photocatalysts Characterization.....	82
3.4.2 Photocatalytic Reforming of Naphthalene	85
3.4.3 Stability of Pt Deposit	92
3.4.4 Effect of Naphthalene Oxidation Products on the H ₂ Evolution.....	93
3.4.5 EPR Study	96
3.5 Experimental	99
3.5.1 Materials	99
3.5.2 Preparation of the Pt-TiO ₂ Photocatalysts.....	99
3.5.3 Photocatalytic Experiments.....	99
3.5.4 Catalyst Characterization.....	101
3.5.5 EPR in Situ Experiments	102
3.6 Conclusions.....	102
3.7 Acknowledgments.....	103

3.8 Author Contributions	103
3.9 References	103
Chapter Four: TiO₂ Photocatalysis: Impact of the Platinum Loading Method on Reductive and Oxidative Half-Reactions	111
4.1 Foreword	111
4.2 Abstract	112
4.3 Introduction	113
4.4 Experimental Section	114
4.4.1 Materials	114
4.4.2 Preparation of the Photocatalysts	115
4.4.3 Photocatalysts Characterization.....	115
4.4.4 Transient Absorption Spectroscopy	116
4.4.5 Electron Paramagnetic Resonance	116
4.4.6 Photocatalytic Studies and Analytical Procedures	117
4.5 Results and Discussion.....	118
4.5.1 Photocatalysts Characterization.....	118
4.5.2 Photocatalytic Activity	121
4.5.3 EPR Investigation.....	126
4.5.4 Transient Absorption Spectroscopy	128
4.5.5 Comparison of the Deposition Methods.....	131
4.6 Conclusions	135
4.7 Supporting Information	137
4.7.1 Photonic Efficiency Determination	137
4.7.2 Photocatalytic Reforming of Methanol	137
4.7.3 Transmission Electron Microscopy (TEM).....	138
4.7.4 Photocatalytic Reforming of Methanol over 1.0 wt% Pt _{LA} -TiO ₂	141
4.7.5 EPR Investigation.....	142

4.8 Acknowledgments	143
4.9 Author Contributions	143
4.10 References	144
Chapter Five: Mechanistic Insights into Hydrogen Evolution by Photocatalytic Reforming of Naphthalene	149
5.1 Foreword	149
5.2 Abstract	150
5.3 Introduction	150
5.4 Experimental Section	152
5.4.1 Raw Materials.....	152
5.4.2 Preparation and Characterization of the Photocatalysts	152
5.4.3 Sample Preparation and Photocatalytic Experiments.....	153
5.4.4 Mineralization Measurements	154
5.4.5 Extraction Procedures.....	155
5.4.6 Analytical Methods	156
5.4.7 EPR in Situ Experiments	157
5.4.8 Transient Absorption Spectroscopy	157
5.5 Results and Discussion.....	157
5.5.1 Naphthalene Degradation and Photoreforming.....	157
5.5.2 Identification of Intermediates	162
5.5.3 Mechanistic Study	166
5.5.3.1 Participation of the TiO ₂ Surface as a Source of Oxygen Atoms.....	166
5.5.3.2 Scavengers and Electron Paramagnetic Resonance (EPR) Spin- Trapping Technique.....	168
5.5.3.3 Diffuse Reflectance Transient Absorption Spectroscopy.....	172
5.5.3.4 Origin of the Evolved Molecular Hydrogen.....	173
5.5.4 Mechanism of the Photocatalytic Reforming of Naphthalene	175

5.6 Conclusions	180
5.7 Supporting Information	181
5.7.1 Material Characterization	181
5.7.1.1 BET Surface Area.....	181
5.7.1.2 X-Ray Diffraction (XRD).....	181
5.7.1.3 Transmission Electron Microscopy (TEM)	182
5.7.1.4 Electron Paramagnetic Resonance (EPR) Technique.....	183
5.7.2 Sample Preparation and Photocatalytic Experiments.....	184
5.7.2.1 Samples Preparation	184
5.7.2.2 Photonic Efficiency Determination	184
5.7.2.3 Initial Photonic Efficiencies, ξ , for Naphthalene Degradation:	185
5.7.2.4 Naphthalene Absorption and Solar Simulator Emission Spectra	185
5.7.2.5 Dark Adsorption	186
5.7.2.6 Photocatalyst Reusability.....	186
5.7.3 Analytical Methods	187
5.7.4 Photocatalytic CO ₂ and H ₂ Evolution During the Reforming of Naphthalene using Quadrupole Mass Spectroscopy.	187
5.7.5 Intermediates Identification.....	188
5.7.6 Mechanistic Study	189
5.7.6.1 EPR Spectra	189
5.7.6.2 Isotopic Labeling Analyses.....	191
5.8 Acknowledgments.....	192
5.9 Author Contributions	192
5.10 References	192
Chapter Six: Summarizing Discussion and Conclusions	201
6.1 Foreword	201
6.2 Photocatalytic Reforming of Naphthalene	201

6.2.1 H ₂ Evolution	202
6.2.2 Naphthalene Conversion	207
6.2.3 Kinetic of the Photocatalytic Reforming of Naphthalene	211
6.3 Effect of Platinum Ratio in Different Types of Commercial TiO ₂	217
6.4 Impact of the Platinization Method	218
6.5 Mechanism of Photocatalytic Reforming of Naphthalene	226
6.6 Conclusions	236
6.7 References	238
Curriculum Vitae.....	246
Publications	248
Oral Presentations	249
Poster Presentations	249

Chapter One: Introduction

1.1 Background

Nowadays, a steady increase in population, paired with rapid urbanization, industrialization, and advanced economic development placed immense strain on fossil fuel consumption, water resources, and the environment. Indeed, fossil fuels are accounted for 84% of the world's primary energy consumption in 2019¹. Although, the corona pandemic pushed down global energy demand by 6% in 2020, the consumption of global energy is expected to increase about 2-fold by 2050 relative to the last century. Apparently, the energy demand will be met mainly from fossil fuels, which will consequently be accompanied by the increase in greenhouse gas emissions to the atmosphere, global warming, and environmental pollution².

Moreover, the exponential use of the planet's resources such as the water reservoir, and the consequential pollution of the environment are other problems accompanied by the energy demand. Human activities have contaminated different natural resources of water, since about 80% of all industrial effluents and municipal wastewater is discharged into the environment without any treatment. In this context, water pollution with a wide range of persistent organic pollutants such as aromatic compounds is considered the foremost challenge and poses great risks and threats to the environment and human health. Polycyclic aromatic hydrocarbons (PAHs) are one example of these pollutants. These compounds, mainly produced by industrial activities and incomplete combustion of fossil fuels, are ubiquitously found in the environment and have a great tendency to bioaccumulate, forming a broad range of deleterious health effects^{3,4}.

Several calls and warnings regarding the necessity of the economic usage of water are released regularly since freshwater resources are limited. This year, the first paragraph written in the United Nations World Water Development Report 2021⁵ is: *“What is water worth? There is no easy answer to this deceptively simple question. On the one hand, water is infinitely valuable – without it, life would not exist. On the other, water is taken for granted – it is wasted every single day”*. Currently, about 26% of the world's population lives in areas suffering from freshwater scarcity, while in 2050, this deficit will extend to about 57%⁶. Corona pandemic and climate change, however, will worsen the situation by 2030⁵. Thus, problems derived from climate change and the spreading of a wide range of

pollutants being present in the environment and wastewater urgently demand the scientific community to focus their concern to develop sustainable and new environmentally friendly technologies.

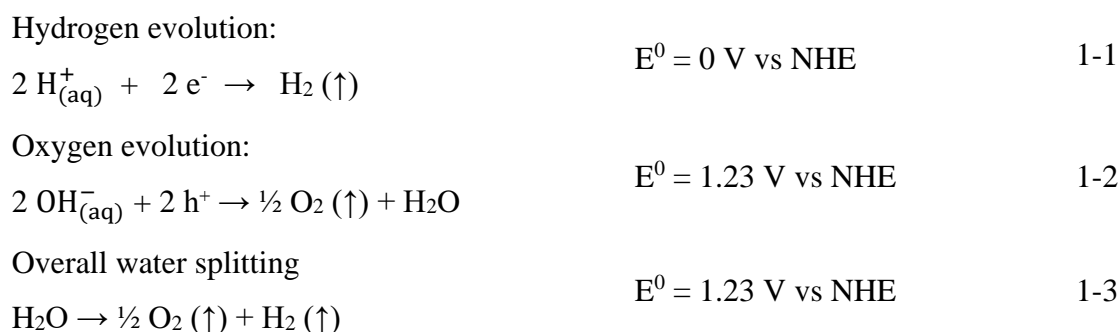
Consequently, sustainable development has become one of the most important strategies worldwide. Several countries have developed a sustainable path for their energy supply. EU has already set its sustainable path to reduce 60% of greenhouse gas emissions by 2050 via transition to renewable energy technologies to achieve continual growth and avoid catastrophic climate change ⁷. From the practical point of view, investment in technology promoted the development of renewable energy technologies in different sectors. In 2019, renewable energy achieved a wide and fast growth rate of about 3.7% in comparison to other resources. Wind power and solar photovoltaic power are the leaders of this achievement, however, wind power growth is the largest ¹.

Given this, solar light represents a huge untapped potential. It has the capability to be an environmentally clean and economically viable sustainable energy. Achieving a fully sustainable energy production system based on sunlight involves the development of multiple and diverse technologies. Since the oil crisis in 1970, molecular hydrogen is being considered the future key energy vector ⁸. H₂ possesses the highest gravimetric gross calorific value among all fuels (142 MJ kg⁻¹), and it burns cleanly yielding only pure water ⁹. Although the "hydrogen economy" is a reasonable approach and compelling vision, practical technological advancements are still the missing key to open this barrier to reality. As solar light is the most abundant clean and renewable energy source, as well, the water is a naturally renewable resource, their combining, and conversion to molecular hydrogen have been accounted as the most viable solution for the development of a low carbon emission economy, in order to counter the increased energy demand and the environmental problems of fossil fuels ¹⁰. Among several methods to produce H₂, solar hydrogen production from water splitting can offer the right renewable and green energy vector.

Since the discovery of the photoelectrochemical splitting of water to H₂ and O₂ by Fujishima and Honda in the 1970s, photocatalysis has received huge attention. The photocatalytic production of molecular hydrogen (H₂) in a solar-driven process is a promising strategy to store sunlight as chemical energy *via* photoinduced reduction of water ^{11,12}. In a photocatalytic system, the reaction that has extremely low kinetics outside this system and thermodynamically unfavored ($\Delta G < 0$), is driven by a semiconductor

through absorption of photons having suitable energy, i.e., the light energy exceeds the energy of the bandgap of the semiconductor¹³. These photons induce the excitation of electrons from the filled valance band (VB) to the empty conduction band (CB) in the photocatalyst, generating electron vacancies in the VB, i.e., the positively charged holes. Afterward, both electrons and holes are relaxed to the bottom of the CB and the top of the VB, respectively. As mobile entities, the charge carrier species (electrons and holes) could recombine or migrate to the surface of the semiconductor, where they can initiate redox reactions via interfacial charge transfer^{14,15}. The photogenerated holes act as oxidants (+1.0 to +3.5 V vs. NHE), while the photogenerated electrons are potential reductants (+0.5 to -1.5 V vs. NHE)¹⁶.

Photocatalytic H₂ production from water-splitting is an uphill reaction and an energetically unfavored process. Thermodynamically, a change in free energy of $\Delta G^0 = 237.2 \text{ kJ mol}^{-1}$ is associated with the splitting of one mole of H₂O to H₂ and ½ O₂. This value corresponds to a potential $\Delta E^0 = 1.23 \text{ V}$ (Equations 1-1 to 1-3)^{17,18}. If the semiconductor will drive this reaction, it must absorb photons of energies higher than 1.23 eV (wavelengths $\leq 1000 \text{ nm}$) and convert the energy into H₂ and O₂¹².



Thus, in the water-splitting reaction, the redox potentials of both H₂ and O₂ generation govern the possible photocatalyst candidate according to the VB and CB positions. The potential photocatalyst for H₂ production should meet the following thermodynamic requirements: (i) energy of the conduction band-edge and the valance band-edge straddle the electrochemical potentials $E^0 (\text{H}^+/\text{H}_2)$ and $E^0 (\text{O}_2/\text{H}_2\text{O})$, respectively, i.e., both potentials should lie within the photocatalyst bandgap. (ii) the bottom of the CB should be more cathodic than the redox potential of (H⁺/H₂), and the top of the VB should be more anodic than the redox potential of (O₂/H₂O)^{19,20}. Therefore, from a thermodynamic point of view, only a few photocatalysts, e.g., TiO₂, are competent to drive the water-splitting reaction.

Titanium dioxide has been one of the most widely studied semiconductors in the last decade as a potential means for the remediation and mineralization of the organic pollutants present in water and air ^{16, 21}, as well as for direct conversion and storage of solar light ²². This is related to its high reactivity, hydrophilicity, low cost and availability, physical and chemical stability, resistance to photocorrosion, and optimal electronic and optical capacity ¹⁴. Since the early part of the 20th century, scientists reported the photoactivity of the TiO₂ for oxidative degradation of organic molecules such as dyes in vacuo and in oxygen ²³. From that time, a dramatic increase in the TiO₂ photocatalysis research had occurred in the environmental remediation and solar energy conversion fields, to develop an applied technology. However, no real technological applications have been accomplished hitherto, due to the drastically low photonic efficiencies ²⁴. Therefore, to realize practical applications three major obstacles must be overcome. Firstly, the rapid recombination of the photogenerated charge carriers, which strongly limits the photocatalytic efficiency ²⁵. Secondly, the poor overlap of the absorption spectrum of TiO₂ with the solar emission spectrum that results in a small fraction of photons being absorbed, mainly in the UV region. And thirdly, the fast backward reaction between the O₂ and H₂ which strongly competes with the splitting of water.

Numerous strategies have been considered to resolve the above-mentioned handicaps and improve the TiO₂'s photocatalytic performance, including sensitization with dyes, doping with metallic or non-metallic species, surface modification, and coupling with other materials ^{26, 27}. The main two approaches for suppressing the charge carrier recombination and the reverse reaction can be achieved by using a specific co-catalyst to form a physical separation between the electron and hole on the surface of the photocatalyst. In addition, using a sacrificial electron donor (SED) leads to push the oxidation half-reaction to achieve acceptable efficiencies ^{11, 12}. By using sacrificial organic molecules such as alcohols, organic acids, and hydrocarbons as electron donors, the holes are scavenged by these molecules and the recombination of the charge carrier can be greatly reduced. Furthermore, since O₂ is not produced by using these sacrificial agents, the back reaction with H₂ to produce water is suppressed, thus, increasing the H₂ formation ²⁸. Indeed, to sustain the H₂ production, the continuous addition of these electron donors is required since they are consumed in the photocatalytic reaction. However, even in the presence of a sacrificial electron donor that should promote the H₂ formation, the quantum efficiency for H₂

production over pristine TiO₂ is still negligible, due to the large overpotential for the reduction of protons^{29, 30}.

Surface decoration with metals (especially Pt, Au, Ag, Cu) is known to greatly improve the efficiency of H₂ production^{31, 32}. According to the Schottky barrier model, such enhancement is attributed to the transfer of the photogenerated holes to the surface and the simultaneous migration of the electrons into the metal nanoparticles induced by the electric field in the space charge layer³³. Amongst the metals that facilitate electron capture, Pt has been reported extensively as the most effective one. Concomitantly, Pt is considered an excellent catalyst in dehydrogenation, oxidation in thermal catalysis, and hydrogenation processes³⁴. However, many structural factors seem to affect the activity of the resulting platinized TiO₂, such as size, dispersion, chemical state of Pt deposits, the interaction between the metal and the support, and the preparation method^{27, 35, 36}.

Moreover, as a hybrid field, dual-functional photocatalysis is a combination of different photocatalytic fields for 2-fold purposes achieved in a single step³⁷. The coupling of H₂ evolution and photocatalytic degradation of organic pollutants yielding CO₂ can be achieved in the so-called photoreforming process (Figure 1-1)^{13, 20, 22, 38}. Such a technique has a great advantage as it can benefit from solar light and treat wastewater. In the photocatalytic reforming process, the photogenerated holes in the valence band can oxidize adsorbed organic substrates (electron donors), whereas the conduction band electrons, trapped by Pt nanoparticles on the surface of the photocatalyst, can reduce the protons (electron acceptor) to molecular hydrogen³⁷.

Although the dual-functional heterogeneous photocatalysis nanotechnology opens up a novel platform to simultaneously remove wastewater pollutants and produce molecular hydrogen, most of the previous studies dealing with the development of this technology have focused on photoreforming of simple organic compounds like methanol, ethanol, formaldehyde, formic acid, etc., as model pollutants. However, in reality, the water and wastewater pollutants consist of a wide range of organic pollutants from different sources such as aliphatic hydrocarbons, phenols, chlorophenols, and chlorobenzenes, pesticides, herbicides, semivolatile organic compounds, dioxins, PAHs, etc. These compounds, in particular PAHs, have been frequently detected in groundwater and wastewater. Among the different PAHs, naphthalene is a particularly noxious member due to its relatively large solubility in water, which leads to increased bioavailability and ultimately to adverse effects

in the environment and on human health. Despite the large number of studies that considered the photocatalysis processes for the removal of PAHs in aerobic conditions (where the reduction half-reaction is the conversion of molecular oxygen to the superoxide radical anion)^{39, 40}, no reports on the remediation of PAHs with the simultaneous production of H₂ were found in the literature.

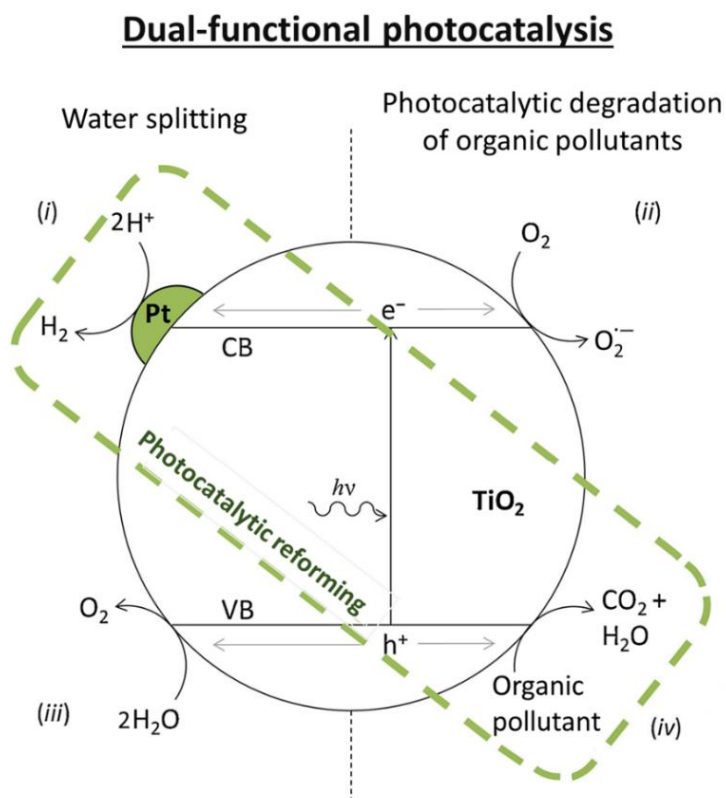


Figure 1-1: Common applications of semiconductor photocatalysis for environmental remediation and water splitting (the green dashed line represents the dual-functional photocatalysis for simultaneous water treatment and energy recovery). Production of hydrogen by the photogenerated electrons (i) and oxygen by the photogenerated holes (iii) during water cleavage, takes place under anaerobic conditions. Oxidation of organic compounds takes place in the presence of O₂ with the participation of photo-generated holes (iv) and O₂^{•-} (ii), producing CO₂ and H₂O. The photo-reforming process combines the H₂ production (i) and oxidation of organic compound (iv) under anaerobic conditions. Adapted with permission from reference 38. Copyright 2016 Elsevier B.V.

1.2 The Objectives of this Thesis

The production of molecular hydrogen from renewable energy sources such as water and sunlight by photocatalytic processes represents a sustainable pathway to green energy as well as eco-friendly methods of degrading organic pollutants. However, the low photocatalytic efficiency and the lack of a detailed mechanistic understanding of the photocatalytic reactions are the main problems that hinder the industrialization of this technology.

This PhD thesis is devoted to investigate and evaluate the photocatalytic reforming of the smallest PAH compound, i.e., naphthalene under simulated solar irradiation. Although there is a wide range of potential candidate semiconductors that can be used to conduct this study, it is preferable and advisable to choose the widely studied photocatalyst to take the advantage of the vast amount of knowledge available in the scientific literature. TiO₂ is by far the most extensively studied photocatalyst. Since it is well acknowledged that the phase composition has a crucial impact on the photocatalytic activity of the TiO₂ materials, the most active commercial TiO₂ types, i.e., Sachtleben Hombikat UV100 (pure anatase) and Evonik Aeroxide P25 (mixed phase of anatase and rutile), were used in this study. By considering that the photocatalytic reforming of the PAHs was not reported previously in the literature, one of the goals of this PhD thesis is to provide the scientific community with comparable values for this reaction. Therefore, the performances of the studied “naphthalene/TiO₂” systems were evaluated in terms of calculating the photonic efficiencies of the hydrogen formation and naphthalene conversion under the same experimental conditions.

Despite that several studies had reported the ability of pristine TiO₂ to produce molecular hydrogen without using a co-catalyst, it is widely accepted that one of the most relevant drawbacks of using pristine TiO₂ as an active photocatalyst for H₂ evolution reaction is the fast recombination of the photogenerated electrons and holes. Considering that the surface catalytic reaction is a successive step of charge separation, the charge carrier recombination process can be controlled by modifying the surface properties of the TiO₂ via loading with metal co-catalyst such as Pt. In this way, the conduction band electrons initiate the reduction reaction of the proton to molecular H₂ on the Pt nanoparticles, while the valence band holes initiate the oxidation reaction on the surface of the TiO₂ (Figure 1-1). In this thesis, the effects of the following factors and parameters on the H₂ production during the photocatalytic reforming of the aromatic compounds were investigated and evaluated:

- i. The type of the TiO₂ photocatalyst.
- ii. The platinum loading method.
- iii. The loading ratio of platinum nanoparticles on the surface of TiO₂.
- iv. The formation of the organic intermediates.

In most of the published investigations dealing with the photocatalytic reforming of the organic pollutants, the researchers paid their main attention only to the H₂ evolution

reaction, while poor and non-systematic documentations for the reaction mechanism were mostly provided. However, from the point of view of the practical application, insights into the detailed mechanistic studies for the kinetic of the charge carrier, as well as, the complete photocatalytic reaction for both half redox reactions i.e., “*The Complete Story*” must be provided. In comparison to the relatively simple sacrificial electron donors like methanol, naphthalene oxidation involves a large number of steps and generates several oxidation intermediates where their involvement in the photocatalytic process may play an undesired role; therefore, mechanistic investigations on both the reductive and oxidative half-reactions are desired. Accordingly, this thesis established and elucidated a systematic method to get more insights into the reaction mechanism of the photocatalytic reforming of the aromatic compounds. By employing and combining different analytical techniques such as HPLC, HPIC, GC-MS, QMS, EPR, and TAS the most possible oxidation half-reaction for photooxidation of naphthalene, as well the reduction half-reaction for molecular hydrogen formation during the photocatalytic reforming of naphthalene were proposed and intensively discussed.

1.3 Thesis Structure

The topics of this doctoral dissertation are extensively discussed in six chapters comprising four peer-reviewed published articles.

Chapter 1 outlines the shortage of freshwater, the environmental pollution, and the global energy issues that necessitated a shift from fossil fuels to green renewable alternatives to decrease the environmental pollution resulted from such use of fossil fuels. Moreover, it presented the basic principle of TiO₂ photocatalysis for generating renewable energy, i.e., H₂ production from the water splitting, and the different limitations that hinder such technology are also discussed. Subsequently, the photocatalytic reforming of the organic water pollutants was introduced as a potential alternative energy technology for H₂ production and remediation of different widespread organic pollutants, as well, some of their major obstacles were highlighted.

Chapter 2 displays a review article entitled “*TiO₂ Photocatalysis for the Transformation of Aromatic Water Pollutants into Fuels*”⁴¹. The first part of this review discussed the different classes of water aromatic pollutants, their environmental hazards, and health threats. Moreover, an overview on the adopted conventional methods and the proposed recent ones for the treatment of these organic pollutants was presented with highlighting

some of their advantages and disadvantages. In the next part, the fundamental and electronic structure of semiconductor-photocatalyst, the significant parameters affecting its performance, and photocatalytic water splitting versus photocatalytic reforming are reviewed and discussed. Moreover, TiO₂ photocatalysis is also presented in this part, emphasizing the photocatalytic properties of its different phases and how to enhance the performance of pristine TiO₂ by loading of noble metals. Finally, and based on the recent research investigations, the current perspective for photocatalytic reforming of aromatic-based pollutants towards H₂ production and water decontamination is reviewed and highlighted.

Chapter 3 includes a research article entitled “*Photocatalytic H₂ Production from Naphthalene by Various TiO₂ Photocatalysts: Impact of Pt Loading and Formation of Intermediates*”⁴². In this article, the photocatalytic reforming of the persistent pollutant naphthalene was systematically investigated over pristine and platinized TiO₂ under illumination by solar light simulator. As a first step to set up the proper conditions for evaluating the efficiency of H₂ evolution during the removal of naphthalene from an aqueous solution, a comparative study between two different commercial TiO₂ photocatalysts, namely, Evonik Aeroxide P25 and Sachtleben Hombikat UV100, was performed. Both photocatalysts were loaded with different fractional ratios of platinum nanoparticles by the photodeposition method. The different photocatalytic activities between the as-prepared Pt-TiO₂ and the impact of the co-catalyst Pt nanoparticles on the photocatalytic activity has been evaluated based on the kinetics of the charge carrier. Moreover, the effect of the intermediate products during the photocatalytic process was also investigated.

Chapter 4 includes a research article entitled “*TiO₂ Photocatalysis: Impact of the Platinum Loading Method on Reductive and Oxidative Half-Reactions*”⁴³. The effect of the platinum-loading methods was assessed for the photoreforming reaction of naphthalene. Platinized TiO₂ (anatase, UV100) was prepared using two alternative methods: photodeposition by reduction of PtCl₆²⁻, and physical mixing of TiO₂ with Pt nanoparticles synthesized by laser ablation. Full physiochemical characterizations were performed for all the samples. The higher photocatalytic activity of the sample prepared by the photodeposition method was explained based on the different charge carrier dynamics by employing transient absorption spectroscopy and electron paramagnetic spectroscopy techniques.

Since the photocatalytic reforming mechanism of polyaromatic hydrocarbons (PAHs) had not been reported previously in the literature, therefore, as a final step in this study, the photoreforming mechanism of the simplest PAH compound, namely, naphthalene has been investigated. Chapter 5 includes a research article entitled “*Mechanistic Insights into Hydrogen Evolution by Photocatalytic Reforming of Naphthalene*”⁴⁴. As a result of the investigations presented in Chapters 3 and 4, the platinumized TiO₂ (anatase, UV100) prepared by loading with the optimum fractional ratio of PtNPs (0.5 wt.%) via the photodeposition method was used in this mechanistic study. Naphthalene/Pt-TiO₂ suspension was employed in different photocatalytic systems to understand the pathways of the half redox reactions during the photoreforming of naphthalene. Different chromatographic, spectroscopic, and isotopic techniques were used, to give an accurate and comprehensive overview for this investigation.

Finally, Chapter 6 displays a summarizing discussion that correlates the presented results in the previous chapters.

1.4 References

1. Agency, I. E. Global energy review 2019: The latest trends in energy and emissions in 2019. <https://webstore.iea.org/download/direct/2994>.
2. Owusu, P. A.; Asumadu-Sarkodie, S., A review of renewable energy sources, sustainability issues and climate change mitigation. *Cogent Eng.* **2016**, *3* (1), 1167990.
3. Mastral, A. M.; Callén, M. S., A review on polycyclic aromatic hydrocarbon (PAH) emissions from energy generation. *Environ. Sci. Technol.* **2000**, *34* (15), 3051-3057.
4. Drwal, E.; Rak, A.; Gregoraszczyk, E. L., Review: Polycyclic Aromatic Hydrocarbons (PAHs)-Action on placental function and health risks in future life of newborns. *Toxicology* **2019**, *411*, 133-142.
5. UNESCO. *The united nations world water development report 2021: Valuing water*; UN-Water: 2021.
6. Boretti, A.; Rosa, L., Reassessing the projections of the World Water Development Report. *npj Clean Water* **2019**, *2* (1), 15.
7. Commission, E. Communication from the commission to the european parliament, the council, the european economic and social committee and the committee of the regions Stepping up Europe’s 2030 climate ambition Investing in a climate-neutral future for the benefit of our people. <https://eur-lex.europa.eu/legal-content/EN/TXT/?uri=CELEX:52020DC0562>.
8. Kulagin, V. A.; Grushevenko, D. A., Will hydrogen be able to become the fuel of the future? *Therm. Eng.* **2020**, *67* (4), 189-201.

9. Niaz, S.; Manzoor, T.; Pandith, A. H., Hydrogen storage: materials, methods and perspectives. *Renew. Sust. Energ. Rev.* **2015**, *50*, 457-469.
10. Ma, Y.; Wang, X.; Jia, Y.; Chen, X.; Han, H.; Li, C., Titanium dioxide-based nanomaterials for photocatalytic fuel generations. *Chem. Rev.* **2014**, *114* (19), 9987-10043.
11. Kennedy, J.; Bahruji, H.; Bowker, M.; Davies, P. R.; Bouleghlimat, E.; Issarapanacheewin, S., Hydrogen generation by photocatalytic reforming of potential biofuels: Polyols, cyclic alcohols, and saccharides. *J. Photochem. Photobiol., A* **2018**, *356*, 451-456.
12. Fajrina, N.; Tahir, M., A critical review in strategies to improve photocatalytic water splitting towards hydrogen production. *Int. J. Hydrog. Energy* **2019**, *44* (2), 540-577.
13. Hakki, A.; AlSalka, Y.; Mendive, C. B.; Ubogui, J.; dos Santos Claro, P. C.; Bahnemann, D., Hydrogen production by heterogeneous photocatalysis. In *Encyclopedia of Interfacial Chemistry*, Wandelt, K., Ed. Elsevier: Oxford, 2018; pp 413-419.
14. Friehs, E.; AlSalka, Y.; Jonczyk, R.; Lavrentieva, A.; Jochums, A.; Walter, J.-G.; Stahl, F.; Scheper, T.; Bahnemann, D., Toxicity, phototoxicity and biocidal activity of nanoparticles employed in photocatalysis. *J. Photochem. Photobiol., C* **2016**, *29*, 1-28.
15. Hernández-Ramírez, A.; Medina-Ramírez, I., Semiconducting materials. In *Photocatalytic semiconductors*, Hernández-Ramírez, A.; Medina-Ramírez, I., Eds. Springer International Publishing: Cham, 2015; pp 1-40.
16. Hoffmann, M. R.; Martin, S. T.; Choi, W.; Bahnemann, D. W., Environmental applications of semiconductor photocatalysis. *Chem. Rev.* **1995**, *95* (1), 69-96.
17. Walter, M. G.; Warren, E. L.; McKone, J. R.; Boettcher, S. W.; Mi, Q.; Santori, E. A.; Lewis, N. S., Solar water splitting cells. *Chem. Rev.* **2010**, *110* (11), 6446-73.
18. Colon, G., Towards the hydrogen production by photocatalysis. *Appl. Catal., A* **2016**, *518*, 48-59.
19. Ohtani, B., Photocatalysis A to Z—What we know and what we do not know in a scientific sense. *J. Photochem. Photobiol., C* **2010**, *11* (4), 157-178.
20. Pichat, P., A brief overview of photocatalytic mechanisms and pathways in water. *Water Sci. Technol.* **2007**, *55* (12), 167-73.
21. Prairie, M. R.; Evans, L. R.; Stange, B. M.; Martinez, S. L., An investigation of titanium dioxide photocatalysis for the treatment of water contaminated with metals and organic chemicals. *Environ. Sci. Technol.* **1993**, *27* (9), 1776-1782.
22. Schneider, J.; Kandiel, T. A.; Bahnemann, D. W., Solar photocatalytic hydrogen production: Current status and future challenges. In *Materials and processes for solar fuel production*, Viswanathan, B.; Subramanian, V.; Lee, J. S., Eds. Springer New York: New York, NY, 2014; pp 41-74.
23. Hashimoto, K.; Irie, H.; Fujishima, A., TiO₂ photocatalysis: A historical overview and future prospects. *Jpn. J. Appl. Phys.* **2005**, *44* (12), 8269-8285.
24. Wei, Z.; Janczarek, M.; Endo, M.; Wang, K.; Balcytis, A.; Nitta, A.; Mendez-Medrano, M. G.; Colbeau-Justin, C.; Juodkazis, S.; Ohtani, B.; Kowalska, E., Noble metal-modified

- faceted anatase titania photocatalysts: Octahedron versus decahedron. *Appl. Catal., B* **2018**, *237*, 574-587.
25. Schneider, J.; Matsuoka, M.; Takeuchi, M.; Zhang, J.; Horiuchi, Y.; Anpo, M.; Bahnemann, D. W., Understanding TiO₂ photocatalysis: Mechanisms and materials. *Chem. Rev.* **2014**, *114* (19), 9919-86.
 26. Kumaravel, V.; Mathew, S.; Bartlett, J.; Pillai, S. C., Photocatalytic hydrogen production using metal doped TiO₂: A review of recent advances. *Appl. Catal., B* **2019**, *244*, 1021-1064.
 27. Wenderich, K.; Mul, G., Methods, mechanism, and applications of photodeposition in photocatalysis: A review. *Chem. Rev.* **2016**, *116* (23), 14587-14619.
 28. Schneider, J.; Bahnemann, D. W., Undesired role of sacrificial reagents in photocatalysis. *J. Phys. Chem. Lett.* **2013**, *4* (20), 3479-3483.
 29. Linsebigler, A. L.; Lu, G. Q.; Yates, J. T., Photocatalysis on TiO₂ surfaces - Principles, mechanisms, and selected results. *Chem. Rev.* **1995**, *95* (3), 735-758.
 30. Wang, Z.; Li, C.; Domen, K., Recent developments in heterogeneous photocatalysts for solar-driven overall water splitting. *Chem. Soc. Rev.* **2019**, *48* (7), 2109-2125.
 31. Park, H.; Reddy, D. A.; Kim, Y.; Lee, S.; Ma, R.; Kim, T. K., Synthesis of ultra-small palladium nanoparticles deposited on CdS nanorods by pulsed laser ablation in liquid: role of metal nanocrystal size in the photocatalytic hydrogen production. *Chemistry* **2017**, *23* (53), 13112-13119.
 32. AlSalka, Y.; Al-Madanat, O.; Curti, M.; Hakki, A.; Bahnemann, D. W., Photocatalytic H₂ evolution from oxalic acid: Effect of cocatalysts and carbon dioxide radical anion on the surface charge transfer mechanisms. *ACS Appl. Energy Mater.* **2020**, *3* (7), 6678-6691.
 33. Li, F. B.; Li, X. Z., The enhancement of photodegradation efficiency using Pt-TiO₂ catalyst. *Chemosphere* **2002**, *48* (10), 1103-1111.
 34. Wang, C.; Yin, L.; Zhang, L.; Liu, N.; Lun, N.; Qi, Y., Platinum-nanoparticle-modified TiO₂ nanowires with enhanced photocatalytic property. *ACS Appl. Mater. Interfaces* **2010**, *2* (11), 3373-7.
 35. Kozlova, E. A.; Lyubina, T. P.; Nasalevich, M. A.; Vorontsov, A. V.; Miller, A. V.; Kaichev, V. V.; Parmon, V. N., Influence of the method of platinum deposition on activity and stability of Pt/TiO₂ photocatalysts in the photocatalytic oxidation of dimethyl methylphosphonate. *Catal. Commun.* **2011**, *12* (7), 597-601.
 36. Wang, C.-y.; Pagel, R.; Bahnemann, D. W.; Dohrmann, J. K., Quantum yield of formaldehyde formation in the presence of colloidal TiO₂-based photocatalysts: Effect of intermittent illumination, platinization, and deoxygenation. *J. Phys. Chem. B* **2004**, *108* (37), 14082-14092.
 37. Kampouri, S.; Stylianou, K. C., Dual-functional photocatalysis for simultaneous hydrogen production and oxidation of organic substances. *ACS Catal.* **2019**, *9* (5), 4247-4270.
 38. Puga, A. V., Photocatalytic production of hydrogen from biomass-derived feedstocks. *Coord. Chem. Rev.* **2016**, *315*, 1-66.

39. Guo, Y.; Dai, Y.; Zhao, W.; Li, H.; Xu, B.; Sun, C., Highly efficient photocatalytic degradation of naphthalene by $\text{Co}_3\text{O}_4/\text{Bi}_2\text{O}_2\text{CO}_3$ under visible light: A novel P–N heterojunction nanocomposite with nanocrystals/lotus-leaf-like nanosheets structure. *Appl. Catal., B* **2018**, *237*, 273-287.
40. Theurich, J.; Bahnemann, D. W.; Vogel, R.; Ehamed, F. E.; Alhakimi, G.; Rajab, I., Photocatalytic degradation of naphthalene and anthracene: GC-MS analysis of the degradation pathway. *Res. Chem. Intermed.* **1997**, *23* (3), 247-274.
41. Al-Madanat, O.; AlSalka, Y.; Ramadan, W.; Bahnemann, D. W., TiO_2 photocatalysis for the transformation of aromatic water pollutants into fuels. *Catalysts* **2021**, *11* (3), 317.
42. Al-Madanat, O.; AlSalka, Y.; Dillert, R.; Bahnemann, D., Photocatalytic H_2 production from naphthalene by various TiO_2 photocatalysts: Impact of Pt loading and formation of intermediates. *Catalysts* **2021**, *11* (1), 107.
43. Al-Madanat, O.; Curti, M.; Günemann, C.; AlSalka, Y.; Dillert, R.; Bahnemann, D. W., TiO_2 photocatalysis: Impact of the platinum loading method on reductive and oxidative half-reactions. *Catal. Today* **2021**, (under review).
44. Al-Madanat, O.; AlSalka, Y.; Curti, M.; Dillert, R.; Bahnemann, D. W., Mechanistic insights into hydrogen evolution by photocatalytic reforming of naphthalene. *ACS Catal.* **2020**, *10* (13), 7398-7412.

Chapter Two: TiO₂ Photocatalysis for the Transformation of Aromatic Water Pollutants into Fuels

2.1 Foreword

This chapter contains the review article “*TiO₂ Photocatalysis for the Transformation of Aromatic Water Pollutants into Fuels*” by Osama Al-Madanat, Yamen AlSalka, Wegdan Ramadan, and Detlef W. Bahnemann. Reproduced with permission from *Catalysts* 2021 (11, 317, DOI: 10.3390/catal11030317). Copyright 2021 MDPI. This chapter aims to provide the reader with the recent reports in solar fuel generation, especially the H₂ production during the photocatalytic degradation of different kinds of aromatic water pollutants based on heterogeneous TiO₂ photocatalysis. The sources and the hazardous effects of these organic pollutants were also presented. Great emphasis was paid to the fundamental of the TiO₂ photocatalysis process, and the adopted strategies for improving the TiO₂ activity. The key factors affecting the efficiencies of photocatalytic processes were also addressed. Besides, the mechanisms of the photocatalytic reforming of some of these aromatic pollutants photocatalytic were presented and discussed.

2.2 Abstract

The growing world energy consumption with reliance on conventional energy sources and the associated environmental pollution are considered the most serious threats faced by mankind. Heterogeneous photocatalysis has become one of the most frequently investigated technologies, due to its dual functionality, i.e., environmental remediation and converting solar energy into chemical energy, especially molecular hydrogen. H₂ burns cleanly and has the highest gravimetric gross calorific value among all fuels. However, the use of a suitable electron donor, in what so-called "photocatalytic reforming", is required to achieve acceptable efficiency. This oxidation half-reaction can be exploited to oxidize the dissolved organic pollutants, thus, simultaneously improving the water quality. Such pollutants would replace other potentially costly electron donors, achieving the dual-functionality purpose. Since the aromatic compounds are widely spread in the environment, they are considered attractive targets to apply this technology. In this review, different aspects are highlighted, including the employing of different polymorphs of pristine titanium dioxide as photocatalysts in the photocatalytic processes, also improving the photocatalytic activity of TiO₂ by loading different types of metal co-catalysts, especially

platinum nanoparticles, and comparing the effect of various loading methods of such metal co-catalysts. Finally, the photocatalytic reforming of aromatic compounds employing TiO₂-based semiconductors is presented.

Keywords: TiO₂, Aromatic compound, PAHs, H₂ production, Photocatalytic reforming, Water remediation.

2.3 Introduction

Water is essential for the existence of all live beings. However, its pollution with organic and inorganic compounds remains a threat and poses great risks to the environment and human health. The water quality is merely a concept reflecting the kind and quantity of contaminants contained in it. Mining and petrochemical industries are instrumental in the economical growth of many countries and their products are regarded as privileges to modern communities ¹. However, the wastes generated from the activities of these industries are toxic and carcinogenic ². Thus, these wastes have been classified as ‘hazardous’ ³, and there is a constant increase in the pollution concerns associated with various petrochemical compounds and their by-products in the form of water, air, and soil pollution. Many of these by-products are still extensively employed, especially in the chemical, medical, and other industrial fields, as irreplaceable and inevitable raw materials ⁴⁻⁷. Aromatic compounds, like benzene, phenol, and chlorobenzene are some of the most encountered volatile organic compounds, VOCs. The primary sources of such VOCs are originated from a large number of anthropogenic activities such as refinery streams, especially from catalytic reforming and cracking, and petroleum refining, petrochemical processing, solvent use, and many other industrial activities ^{8,9}. Other VOCs like methane and chlorofluorocarbons “greenhouse gases” which cause global warming.

The aromatic ring is the basic constituent of many organic pollutants, such as polyaromatic hydrocarbons (PAHs), dyes, pesticides, and pharmaceuticals. Aromatic compounds, such as benzene, phenols, and benzoic acid, are the most frequently used model substrates to investigate the photocatalytic mechanism and to test the activity of the photocatalysts ¹⁰⁻¹³. Detailed studies have been made on the harm caused by the aromatic compounds, for example, the potential relationship between the benzene-related compounds and the risk of hematologic cancers, like lymphoid malignancies ¹⁴. Also, long-term exposure to a low concentration of such compounds could predispose to the development of type 2 diabetes

(T2D) and affect human metabolism^{15, 16}. Aromatic organic compounds also contribute to serious environmental problems such as water pollution, which may result in the demise of scarce species, and biological genetic variation which in many cases is an irreversible problem^{17, 18}.

Semiconductor photocatalysis has been extensively studied in the past 30 years as a promising method of environmental cleanup and sterilization. However, an earlier description of the photocatalytic properties of some metal oxides was given in 1955 by Markham¹⁹, who dealt with ZnO, Sb₂O₃, and TiO₂ and the various types of photochemical changes that these oxides could undergo, including the catalyzed oxidation of organic compounds under UV irradiation. Later and in 1972 a short note published in Nature by Fujishima and Honda²⁰ demonstrated that water could be photolyzed electrochemically at an illuminated TiO₂ and Pt electrode combination to yield stoichiometric quantities of H₂ and O₂. What followed soon thereafter was a frenzied series of studies in search of the photocatalytic materials to produce H₂ fuel as part of the beginnings of the hydrogen economy. Many semiconductors showed photocatalytic properties like MoS₂²¹, WO₃²², BiFeO₃²³, Fe₂O₃²⁴, and CdTe^{25, 26}, but only a few of them fulfill the thermodynamic requirements for overall water splitting like KTaO₃, SrTiO₃, TiO₂, ZnS and SiC. What seems a simple basic function like the excitation of the semiconductor by absorption of light results in the formation of the charge carrier, i.e., the valance band holes, h_{vb}^+ , and the conduction band electrons, e_{cb}^- . However, because of the strong oxidation ability of h_{vb}^+ and reactive oxygen species like •OH, •OOH, and H₂O₂, which are formed from the h_{vb}^+ oxidation of H₂O and e_{cb}^- reduction of O₂, most organic compounds can be oxidized, even mineralized to CO₂ and H₂O in the photocatalytic systems. Due to the challenges that remain in achieving overall pure water splitting, the alternative approach is to combine light-induced splitting of water and photooxidation of organic substrates into a single process in so-called photocatalytic reforming²⁷.

TiO₂ is one of the most studied photocatalysts, it was greatly debated in many aspects like the nature of the oxidative agent (OH^\bullet vs h^+), the site at which the reaction takes place (surface versus bulk solution), how to improve performance, and efficiency of TiO₂ photocatalytic properties. Unfortunately, TiO₂ has a relatively large bandgap (3.2 eV) so that only UV radiation can activate it, its conduction band is somewhat positive in relation to the redox potential for H₂ evolution. Clearly, new semiconductor-based nanostructured materials are needed that would use lower-energy photons available in the visible spectral

region. A strategy developed mostly in the past decade was to push the absorption onset of TiO₂ toward longer wavelengths (≥ 387 nm) by doping TiO₂ with anions and/or cations (N, C, S, F, ..., and metal ions) ²⁸. Despite the many studies carried out with TiO₂, no other metal oxide has yet been found that might act as an efficient photoanode with conduction and valence band edges that straddle the redox potentials of water and many water organic pollutants.

In the first part of this review, we discuss the different classes of aromatic organic hydrocarbons pollutants with an emphasis on their chemical, structural, and physical properties. Their environmental hazards, health threats, and their ability to leak into the different components of the environment especially the aquatic environment are also discussed. In the following parts of this review, we provide the reader with an overview of the conventional methods adopted for the treatment of organic pollutants against the recent methods used and the new trends to be evaluated and debated. The fundamental and electronic structure of semiconductor-photocatalyst, the significant parameters affecting its performance, and photocatalytic water splitting versus photocatalytic reforming are reviewed in detail. The next part of this review is dedicated to TiO₂, which is one of the most widely studied semiconductors, with emphasis on the photocatalytic properties of its different phases and how to enhance the performance of pristine TiO₂ by the loading of noble metals. Finally, and based on the recent research investigations, the current perspective for photocatalytic reforming of aromatic-based pollutants towards H₂ production and water decontamination is reviewed and highlighted.

2.4 Aromatic Hydrocarbons as Water Pollutants

Many pollutants discarded into the environment contain non-degradable substances like heavy metals and organic pollutants ²⁹⁻³¹. The persistent organic pollutants such as Pesticides ³², aromatic organic compounds (OCs) ^{33, 34}, semi-volatile organic compounds (SVOCs) ³⁵⁻³⁷, and organic dyes ^{38, 39} are gaining great environmental concerns due to their impacts on health and environment. These compounds have grasped much attention due to their carcinogenic potential and ubiquitous presence in the environment, which pose a major threat to water reservoirs and the surrounding ecosystem.

The aromatic organic compounds, such as benzene, toluene, ethylbenzene, and xylenes (BTEX), polyaromatic hydrocarbons (PAHs), phenols, and their derivatives are frequently detected in different wastewater resources ⁴⁰. The removal of these organic pollutants is a

must to reuse this water since such pollutants can't be eliminated efficiently during conventional treatment processes. The reuse of this treated water, especially in irrigation of crops, contains great risks due to the transfer of these pollutants to plants, thus, through the food chain to living organisms^{32, 35}. The following subsections provide a brief description of the main types of these pollutants.

2.4.1 Phenols

Phenolic compounds are a class of organic compounds that consist of a hydroxyl group(s) directly bonded to one or more aromatic rings. The phenolic compounds are classified as priority pollutants due to their carcinogenic, mutagenic properties, and high toxicity even at low concentrations⁴¹. These compounds represent serious threats to human health, e.g., skin and eye irritations, anemia, respiratory, and vertigo⁴². The Environmental Protection Agency (EPA) sets the level standard of phenols in the surface water to less than 1 µg L⁻¹, while, the toxicity levels for both humans and aquatic life are usually in the range 9–25 mg L⁻¹⁴¹. Phenols are one of the main intermediates for household and industrial productions of cleaners, dyes, pesticides, herbicides, paint, pharmaceuticals, petrochemicals, cooking operations, resin manufacturing, plastics, pulp, paper, and wood products^{33, 42}. They are usually detected in the wastewater effluents in very high concentrations up to thousands of mg L⁻¹⁴³.

The first member of this category of organic compounds is phenol with the chemical formula of C₆H₅OH. All other members of the group are derivatives of phenol⁴⁴. Chlorophenols are the largest group and most spread group of phenols. They are formed in the environment by chlorination of mono and polyaromatic compounds present in soil and water⁴². Moreover, the reaction of hypochlorite with phenolic acids during the treatments and disinfection processes leads to the formation of such chlorinated compounds. Chlorinated phenols e.g., 2-chlorophenol, 2,4-dichlorophenol, 2,4,6-trichlorophenol, and pentachlorophenol (Chart 2-1), are listed by the US-EPA as priority organic pollutants^{45, 46}.

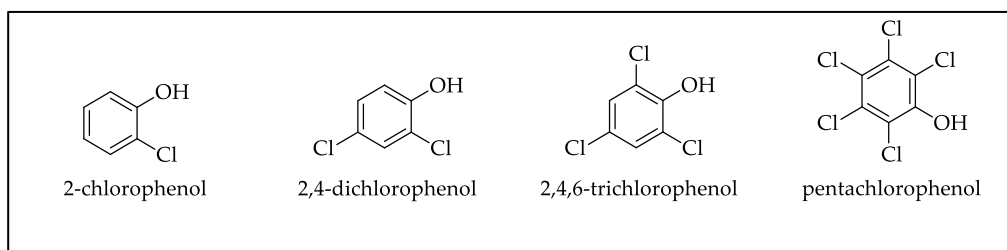


Chart 2-1: The most common priority pollutants chlorinated phenols.

2.4.2 Polyaromatic Hydrocarbons

Another kind of organic pollutants that causes water contamination is the PAHs, which are classified as hazardous persistent environmental pollutants⁴⁷. They are a group of over 100 different organic compounds containing two or more fused aromatic benzene rings connected linearly, angularly, or in a cluster arrangement^{48, 49}. PAHs are found naturally and released into the environment by anthropogenic sources. The incomplete combustion of wood, coal, oil, gas, garbage, and other organic substances, pyrosynthesis or pyrolysis of hydrocarbons (petrogenesis), and the leakage of crude oil and refined petroleum products are considered the main sources of the PAHs^{47, 50, 51}. The surface runoff from roads is another major source of the PAHs in the aquatic system^{52, 53}. Surface-active compounds and humic substances increase the solubility of PAHs several times. Huang and Buekens⁵⁴ reported the formation of the PAHs under insufficient combustion conditions of the aliphatic fuels. Under these conditions, carbon containing-compounds are not oxidized completely to carbon dioxide, rather, hydrocarbon fragments that are generated during incomplete combustion interact with each other to yield complex polycyclic structures. Many other resources for the PAHs^{49, 53} are shown in Figure 2-1.

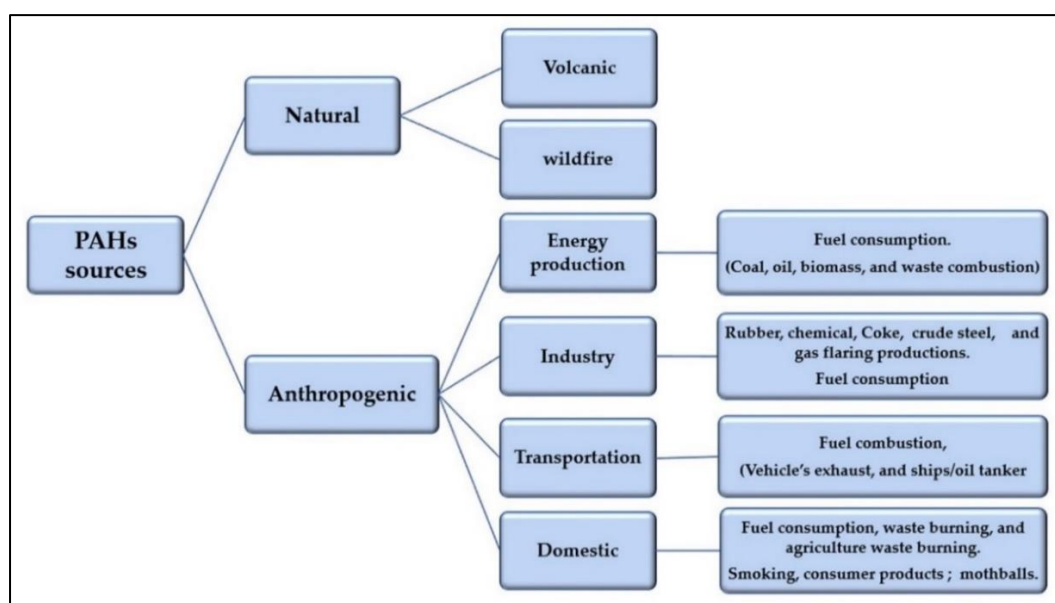
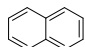
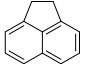
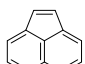
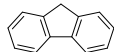
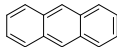
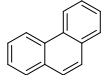
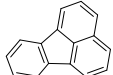
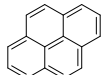
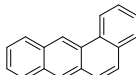
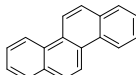
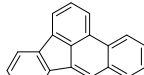
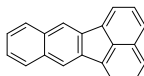
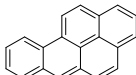
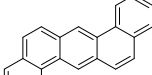
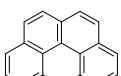
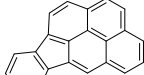


Figure 2-1: Different sources of PAHs generation.

PAHs have low aqueous solubility and are considered lipophilic organic compounds that are widely distributed in the environment and characterized by their high toxicity, genotoxicity, and carcinogenicity^{49, 55}. Table 2-1 shows the physicochemical properties of 16 compounds of the PAHs that have been listed as priority pollutants by the United States Environmental Protection Agency^{50, 56}.

Chapter Two: TiO₂ Photocatalysis for the Transformation of Aromatic Water Pollutants into Fuels

Table 2-1: Physiochemical properties of the 16 US-EPA PAHs^{53, 72, 73}.

Compound Name	Chemical structure	Chemical Formula	number of rings	Molecular Weight (g/mol)	Melting Point (°C)	Boiling Point (°C)	Aqueous solubility (mg/l)	Vapor pressure (Pa)	Log K _{ow}
Naphthalene		C ₁₀ H ₈	2	128.17	80.26	218	31	1.0x10 ²	3.37
Acenaphthene		C ₁₂ H ₁₀	3	154.21	93.4	279	3.8	3.0x10 ⁻¹	3.92
Acenaphthylene		C ₁₂ H ₈	3	152.19	92-93	265-275	16	9.0x10 ⁻¹	4.00
Fluorene		C ₁₃ H ₁₀	3	166.22	116-117	295	1.9	9.0x10 ⁻²	4.18
Anthracene		C ₁₄ H ₁₀	3	178.23	218	340-342	0.045	1.0x10 ⁻³	4.54
Phenanthrene		C ₁₄ H ₁₀	3	178.23	100	340	1.1	2.0x10 ⁻²	4.57
Fluoranthene		C ₁₆ H ₁₀	4	202.25	110.8	375	0.26	1.2x10 ⁻³	5.22
Pyrene		C ₁₆ H ₁₀	4	202.25	156	393-404	0.13	6.0x10 ⁻⁴	5.18
Benzo[a]anthracene		C ₂₀ H ₁₂	4	228.29	158	438	0.011	2.8x10 ⁻⁵	5.91
Chrysene		C ₁₈ H ₁₂	4	228.29	254	448	0.006	5.7x10 ⁻⁷	5.91
Benzo[b]fluoranthene		C ₂₀ H ₁₂	5	252.31	168.3	No data	0.0015	-	5.80
Benzo[k]fluoranthene		C ₂₀ H ₁₂	5	252.31	215.7	480	0.0008	5.2x10 ⁻⁸	6.00
Benzo[a]pyrene		C ₂₀ H ₁₂	5	252.31	179-179.3	495	0.0038	7.0x10 ⁻⁷	5.91
Dibenzo[a,h]anthracene		C ₂₂ H ₁₄	6	278.35	262	No data	0.0006	3.7x10 ⁻¹⁰	6.75
Benzo[ghi]perylene		C ₂₂ H ₁₂	6	276.33	273	550	0.00026	1.4x10 ⁻⁸	6.50
Indeno[1,2,3-cd]pyrene		C ₂₂ H ₁₂	6	276.33	163.6	530	0.00019	-	6.50

PAHs of two and three aromatic rings, e.g., naphthalene and anthracene, are known as low molecular weight (LMW). Those compounds possess higher solubility in water and higher volatility than that of the high molecular weight (HMW) PAHs⁵⁷. In fact, higher concentrations of the LMW PAHs have been reported in wastewater influent and effluent comparing to the HMW PAHs, which can be related to their higher water solubility^{35, 40, 58-61}.

Naphthalene (C₁₀H₈) is the simplest form of PAHs and possesses higher volatility besides its higher solubility in water (31.7 mg l⁻¹ at 25 °C) compared to other PAH compounds. Naphthalene is widely used in industry as an intermediate in the production of pesticides, phthalic anhydride, dyes, resins, and surfactants^{62, 63}. Moreover, it is found in many consumer products like mothballs and some insect repellent products that are used to kill moths in airtight spaces, and to repel vertebrate pests in attics and wall voids spaces⁶⁴. In general, naphthalene was found the most ubiquitous and abundant PAH in wastewater with concentrations ranged between ng L⁻¹ to µg L⁻¹^{47, 59-61, 65, 66}.

2.4.3 Organic Dyes

Dyes are colored substances that have an affinity for the substrate to which they are being applied. They have colors due to their absorption of light at a certain wavelength in the visible range. Due to their high molar extinction coefficients, a small amount of dye in an aqueous solution can produce a vivid color^{67, 68}. Synthetic dyes possess very different chemical and physical properties. Azo, anthraquinone, xanthene, indigoid, triphenylmethane, and phthalocyanine derivatives are the most frequent chemical classes of dyes employed in the industry (Chart 2-2)⁶⁷⁻⁷¹.

Synthetic organic dyes are introduced in the aquatic environment^{74, 75} because of their extensive usage in printing, paint, and textile industries. These compounds are characterized especially by their non-reactivity, long-lasting coloring, and highly stable structures⁷⁴. Besides their carcinogenic effect, many dyes affect human life such as dysfunction of the central nervous system (CNS), kidney, reproductive system, brain, and liver^{74, 76, 77}. Wastewaters from textile and other dyes industrial processes contain large quantities of these organic pollutants, which are difficult to degrade during the standard biological methods and resist aerobic degradation. Moreover, Due to their high solubility in water, the removal of the dyes from wastewater through conventional methods is very difficult and ineffective^{71, 78}. Degradation of certain types of dye produces more hazardous

pollutants than the dye itself. For example, under anaerobic conditions, organic dyes such as Azo-dye can be reduced to potentially carcinogenic aromatic amine^{68,79}.

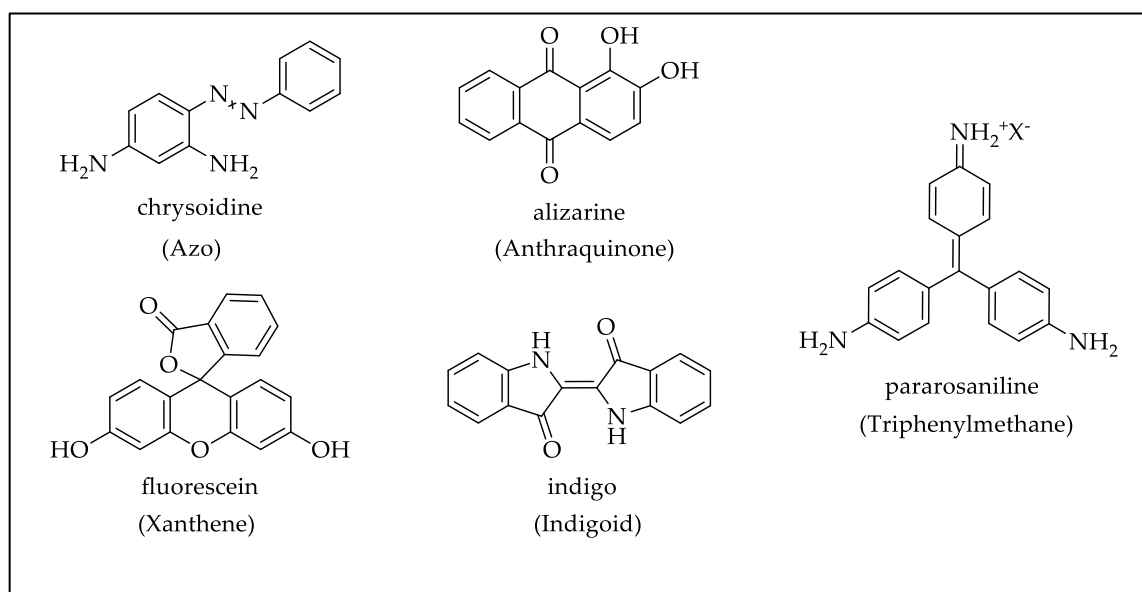


Chart 2-2: The chemical structure of some common synthetic dyes.

2.5 Methods of Treatment

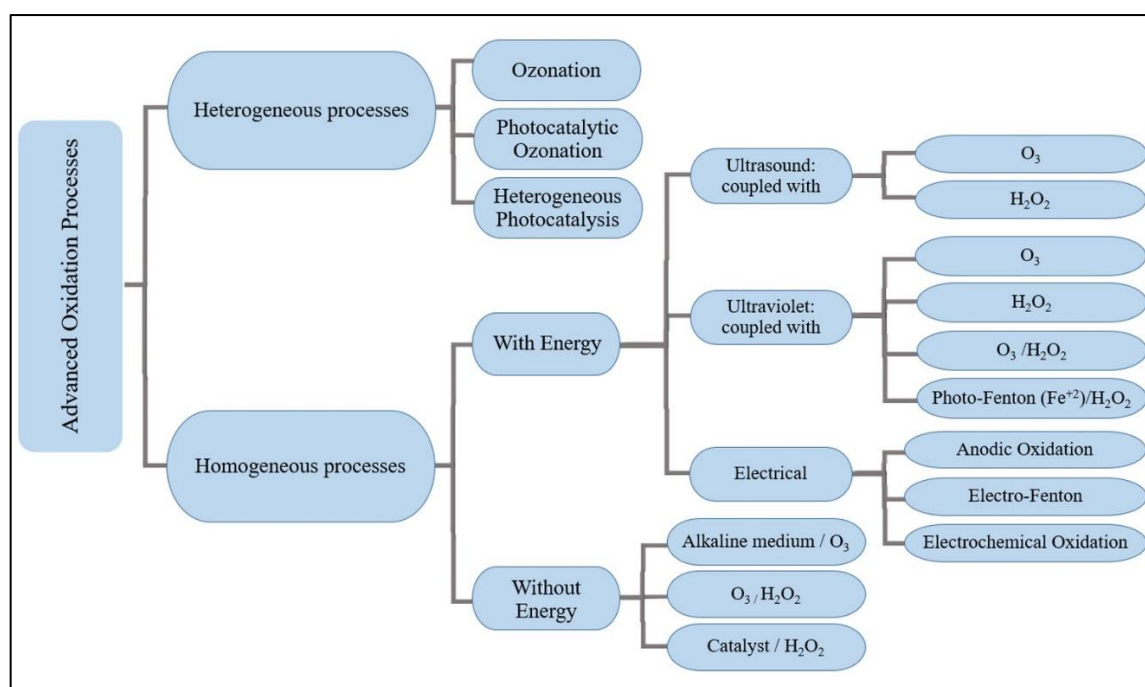
As outlined beforehand, toxic organic pollutants are widespread in the environment, thus, it is highly recommended to eliminate or reduce the concentration of such pollutants in the aquatic environment to safe levels^{53, 80-83}. Numerous conventional treatment processes have been applied and tested for wastewater treatment such as adsorption, coagulation, precipitation, biodegradation, ozonation, electrochemical oxidation, and advanced oxidation processes^{43, 47, 83-88}. Besides that, combining some of these processes, such as the biological-physical or chemical processes, has been successfully applied in many wastewater treatments plants⁸⁹⁻⁹². Although many of these processes have been considered effective and efficient for removing a wide spectrum of organic pollutants from the wastewater, however, each process has disadvantages that limit the large-scale application, e.g., small capacity, high costs, pH-dependency, limited recyclability, high-energy requirements, incomplete pollutant removal, and generation of toxic secondary materials (Table 2-2)^{87, 93-96}.

Table 2-2: Different removal techniques used for wastewater treatment and their advantage(s) and disadvantage(s).

Removal techniques	Advantage(s)	Disadvantage(s)
a) Coagulation	<ul style="list-style-type: none"> The additive coagulants easily settled with the suspended particle. Rapid and efficient for insoluble contaminants. Low-cost operation. 	<ul style="list-style-type: none"> pH monitoring of the effluent. The dissolved organic pollutants are not completely removed. Formation of sludge and secondary pollutants.
b) Electrochemical oxidation	<ul style="list-style-type: none"> Recycling of valuable metals. Increases biodegradability. Not require auxiliary chemicals or high temperatures. 	<ul style="list-style-type: none"> Required pre-filtration; formation of sludge. High initial cost of the equipment. Low selectivity and low reaction rates.
c) Biological process	<ul style="list-style-type: none"> Simple, economically attractive. Ecologically favorable process. 	<ul style="list-style-type: none"> Poor decolorization. Formed uncontrolled degradation products. High capital and operational cost. the secondary sludge problems.
d) Adsorption	<ul style="list-style-type: none"> Cost-effective and simple method. The most profitable process and more efficient than the conventional methods (i.e., precipitation, solvent extraction, membrane filtration, etc.). 	<ul style="list-style-type: none"> Removes the pollutants from one phase (aqueous) to another (solid matrix). Expensive regeneration process especially if the pollutants are strongly bound to the adsorbents.
e) Chemical precipitation	<ul style="list-style-type: none"> Adapted to high pollutant loads. Simple equipment and processes. 	<ul style="list-style-type: none"> Chemical consumption. High sludge production.
f) Advanced oxidation processes (AOP)		
I. Ozonation	<ul style="list-style-type: none"> Powerful oxidation technique for a large number of pollutants. 	<ul style="list-style-type: none"> Complex technology. High capital/operational cost. High electric consumption.
II. UV	<ul style="list-style-type: none"> An effective method that typically does not produce harmful by-products. 	<ul style="list-style-type: none"> low efficiency when the wastewater contains a high number of particulates that absorb UV light.
III. UV/H ₂ O ₂	<ul style="list-style-type: none"> An effective technique in the oxidation and mineralization of most organic pollutants. Ease formation of •OH radicals. 	<ul style="list-style-type: none"> Less effective, when the wastewater has high absorbance. High operational cost.
V. O ₃ /UV/H ₂ O ₂	<ul style="list-style-type: none"> Most effective process due to the fast generation of •OH radicals. Can treat a wide variety of contaminants. 	<ul style="list-style-type: none"> Needs to compete with high turbidity, solid particles, and heavy metal ions in the aqueous stream. High operational cost.
V. Fenton reaction	<ul style="list-style-type: none"> Simple process. Easy availability of chemicals. 	<ul style="list-style-type: none"> Production of iron sludge waste, bringing logistical problems with handling.
VI. Photo-Fenton reaction	<ul style="list-style-type: none"> Reduction of sludge iron waste compared to the original Fenton reaction. Effective and fast degradation. 	<ul style="list-style-type: none"> Requires a controlled pH medium for better performance.
II. Heterogeneous photocatalysis	<ul style="list-style-type: none"> Long-term stability at high temperature. Resistance to attrition. Low-cost and environmentally benign treatment technology. 	<ul style="list-style-type: none"> formation a harmful byproduct to the environment. Requires efficient catalysts that can absorb a wide range of light.

Among many developed and examined methods for eliminating the persistent organic pollutants from the environment (especially aquatic environment), advanced oxidation processes (AOPs) are the most promising techniques. They are also the most studied and the best environmental-friendly techniques for removing these pollutants. These processes are based on the formation of in-situ highly reductive or oxidative free radicals, e.g., hydroxyl radicals ($\bullet\text{OH}$), at sufficient concentration to effectively mineralize the hazardous organic compounds and decontaminate water under ambient conditions^{95,97}.

Several AOP techniques have been explored to decompose the organic pollutants in the water resources by chemical oxidation or reduction such as ozonation, H₂O₂ photolysis, Fenton process, photo-Fenton process, and heterogeneous photocatalysis⁹⁷⁻¹⁰⁰. Scheme 2-1 shows the types and the general classification of the AOP¹⁰⁰.



Scheme 2-1: General classification of the AOP. Adapted with permission from reference 100.

By far, heterogeneous photocatalysis has gained the most attention as one of the most realistic and viable solutions due to its ability to clean-up a wide range of environmental pollutants besides the use of low-cost and chemical stable photocatalysts¹⁰¹⁻¹⁰⁸. This promising approach relies on the excitation of a semiconductor with suitable light, e.g., the sunlight, to drive different redox reactions. Heterogeneous photocatalysis is a process that includes a large variety of reactions such as oxidation, dehydrogenation, water splitting (reduction, H₂ production; oxidation, O₂ production), organic synthesis, photoreduction, metal deposition, hydrogen production, gaseous pollutant removal, and water purification¹⁰⁹.

Photocatalysis is a sustainable and economical technology that can exploit the inexhaustibly abundant clean energy of the sun^{104, 109, 110}. The use of an efficient nanoparticulate semiconductor is required for the detoxification of the wastewater via photocatalysis, which has the potential to degrade the toxic substances in the water like contaminants and microorganisms¹¹¹⁻¹¹³. Due to their narrow bandgap and distinct electronic structure (unoccupied conduction band and occupied valence band)^{20, 114, 115}, various kinds of photocatalysts, including TiO₂, Gr-TiO₂, CdS, SnO₂, WO₃, SiO₂, ZnO, Nb₂O₃, Fe₂O₃, have been studied to degrade a variety of organic and inorganic pollutants^{102, 115-117}.

Nowadays, the photooxidation of organic pollutants based on TiO₂ nanomaterials is still gain huge attention. Several recent studies have shown the effective role of TiO₂ in oxidizing and mineralizing a wide range of hazardous organic contaminants^{118, 119}, such as alcohol^{120, 121}, organic acids¹²², aromatic hydrocarbons¹⁰⁴, phenols¹²³, dyes¹²⁴, pharmaceuticals^{125, 126}, and pesticides¹²⁶. The photocatalytic oxidation of organic pollutants proceeds either by the direct attack of the photogenerated holes or via the attack of the highly reactive hydroxyl radicals generated at the surface of the photocatalyst¹¹⁰. The photocatalytically generated •OH radicals can abstract hydrogen atoms from the organic molecules, causing a chain of reactions toward lower molecular intermediates and may end up in the complete mineralization of the pollutants¹²⁷.

Another major field in photocatalysis includes light-driven water splitting into H₂ and O₂¹²⁸. H₂ is regarded as the most recommended replacement for fossil fuels since its energy cycle is free of pollutants and greenhouse gases^{105, 129, 130}. Achieving dual-functional photocatalysis, i.e., the photocatalytic degradation of organic pollutants and the simultaneous production of hydrogen gas is an added value of this technique¹³¹. Unfortunately, as will be discussed in the following sections, different operational conditions should be applied for each process to achieve its optimal reaction yield¹¹.

2.6 Semiconductor-Based Heterogeneous Photocatalysis

A photocatalytic system is thermodynamically defined as a system, in which a reaction with $\Delta G < 0$ is driven through the photon absorption by a suitable material, i.e., the light energy is exploited to drive a reaction having extremely low kinetics outside this system¹³². The photons are absorbed by such a system to generate accordingly charge carriers, i.e., electrons and holes, which induce a redox reaction. The semiconductors could be the light-absorbing materials in heterogeneous systems and they are then known as photocatalysts¹³³.

Thus, heterogeneous photocatalysis depends on the distinctive properties of powdered semiconductor materials in harvesting incident light, generating charge carriers, and subsequently initiating surface reactions. This may provide a simple means for environmental remediation and photochemical energy conversion into fuels^{134, 135}.

2.6.1 The Electronic Structure of a Semiconductor-Photocatalyst

The band model based on the concept of molecular orbitals can be used to explain the electronic structure of a semiconductor. The electronic orbitals merge and split into two bands, i.e., the valence band (VB) and the conduction band (CB). VB and CB of a semiconductor are formed from the highest occupied molecular orbitals (HOMO) and the lowest unoccupied molecular orbitals (LUMO), respectively¹³⁶. At 0 K, the VB is the lower band that is completely filled with electrons, while the CB is the higher band that is empty¹³⁷. The difference in energy between the highest energy level in the VB and the lowest energy level in the CB creates a region known as the energy bandgap (E_g)¹³⁸. The interaction between the electronic orbitals, forming the band structure of a semiconductor is shown in Figure 2-2.

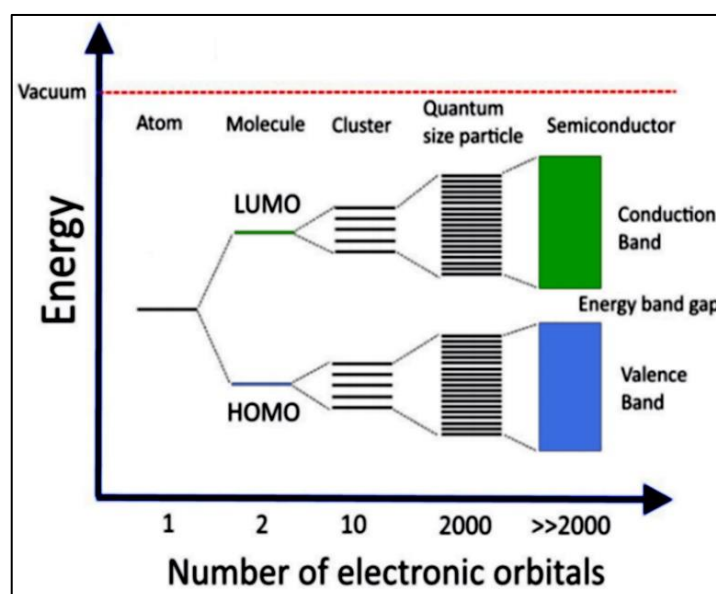


Figure 2-2: Band structure of a semiconductor as an interaction of atomic orbitals, adapted from reference 144. Copyright 1997 Elsevier B.V.

Interestingly, the E_g values for semiconductors are sufficiently small that the electrons promotion from the VB to the CB can be initiated through an energy transfer to those materials¹³². The light energy that is higher or equal to E_g induces the excitation of electrons from the VB to occupy partially filled states in the CB generating an electron vacancy in the VB, which is known as the positively charged hole¹³⁹. This hole is

considered as a mobile entity since it can be filled by another electron creating a vacancy in the space where it has been transferred from¹⁴⁰. The electrons in the CB are, likewise, mobile entities having often higher mobility than those of the holes (e.g., for Si, $\mu_{n(\text{electrons})} = 1500 \text{ cm}^2 \text{ V}^{-1} \text{ s}^{-1} > \mu_{p(\text{holes})} = 450 \text{ cm}^2 \text{ V}^{-1} \text{ s}^{-1}$ ¹⁴¹). Electrons have consequently a higher diffusion coefficient than holes, however, the trapping of the electrons leads to a decrease in their mobilities¹⁴². The e^-/h^+ species migrate then to the surface of the semiconductor, where they can react with the adsorbed molecules. The photogenerated holes act as oxidants (+1.0 to +3.5 V vs. NHE), while the photogenerated electrons are potential reductants (+0.5 to -1.5 V vs. NHE)¹⁴³.

Semiconductor photocatalysis is considered, from this point of view, as a multi-step process, which is illustrated in Figure 2-3. Such a process is initiated by the photoexcitation with electromagnetic radiation equal to or exceeding E_g (1), the separation of the charge carrier pairs (2), the diffusion of e^-/h^+ species within the material towards the surface, and the surface charge transfer for the reduction of adsorbed electron acceptors (3) and the oxidation of adsorbed electron donors (4), respectively^{145, 146}. Accordingly, the photo-induced electrons and holes should migrate to reach the surface of the material and react with adsorbed chemical species via surface charge transfer¹⁴⁴. Therefore, the E_g of a semiconductor is the minimum thermodynamic requirement for photocatalysis¹⁴⁷.

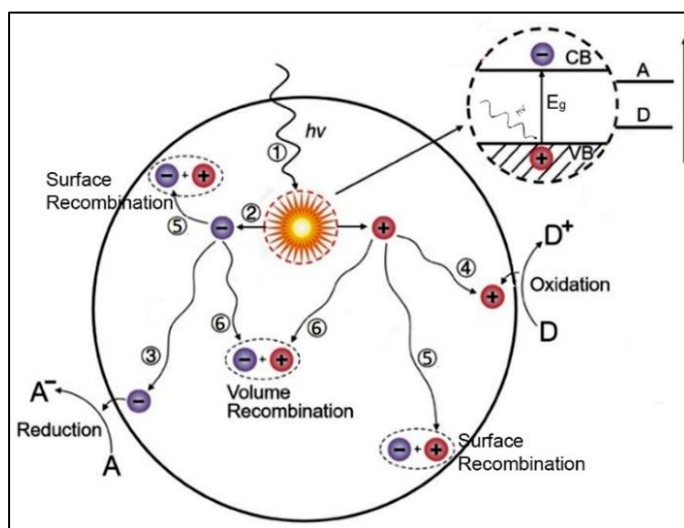


Figure 2-3: Pathways of the photogenerated charge carriers in a semiconductor photocatalyst. Adapted with permission from reference 149. Copyright 2013 John Wiley and Sons.

One of the other main limitations of semiconductor photocatalysis is the recombination of the photogenerated charge carriers, dissipating the absorbed energy as heat¹³⁸ and affecting negatively the lifetime of the electrons and holes¹⁴⁴. This undesired recombination

occurred either indirectly, i.e., via surface defects (5), or directly, i.e., by band-to-band recombination (6). Such phenomena are highly reliant on the crystal structure of the semiconductor. To enhance effectively the redox reactions while minimizing recombination, the photogenerated charge carriers must migrate to the liquid junction through the solid and must react with adsorbed species directly at the semiconductor surface ¹⁴⁸.

2.6.2 Photocatalytic Water-Splitting vs. Photocatalytic Reforming

Photocatalytic H₂ production from water-splitting is accomplished under ambient operating conditions and consists of two half-reactions as shown in Equations 2-1 and 2-2, i.e., the reduction of proton and the 4-electron oxidation of water, respectively ¹⁵⁰. A change in free energy of $\Delta G^0 = 237.2 \text{ kJ mol}^{-1}$ is associated with the splitting of one H₂O molecule to H₂ and ½ O₂, which equals to $\Delta E^0 = 1.23 \text{ V}$ according to the Nernst equation ¹⁵¹. Thus, the semiconductor should absorb photon energy of more than 1.23 eV (wavelengths shorter than 1000 nm) to drive the water-splitting photoreaction. The semiconductor can use their photogenerated electrons/holes to convert the photon energy into H₂ and O₂ when the energy of the conduction band-edge and the valance band-edge straddle the electrochemical potentials $E^0(\text{H}^+/\text{H}_2)$ and $E^0(\text{O}_2/\text{H}_2\text{O})$, respectively ¹⁵⁰ (Figure 2-4).

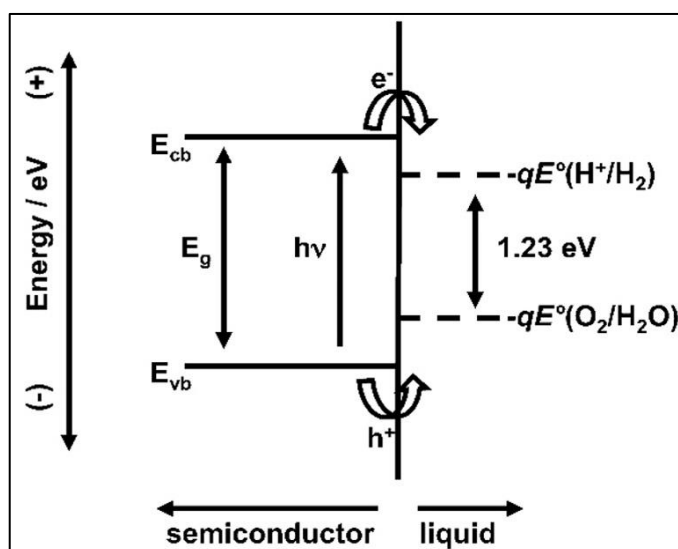


Figure 2-4: Photocatalytic water-splitting at the surface of an irradiated semiconductor, reprinted from reference 159. Copyright 2010 American Chemical Society.

Accordingly, the thermodynamic requirement for the water-splitting is more cathodic and more anodic energy levels of the CB bottom and VB top of a photocatalyst compared to the standard electrode potential of (H⁺/H₂) and (O₂/H₂O), respectively ^{152, 153}. Therefore, from a thermodynamic point of view, only a few photocatalysts, e.g., TiO₂, are proficient to drive the water-splitting reaction. However, the efficiencies of heterogeneous photocatalytic water-splitting remain relatively low due to many reasons outlined in the next sections.

As a hybrid field, dual-functional photocatalysis is a combination of different photocatalytic fields for 2-fold purposes achieved in a single step ¹³⁰. The coupling of H₂ evolution and photocatalytic degradation of organic pollutants yielding CO₂ can be achieved in the so-called photoreforming process ^{38, 132, 153-156}. Such a technique has a great advantage as it can benefit from solar light and treat wastewater, meanwhile, the evolved CO₂ can be consumed by natural photosynthesis ¹⁵⁷. In the photocatalytic reforming process, the photogenerated holes in the valence band can oxidize adsorbed organic substrates (electron donors or sacrificial reagents), whereas the photogenerated electrons in the conduction band can reduce the protons (electron acceptor) to H₂ ^{104, 105, 130, 158}. Such an adsorbed organic substrate can react irreversibly with the photogenerated holes, minimizing the undesired electron/hole recombination ¹⁵⁰.

Despite the fact that H₂ can be formed simultaneously with other processes, e.g., the organic synthesis of organic compounds ^{160, 161}, however, such processes should not be considered as a dual function process ¹³⁰. The reforming process can be considered as a dual function photocatalysis process only when some requirements have been met: (i) H₂ is mainly derived from the reduction of water and (ii) target organic molecules are pollutants or they are oxidized to synthesize other value-added products like aldehyde, organic acid, and imine ^{130, 162}. Consequently, photocatalytic reforming is an intermediate process between photocatalytic water-splitting and the photocatalytic oxidation of organic pollutants as shown in Figure 2-5.

Organic substrates are generally stronger reducing agents than water, hence, a less positive potential is necessary to oxidize these compounds. Accordingly, the energetic separation of the redox half-reactions in photoreforming is narrower compared to that of the overall water splitting ¹⁶³. As O₂ is not produced in these systems, the back reaction to produce water is suppressed, avoiding a subsequent gas separation stage ¹⁶⁴. A wide range of organic

compounds such as alcohols, organic acids, and hydrocarbons had proven activity as electron donors for photocatalytic H₂ production^{101, 104, 105, 131, 150, 165-167}. The evolution of H₂ and its kinetic reactions pathway is dependent on the concentration and the nature of the organic substrate^{168, 169}.

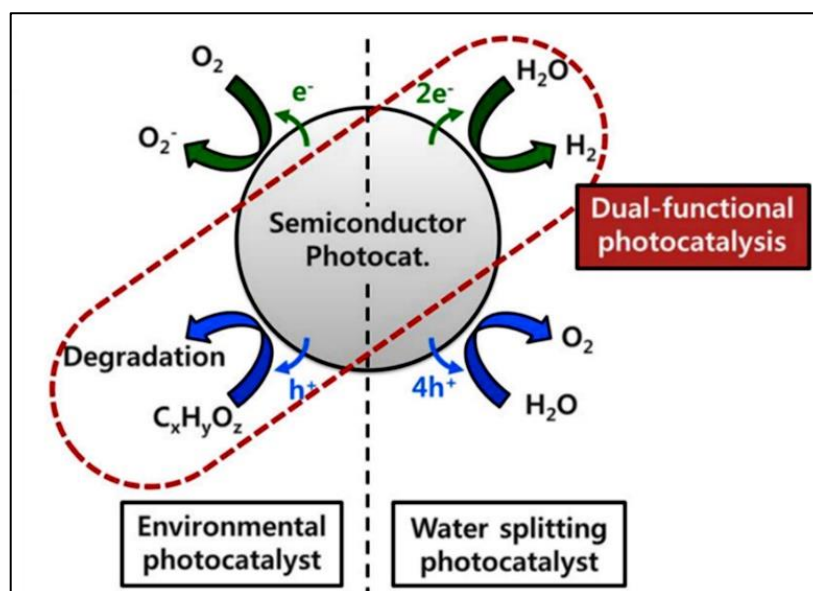


Figure 2-5: Dual-function photocatalysis process. Reprinted with permission from reference 158. Copyright 2018 American Chemical Society.

2.6.3 Titanium dioxide (TiO₂) as a photocatalyst

Titanium dioxide has been one of the most widely studied semiconductors in the last decade for various photocatalytic applications¹⁷⁰. This is related to its high reactivity, hydrophilicity, low cost and availability, physical and chemical stability, resistance to photocorrosion, and optimal electronic and optical capacity^{97, 111, 139}. TiO₂ is a transition-metal oxide semiconductor composed of Ti⁴⁺ atoms and six O²⁻ coordinated together to form a TiO₆ octahedron¹⁷¹. Like other transition metal oxides, TiO₂ is often nonstoichiometric with oxygen vacancies (O_v) as predominant defects at the near-atmospheric oxygen pressure, granting it the properties of an intrinsic n-type semiconductor¹⁷². The oxygen vacancies (O_v) at the surface of n-type TiO₂ appear as extra unpaired electrons in the CB^{164, 173}, which act as donor-like states. This creates an accumulation layer in the surface, resulting in a downward band bending¹⁷⁴.

The photocatalytic activity of TiO₂ is highly related to its charge carrier dynamics. The electron/hole pairs are generated within a few femtoseconds upon irradiation and they can recombine easily either in the bulk or at the surface. However, other charge carriers escape recombination and migrate to the surface, where they might be trapped before the interfacial

charge transfer in redox reactions¹⁷⁵. Figure 2-6 (a) and Equations (2-3) to (2-6) demonstrate the potential fates of charge carriers upon the irradiation of TiO₂, while Figure 2-6 (b) reports the time scale of each process^{143, 176}.

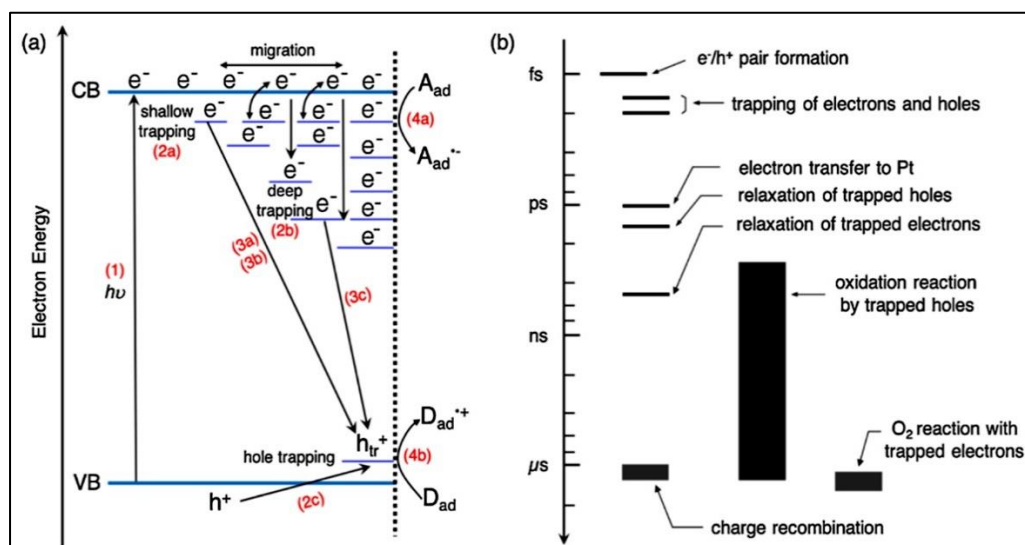


Figure 2-6: The possible charge carrier pathways on irradiated TiO₂. Reprinted with permission from reference 175. Copyright 2019 Elsevier B.V.

Serpone et al. found that in the absence of scavengers, more than 90% of the initially formed charge carriers recombine rapidly within 10 ns upon the irradiation of TiO₂ in aqueous media. Such high recombination results in less than 10% quantum yields of photooxidation¹⁷⁷.

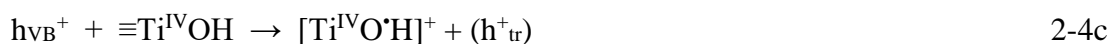
On the other hand, the photogenerated charge carriers can be trapped either in the bulk or at the surface as trapped holes and trapped electrons, with the surface trapping being preferred for the subsequent interfacial charge transfer reactions¹⁷⁸. Yoshihara et al. showed in their Transient Absorption Spectroscopy study that both trapped holes and electrons are found to be localized at the surface of photoexcited TiO₂ particles, while free electrons are distributed in the bulk¹⁷⁹. Howe and Gratzel demonstrated in their EPR studies on irradiated TiO₂ that the photogenerated electrons are localized in the d orbitals of Ti⁴⁺ while the photogenerated holes are trapped at the lattice oxygen atoms, forming EPR-active paramagnetic centers, i.e., Ti³⁺ and O^{•-}, respectively^{180, 181}. Simultaneously, upon the generation, separation, and transport of charge carriers in TiO₂, e^-/h^+ pairs might participate in redox reactions *via* interfacial charge carrier transfer. In aqueous media, water layers adsorb, physically and chemically, on the TiO₂ surface creating a TiO₂/H₂O interface¹⁸². The photogenerated holes can react on the surface either with hydroxyl groups or with H₂O resulting in the formation of hydroxyl radicals, $\bullet OH$. Therefore, not only h^+ is

produced by the photoexcitation of TiO₂ but also hydroxyl radicals can be formed on hydrated TiO₂ surfaces.

Photogeneration of the charge carriers:



Trapping of the charge carriers:



Recombination of the charge carriers:



Interfacial charge transfer to the acceptor (A) or donor (D) adsorbed on the surface:



TiO₂ has three main crystal phases: anatase, rutile, and brookite. While anatase and rutile exhibit the same tetragonal crystal structures, brookite has an orthorhombic crystal structure. These three polymorphs have also different E_g values, i.e., 3.2 eV, 3.0 eV, and 3.3 eV for anatase, rutile, and brookite, respectively³⁰. Anatase has been generally considered as the most active phase of the three TiO₂ polymorphs for photocatalytic applications^{183, 184}.

Anatase and rutile TiO₂ have shown differences in their respective charge carrier recombination kinetics^{185, 186}. Using transient absorption spectroscopy, Sachs et al.¹⁸⁵ compare the ultrafast charge carrier kinetics for anatase and rutile in dense and nanostructured TiO₂ films. They found that bulk rather than surface recombination was the key determinant of charge carrier lifetime. They also monitored that recombination was dependent on the crystal phase. Rutile shows faster recombination than anatase, which is consistent with the doping density (n-type doping due to oxygen vacancies) in rutile being higher than in anatase. Besides, Wang et al.¹⁸⁷ investigated anatase and rutile TiO₂ with photoluminescence spectroscopy under weak excitation conditions. Anatase showed a

visible emission, while a NIR emission was reported in rutile, however, both emission spectra exhibited long lifetimes up to milliseconds. They explained that the NIR luminescence band in rutile TiO₂ was due to the recombination of trapped electrons with free holes. Hence, trap states in TiO₂ may play a very important role in the photocatalysis processes. The depth of trap states in rutile TiO₂ is much deeper than that in anatase TiO₂, which has shallowed-trapped electrons in addition to a higher number of free electrons as shown in Figure 2-7 (a and b). On the other hand, Durrant et al.¹⁸⁸ employed transient absorption spectroscopy (TAS) to investigate the kinetic of photocatalysis in anatase and rutile TiO₂ films. Although rutile exhibited 10 times slower recombination kinetics than anatase, mesoporous anatase film was around 30 times more efficient than mesoporous rutile film in the photocatalysis of the “intelligent ink” model system. They found also that in the presence of alcohols, faster and irreversible hole scavenging was achieved on anatase than in the case of rutile, resulting in the creation of long-lived electrons ($\tau \approx 0.7$ s). The authors explained the lower activity of rutile to the deficiency of rutile holes to drive efficient and irreversible alcohol oxidation rather than to the differences in recombination kinetics.

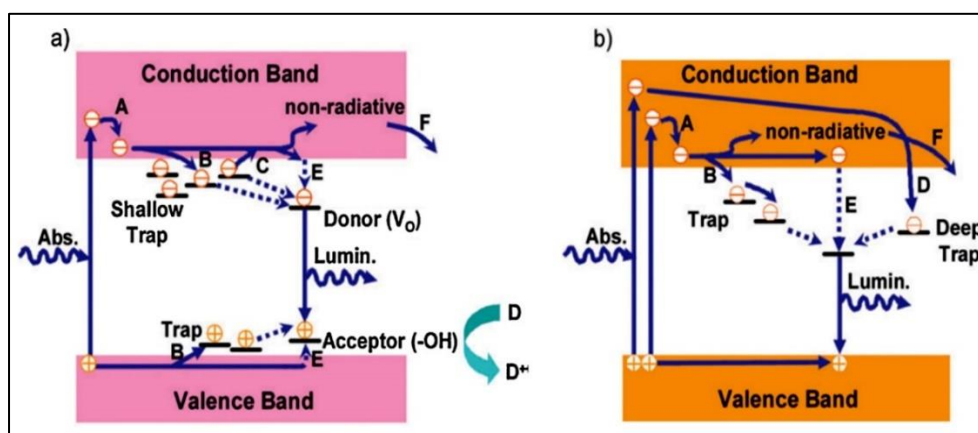


Figure 2-7: Tapping and recombination of photogenerated charge carriers in anatase (a) and rutile (b), reprinted with permission from reference 175. Copyright 2019 Elsevier B.V.

Choi et al.¹⁸⁹ compared the recombination kinetics in anatase and rutile using time-resolved diffuse reflectance (TDR) spectroscopy. They demonstrated that during the 355 nm laser excitation, the time-resolved decay at 550 nm was slower in anatase than rutile as shown in Figure 2-8 (a). This results in a longer lifetime of photogenerated charge carriers with subsequent higher ROS generation in anatase. The authors observed also the generation and the diffusion of $\bullet\text{OH}$ from the illuminated TiO₂ surface to the solution bulk using a single-molecule detection method. They found that only anatase generates mobile $\bullet\text{OH}$

radicals, therefore, the photocatalytic oxidation on rutile is limited to adsorbed species. Schindler and Kunst¹⁹⁰ studied the excess charge carrier kinetics in anatase and rutile TiO₂ powders using the time-resolved microwave conductivity (TRMC) method. Figure 2-8 (b) shows the transient change of the reflected microwave power after excitation by a 20-ns laser pulse at 266 nm. The photoconductivity in anatase decays very slowly compared to rutile powder. They demonstrated that this signal can be attributed to excess electrons in the CB because of the n-doping characteristics and the larger electron mobility compared to the hole mobility. Therefore, the short electron lifetime in rutile could be due to a higher recombination rate, while in anatase fast trapping of the minority charge carriers (holes) may take place. This would decrease the availability of holes for recombination and reduce the recombination probability, leading to a longer lifetime in anatase.

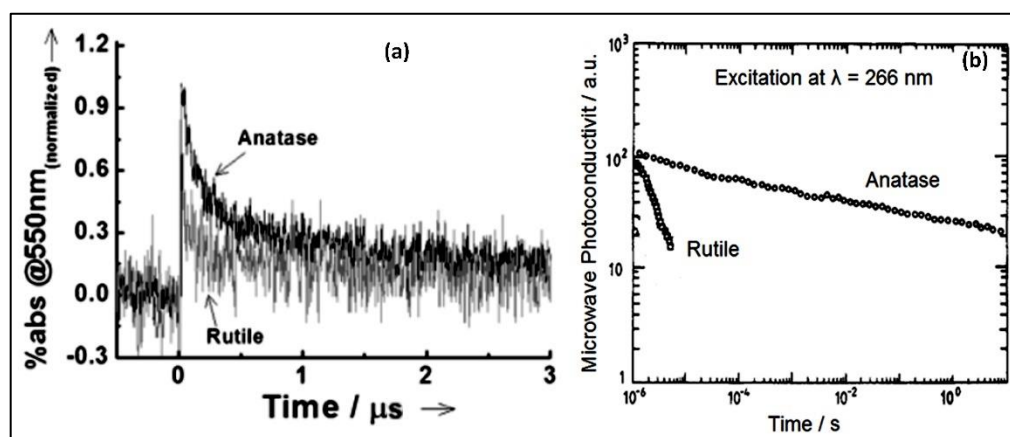


Figure 2-8: (a) Time-resolved diffuse reflectance spectroscopy measurements with normalized absorbance at 550 nm during the 355 nm laser excitation ($1.5 \text{ mJ pulse}^{-1}$) of aqueous suspensions of anatase and rutile TiO₂ in water. Adapted with permission from reference 189. Copyright 2013 John Wiley and Sons. (b) Photoconductivity of TiO₂ powders after a laser flash excitation at 266 nm with energies of 0.5 and 1 mJ cm^{-2} for anatase and rutile, respectively. Adapted with permission from reference 190. Copyright 1990 American Chemical Society.

The development of TiO₂ materials has led to mixed-phase titania photocatalysts. One example is P25-TiO₂, which is a mixture of anatase and rutile (75:25). Due to its higher activity, anatase is conventionally considered to be the active component in P25, with rutile serving as an electron sink. Some reports showed that such mixed-phase titania has slower rates of charge carrier recombination, higher photo-efficiencies, and lower energy light activation¹⁹¹. Knorr et al.¹⁸⁶ studied the room-temperature photoluminescence spectra of nanocrystalline TiO₂ in the anatase and rutile phases and mixed-phase films. They showed that the photoluminescence of anatase results from at least two spatially isolated trap-state distributions, i.e., trapped electrons and trapped holes, which are, respectively, about 0.7–1.6 eV and 1.8–2.5 eV below the conduction band edge. The signal of trapped electrons

was largely quenched in P25 and the presence of hole scavengers. The authors, hence, concluded a bidirectional electron transport between anatase and rutile phases in P25, with solvents having a strong impact on the competition for electrons between the two phases.

Additional recombination or trapping in the rutile part decreases the lifetime of electrons compared to pure anatase, but it would be much longer than in pure rutile due to the deep trapping of the holes in the anatase part. On the other hand, Hurum et al.¹⁹¹ studied the charge separation characteristics of P25 by EPR spectroscopy. They showed, as presented in Figure 2-9, that the visible light irradiation of rutile produced charge carriers, which are stabilized through electron transfer to lower energetic trapping sites in the lattice of anatase. The authors suggested that the morphology of nanoclusters P25 consists of small rutile crystallites interwoven with anatase crystallites. The transition points between these two phases permit a rapid electron transfer from rutile to anatase. Hence, rutile in P25 acts as an antenna to extend the photoactivity into visible wavelengths and the structural arrangement creates catalytic “hot spots” at the rutile–anatase interface.

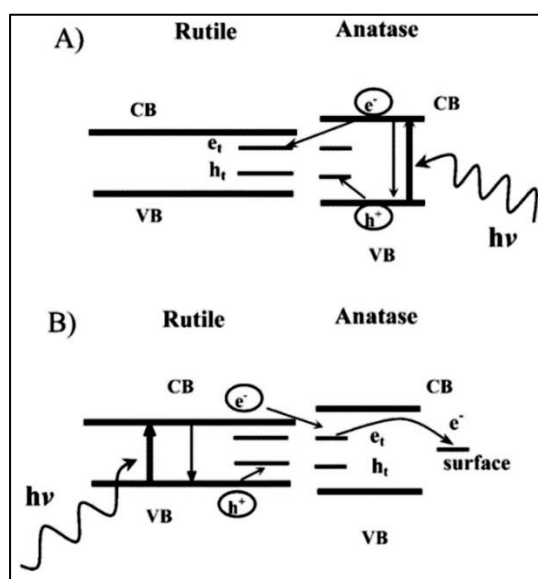


Figure 2-9: (a) Conventional model of P25 activity where charge separation occurs on anatase while rutile acts as electrons sink. (b) Proposed model of a rutile antenna and subsequent charge separation. Adapted with permission from reference 191. Copyright 1990 American Chemical Society.

Using the time-resolved microwave conductivity (TRMC) method, Schindler and Kunst¹⁹⁰ found that the transient photoconductivity in P25 was rather more like the decay behavior observed in anatase than that in rutile shown in Figure 2-8 (b). They expected that in the mixed powder, fast recombination like in rutile for the electron-hole pairs created in the

rutile part. Nevertheless, the deep trapping of holes in the anatase part would prevent the transfer of holes to the rutile part for the electron-hole pairs created in the anatase part.

2.6.4 Enhancing the Performance of Pristine TiO₂

As discussed above, although pristine TiO₂ exhibits advantages, some limitations are also presented. The main drawbacks to using pristine TiO₂ as an active photocatalyst are the lack of visible light activation, the fast recombination of the photogenerated electrons and holes, the relatively low charge carrier mobility.

Various attempts have been made to improve the capability to exploit visible photons for the TiO₂ photocatalytic process. Doping with transition metal ions is one approach that has been extensively employed, especially the incorporation of Fe³⁺ into the TiO₂ matrix¹⁶⁴. This has been proven as a promising method to create additional states in the bandgap and, consequently, to an increase in the absorption of the visible light¹⁰². It can introduce also electron capture centers, resulting in a decrease in electron/hole recombination centers¹⁶⁴. Compared to pristine TiO₂, Fe-doped TiO₂ has enhanced light-harvesting; however, controversial results on its photocatalytic activity have been reported¹⁰². Choi et al.¹⁹² studied the photocatalytic oxidation of chloroform using TiO₂ doped with 21 transition metal ions and discovered that the doping with Fe³⁺, Mo⁵⁺, Ru³⁺, Os³⁺, Re⁵⁺, V⁴⁺, and Rn³⁺ cations is beneficial. Moreover, nonmetal doping has been widely studied, especially with N, C, F, B, and other elements having an atomic radius similar to that of the O atom. Among them, nitrogen has attracted much attention. Asahi et al.¹⁹³, for example, showed that nitrogen-doped TiO₂ exhibits enhanced visible light absorption and photocatalytic activity. Other strategies are the use of noble metals (e.g., Pt, Au, Pd, Rh, Ni, Cu, and Ag) as a cocatalyst to decrease the recombination of the charge carriers and provide additional active sites for H₂ evolution¹⁰². We will focus in the next sections on the modification of pristine TiO₂ with noble-metal co-catalysts, particularly platinum nanoparticles, due to their higher catalytic performance driving the reduction reaction of protons¹⁰⁴, hence, increasing the photocatalytic reforming of organic compounds.

The energy of the photogenerated electrons in the conduction band for both rutile ($E_{CB} = -0.11$ V at pH 0) and anatase ($E_{CB} = -0.32$ V at pH 0)¹⁴⁵ is sufficient to form H₂ by reducing water. However, pristine TiO₂ has been reported as an inactive photocatalyst for H₂ production because of the fast recombination of charge carriers and the inability to reduce protons to H₂ due to the higher overpotential for hydrogen evolution reaction (0.05

V) ¹⁹⁴. Hence, even in the presence of an electron donor, pristine TiO₂ has shown an inability to catalyze the hydrogen evolution reaction ¹³¹. TAS data revealed that the generated electrons are trapped as blue Ti³⁺ ions instead of reducing H⁺ upon the consumption of holes by the electron donor ^{105,195}. Consequently, it is highly recommended to modify pristine TiO₂ with an appropriate co-catalyst, which can effectively catalyze the cathodic H₂ evolution reaction. One successful strategy is the surface modification with noble metal nanoparticles, e.g., Pt and Au NPs. Noble-metal-modified TiO₂ photocatalysts have been widely studied in the literature, in which the noble-metal NPs act as Hydrogen Evolution Reaction (HER) catalysts.

HER on metallic platinum, as an example, induces via the Volmer reaction, in which H^{*}_{ads} atoms are produced when the accumulated electrons in Pt transfer to the proton adsorbed H⁺_{ads} and H₂O_{ads}, respectively, as described in Equations. (2-7a) and (2-7b) ¹⁹⁶. The reaction proceeds afterward through two possible pathways, either the Heyrovsky reaction (Equation 2-7c) or the Tafel reaction (Equation 2-7d), in which H^{*}_{ads} react with H⁺_{ads} or/and the direct recombination of two H^{*}_{ads} with each other, respectively ¹⁵⁵. Figure 2-10 illustrates the two-electron transfer reaction that occurs on the metal surface in acidic solutions. HER on Pt has been shown to exhibit pseudo-first-order kinetics, which indicates that the rate-determining step of the HER is the Volmer reaction ¹⁹⁷. Rabani et al. ¹⁹⁷ have presented a linear increase in e⁻_{TiO2} decay rate while increasing H⁺ concentration at a given Pt concentration, suggesting that H₂ is most likely generated by reduction of H⁺ rather than the reduction of H₂O. They have also highlighted that the presence of Pt is vital for reactions 2-7a and 2-7b to occur.

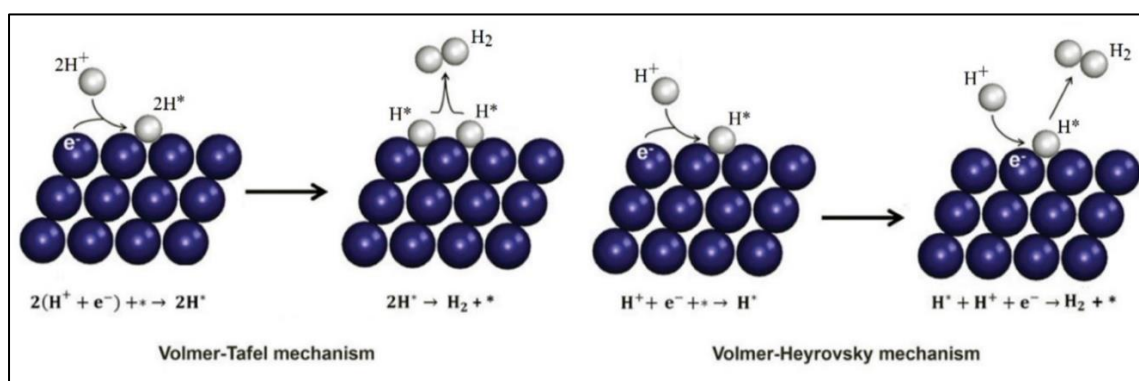
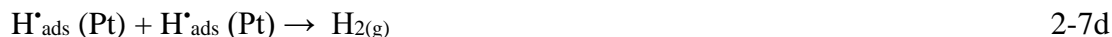
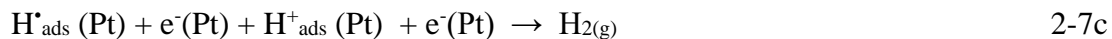


Figure 2-10: The possible mechanisms of HER on the catalyst surface in acidic solutions. The (*) refers to the active sites of the catalyst, H^{*} refers to the adsorbed H^{*} atom at the active site of the catalyst. Reprinted with permission from reference 198.



It has been widely accepted that enhancement of the activity through the modification of TiO₂ with noble-metal NPs is due to a better charge separation according to the Schottky barrier model. Noble-metal NPs have higher Fermi level energy, i.e., 5.65 eV and 5.10 eV for Pt and Au, respectively¹⁹⁹ compared to that of TiO₂, i.e., 4.2 eV²⁰⁰. Therefore, photogenerated electrons can transfer from TiO₂ to the metal NPs through the interface until a thermodynamic equilibrium is achieved¹¹⁰ as shown in Figure 2-11 (a-d).

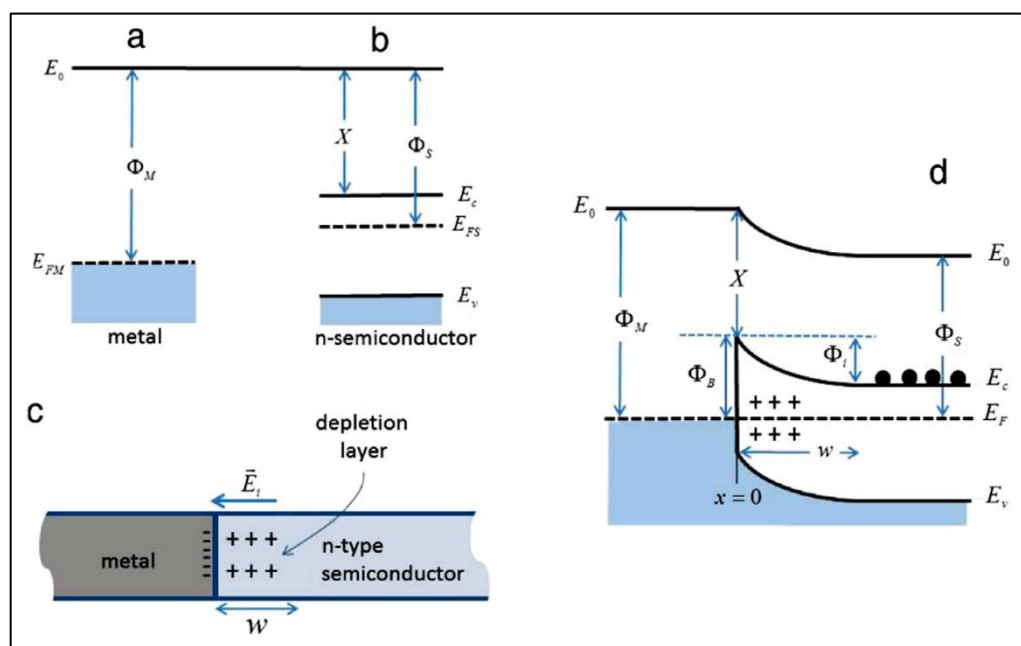


Figure 2-11: A Schottky barrier formed by a metal of higher work function contacting an n-type semiconductor. (a) Metal workfunction Φ_M and Fermi energy E_{FM} . (b) Semiconductor workfunction Φ_S , electron affinity X and band structure with a bandgap between E_c and E_v and Fermi energy E_{FS} . (c) Charge at the metal/semiconductor (M/S) junction. (d) Idealized equilibrium band diagram for the M/S junction. Φ_i is the energy barrier to the flow of electrons (black dots) from the semiconductor to the metal, while Φ_B is the Schottky barrier height for the electron flow in the opposite direction. w is the extension of the depletion layer. Reprinted with permission from reference 201. Copyright 2015 Elsevier B.V.

Schottky barrier Φ_B defines as the barrier against the flow of electrons from the metal to the n-type semiconductor, i.e., TiO₂²⁰¹. During the irradiation, this thermodynamic

equilibrium will be unsettled, permitting the photogenerated electrons to continuously flow from the CB of TiO₂ to the metal NPs^{110, 202}. It has been generally recognized that such a Schottky barrier smooths electron trapping by the metal, providing better charge separation. The trapped electrons have, therefore, a longer lifetime to promote the reduction reactions^{203, 204}. Correlations between photocatalytic H₂ evolution rates and metal work functions have been thoroughly established^{105, 205, 206}. However, EPR experiments for irradiated Pt/TiO₂ revealed simultaneously signals for the Ti³⁺ centers, which confirms that the photogenerated electrons are not transferred completely to the Pt NPs, rather a certain number of them are trapped as Ti³⁺ ions in TiO₂^{105, 110, 181}. Scavenging the photogenerated electrons from TiO₂ by the noble-metal NPs is essential but is not the only factor that enhances the HER. According to the Sabatier principle²⁰⁷, an ideal catalyst for (HER) is characterized by its optimal binding energy with adsorbed atomic hydrogen (H^{*}_{ads}). This binding energy should be neither too strong nor too weak. On the one hand, the active sites for the HER reaction can be blocked and the desorption of H₂ becomes rate-limiting in the case of a strong binding. On the other hand, proton reduction is rate-limiting in the case of weak binding energy with H^{*}_{ads}²⁰⁸. Consequently, a volcano-type dependence between HER rates and metal-H^{*}_{ads} bond strength has been proposed²⁰⁹, in which platinum provides the best activity to drive the HER as shown in Figure 2-12.

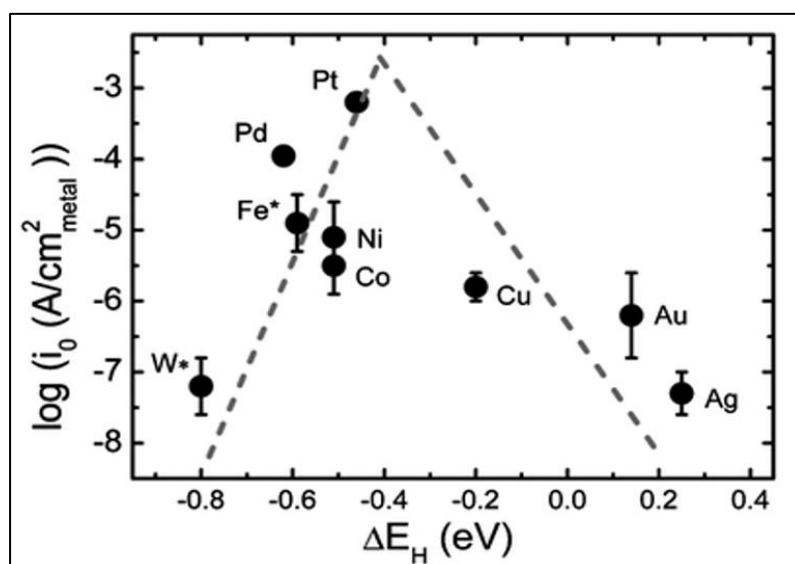


Figure 2-12: Exchange current densities, $\log(i_0)$, on monometallic surfaces plotted as a function of the calculated hydrogen binding energy. Reprinted with permission from reference 211. Copyright 2013 from the Royal Society of Chemistry.

In conclusion, Pt/TiO₂ has been demonstrated to exhibit the highest photocatalytic activity towards H₂ production compared to other metal-loaded TiO₂^{105, 155, 210}, such as Au/TiO₂.

This has been explained by the highest work function of Pt that enhances electrons “sinking” properties, the lowest overpotential for H₂ formation, and the optimal binding energy adsorbing atomic hydrogen.

2.6.5 Effect of the Loading Method on H₂ Production

As discussed in section 2.6.4, surface decoration of metal (e.g., Au, Ag, Cu, and especially Pt) on TiO₂ nanoparticles is an outstanding technique to revamp the electronic properties of TiO₂ without affecting its original crystallinity, thus, enhance the photocatalytic activity and enrich the H₂ production efficiency^{212, 213}. Different co-catalyst loading methods “techniques” have been successfully applied^{38, 214, 215}, however, the structure and the properties of the co-catalyst were found to play a critical role in achieving superior photocatalytic activity²¹⁶. It has been reported that many structural factors affect the activity of the platinized TiO₂, such as the size of Pt NPs^{213, 217, 218}, their dispersion of Pt NPs^{219, 220}, the interaction between the metal and the support²²¹⁻²²³, and the chemical state of Pt deposits^{220, 224}. Nevertheless, all these factors can be optimized by using proper preparation methods^{210, 214, 220, 225, 226}.

The most commonly adopted techniques for the loading of Pt nanoparticles on the surface of TiO₂ include photodeposition^{104, 105, 131, 167, 210, 227}, deposition-precipitation²¹⁰, chemical reduction^{212, 228}, impregnation²²⁷, electrode-position²²⁹, and physical mixing²¹⁰. Some of these methods require adding a reducing agent, such as NaBH₄, to reduce the metal ions to metal particles. However, the weak adhering of the metal nanoparticles to the semiconductor surface, the larger size of the metal nanoparticles, and the nucleation of isolated metal nanoparticles in the electrolyte are the main problems associated with such methods. Such a poor interaction between the metal nanoparticles and the semiconductor surface negatively affects the electron transfer to the metal, increasing the electron/hole recombination rate^{212, 230, 231}. On the other hand, some techniques need elevated temperatures or an applied bias, and a longer preparation period^{128, 210, 214, 232, 233}.

Photocatalytic hydrogen production over Eosin Y-sensitized Pt-loaded TiO₂-ZrO₂ mixed oxide photocatalysts was investigated under visible light irradiation by Sreethawong and Yoshikawab²³⁴. The authors prepared the platinized material by using two different methods, i.e., single-step sol-gel (SSSG) and photochemical deposition (PCD). At the optimum loading ratio (0.5 wt%) of Pt, the authors found that the platinized photocatalyst prepared by the PCD method exhibited a higher H₂ production rate of 2.37 mL/h g

comparing to 1.42 mL/h g to that prepared by the SSSG method. They attributed the difference in the photocatalytic activity to the different oxidation states of Pt in both samples. The loaded Pt nanoparticles synthesized by the SSSG method were partly in the oxide form, whereas those prepared via the PCD method consisted of particles in their metallic form having better-dispersion on the surface of the semiconductor. Accordingly, the latter provided an efficient charge carrier separation at the interfacial contact between the photochemical-deposited Pt nanoparticles and the TiO₂-ZrO₂.

Alternatively, the photodeposition method is the most adopted and recommended technique among other loading methods to prepare Pt/TiO₂ ^{128, 214}. The interest of the scientific community with the photodeposition method has greatly expanded since 1978 when Kraeutler and Bernhard employed this technique to synthesize well-dispersed Pt nanoparticles on TiO₂ to use this composite in the photocatalytic decomposition of acetic acid to methane ^{214, 235}. Many beneficial features can be controlled during the photodeposition method such as well-defining of co-catalyst nanoparticles, preparing facet-engineered nanoparticles, geometrical distributing of nanoparticles, controlling the size and the oxidation state of the deposited nanoparticles. During the photodeposition process, the metal ions are reduced by the conduction band photogenerated electrons, which leads to a uniform dispersion of the metal nanoparticles on the photocatalyst surface and avoids the self-nucleation of metal particles in the solution ²³⁶.

Several structural properties contribute to the photoactivity of the loaded photocatalyst, such as aggregation, Pt-assisted network formation, and Pt dispersion. Wang et al. ²²² studied a 1 w% platinization of colloidal TiO₂ by two methods, i.e., the photodeposition and the mixing with colloidal Pt prepared by chemical reduction of Pt⁴⁺. The authors found that during the photocatalytic oxidation of methanol, the quantum yields of HCHO formation increased by 70% and 50%, for the photocatalyst prepared by photodeposition and mixing, respectively. They showed, additionally, that in a deoxygenated system, the platinized-TiO₂ prepared by photodeposition method was more efficient for photocatalytic H₂ and HCHO formation than the other platinized sample prepared by physical mixing during the reforming of CH₃OH. The authors explained that Pt clusters on the TiO₂ surface were formed via the photodeposition process, while, Pt particles were surrounded by TiO₂ particles by mixing colloidal Pt with colloidal TiO₂, as shown in Figure 2-13. Therefore, the better activity of the former attributed to the better dispersity and the stronger contact between the Pt particles with the TiO₂ surface.

Moreover, the deposition of Pt on the surface of TiO₂ enhances the optical property of the Pt-TiO₂. Chen et al.²³⁷ reported that the deposition of Pt on TiO₂ surface via the photodeposition method promoted the optical absorption property of the prepared material to the visible region of light. The authors attributed this enhancement to the formation of Ti⁺³ due to the reduction of the Ti⁺⁴ during the photodeposition of the Pt. Similarly, F. Li and X. Li²²⁴ found that the deposition of Pt nanoparticles on the TiO₂ surface enhanced the photocatalytic activity due to the formation of a defect energy level near the valance band of TiO₂, as a result of the Ti^{III} formation in the lattice. The authors attributed the formation of Ti^{III} to the interaction between Pt and TiO₂ during the photoreduction process.

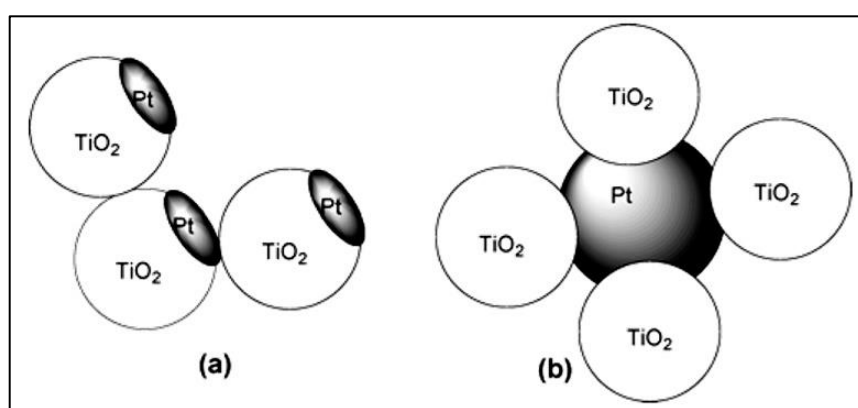


Figure 2-13: Models of Pt-TiO₂ formed by (a) photodeposition of Pt, and (b) physical mixing of colloidal Pt and TiO₂. Reprinted with permission from reference 222. Copyright 2004 American Chemical Society.

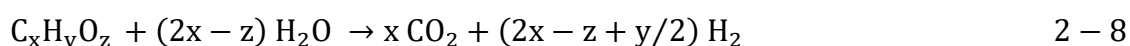
Despite many reports have shown that the photodeposition technique produces a high active photocatalyst system^{210, 212}, several reports of the metal/semiconductor prepared with other techniques have claimed the contrary^{213, 225, 238}, thus, no general conclusion could be deduced. Apparently, the shape and the nature of Pt NPs besides their interaction with the support are expected to be different by the various platinization methods, which results in diverse photocatalytic behaviors.

2.7 Photocatalytic Reforming of Aromatic Compounds

Aromatic compounds such as phenols, dyes, and PAHs are important industrial chemicals due to their wide usage. Therefore, the development of novel and simple processes is desired to remove these compounds from the environment from the viewpoint of “green chemistry”²³⁹. Several investigations of photooxidation of such pollutants have been carried out by using TiO₂ and Pt/TiO₂ photocatalysts in the presence of molecular oxygen^{113, 117, 124, 240-246}.

Due to the low efficiency of overall photocatalytic water-splitting, the photoreforming of the organic compounds has shown significantly higher rates and longer-term stability of H₂ production. Therefore, a huge number of photocatalytic reforming studies have been reported. However, simple organic compounds like methanol (the most studied), ethanol, formaldehyde, ..., and formic acid have been mostly used as model pollutants. In this section, we will focus on the reported investigations that using aromatic compounds like benzene, phenols, dyes, and PAHs as electron donors (hole scavengers), especially over modified TiO₂ materials for the same goal.

As mentioned in section 2.6.2, surface-modified TiO₂ and other semiconductors like Cu₂O, WO₃, have been widely used as photocatalysts for the photooxidation and the reforming of the hazardous organic pollutants found in wastewater^{38, 105, 130, 247}. Upon the total mineralization, the photoreforming process is demonstrated by the following stoichiometrical reaction (Equation 2-8)²⁴⁸.



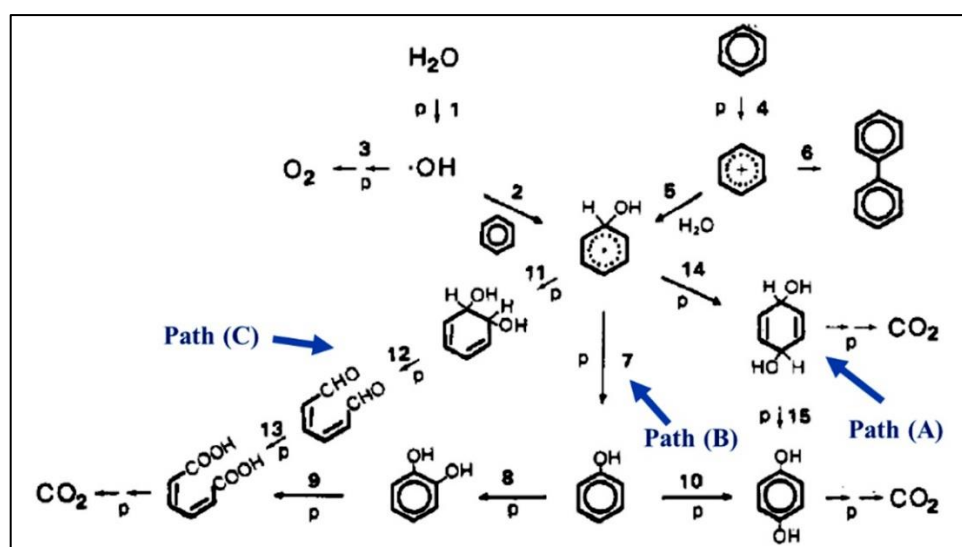
2.7.1 Monoaromatic and Phenolic-Based Compounds

Benzene is considered a toxic and carcinogenic pollutant. It naturally exists in the environment and artificially made the human through a wide range of products such as plastics, paints, mucilage, rubber, and gasoline. It was confirmed that exposure to benzene for a high level or long-time results in several ailments like drowsiness, nausea, headache, lightheadedness, dizziness, and cancers. Therefore, it was classified in Category A as a carcinogenic compound by the Environmental Protection Agency.

Hashimoto et al.²⁴⁷ investigated the photocatalytic H₂ production from different solutions of aliphatic and aromatic compounds using Pt-TiO₂ photocatalyst. Assisted by light energy and in the presence of the photocatalyst, both types of hydrocarbons produced H₂ by reacting with water at room temperature. The maximum H₂ formation was obtained at a 30:1 ratio between the water/benzene mixtures while increasing the benzene ratio decreased the H₂ formation. The authors have claimed that water is the main source of H₂ since no H₂ was detected upon the use of pure benzene in the presence of the Pt-TiO₂ under irradiation. Comparing to the water-alcohol mixture, the authors observed that H₂ and CO₂ are produced at an early stage of irradiation, and the aromatic hydrocarbons produced a higher CO₂ amount than their corresponding derivatives like phenol, hydroquinone, and catechol. Therefore, they suggested a higher reactivity of the aromatic hydrocarbons comparing to

the hydroxylated aromatic compounds. The authors, hence, proposed that the direct oxidation of benzene by photogenerated holes is the main reaction pathway, followed by the ring-opening producing the corresponding organic acid that decomposes via photo-Kolb reaction (*Path C* in Scheme 2-2). The authors have excluded phenol and catechol as the main intermediates in this path since benzene swiftly oxidized to muconic acid, whose reactivity is larger than that of benzene itself.

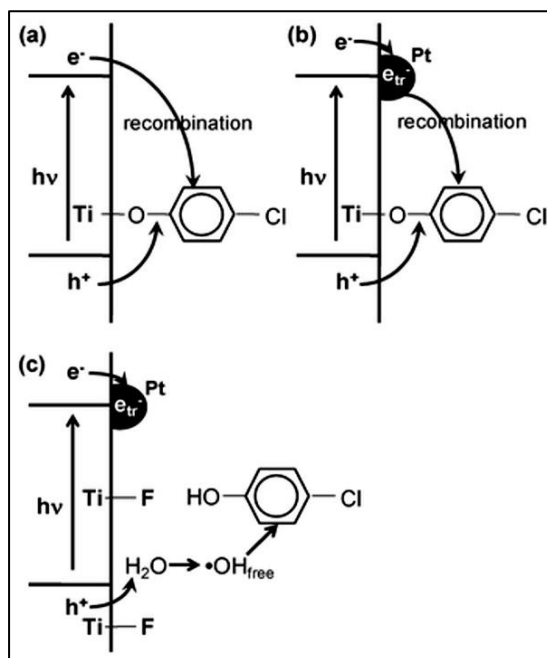
Many other investigations have documented the H₂ formation during the photocatalytic transformation of benzene, however, they have mainly discussed the H₂ formation as a secondary product. Such reports focused on other purposes, such as the mechanistic studies of the photocatalytic reaction^{12, 13, 249-251} and the chemical synthesis^{162, 250, 252}, rather than the transformation of the aromatic water pollutants into fuels H₂.



Scheme 2-2: Reaction scheme of photocatalytic oxidation of benzene in water. Adapted with permission from reference 247. Copyright 1984 American Chemical Society.

On the other hand, phenolic compounds - as we mentioned previously - are one of the most abundant aromatic pollutants in wastewater. Few research groups reported the transformation of these kinds of pollutants into fuels. In 2008, Choi et al.²⁵³ reported the photocatalytic degradation of 4-chlorophenol and bisphenol A on the surface of bare TiO₂ (P25), F-TiO₂, Pt/TiO₂, and F-TiO₂/Pt under anoxic conditions. The authors found that F-TiO₂/Pt exhibited the highest photocatalytic activity towards the conversion of these compounds compared to the other materials. They attributed this activity to the unique synergic effect of two different surface species, i.e., fluoride and platinum, on the photo-induced charge transfer process. Such an effect inhibits the charge recombination on F-TiO₂/Pt as shown in Scheme 2-3. However, the mineralization of these aromatic

compounds could not be achieved for all photocatalysts, since the total organic carbon content in the suspensions remained unaltered during the irradiation. Nevertheless, the authors did not discuss the possibility of molecular hydrogen formation in anoxic conditions, and they ignored it in their reaction mechanism.



Scheme 2-3: Photo-induced charge transfer/recombination processes occurring on (a) bare TiO₂, (b) Pt/TiO₂, and (c) F-TiO₂/Pt in the presence of 4-CP and the absence of O₂. Reprinted with permission from reference 253. Copyright 2008 Royal Society of Chemistry.

Two years after, the same research group presented similar results, taking into account the simultaneous production of H₂ during the photooxidation of such organic compounds²⁴⁸. Interestingly, the authors found that the % photonic efficiencies for H₂ formation during the photooxidation of the simple organic compounds, i.e., dichloroacetic acid and *N*-nitrosodimethyl amine were found 0.122 and 0.139, respectively over Pt/TiO₂. These values were higher than those reported for F-TiO₂/Pt, i.e., 0.046 and 0.1, respectively. In contrast, using other aromatic compounds, i.e., hydroquinone, 4-chlorophenol, 4-chlorobenzoic acid, and bisphenol, higher % photonic efficiencies for H₂ were achieved over F-TiO₂/Pt (0.094, 0.116, 0.249, 0.334, respectively) than those over Pt/TiO₂ (0.052, 0.003, 0.002, 0.044, respectively). The authors reported, additionally, a complete TOC removal in the 4-chlorophenol / F-TiO₂/Pt suspension after 8-hour irradiation.

It is well known that the adsorption of the photodegraded organic intermediates to the photocatalyst surface and the insufficient management of the photo-generated charge carrier inhibits the H₂ evolution reaction and/or the photocatalytic degradation of the

organic pollutants in the dual-functional photocatalysis process^{38, 104, 254}. To this end, Kim et al.,¹¹ studied the enhancement of the dual-functional photocatalysis process by modifying titania photocatalysts with fluoride or phosphate beside the deposition of different metals, i.e., Pt, Pd, Au, Ag, Cu, or Ni. The authors found that the dual-function photocatalysis worked only when both the anion and the metal coexisted on the surface of TiO₂, whereas TiO₂ modified with a single surface component such as F-TiO₂, P-TiO₂, or M/TiO₂ was inactive under the same experimental condition (Figure 2-14 a). Almost similar dual-functional photocatalysis activities were reported for F-TiO₂/Pt and P-TiO₂/Pt, however, the synergistic effect greatly depended on the kind of deposited metal and the pH (Figure 2-14 a and b). F-TiO₂/Pt was found to be active in the acidic pH region since its activity gradually decreased with increasing pH. In contrast, P-TiO₂/Pt exhibited a consistent activity over a wide range of pH, due to the strong chemical bonding of phosphates on TiO₂. Therefore, they suggested that P-TiO₂/Pt could be more appropriate for practical dual-functional applications (Figure 2-14 c). The authors claimed that the modification of the TiO₂ surface with fluorides or phosphates with the deposition of metal act synergistically to reduce the charge recombination and enhance the interfacial electron transfer which enhancing the photocatalytic activity.

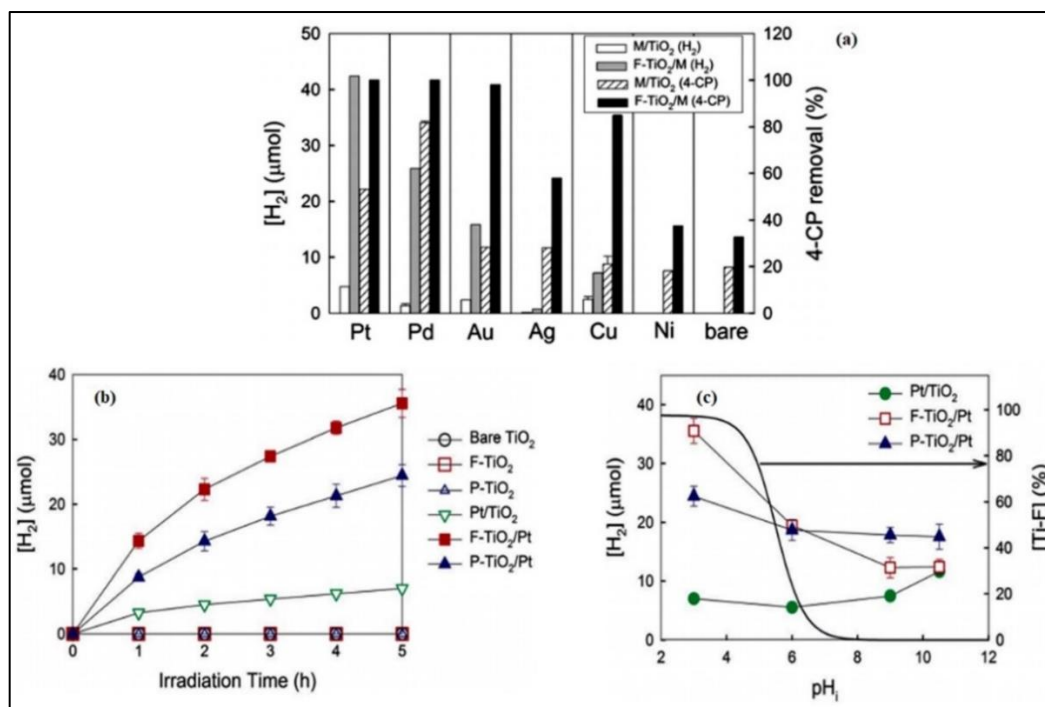


Figure 2-14: (a) Production of H₂ with the simultaneous degradation of 4-CP in the suspension of M/TiO₂ and F-TiO₂/M (M= Pt, Pd, Au, Ag, Cu, and Ni), (b) Production of H₂ in the suspension of bare TiO₂, F-TiO₂, P-TiO₂, Pt/TiO₂, F-TiO₂/Pt, and P-TiO₂/Pt with 4-CP, and (c) effect of pH on the production of H₂. Adapted with permission from reference 11. Copyright 2012 Royal Society of Chemistry.

Furthermore, the enhancement of the dual-functional photocatalytic process toward the simultaneous H₂ formation and 4-chlorophenol degradation was achieved by designing a ternary components photocatalyst¹⁵⁶. Cr₂O₃/Rh/SrTiO₃ was prepared by covering the Rh nanoparticles on the surface of SrTiO₃ with a thin barrier layer of Cr₂O₃ to selectively control and maximize the dual-functional photocatalytic activity. Under the same experimental condition, the as-prepared Cr₂O₃/Rh/SrTiO₃ photocatalyst exhibited a higher activity towards H₂ production and 4-chlorophenol degradation than that of F-TiO₂/Pt and was unaffected by the pH change from the acidic medium to neutral medium (Figure 2-15).

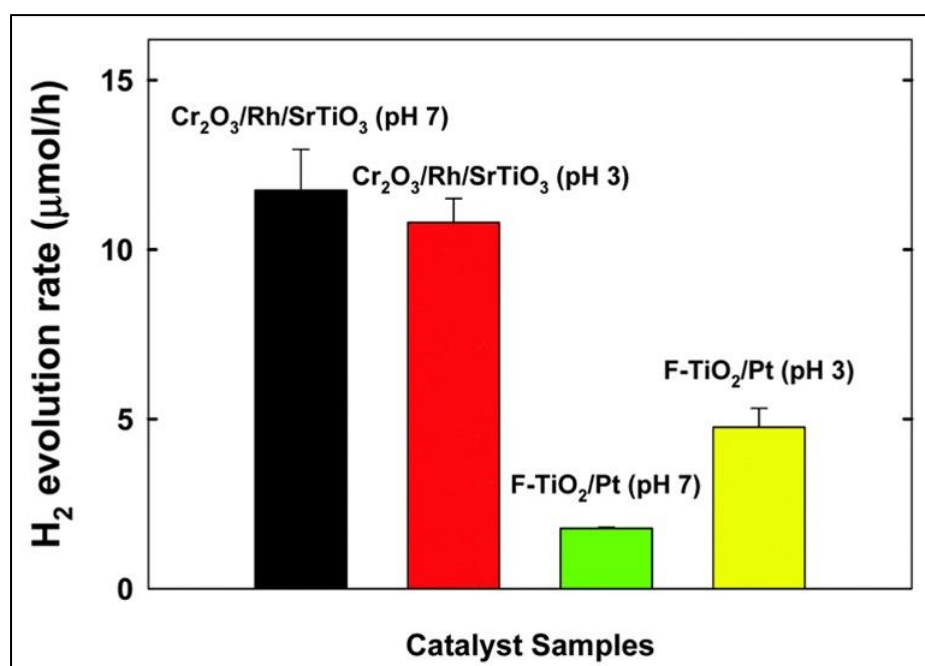
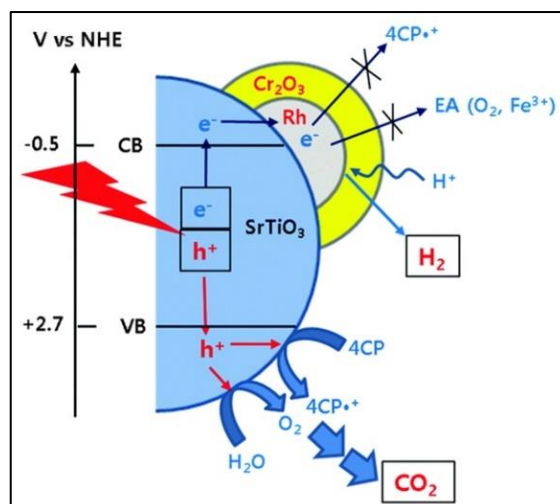


Figure 2-15: Comparison of the initial photocatalytic H₂ production rate between Cr₂O₃/Rh/SrTiO₃ and F-TiO₂/Pt photocatalytic systems in the presence of 4-CP. Reprinted from reference 156. Published by the Royal Society of Chemistry.

According to the authors, the better photocatalytic behavior of Cr₂O₃/Rh/SrTiO₃ can be related to two features. Firstly, the Cr₂O₃ barrier layer selectively allows the conduction band electrons to be consumed by protons, hindering their transfer to O₂ or other electron acceptors. Secondly, the valence band holes are utilized to oxidize both the 4-chlorophenol and H₂O (to O₂), since the in-situ generated O₂ simultaneously and immediately consumed in the oxidation reaction to help in the mineralization of the organic pollutants, as shown in Scheme 2-4.

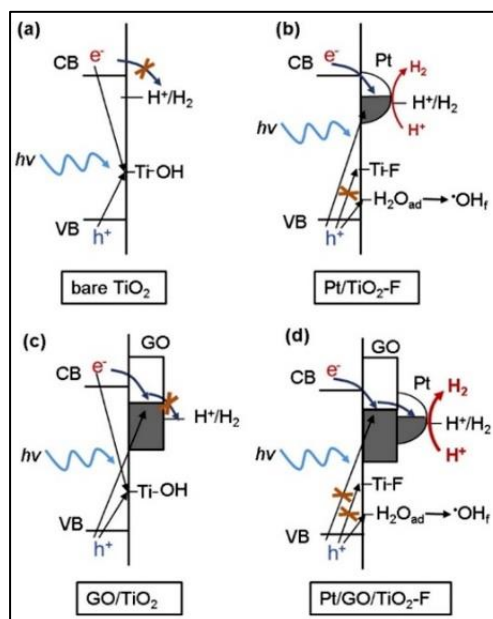


Scheme 2-4: Schematic illustrations of photocatalytic reaction mechanisms occurring on the surface of Cr₂O₃/Rh/SrTiO₃. Reprinted from reference 156. Published by the Royal Society of Chemistry.

Cho et al.²⁵⁵ modified the TiO₂ surface by adding the graphene oxide (GO) as a ternary component besides the modification with F and Pt to enhance the dual-functional photocatalytic activity. Pt/GO/TiO₂-F showed 1.7 and 3.8 times higher H₂ production than Pt/TiO₂-F and Pt/GO/TiO₂, respectively, during the photocatalytic degradation of 4-chlorophenol. Since the GO attracts electrons, the interfacial electron transfer was facilitated by the direct contact between GO and the TiO₂ surface, while holes are kept in TiO₂. Such an electron transfer to GO reduces the possibility of recombination of photogenerated charge carriers and extends the lifetime of charge carriers. Moreover, as the work function of Pt is higher than that of GO, i.e., 5.64 and 4.42 eV, respectively, the transfer of photogenerated electrons from GO to Pt is energetically favorable, which enhances the H₂ production. On the other hand, F ions replace the surface hydroxyl groups on the TiO₂ surface which act as the main hole trap sites. This in turn reduces hole-trapping efficiency and hinders the chemisorption of organic substrates, thus, prevents the direct attack of the organic molecules by the trapped hole. Since the electrons are trapped by Pt, the preferred path of holes is to react with H₂O to generate unbound •OH radicals that can diffuse out from the surface and react with the organic molecules in the medium. The authors explained that such a ternary hybrid system retards the recombination of the charge carrier and enhances both the H₂ production and 4-chlorophenol degradation, as shown in Scheme 2-5.

Recently, many efforts have been made to use visible-light active dual-functional photocatalysts. For example, the 2D Black phosphorous/2D carbon nitride (2D BP/2D

C₃N₄) was synthesized and employed for efficient H₂ evolution with the simultaneous photodegradation of bisphenol A pollutant (BPA)²⁵⁶.



Scheme 2-5: Schematic illustrations of interfacial charge transfer and recombination occurring on (a) bare TiO₂, (b) Pt/TiO₂-F, (c) GO/TiO₂, and (d) Pt/GO/TiO₂-F in the absence of O₂. Reprinted with permission from reference 255. Copyright 2015 Elsevier B.V.

The H₂ evolution rate and the BPA removal over 2D C₃N₄ nanosheets were found to be ~45 μmol h⁻¹ g⁻¹ and 43%, respectively. Upon the introduction of 2D BP, both the H₂ production rate and the simultaneous BPA removal were improved. The optimum ratio of 5% 2D BP exhibits an H₂ evolution rate of 259.04 μmol h⁻¹ g⁻¹ and BPA removal rate of 88% with an external quantum efficiency of 0.56% at 420 nm (Figure 2-16 (a)). The authors attributed the high efficiency of this material to the intimate electronic interaction between 2D BP and 2D C₃N₄, besides the excellent charge mobility between the two composites.

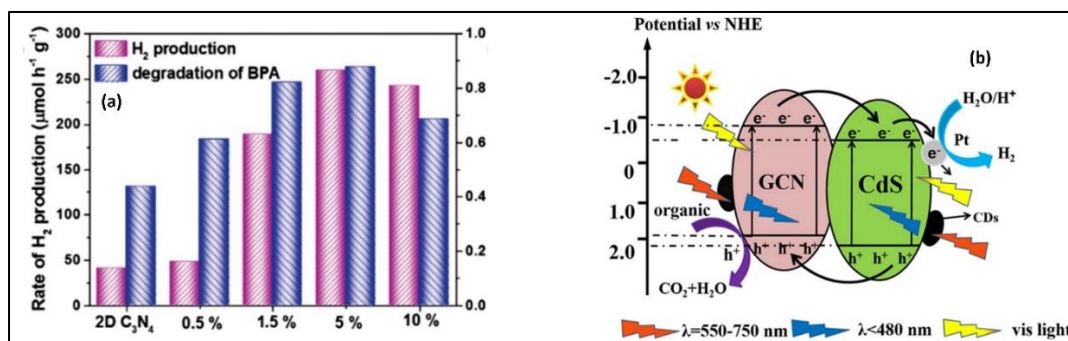


Figure 2-16: (a) Production of H₂ with simultaneous degradation in the presence of BPA over 2D C₃N₄ coupled with different amounts of 2D BP. Reprinted with permission from reference 256. Copyright 2019 Elsevier B.V. (b) Illustration for the Photocatalytic Mechanism over the 3%CDs/10%CdS/GCN Catalyst under Visible-Light Irradiation. Reprinted with permission from reference 257. Copyright 2018 Royal Society of Chemistry.

Another effort was exerted towards the development of new materials possessing optical properties in the visible light region. Jiang et al.²⁵⁷ prepared a photocatalyst consists of carbon quantum dots/CdS quantum dots/g-C₃N₄ (CDs/CdS/GCN) photocatalyst composite. The photocatalytic activity of this material under visible-light illumination was evaluated for concurrent H₂ production and the decomposition of typical wastewater pollutants like p-chlorophenol (4-NP), bisphenol A (BPA), and tetracycline (TTC). The 3%CDs/10%CdS/GCN photocatalyst exhibited the best photocatalytic efficiency under the visible-light irradiation for H₂ evolution from water splitting in an aqueous solution containing organic pollutants (Figure 2-16 (b)). The addition of 4-NP decreased the photocatalytic H₂ evolution rate compared with the pure water system, due to the consumption of some photogenerated electrons in the degradation of 4-NP. Although the photocatalytic degradation rate of 4-NP was higher than those of BPA and TTC, the H₂ evolution rate increased with the addition of BPA or TTC. The authors have explained such a result by the consumption of all photogenerated electrons to split water for H₂ production.

On the other hand, some reports have shown the inability to use phenol as a sacrificial reagent in the dual functional photocatalytic processes. Mogyorósi et al.²⁵⁸ investigated the photocatalytic H₂ production and the decomposition of various organics using 1% Pt-, Au- and Ag-deposited on the surface of Degussa P25 photocatalysts. The photocatalytic decomposition of oxalic acid and formic acid was increased upon the deposition of noble metals compared to that of the bare photocatalyst. However, in phenol containing system, the authors reported a decrease in the decomposition activity, indicating that the noble metals block the active sites on the surface of the photocatalyst. On the other hand, they practically reported no H₂ production over the bare and the modified P25 in the presence of phenol as a sacrificial reagent. While a very high quantum yield for H₂ production over Pt-TiO₂ photocatalyst was reported in the presence of oxalic and formic acids. They have concluded that O₂ was a requirement for the photooxidation of phenol in presence of any photocatalysts since no decomposition was detected in its absence. Hence, the inhibition of phenol photooxidation in anoxic conditions negatively affects the ability of H₂ production.

2.7.2 Dyes and Polyaromatic-Based Pollutants.

A wide variety of photocatalysts were designed to achieve the goal of the dual-functional photocatalysis technology; simultaneous H₂ production and wastewater purification by the degradation of the persistent dyes^{38, 39, 189, 259-262}. The production of hydrogen with a

simultaneous degradation of Azo-dye solution (commercial name Acid Orange 7; AO7) using the well-known photocatalyst Pt/TiO₂ suspensions was examined by Patsoura²⁶¹ under UV–vis light. The authors have investigated the effect of the dye concentration, the pH, and the temperature on the H₂ production rate. Besides, the effect of the Pt loading ratio on the H₂ formation rate was thermodynamically investigated through the dynamic of the charge carrier during the reaction. In the absence of the Azo-dye and after the deposition of Pt (0.5 wt.%) on the TiO₂ surface, the H₂ production rate increased to a maximum during the irradiation before dropping to a very low steady-state rate value comparable to those obtained over bare TiO₂. Although, it is well known that bare TiO₂ is inactive for the H₂ production due to the driving force for this reaction is small and the presence of a large overpotential for the H₂ evolution²⁶³, the authors attributed such activity to the presence of i) metal or organic impurities in the semiconductor, ii) partially reduced titania species, iii) small size semiconductor particles that exhibit a higher efficiency in photocatalytic reactions. The authors also reported an improvement in the H₂ formation during the photo-induced water splitting reaction over Pt/TiO₂ by increasing the pH and the temperature. Interestingly, the presence of a small quantity of Azo-dye in the reaction medium significantly enhanced the H₂ formation rate, which depends on dye concentration, solution pH, and to a lesser extent to the solution temperature. They found that using a higher dye concentration resulted in increasing H₂ formation over a longer reaction period. However, afterward, the formation rate was decreased to a steady-state value comparable to that obtained in the absence of the Azo-dye. The authors have attributed this decrease to the complete mineralization of the AO7 by-products in the reaction solution, due to their oxidation by consuming the photogenerated oxygen from the surface of the photocatalyst.

Moreover, in the same study, the authors examined if the beneficial effect of the presence of AO7 on the rate of H₂ production is general phenomena, another two different Azo-dyes, namely Basic Blue 41 and Basic Red 46 have been tested at neutral pH solution. Similar behavior to the addition of AO7 was observed for the other Azo-dyes. The H₂ formation rate increases during the first few hours of irradiation and then progressively drops to steady-state values similar to those obtained for pure water.

The authors have also highlighted a very important point in this study. The adsorption of the reaction intermediates on Pt, which cannot be effectively removed under the experiment conditions, leads to retarding the H₂ evolution. This behavior had been observed in many similar photocatalytic systems dealing with the TiO₂ and aromatic compounds^{104, 167, 247, 250}.

On the other hand, increasing pH from 4 to 10 resulted in a significant increase in the maximum formation rate from 0.28 to 0.67 $\mu\text{mol}/\text{min}$, which was related to the enhanced kinetics of dye degradation with increasing the solution pH. According to these authors, this enhancement indicating that the rate of H₂ production is limited by the rate of consumption of photogenerated O₂. Therefore, they conclude that the azo-dye acts as a sacrificial agent that rapidly remove the photogenerated holes and consume the photogenerated oxygen. This suppresses electron-hole and O₂-H₂ recombination, enhancing the H₂ production until complete degradation of the dye to CO₂ and inorganic ions.

The modification of the TiO₂ in a way that increases the adsorption of the organic molecules on its surface is considered one of the methods that enhance the photocatalytic activity since the direct hole transfer to the organic molecules is dominant^{264, 265}. Bifunctional TiO₂ photocatalysts have been developed by Kim et al.²⁶⁶ through the modification of the surface of TiO₂ with two different components, platinum, and Nafion (Pt/TiO₂/Nf). The simultaneous H₂ production and rhodamine B (RhB) degradation was successfully achieved using Pt/TiO₂/Nf under visible light ($\lambda > 420 \text{ nm}$). Pt/TiO₂/Nf exhibited high activity for H₂ production in the presence of RhB as a photosensitizer and organic dye pollutant, besides EDTA as an electron donor. However, the modification with only one component, i.e., Pt or Nf, resulted in a negligible activity for H₂ production under the same experimental conditions. According to the authors, the negative charge of the Nafion layer improves the adsorption of cationic RhB and pulls protons to the surface of TiO₂ through electrostatic attraction, enhancing the RhB photooxidation. Simultaneously, these protons are reduced to H₂ on the deposited Pt that acts as an electron sink and a temporary electron reservoir for the reduction half-reaction. The authors found that RhB was not degraded in the absence of EDTA, which is involved in the reaction mechanism by converting the RhB to *N*-deethylation. In this dual-functional photocatalytic system, a 20 μM (0.6 μmol) of RhB approximately produced 70 μmol of H₂, while the RhB and its intermediates were completely removed over 12 h period.

Polycyclic aromatic hydrocarbons (PAHs) are a kind of semi-volatile persistent aromatic pollutants²⁶⁷. These compounds are frequently detected in different types of wastewater^{58, 267}. As for many other pollutants, advanced oxidative processes based on photocatalysis have often been reported for the removal of PAHs^{268, 269}. Although several studies have explored their photocatalytic degradation in anoxic conditions^{268, 270, 271}, however, very limited

reports on the remediation of PAHs with simultaneous H₂ production had been documented in the literature^{104, 167}. On the other hand, several reports on the simplest aromatic compound benzene have proved its ability to act as a sacrificial electron donor (hole scavenger) to photo-catalyze molecular hydrogen^{247, 250, 251}. Bahnemann's research group has considered this shortage in the literature and spotted the light on employing these compounds as sacrificial electron donors (SEDs) in the dual-functional photocatalysis system^{104, 167, 272}.

The hydrogen production with the simultaneous degradation of the simplest PAH compounds naphthalene based on Pt/TiO₂ has been investigated by the Bahnemann research group¹⁶⁷. In this study, two different commercial TiO₂ photocatalysts, Aeroxide P25 (ATiO₂) and Sachtleben Hombikat UV100 (HTiO₂) were loaded with different fractional ratios of Pt nanoparticles using the photodeposition method. The aim was to evaluate the role of the loaded Pt on hydrogen production and the simultaneous degradation of naphthalene. The 0.5 wt% Pt was found to be the optimum loading ratio on the surface of HTiO₂, which increased the conversion of naphthalene from 71% for bare HTiO₂ to 82% and produces 6 μmol of H₂ (Figure 2-17). However, the authors found that using a higher Pt content than the optimal platinization ratio inhibited both processes, the H₂ formation, and naphthalene photooxidation. On the other hand, they claimed that loading ATiO₂ with the Pt nanoparticles regardless of the platinization ratio decreased naphthalene conversion, while no dependency between the Pt ratio and the H₂ formation rate was found since all the platinized ATiO₂ materials showed a similar H₂ formation of around 3 μmol.

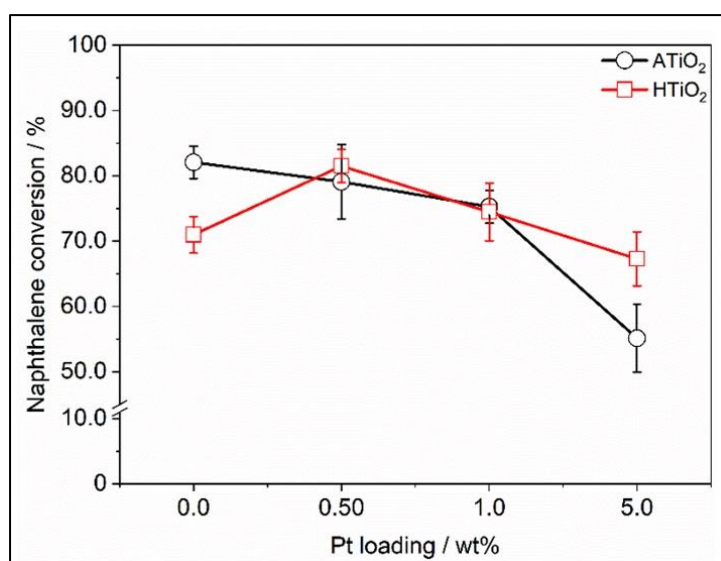


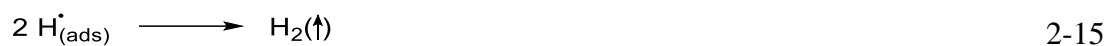
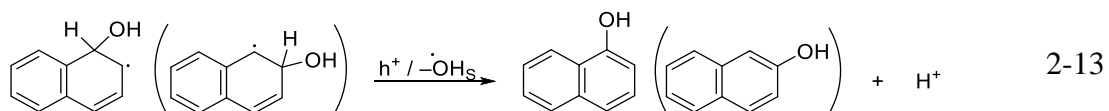
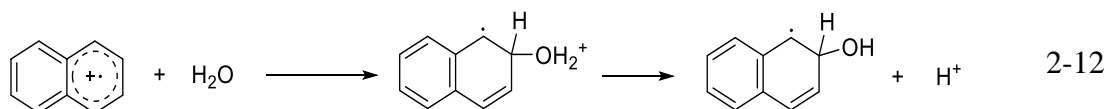
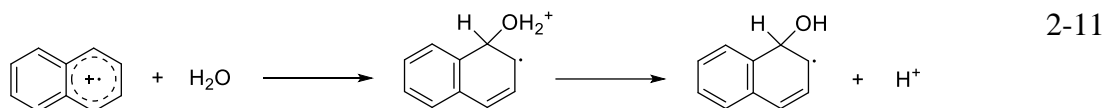
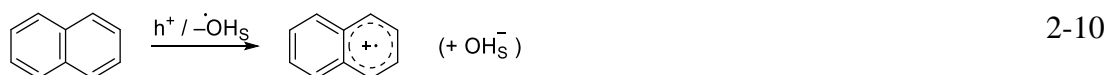
Figure 2-17: Naphthalene conversion in the presence of TiO₂-based photocatalysts loaded with different % of Pt nanoparticles. Reprinted with permission from reference 167.

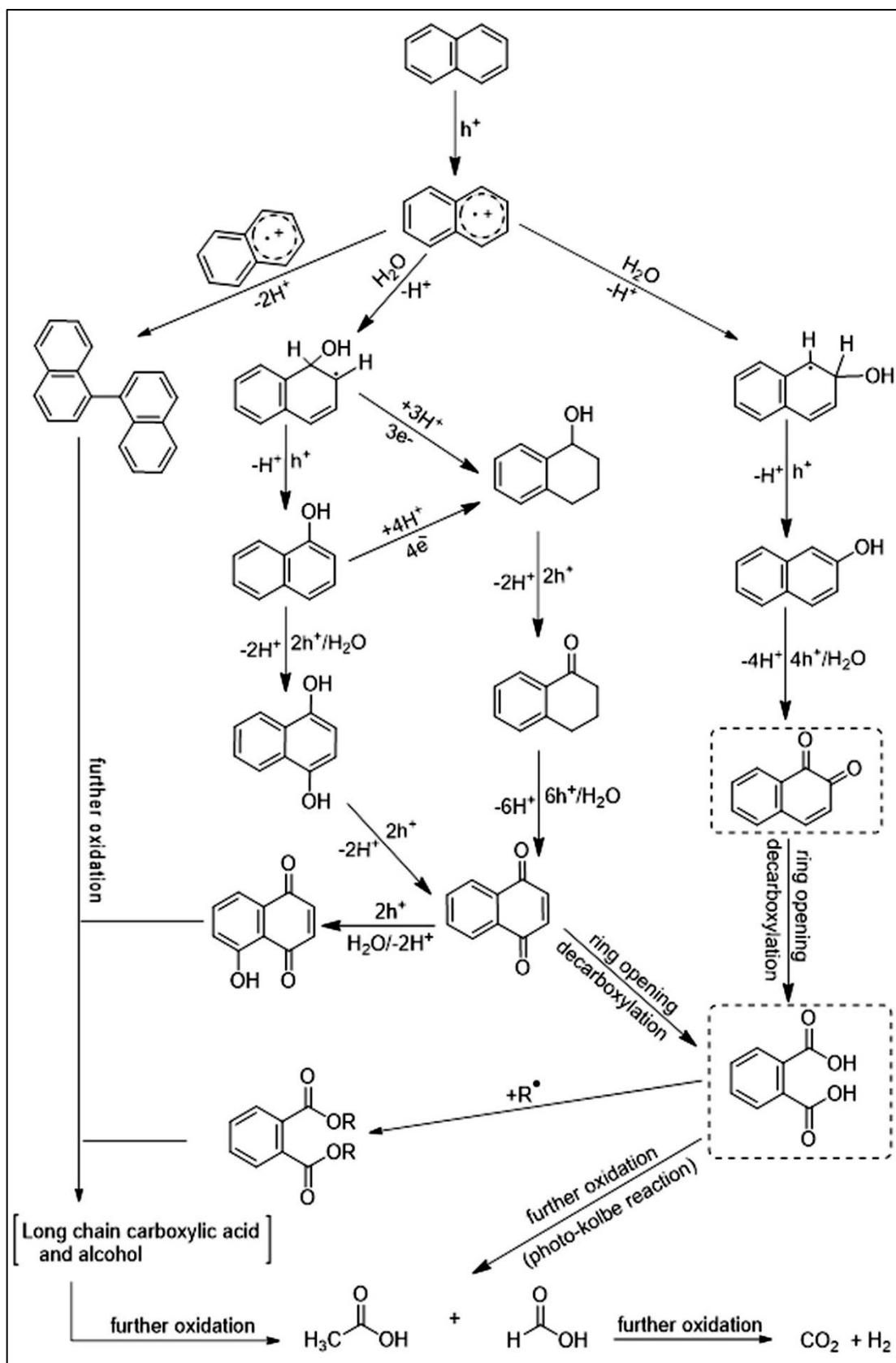
Based on the EPR technique, the authors concluded that the Pt NPs on ATiO₂ acted as recombination centers for the photogenerated charge carrier. They have additionally related the decreases of H₂ formation rate and naphthalene conversion during the photocatalytic process to the deactivation of the photocatalyst due to adsorption of the formed intermediates on the surface of the photocatalyst. Interestingly, the authors demonstrated that the reforming of PAHs over the Pt-HTiO₂ exhibits higher photonic efficiencies than that of their corresponding hydroxylated compounds, such as 1 and 2-naphthols.

In another study, the effect of the co-catalyst loading methods on the physicochemical properties of the dual-functional photocatalyst was studied by the same research group²⁷². Anatase TiO₂ (Sachtleben Hombikat UV100) was loaded with Pt nanoparticles using two alternative methods: photodeposition by reduction of PtCl₆²⁻ (Pt_{PD}-TiO₂) and physical mixing of TiO₂ with Pt nanoparticles synthesized by laser ablation (Pt_{LA}-TiO₂). Both as-prepared materials were fully characterized, and their photocatalytic activities were evaluated for the photoreforming of naphthalene and methanol. Over both photocatalysts, the authors reported a huge difference in H₂ formation between the two-electron donors, which can be related to the different nature of the organic compounds. Methanol reacts swiftly with the photogenerated holes, while the reaction of naphthalene involved multi-complicated steps. On the other hand, Pt_{PD}-TiO₂ exhibited better photocatalytic activity toward naphthalene oxidation and H₂ formation compared to Pt_{LA}-TiO₂. Based on the transient absorption spectroscopy and the electron paramagnetic spectroscopy techniques, the higher activity of Pt_{PD}-TiO₂ was related to the better charge carrier transfer between the TiO₂ and the loaded Pt nanoparticles. The authors explained these results by the better dispersion of Pt nanoparticles and their strong interaction with the surface of TiO₂.

The mechanism of the dual-functional photocatalysis process for molecular hydrogen formation concurrent with naphthalene degradation over Pt-TiO₂ (Hombikat UV100) has been investigated¹⁰⁴. The authors reported photonic efficiencies of 0.33% and 0.970% for naphthalene conversion and H₂ formation, respectively, under simulated sunlight. After 4h irradiation, the authors were able to determine the formed organic by-products in the system by the mean of GC-MS, HPLC-UV, and HPIC techniques. Moreover, through the spin-trapping experiments, they evinced that only the photogenerated holes play the main role in the photooxidation of naphthalene, while, the isotopic labeling analyses showed that the evolved H₂ originated mainly from water. According to these results, the authors suggested

the following mechanism for hydroxylation of naphthalene (Equations 2-9 to 2-15), while the total mineralization mechanism was shown in Scheme 2-6.





Scheme 2-6: Proposed mechanism for the photocatalytic reforming of naphthalene over Pt-UV100 under simulated sunlight. Note: Compounds inside the dashed square were not detected during the by-products identification. Reprinted with permission from reference 104. Copyright 2020 Royal Society of Chemistry.

2.8 Conclusions

The increase in the quantity and quality of pollutants associated with industrial progress and population growth makes it necessary to match this increase with efficient and sustainable ways to treat it. Hence, the urge to develop new materials or to modify and/or enhance the performance of some existing materials. There is no doubt that abundance and low cost are advantages that every semiconductor must meet for their application in large-scale photocatalytic systems. These two properties turned TiO₂ into an attractive material in this field. Attractive enough to devote large scientific efforts to overcome its main limitations: fast charge carrier recombination rates and a relatively large bandgap (3.2 eV) so that only UV radiation can activate it. However, the adopted strategies to improve TiO₂ performance and make it more appealing for large-scale applications, some of these strategies are discussed in this review, are and to large extent working and seem promising. However, miniaturizing or synthesizing in the nanoscale is not the only way to achieve high efficiency. The fast recombination of the photogenerated charges could be significantly reduced by the loading of co-catalyst which is normally noble metal nanoparticles. The high cost of the noble metals and their limited availability make them a not idealistic choice. One more time, cost-effectiveness comes into play but this time as a limiting factor. The search for co-catalysts that demonstrate high efficiency combined with cost efficiency is a challenging issue in photocatalysis. The wide scale of chemical and physical properties of both pollutants and semiconductors could anticipate the use of oxide-oxide or metal-oxide hetero nanostructures to create new properties that achieve higher performance and enhanced ability to remove, reform, or degrade pollutants. Not to mention that heterostructures could demonstrate the same function as a catalyst and cocatalyst without the resolve to high-cost noble metals which could be a working strategy with enormous numbers of materials. Finally, despite a large amount of photocatalytic reforming studies, there is a huge deficiency in the investigation of the photocatalytic reforming of aromatic-based pollutants, especially the PAHs. Such pollutants have shown the ability for photocatalytic oxidation in the oxygen atmosphere; however, few reports have been published that deal with the H₂ production based on their photoreforming. Hence, this research line can be a rich area for further future investigation.

2.9 Acknowledgments

Financial support from the Katholischer Akademischer Ausländer-Dienst (KAAD), Graduiertenakademie and Institut für Technische Chemie at Gottfried Wilhelm Leibniz Universität Hannover are gratefully acknowledged for providing scholarships and a job for Osama Al-Madanat to perform his Ph.D. Wegdan Ramadan would like to thank the Alexander von Humboldt Foundation for the fund received allocated for the purchase of equipment.

2.10 Author Contributions

Conceptualization, resources, validation, data curation, and writing—original draft preparation: **Osama Al-Madanat, Yamen AlSalka**. Writing—review and editing: **Osama Al-Madanat, Yamen AlSalka, Wegdan Ramadan**. Supervision: **Detlef W. Bahnemann**.

2.11 References

1. Liew, W. T.; Adhitya, A.; Srinivasan, R., Sustainability trends in the process industries: A text mining-based analysis. *Comput. Ind.* **2014**, 65 (3), 393-400.
2. Mechhoud, E.; Rouainia, M.; Rodriguez, M., A new tool for risk analysis and assessment in petrochemical plants. *Alex. Eng. J.* **2016**, 55 (3), 2919-2931.
3. Rovira, E.; Cuadras, A.; Aguilar, X.; Esteban, L.; Borràs-Santos, A.; Zock, J.-P.; Sunyer, J., Asthma, respiratory symptoms and lung function in children living near a petrochemical site. *Environ. Res.* **2014**, 133, 156-163.
4. Villanueva, F.; Tapia, A.; Lara, S.; Amo-Salas, M., Indoor and outdoor air concentrations of volatile organic compounds and NO₂ in schools of urban, industrial and rural areas in Central-Southern Spain. *Sci. Total Environ.* **2018**, 622-623, 222-235.
5. Bari, M. A.; Kindzierski, W. B., Ambient volatile organic compounds (VOCs) in communities of the Athabasca oil sands region: Sources and screening health risk assessment. *Environ. Pollut.* **2018**, 235, 602-614.
6. Matthews, R. W., Purification of water with near—u.v. illuminated suspensions of titanium dioxide. *Water Res.* **1990**, 24 (5), 653-660.
7. Matthews, R. W., An adsorption water purifier with in situ photocatalytic regeneration. *J. Catal.* **1988**, 113 (2), 549-555.
8. Grigoryan, H.; Edmands, W. M. B.; Lan, Q.; Carlsson, H.; Vermeulen, R.; Zhang, L.; Yin, S. N.; Li, G. L.; Smith, M. T.; Rothman, N.; Rappaport, S. M., Adductomic signatures of benzene exposure provide insights into cancer induction. *Carcinogenesis* **2018**, 39 (5), 661-668.

9. He, C.; Cheng, J.; Zhang, X.; Douthwaite, M.; Pattison, S.; Hao, Z., Recent advances in the catalytic oxidation of volatile organic compounds: A review based on pollutant sorts and sources. *Chem. Rev.* **2019**, *119* (7), 4471-4568.
10. Alegría, M.; Aliaga, J.; Ballesteros, L.; Sotomayor-Torres, C.; González, G.; Benavente, E., Layered nanocomposite 2D-TiO₂ with Cu₂O nanoparticles as an efficient photocatalyst for 4-Chlorophenol degradation and hydrogen evolution. *Top. Catal.* **2020**.
11. Kim, J.; Monllor-Satoca, D.; Choi, W., Simultaneous production of hydrogen with the degradation of organic pollutants using TiO₂ photocatalyst modified with dual surface components. *Energy Environ. Sci.* **2012**, *5* (6), 7647-7656.
12. Montoya, J. F.; Bahnemann, D. W.; Peral, J.; Salvador, P., Catalytic role of TiO₂ terminal oxygen atoms in liquid-phase photocatalytic reactions: oxidation of aromatic compounds in anhydrous acetonitrile. *ChemPhysChem* **2014**, *15* (11), 2311-2320.
13. Montoya, J. F.; Ivanova, I.; Dillert, R.; Bahnemann, D. W.; Salvador, P.; Peral, J., Catalytic role of surface oxygens in TiO₂ photooxidation reactions: Aqueous benzene photooxidation with Ti¹⁸O₂ under anaerobic conditions. *J. Phys. Chem. Lett.* **2013**, *4* (9), 1415-22.
14. Teras, L. R.; Diver, W. R.; Deubler, E. L.; Krewski, D.; Flowers, C. R.; Switchenko, J. M.; Gapstur, S. M., Residential ambient benzene exposure in the United States and subsequent risk of hematologic malignancies. *Int. J. Cancer* **2019**, *145* (10), 2647-2660.
15. Mustieles, V.; Fernández, M. F.; Martín-Olmedo, P.; González-Alzaga, B.; Fontalba-Navas, A.; Hauser, R.; Olea, N.; Arrebola, J. P., Human adipose tissue levels of persistent organic pollutants and metabolic syndrome components: Combining a cross-sectional with a 10-year longitudinal study using a multi-pollutant approach. *Environ. Int.* **2017**, *104*, 48-57.
16. Zhang, X.; Gao, B.; Creamer, A. E.; Cao, C.; Li, Y., Adsorption of VOCs onto engineered carbon materials: A review. *J Hazard Mater.* **2017**, *338*, 102-123.
17. Liu, L.; Li, J.; Zhang, H.; Li, L.; Zhou, P.; Meng, X.; Guo, M.; Jia, J.; Sun, T., In situ fabrication of highly active γ -MnO₂/SmMnO₃ catalyst for deep catalytic oxidation of gaseous benzene, ethylbenzene, toluene, and o-xylene. *J. Hazard. Mater.* **2019**, *362*, 178-186.
18. Mosmeri, H.; Gholami, F.; Shavandi, M.; Dastgheib, S. M. M.; Alaie, E., Bioremediation of benzene-contaminated groundwater by calcium peroxide (CaO₂) nanoparticles: Continuous-flow and biodiversity studies. *J. Hazard. Mater.* **2019**, *371*, 183-190.
19. Markham, S. C., Photocatalytic properties of oxides. *J. Chem. Educ.* **1955**, *32* (10), 540.
20. Fujishima, A.; Honda, K., Electrochemical photolysis of water at a semiconductor electrode. *Nature* **1972**, *238* (5358), 37-8.
21. Sabarinathan, M.; Harish, S.; Archana, J.; Navaneethan, M.; Ikeda, H.; Hayakawa, Y., Highly efficient visible-light photocatalytic activity of MoS₂-TiO₂ mixtures hybrid photocatalyst and functional properties. *RSC Adv.* **2017**, *7* (40), 24754-24763.
22. Liu, X.; Zhai, H.; Wang, P.; Zhang, Q.; Wang, Z.; Liu, Y.; Dai, Y.; Huang, B.; Qin, X.; Zhang, X., Synthesis of a WO₃ photocatalyst with high photocatalytic activity and stability using synergetic internal Fe³⁺ doping and superficial Pt loading for ethylene degradation under visible-light irradiation. *Catal. Sci. Technol.* **2019**, *9* (3), 652-658.

23. Ramadan, W.; Shaikh, P. A.; Ebrahim, S.; Ramadan, A.; Hannoyer, B.; Jouen, S.; Sauvage, X.; Ogale, S., Highly efficient photocatalysis by BiFeO₃/α(γ)-Fe₂O₃ ferromagnetic nano p/n junctions formed by dopant-induced phase separation. *J. Nanopart. Res.* **2013**, *15* (8), 1848.
24. Mishra, M.; Chun, D.-M., α-Fe₂O₃ as a photocatalytic material: A review. *Appl. Catal., A* **2015**, *498*, 126-141.
25. Ebrahim, S.; Ramadan, W.; Ali, M., Structural, optical and ferromagnetic properties of cobalt doped CdTe quantum dots. *J. Mater. Sci: Mater. Electron* **2016**, *27* (4), 3826-3833.
26. Kaur, R.; Rana, A.; Singh, R. K.; Chhabra, V. A.; Kim, K.-H.; Deep, A., Efficient photocatalytic and photovoltaic applications with nanocomposites between CdTe QDs and an NTU-9 MOF. *RSC Adv.* **2017**, *7* (46), 29015-29024.
27. Huang, C.-W.; Nguyen, B.-S.; Wu, J. C. S.; Nguyen, V.-H., A current perspective for photocatalysis towards the hydrogen production from biomass-derived organic substances and water. *Int. J. Hydrog. Energy* **2020**, *45* (36), 18144-18159.
28. Serpone, N., Is the band gap of pristine TiO₂ narrowed by anion- and cation-doping of titanium dioxide in second-generation photocatalysts? *J. Phys. Chem. B* **2006**, *110* (48), 24287-93.
29. Fouda, A.; Hassan, S.E.-D.; Saied, E.; Azab, M.S. An eco-friendly approach to textile and tannery wastewater treatment using maghemite nanoparticles (γ-Fe₂O₃-NPs) fabricated by *Penicillium expansum* strain (K-w). *J. Environ. Chem. Eng.* **2021**, *9*, 104693.
30. Angaru, G. K. R.; Choi, Y. L.; Lingamdinne, L. P.; Choi, J. S.; Kim, D. S.; Koduru, J. R.; Yang, J. K.; Chang, Y. Y., Facile synthesis of economical feasible fly ash-based zeolite-supported nano zerovalent iron and nickel bimetallic composite for the potential removal of heavy metals from industrial effluents. *Chemosphere* **2021**, *267*, 128889.
31. Al-Madanat, O.; Jiries, A.; Batarseh, M.; Al-Nasir, F., Indoor and outdoor pollution with heavy metals in Al-Karak city, Jordan. *J. Int. Environ. Appl. Sci.* **2017**, *12*, 131-139.
32. Al-Nasir, F. M.; Jiries, A. G.; Al-Rabadi, G. J.; Alu'datt, M. H.; Tranchant, C. C.; Al-Dalain, S. A.; Alrabadi, N.; Madanat, O. Y.; Al-Dmour, R. S., Determination of pesticide residues in selected citrus fruits and vegetables cultivated in the Jordan Valley. *Lwt* **2020**, *123*, 109005.
33. Lei, M.; Gao, Q.; Zhou, K.; Gogoi, P.; Liu, J.; Wang, J.; Song, H.; Wang, S.; Liu, X., Catalytic degradation and mineralization mechanism of 4-chlorophenol oxidized by phosphomolybdic acid/H₂O₂. *Sep. Purif. Technol.* **2021**, *257*, 117933.
34. Kuttiani Ali, J.; Maher Chabib, C.; Abi Jaoude, M.; Alhseinat, E.; Teotia, S.; Patole, S.; Hussain Anjum, D.; Qattan, I., Enhanced removal of aqueous phenol with polyimide ultrafiltration membranes embedded with deep eutectic solvent-coated nanosilica. *Chem. Eng. J.* **2021**, *408*, 128017.
35. Al Nasir, F.; Batarseh, M. I., Agricultural reuse of reclaimed water and uptake of organic compounds: pilot study at Mutah University wastewater treatment plant, Jordan. *Chemosphere* **2008**, *72* (8), 1203-14.
36. Torres-Pinto, A.; Sampaio, M. J.; Silva, C. G.; Faria, J. L.; Silva, A. M. T., Metal-free carbon nitride photocatalysis with in situ hydrogen peroxide generation for the degradation of aromatic compounds. *Appl. Catal., B* **2019**, *252*, 128-137.

37. Alrabadi, G.; Al-Nasir, F.; Jiries, A.; Al-Dmour, R.; Madanat, O.; Al-Dalain, S., Polychlorinated biphenyls residue in citrus and vegetables in the Jordan Valley, Jordan. *JJEES* **2019**, *10* (4), 247-251.
38. Lin, Z.; Li, L.; Yu, L.; Li, W.; Yang, G., Dual-functional photocatalysis for hydrogen evolution from industrial wastewaters. *Phys. Chem. Chem. Phys.* **2017**, *19* (12), 8356-8362.
39. Puga, A. V.; Barka, N.; Imizcoz, M., Simultaneous H₂ production and bleaching via solar photoreforming of model dye-polluted wastewaters on metal/titania. *Chem.Cat.Chem.* **2020**, *13*, 1513.
40. AlSalka, Y.; Karabet, F.; Hashem, S., Development and optimisation of quantitative analytical method to determine BTEX in environmental water samples using HPLC-DAD. *Anal. Methods* **2010**, *2* (8), 1026-1035.
41. Villegas, L. G. C.; Mashhadi, N.; Chen, M.; Mukherjee, D.; Taylor, K. E.; Biswas, N., A short review of techniques for phenol removal from wastewater. *Curr. Pollut. Rep.* **2016**, *2* (3), 157-167.
42. Michałowicz, J.; Duda, W., Phenols - Sources and toxicity. *Pol. J. Environ. Stud.* **2007**, *16* (3), 347-362.
43. Zango, Z. U.; Sambudi, N. S.; Jumbri, K.; Ramli, A.; Abu Bakar, N. H. H.; Saad, B.; Rozaini, M. N. H.; Isiyaka, H. A.; Osman, A. M.; Sulieman, A., An overview and evaluation of highly porous adsorbent materials for polycyclic aromatic hydrocarbons and phenols removal from wastewater. *Water* **2020**, *12* (10), 2921.
44. Anku, W. W.; Mamo, M. A.; Govender, P. P., Phenolic compounds in water: Sources, reactivity, toxicity and treatment methods, phenolic compounds - Natural sources, importance and applications. IntechOpen-Open Science Open Minds: London, UK., 2017.
45. Igbinosa, E. O.; Odjadjare, E. E.; Chigor, V. N.; Igbinosa, I. H.; Emoghene, A. O.; Ekhaise, F. O.; Igiehon, N. O.; Idemudia, O. G., Toxicological profile of chlorophenols and their derivatives in the environment: The public health perspective. *Sci. World J.* **2013**, *2013*, 460215.
46. Tang, W. Z.; Huang, C. P., Effect of chlorine content of chlorinated phenols on their oxidation kinetics by Fenton's reagent. *Chemosphere* **1996**, *33* (8), 1621-1635.
47. AlSalka, Y.; Karabet, F.; Hashem, S., Evaluation of electrochemical processes for the removal of several target aromatic hydrocarbons from petroleum contaminated water. *J. Environ. Monit.* **2011**, *13* (3), 605-13.
48. Drwal, E.; Rak, A.; Gregoraszczyk, E. L., Review: Polycyclic aromatic hydrocarbons (PAHs)-Action on placental function and health risks in future life of newborns. *Toxicology* **2019**, *411*, 133-142.
49. Patel, A. B.; Shaikh, S.; Jain, K. R.; Desai, C.; Madamwar, D., Polycyclic aromatic hydrocarbons: Sources, toxicity, and remediation approaches. *Front. Microbiol.* **2020**, *11*, 562813.

50. Abdel-Shafy, H. I.; Mansour, M. S. M., A review on polycyclic aromatic hydrocarbons: Source, environmental impact, effect on human health and remediation. *Egypt. J. Pet.* **2016**, 25 (1), 107-123.
51. Mastral, A. M.; Callén, M. S., A review on polycyclic aromatic hydrocarbon (PAH) emissions from energy generation. *Environ. Sci. Technol.* **2000**, 34 (15), 3051-3057.
52. Jiries, A. G.; Hussein, H. H.; Lintelmann, J., Polycyclic aromatic hydrocarbon in rain and street runoff in Amman, Jordan. *J. Environ. Sci. (China)* **2003**, 15 (6), 848-53.
53. Forsgren, A.J. *Wastewater Treatment: Occurrence and Fate of Polycyclic Aromatic Hydrocarbons (PAHs)*, 1st ed.; CRC Press: Boca Raton, FL, USA.
54. Huang, H.; Buekens, A., Chlorinated dioxins and furans as trace products of combustion: Some theoretical aspects. *Toxicol. Environ. Chem.* **2000**, 74 (3-4), 179-193.
55. Novotna, B.; Topinka, J.; Solansky, I.; Chvatalova, I.; Lnenickova, Z.; Sram, R.J. Impact of air pollution and genotype variability on DNA damage in Prague policemen. *Toxicol. Lett.* **2007**, 172, 37-47.
56. Batarseh, M. I.; Kreuzig, R.; Bahadir, M., Residue analysis of organic pollutants in sediments from the Amman/Zarqa area in Jordan. Part 1: Development of analytical methods and distribution patterns of PAHs. *Fresenius Environ. Bull.* **2003**, 12 (9), 972-978.
57. Majumdar, D.; Rajaram, B.; Meshram, S.; Suryawanshi, P.; Chalapati Rao, C.V. Worldwide distribution of polycyclic aromatic hydrocarbons in urban road dust. *Int. J. Environ. Sci. Technol.* **2016**, 14, 397-420.
58. Jiries, A.; Hussain, H.; Lintelmann, J., Determination of polycyclic aromatic hydrocarbons in wastewater, sediments, sludge and plants in Karak Province, Jordan. *Water Air Soil Pollut.* **2000**, 121 (1/4), 217-228.
59. Tian, W.; Bai, J.; Liu, K.; Sun, H.; Zhao, Y. Occurrence and removal of polycyclic aromatic hydrocarbons in the wastewater treatment process. *Ecotoxicol. Environ. Saf.* **2012**, 82, 1-7.
60. Wang, X.; Xi, B.; Huo, S.; Sun, W.; Pan, H.; Zhang, J.; Ren, Y.; Liu, H. Characterization, treatment and releases of PBDEs and PAHs in a typical municipal sewage treatment plant situated beside an urban river, East China. *J. Environ. Sci. (China)* **2013**, 25, 1281-1290.
61. Sun, H.M.; Tian, W.J.; Wang, Y.M. Occurrence and fate of polycyclic aromatic hydrocarbons in the anaerobic-anoxic-oxic wastewater treatment process. *Adv. Mater. Res.* **2012**, 610-613, 1722-1725.
62. Jia, C.; Batterman, S., A critical review of naphthalene sources and exposures relevant to indoor and outdoor air. *Int. J. Environ. Res Public Health* **2010**, 7 (7), 2903-39.
63. Robles, H., Naphthalene. In *Encyclopedia of Toxicology*, Wexler, P., Ed. Academic Press: Oxford, 2014; pp 437-439.
64. Sudakin, D.L.; Stone, D.L.; Power, L. Naphthalene mothballs: Emerging and recurring issues and their relevance to environmental health. *Curr. Top. Toxicol.* **2011**, 7, 13-19.

65. Arizavi, A.; Mirbagheri, N. S.; Hosseini, Z.; Chen, P.; Sabbaghi, S., Efficient removal of naphthalene from aqueous solutions using a nanoporous kaolin/Fe₃O₄ composite. *Int. J. Environ. Sci. Technol.* **2020**, *17* (4), 1991-2002.
66. Nesterenko-Malkovskaya, A.; Kirzhner, F.; Zimmels, Y.; Armon, R., Eichhornia crassipes capability to remove naphthalene from wastewater in the absence of bacteria. *Chemosphere* **2012**, *87* (10), 1186-91.
67. Pereira, L.; Alves, M., Dyes—Environmental Impact and Remediation. In *Environmental Protection Strategies for Sustainable Development*, Malik, A.; Grohmann, E., Eds. Springer Netherlands: Dordrecht, 2012; pp 111-162.
68. Hunger, K.; Gregory, P.; Miederer, P.; Berneth, H.; Heid, C.; Mennicke, W., Important Chemical Chromophores of Dye Classes. In *Industrial Dyes*, Hunger, K., Ed. John Wiley & Sons, Inc: Germany, 2002; pp 13-112.
69. Benkhaya, S.; M'rabet, S.; El Harfi, A., A review on classifications, recent synthesis and applications of textile dyes. *Inorg. Chem. Commun.* **2020**, *115*, 107891.
70. Berradi, M.; Hsissou, R.; Khudhair, M.; Assouag, M.; Cherkaoui, O.; El Bachiri, A.; El Harfi, A., Textile finishing dyes and their impact on aquatic environs. *Heliyon* **2019**, *5* (11), e02711.
71. Forgacs, E.; Cserháti, T.; Oros, G., Removal of synthetic dyes from wastewaters: a review. *Environ. Int.* **2004**, *30* (7), 953-971.
72. Yan, J.; Wang, L.; Fu, P.P.; Yu, H. Photomutagenicity of 16 polycyclic aromatic hydrocarbons from the US EPA priority pollutant list. *Mutat. Res. Genet. Toxicol. Environ. Mutagen.* **2004**, *557*, 99–108.
73. Ravindra, K.; Sokhi, R.; Van Grieken, R., Atmospheric polycyclic aromatic hydrocarbons: Source attribution, emission factors and regulation. *Atmospheric Environment* **2008**, *42* (13), 2895-2921.
74. Ghodke, S. A.; Sonawane, S. H.; Bhanvase, B. A.; Potoroko, I., Advanced engineered nanomaterials for the treatment of wastewater. In *Handbook of nanomaterials for industrial applications*, Mustansar Hussain, C., Ed. Elsevier: 2018; pp 959-970.
75. Naushad, M.; Alqadami, A. A.; AlOthman, Z. A.; Alsohaimi, I. H.; Algamdi, M. S.; Aldawsari, A. M., Adsorption kinetics, isotherm and reusability studies for the removal of cationic dye from aqueous medium using arginine modified activated carbon. *J. Mol. Liq.* **2019**, *293*, 111442.
76. Kadirvelu, K.; Kavipriya, M.; Karthika, C.; Radhika, M.; Vennilamani, N.; Pattabhi, S., Utilization of various agricultural wastes for activated carbon preparation and application for the removal of dyes and metal ions from aqueous solutions. *Bioresour. Technol.* **2003**, *87* (1), 129-132.
77. Katheresan, V.; Kansedo, J.; Lau, S. Y., Efficiency of various recent wastewater dye removal methods: A review. *J. Environ. Chem. Eng.* **2018**, *6* (4), 4676-4697.
78. Pai, S.; Kini, M.S.; Selvaraj, R. A review on adsorptive removal of dyes from wastewater by hydroxyapatite nanocomposites. *Environ. Sci. Pollut. Res. Int.* **2019**.

79. Kiriakidou, F.; Kondarides, D. I.; Verykios, X. E., The effect of operational parameters and TiO₂-doping on the photocatalytic degradation of azo-dyes. *Catal. Today* **1999**, *54* (1), 119-130.
80. Adeola, A. O.; Forbes, P. B. C., Advances in water treatment technologies for removal of polycyclic aromatic hydrocarbons: Existing concepts, emerging trends, and future prospects. *Water Environ. Res* **2020**.
81. Amin, M. T.; Alazba, A. A.; Manzoor, U., A review of removal of pollutants from water/wastewater using different types of nanomaterials. *Adv. Mater. Sci. Eng.* **2014**, *2014*, 1-24.
82. Hlongwane, G. N.; Sekoai, P. T.; Meyyappan, M.; Moothi, K., Simultaneous removal of pollutants from water using nanoparticles: A shift from single pollutant control to multiple pollutant control. *Sci. Total Environ.* **2019**, *656*, 808-833.
83. Rajasekhar, B.; Nambi, I. M.; Govindarajan, S. K., Investigating the degradation of nC₁₂ to nC₂₃ alkanes and PAHs in petroleum- contaminated water by electrochemical advanced oxidation process using an inexpensive Ti/Sb-SnO₂/PbO₂ anode. *Chem. Eng. J.* **2021**, *404*, 125268.
84. Singa, P. K.; Isa, M. H.; Lim, J. W.; Ho, Y. C.; Krishnan, S., Photo-Fenton process for removal of polycyclic aromatic hydrocarbons from hazardous waste landfill leachate. *Int. J. Environ. Sci. Technol.* **2020**.
85. Wilson, S. C.; Jones, K. C., Bioremediation of soil contaminated with polynuclear aromatic hydrocarbons (PAHs): A review. *Environ. Pollut.* **1993**, *81* (3), 229-49.
86. Manariotis, I. D.; Karapanagioti, H. K.; Chrysikopoulos, C. V., Degradation of PAHs by high frequency ultrasound. *Water Res.* **2011**, *45* (8), 2587-94.
87. Khulbe, K. C.; Matsuura, T., Removal of heavy metals and pollutants by membrane adsorption techniques. *Appl. Water Sci.* **2018**, *8* (1), 19.
88. Trojanowicz, M. Removal of persistent organic pollutants (POPs) from waters and wastewaters by the use of ionizing radiation. *Sci. Total. Environ.* **2020**, *718*, 134425.
89. Zhang, W.; Wei, C.; An, G., Distribution, partition and removal of polycyclic aromatic hydrocarbons (PAHs) during coking wastewater treatment processes. *Environ. Sci.: Process Impacts* **2015**, *17* (5), 975-84.
90. Fatone, F.; Di Fabio, S.; Bolzonella, D.; Cecchi, F., Fate of aromatic hydrocarbons in Italian municipal wastewater systems: an overview of wastewater treatment using conventional activated-sludge processes (CASP) and membrane bioreactors (MBRs). *Water Res.* **2011**, *45* (1), 93-104.
91. Zhu, X.; Ni, J.; Lai, P., Advanced treatment of biologically pretreated coking wastewater by electrochemical oxidation using boron-doped diamond electrodes. *Water Res.* **2009**, *43* (17), 4347-55.
92. Sakulthaew, C.; Comfort, S.; Chokejaroenrat, C.; Harris, C.; Li, X., A combined chemical and biological approach to transforming and mineralizing PAHs in runoff water. *Chemosphere* **2014**, *117*, 1-9.

93. Anjum, M.; Miandad, R.; Waqas, M.; Gehany, F.; Barakat, M. A., Remediation of wastewater using various nano-materials. *Arabian J. Chem.* **2019**, *12* (8), 4897-4919.
94. Waclawek, S.; Padil, V. V. T.; Černík, M., Major advances and challenges in heterogeneous catalysis for environmental applications: A review. *Ecol. Chem. Eng. S* **2018**, *25* (1), 9-34.
95. Rasalingam, S.; Peng, R.; Koodali, R.T. Removal of hazardous pollutants from wastewaters: Applications of TiO₂-SiO₂ mixed oxide materials. *J. Nanomater.* **2014**, *2014*, 1-42.
96. Crini, G.; Lichtfouse, E. Advantages and disadvantages of techniques used for wastewater treatment. *Environ. Chem. Lett.* **2019**, *17*, 145-155.
97. Oturan, M.A.; Aaron, J.-J. Advanced oxidation processes in water/wastewater treatment: Principles and applications. A review. *Crit. Rev. Env. Sci. Tec.* **2014**, *44*, 2577-2641.
98. Lee, S.-Y.; Park, S.-J., TiO₂ photocatalyst for water treatment applications. *J. Ind. Eng. Chem.* **2013**, *19* (6), 1761-1769.
99. Mousavi, M.; Habibi-Yangjeh, A.; Pourn, S.R. Review on magnetically separable graphitic carbon nitride-based nanocomposites as promising visible-light-driven photocatalysts. *J. Mater. Sci. Mater. Electron.* **2018**, *29*, 1719-1747.
100. Mokhbi, Y.; Korichi, M.; Akchiche, Z. Combined photocatalytic and Fenton oxidation for oily wastewater treatment. *Appl. Water Sci.* **2019**, *9*, 35.
101. Ramadan, W.; Dillert, R.; Koch, J.; Tegenkamp, C.; Bahnemann, D.W. Changes in the solid-state properties of bismuth iron oxide during the photocatalytic reformation of formic acid. *Catal. Today* **2019**, *326*, 22-29.
102. AlSalka, Y.; Granone, L.I.; Ramadan, W.; Hakki, A.; Dillert, R.; Bahnemann, D.W. Iron-based photocatalytic and photoelectrocatalytic nano-structures: Facts, perspectives, and expectations. *Appl. Catal. B* **2019**, *244*, 1065-1095.
103. Raza, W.; Haque, M.M.; Muneer, M.; Bahnemann, D. Synthesis of visible light driven TiO₂ coated carbon nanospheres for degradation of dyes. *Arab. J. Chem.* **2019**, *12*, 3534-3545.
104. Al-Madanat, O.; AlSalka, Y.; Curti, M.; Dillert, R.; Bahnemann, D.W. Mechanistic insights into hydrogen evolution by photocatalytic reforming of naphthalene. *ACS Catal.* **2020**, *10*, 7398-7412.
105. AlSalka, Y.; Al-Madanat, O.; Curti, M.; Hakki, A.; Bahnemann, D. W., Photocatalytic H₂ evolution from oxalic acid: effect of cocatalysts and carbon dioxide radical anion on the surface charge transfer mechanisms. *ACS Appl. Energy Mater.* **2020**, *3* (7), 6678-6691.
106. Megatif, L.; Dillert, R.; Bahnemann, D. W., Reaction rate study of the photocatalytic degradation of dichloroacetic acid in a black body reactor. *Catalysts* **2019**, *9* (8), 635.
107. Faycal Atitar, M.; Ismail, A. A.; Dillert, R.; Bahnemann, D. W., Photodegradation of herbicide imazapyr and phenol over mesoporous bicrystalline phases TiO₂: A Kinetic study. *Catalysts* **2019**, *9* (8), 640.
108. Jagadale, T.; Kulkarni, M.; Pravarthana, D.; Ramadan, W.; Thakur, P. Photocatalytic degradation of azo dyes using Au:TiO₂, gamma-Fe₂O₃:TiO₂ functional nanosystems. *J. Nanosci. Nanotechnol.* **2012**, *12*, 928-936.

109. Fox, M.A.; Dulay, M.T. Heterogeneous photocatalysis. *Chem. Rev.* **1993**, *93*, 341–357.
110. Schneider, J.; Matsuoka, M.; Takeuchi, M.; Zhang, J.; Horiuchi, Y.; Anpo, M.; Bahnemann, D. W., Understanding TiO₂ photocatalysis: mechanisms and materials. *Chem. Rev.* **2014**, *114* (19), 9919-86.
111. Shayegan, Z.; Lee, C.-S.; Haghghat, F., TiO₂ photocatalyst for removal of volatile organic compounds in gas phase – A review. *Chem. Eng. J.* **2018**, *334*, 2408-2439.
112. Pelaez, M.; Nolan, N. T.; Pillai, S. C.; Seery, M. K.; Falaras, P.; Kontos, A. G.; Dunlop, P. S. M.; Hamilton, J. W. J.; Byrne, J. A.; O'Shea, K.; Entezari, M. H.; Dionysiou, D. D., A review on the visible light active titanium dioxide photocatalysts for environmental applications. *Appl. Catal., B* **2012**, *125*, 331-349.
113. Choquette-Labbé, M.; Shewa, W.; Lalman, J.; Shanmugam, S., Photocatalytic degradation of phenol and phenol derivatives using a nano-TiO₂ catalyst: Integrating quantitative and qualitative factors using response surface methodology. *Water* **2014**, *6* (6), 1785-1806.
114. Kamat, P.V. Meeting the clean energy demand: Nanostructure architectures for solar energy conversion. *J. Phys. Chem. C* **2007**, *111*, 2834–2860.
115. Etacheri, V.; Di Valentin, C.; Schneider, J.; Bahnemann, D.; Pillai, S. C., Visible-light activation of TiO₂ photocatalysts: Advances in theory and experiments. *J. Photochem. Photobiol., C* **2015**, *25*, 1-29.
116. Rachna; Rani, M.; Shanker, U., Sunlight mediated improved photocatalytic degradation of carcinogenic benz[a]anthracene and benzo[a]pyrene by zinc oxide encapsulated hexacyanoferrate nanocomposite. *J. Photochem. Photobiol., A* **2019**, *381*, 111861.
117. Fu, J.; Kyzas, G. Z.; Cai, Z.; Deliyanni, E. A.; Liu, W.; Zhao, D., Photocatalytic degradation of phenanthrene by graphite oxide-TiO₂-Sr(OH)₂/SrCO₃ nanocomposite under solar irradiation: Effects of water quality parameters and predictive modeling. *Chem. Eng. J.* **2018**, *335*, 290-300.
118. El-Mekkawi, D. M.; Abdelwahab, N. A.; Mohamed, W. A. A.; Taha, N. A.; Abdel-Mottaleb, M. S. A., Solar photocatalytic treatment of industrial wastewater utilizing recycled polymeric disposals as TiO₂ supports. *J. Cleaner Prod.* **2020**, *249*, 119430.
119. Horikoshi, S.; Serpone, N., Can the photocatalyst TiO₂ be incorporated into a wastewater treatment method? Background and prospects. *Catal. Today* **2020**, *340*, 334-346.
120. Zhai, S.; Zhu, G.; Wei, X.; Ge, M. Enhanced catalytic degradation of polyvinyl alcohol from aqueous solutions by novel synthesis of MnCoO₃@ γ -Al₂O₃ nanocomposites: Performance, degradation intermediates and mechanism. *J. Mol. Liq.* **2021**, *323*, 114569.
121. Sola, A. C.; Ramírez de la Piscina, P.; Homs, N., Behaviour of Pt/TiO₂ catalysts with different morphological and structural characteristics in the photocatalytic conversion of ethanol aqueous solutions. *Catal. Today* **2020**, *341*, 13-20.
122. Ivanova, I.; Schneider, J.; Gutzmann, H.; Kliemann, J.-O.; Gärtner, F.; Klassen, T.; Bahnemann, D.; Mendive, C. B., Photocatalytic degradation of oxalic and dichloroacetic acid on TiO₂ coated metal substrates. *Catal. Today* **2013**, *209* (Supplement C), 84-90.

123. Hasan, I.; Shekhar, C.; Bin, S., II; Khan, R. A.; Alsalmeh, A., Ecofriendly green synthesis of the ZnO-doped CuO@Alg bionanocomposite for efficient oxidative degradation of p-nitrophenol. *ACS Omega* **2020**, *5* (49), 32011-32022.
124. Wu, S.; Li, X.; Tian, Y.; Lin, Y.; Hu, Y. H., Excellent photocatalytic degradation of tetracycline over black anatase-TiO₂ under visible light. *Chem. Eng. J.* **2021**, *406*, 126747.
125. Miao, Y.; Xu, X.; Liu, K.; Yu, S.; Wang, Y.; Yang, S., Preparation and activity evaluation of the novel Cu/TiO₂ nanometer photocatalytic materials. *Sci. Adv. Mater.* **2020**, *12* (7), 1027-1033.
126. Rani, M.; Shanker, U.; Yadav, J.; Keshu, Degradation of pesticides residue by engineered nanomaterials. In *Sustainable agriculture reviews 48*, Inamuddin; Ahamed, M. I.; Lichtfouse, E., Eds. Springer International Publishing: Cham, 2021; pp 259-310.
127. Park, H.; Kim, H.-i.; Moon, G.-h.; Choi, W. Photoinduced charge transfer processes in solar photocatalysis based on modified TiO₂. *Energy Environ. Sci.* **2016**, *9*, 411-433.
128. Kumaravel, V.; Mathew, S.; Bartlett, J.; Pillai, S. C., Photocatalytic hydrogen production using metal doped TiO₂: A review of recent advances. *Appl. Catal., B* **2019**, *244*, 1021-1064.
129. Pellegrino, F.; Sordello, F.; Mino, L.; Minero, C.; Hodoroaba, V.-D.; Martra, G.; Maurino, V., Formic acid photoreforming for hydrogen production on shape-controlled anatase TiO₂ nanoparticles: Assessment of the role of fluorides, (101)/(001) surfaces ratio, and platinization. *ACS Catal.* **2019**, *9* (8), 6692-6697.
130. Kampouri, S.; Stylianou, K. C., Dual-functional photocatalysis for simultaneous hydrogen production and oxidation of organic substances. *ACS Catal.* **2019**, *9* (5), 4247-4270.
131. AlSalka, Y.; Hakki, A.; Fleisch, M.; Bahnemann, D.W. Understanding the degradation pathways of oxalic acid in different photocatalytic systems: Towards simultaneous photocatalytic hydrogen evolution. *J. Photochem. Photobiol. A* **2018**, *366*, 81-90.
132. Hakki, A.; AlSalka, Y.; Mendive, C. B.; Ubogui, J.; dos Santos Claro, P. C.; Bahnemann, D., Hydrogen production by heterogeneous photocatalysis. In *Encyclopedia of Interfacial Chemistry*, Wandelt, K., Ed. Elsevier: Oxford, 2018; pp 413-419.
133. Sivula, K.; Van De Krol, R., Semiconducting materials for photoelectrochemical energy conversion. *Nat. Rev. Mater.* **2016**, *1* (2), 15010.
134. Takanabe, K.; Domen, K., Toward visible light response: overall water splitting using heterogeneous photocatalysts. *Green* **2011**, *1* (5-6), 313-322.
135. Maeda, K.; Domen, K. Photocatalytic water splitting: Recent progress and future challenges. *J. Phys. Chem. Lett.* **2010**, *1*, 2655-2661.
136. Cao, W., Semiconductor Photocatalysis: Materials, Mechanisms and Applications. BoD-Books on Demand: 2016.
137. Jiang, C.; Moniz, S.J.; Wang, A.; Zhang, T.; Tang, J. Photoelectrochemical devices for solar water splitting—materials and challenges. *Chem. Soc. Rev.* **2017**, *46*, 4645-4660.
138. Kisch, H., Semiconductor Photocatalysis Principle and Applications. Wiley-VCH: 2015.

139. Friehs, E.; AlSalka, Y.; Jonczyk, R.; Lavrentieva, A.; Jochums, A.; Walter, J.-G.; Stahl, F.; Scheper, T.; Bahnemann, D., Toxicity, phototoxicity and biocidal activity of nanoparticles employed in photocatalysis. *J. Photochem. Photobiol., C* **2016**, *29*, 1-28.
140. Hernández-Ramírez, A.; Medina-Ramírez, I., Semiconducting materials. In *Photocatalytic semiconductors*, Hernández-Ramírez, A.; Medina-Ramírez, I., Eds. Springer International Publishing: Cham, 2015; pp 1-40.
141. Barr, A., Electrical properties of semiconductors. In *Electronic Materials*, Miller, L. S.; Mullin, J. B., Eds. Springer US: Boston, MA, 1991; pp 19-24.
142. Fonash, S. J., Structures, materials, and scale. In *Solar cell device physics*, Fonash, S. J., Ed. Academic Press: Boston, 2010; pp 67-120.
143. Hoffmann, M.R.; Martin, S.T.; Choi, W.; Bahnemann, D.W. Environmental applications of semiconductor photocatalysis. *Chem. Rev.* **1995**, *95*, 69–96.
144. Mills, A.; Le Hunte, S., An overview of semiconductor photocatalysis. *J. Photochem. Photobiol., A* **1997**, *108* (1), 1-35.
145. Linsebigler, A. L.; Lu, G.; Yates Jr, J. T., Photocatalysis on TiO₂ surfaces: Principles, mechanisms, and selected results. *Chem. Rev.* **1995**, *95* (3), 735-758.
146. Wang, F.; Li, Q.; Xu, D., Recent progress in semiconductor-based nanocomposite photocatalysts for solar-to-chemical energy conversion. *Adv. Energy Mater.* **2017**, *7* (23), 1700529.
147. Takanabe, K. Photocatalytic water splitting: Quantitative approaches toward photocatalyst by design. *ACS Catal.* **2017**, *7*, 8006–8022.
148. Peter, L. M., Photoelectrochemistry: from basic principles to photocatalysis. In *Photocatalysis: Fundamentals and perspectives*, The Royal Society of Chemistry: 2016; pp 1-28.
149. Habisreutinger, S. N.; Schmidt-Mende, L.; Stolarczyk, J. K., Photocatalytic reduction of CO₂ on TiO₂ and other semiconductors. *Angew. Chem. Int. Ed.* **2013**, *52* (29), 7372-7408.
150. AlSalka, Y.; Hakki, A.; Schneider, J.; Bahnemann, D. W., Co-catalyst-free photocatalytic hydrogen evolution on TiO₂: Synthesis of optimized photocatalyst through statistical material science. *Appl. Catal., B* **2018**, *238*, 422-433.
151. Walter, M. G.; Warren, E. L.; McKone, J. R.; Boettcher, S. W.; Mi, Q.; Santori, E. A.; Lewis, N. S., Solar water splitting cells. *Chem. Rev.* **2010**, *110* (11), 6446-73.
152. Ohtani, B., Photocatalysis A to Z—What we know and what we do not know in a scientific sense. *J. Photochem. Photobiol., C* **2010**, *11* (4), 157-178.
153. Pichat, P., A brief overview of photocatalytic mechanisms and pathways in water. *Water Sci. Technol.* **2007**, *55* (12), 167-73.
154. Ni, M.; Leung, M. K.; Leung, D. Y.; Sumathy, K., A review and recent developments in photocatalytic water-splitting using TiO₂ for hydrogen production. *Renewable and Sustainable Energy Reviews* **2007**, *11* (3), 401-425.
155. Schneider, J.; Kandiel, T. A.; Bahnemann, D. W., Solar photocatalytic hydrogen production: Current status and future challenges. In *Materials and processes for solar fuel production*,

- Viswanathan, B.; Subramanian, V.; Lee, J. S., Eds. Springer New York: New York, NY, 2014; pp 41-74.
156. Cho, Y. J.; Moon, G. H.; Kanazawa, T.; Maeda, K.; Choi, W., Selective dual-purpose photocatalysis for simultaneous H₂ evolution and mineralization of organic compounds enabled by a Cr₂O₃ barrier layer coated on Rh/SrTiO₃. *Chem. Commun.* **2016**, 52 (62), 9636-9639.
157. Shimura, K.; Yoshida, H. Heterogeneous photocatalytic hydrogen production from water and biomass derivatives. *Energy Environ. Sci.* **2011**, 4, 2467-2481.
158. Jeon, T.H.; Koo, M.S.; Kim, H.; Choi, W. Dual-functional photocatalytic and photoelectrocatalytic systems for energy- and resource-recovering water treatment. *ACS Catal.* **2018**, 8, 11542-11563.
159. Ohtani, B. Photocatalysis A to Z—What we know and what we do not know in a scientific sense. *J. Photochem. Photobiol. C* 2010, 11, 157-178.
160. Balayeva, N. O.; Zheng, N.; Dillert, R.; Bahnemann, D. W., Visible-light-mediated photocatalytic aerobic dehydrogenation of N-heterocycles by surface-grafted TiO₂ and 4-amino-TEMPO. *ACS Catal.* **2019**, 9 (12), 10694-10704.
161. Zhang, L.; Jiang, D.; Irfan, R. M.; Tang, S.; Chen, X.; Du, P., Highly efficient and selective photocatalytic dehydrogenation of benzyl alcohol for simultaneous hydrogen and benzaldehyde production over Ni-decorated Zn_{0.5}Cd_{0.5}S solid solution. *J. Energy Chem.* **2019**, 30, 71-77.
162. Zheng, Y.W.; Chen, B.; Ye, P.; Feng, K.; Wang, W.; Meng, Q.Y.; Wu, L.Z.; Tung, C.H. Photocatalytic hydrogen-evolution cross-couplings: Benzene C-H amination and hydroxylation. *J. Am. Chem. Soc.* **2016**, 138, 10080-10083.
163. Puga, A. V., Photocatalytic production of hydrogen from biomass-derived feedstocks. *Coord. Chem. Rev.* **2016**, 315, 1-66.
164. Schneider, J.; Bahnemann, D. W., Undesired role of sacrificial reagents in photocatalysis. *J. Phys. Chem. Lett.* **2013**, 4 (20), 3479-3483.
165. Chen, X.; Shen, S.; Guo, L.; Mao, S. S., Semiconductor-based photocatalytic hydrogen generation. *Chem. Rev.* **2010**, 110 (11), 6503-70.
166. Kandiel, T. A.; Ivanova, I.; Bahnemann, D. W., Long-term investigation of the photocatalytic hydrogen production on platinumized TiO₂: an isotopic study. *Energy Environ. Sci.* **2014**, 7 (4), 1420-1425.
167. Al-Madanat, O.; AlSalka, Y.; Dillert, R.; Bahnemann, D., Photocatalytic H₂ production from naphthalene by various TiO₂ photocatalysts: Impact of Pt loading and formation of intermediates. *Catalysts* **2021**, 11 (1), 107.
168. Bahruji, H.; Bowker, M.; Davies, P.R.; Morgan, D.J.; Morton, C.; Egerton, T.; Kennedy, J.; Jones, W. Rutile TiO₂-Pd photocatalysts for hydrogen gas production from methanol reforming. *Top. Catal.* **2015**, 58, 70-76.

169. Ismail, A.A.; Robben, L.; Bahnemann, D.W. Study of the efficiency of UV and visible-light photocatalytic oxidation of methanol on mesoporous RuO₂-TiO₂ nanocomposites. *ChemPhysChem* **2011**, *12*, 982–991.
170. Prairie, M. R.; Evans, L. R.; Stange, B. M.; Martinez, S. L., An investigation of titanium dioxide photocatalysis for the treatment of water contaminated with metals and organic chemicals. *Environ. Sci. Technol.* **1993**, *27* (9), 1776-1782.
171. Mo, S. D.; Ching, W. Y., Electronic and optical properties of three phases of titanium dioxide: Rutile, anatase, and brookite. *Phys. Rev. B* **1995**, *51* (19), 13023-13032.
172. Enke, C. G., Nonstoichiometry, diffusion, and electrical conductivity in binary metal oxides. (Wiley series on the science and technology of materials). P. Kofstad. 160 Abb. 11 Tab. XI, 382 S. Ca. 1060 Schrifttumshinweise. Format 15.5 × 23 cm. Wiley Interscience (J. Wiley & Sons, Inc.) New York-London-Sydney-Toronto, 1972. Gebunden ca. DM 52. *Werkst. Korros.* **1974**, *25* (10), 801-802.
173. Chretien, S.; Metiu, H. Electronic structure of partially reduced rutile TiO₂ (110) surface: Where are the unpaired electrons located? *J. Phys. Chem. C* **2011**, *115*, 4696–4705.
174. Diebold, U., The surface science of titanium dioxide. *Surf. Sci. Rep.* **2003**, *48* (5-8), 53-229.
175. Qian, R.; Zong, H.; Schneider, J.; Zhou, G.; Zhao, T.; Li, Y.; Yang, J.; Bahnemann, D.W.; Pan, J.H. Charge carrier trapping, recombination and transfer during TiO₂ photocatalysis: An overview. *Catal. Today* **2019**, *335*, 78–90.
176. Kohtani, S.; Kawashima, A.; Miyabe, H., Reactivity of trapped and accumulated electrons in titanium dioxide photocatalysis. *Catalysts* **2017**, *7* (10), 303.
177. Serpone, N.; Lawless, D.; Khairutdinov, R., Size effects on the photophysical properties of colloidal anatase TiO₂ particles: size quantization versus direct transitions in this indirect semiconductor? *J Phys Chem-US* **1995**, *99* (45), 16646-16654.
178. Stevanovic, A.; Yates Jr, J. T., Probe of NH₃ and CO adsorption on the very outermost surface of a porous TiO₂ adsorbent using photoluminescence spectroscopy. *Langmuir* **2012**, *28* (13), 5652-5659.
179. Yoshihara, T.; Katoh, R.; Furube, A.; Tamaki, Y.; Murai, M.; Hara, K.; Murata, S.; Arakawa, H.; Tachiya, M., Identification of reactive species in photoexcited nanocrystalline TiO₂ films by wide-wavelength-range (400– 2500 nm) transient absorption spectroscopy. *J Phys Chem B* **2004**, *108* (12), 3817-3823.
180. Howe, R.F.; Gratzel, M. EPR study of hydrated anatase under UV irradiation. *J. Phys. Chem.* **1987**, *91*, 3906–3909.
181. Howe, R. F.; Gratzel, M., EPR observation of trapped electrons in colloidal titanium dioxide. *J. Phys. Chem.* **1985**, *89* (21), 4495-4499.
182. Wu, C.-Y.; Tu, K.-J.; Deng, J.-P.; Lo, Y.-S.; Wu, C.-H., Markedly enhanced surface hydroxyl groups of TiO₂ nanoparticles with superior water-dispersibility for photocatalysis. *Materials* **2017**, *10* (5), 566.
183. Augustynski, J. The role of the surface intermediates in the photoelectrochemical behaviour of anatase and rutile TiO₂. *Electrochim. Acta* **1993**, *38*, 43–46.

184. Zhang, J.; Zhou, P.; Liu, J.; Yu, J. New understanding of the difference of photocatalytic activity among anatase, rutile and brookite TiO₂. *PCCP* **2014**, *16*, 20382–20386.
185. Sachs, M.; Pastor, E.; Kafizas, A.; Durrant, J.R. Evaluation of surface state mediated charge recombination in anatase and rutile TiO₂. *J. Phys. Chem. Lett.* **2016**, *7*, 3742–3746.
186. Knorr, F.J.; Mercado, C.C.; McHale, J.L. Trap-state distributions and carrier transport in pure and mixed-phase TiO₂: Influence of contacting solvent and interphasial electron transfer. *J. Phys. Chem. C* **2008**, *112*, 12786–12794.
187. Wang, X.; Feng, Z.; Shi, J.; Jia, G.; Shen, S.; Zhou, J.; Li, C. Trap states and carrier dynamics of TiO₂ studied by photoluminescence spectroscopy under weak excitation condition. *PCCP* **2010**, *12*, 7083–7090.
188. Wang, X.; Kafizas, A.; Li, X.; Moniz, S.J.A.; Reardon, P.J.T.; Tang, J.; Parkin, I.P.; Durrant, J.R. Transient absorption spectroscopy of anatase and rutile: The impact of morphology and phase on photocatalytic activity. *J. Phys. Chem. C* **2015**, *119*, 10439–10447.
189. Kim, W.; Tachikawa, T.; Moon, G. H.; Majima, T.; Choi, W., Molecular-level understanding of the photocatalytic activity difference between anatase and rutile nanoparticles. *Angew. Chem. Int. Ed.* **2014**, *53* (51), 14036-41.
190. Schindler, K.M.; Kunst, M. Charge-carrier dynamics in titania powders. *J. Phys. Chem.* **1990**, *94*, 8222–8226.
191. Hurum, D.C.; Agrios, A.G.; Gray, K.A.; Rajh, T.; Thurnauer, M.C. Explaining the enhanced photocatalytic activity of degussa P25 mixed-phase TiO₂ using EPR. *J. Phys. Chem. B* **2003**, *107*, 4545–4549.
192. Choi, W.; Termin, A.; Hoffmann, M.R. The role of metal ion dopants in quantum-sized TiO₂: Correlation between photoreactivity and charge carrier recombination dynamics. *J. Phys. Chem.* **1994**, *98*, 13669–13679.
193. Asahi, R.; Morikawa, T.; Ohwaki, T.; Aoki, K.; Taga, Y., Visible-light photocatalysis in nitrogen-doped titanium oxides. *Science* **2001**, *293* (5528), 269-71.
194. Weber, M. F.; Dignam, M. J., Efficiency of splitting water with semiconducting photoelectrodes. *J. Electrochem. Soc.* **1984**, *131* (6), 1258-1265.
195. Bahnemann, D.; Henglein, A.; Lilie, J.; Spanhel, L., Flash photolysis observation of the absorption spectra of trapped positive holes and electrons in colloidal titanium dioxide. *J. Phys. Chem.* **1984**, *88* (4), 709-711.
196. Erdey-Grúz, T.; Volmer, M., Zur theorie der wasserstoff überspannung. *Z. Phys. Chem.* **1930**, *150* (1), 203-213.
197. Kasarevic-Popovic, Z.; Behar, D.; Rabani, J. Role of excess electrons in TiO₂ nanoparticles coated with Pt in reduction reactions studied in radiolysis of aqueous solutions. *J. Phys. Chem. B* **2004**, *108*, 20291–20295.
198. Hu, C.; Lv, C.; Liu, S.; Shi, Y.; Song, J. F.; Zhang, Z.; Cai, J. G.; Watanabe, A., Nickel phosphide electrocatalysts for hydrogen evolution reaction. *Catalysts* **2020**, *10* (2), 188.

199. Michaelson, H. B., The work function of the elements and its periodicity. *J. Appl. Phys.* **1977**, *48* (11), 4729-4733.
200. Xiong, G.; Shao, R.; Droubay, T. C.; Joly, A. G.; Beck, K. M.; Chambers, S. A.; Hess, W. P., Photoemission electron microscopy of TiO₂ anatase films embedded with rutile nanocrystals. *Adv. Funct. Mater.* **2007**, *17* (13), 2133-2138.
201. Di Bartolomeo, A., Graphene Schottky diodes: An experimental review of the rectifying graphene/semiconductor heterojunction. *Phys. Rep.* **2016**, *606*, 1-58.
202. Iwata, K.; Takaya, T.; Hamaguchi, H.-o.; Yamakata, A.; Ishibashi, T.-a.; Onishi, H.; Kuroda, H., Carrier dynamics in TiO₂ and Pt/TiO₂ powders observed by femtosecond time-resolved near-infrared spectroscopy at a spectral region of 0.9– 1.5 μm with the direct absorption method. *J. Phys. Chem. B* **2004**, *108* (52), 20233-20239.
203. Yamakata, A.; Ishibashi, T.-a.; Kato, H.; Kudo, A.; Onishi, H., Photodynamics of NaTaO₃ catalysts for efficient water splitting. *J. Phys. Chem. B* **2003**, *107* (51), 14383-14387.
204. Yamakata, A.; Ishibashi, T.-a.; Onishi, H., Water-and oxygen-induced decay kinetics of photogenerated electrons in TiO₂ and Pt/TiO₂: a time-resolved infrared absorption study. *J. Phys. Chem. B* **2001**, *105* (30), 7258-7262.
205. Fu, X.; Long, J.; Wang, X.; Leung, D.; Ding, Z.; Wu, L.; Zhang, Z.; Li, Z.; Fu, X. Photocatalytic reforming of biomass: A systematic study of hydrogen evolution from glucose solution. *Int. J. Hydrog. Energy* **2008**, *33*, 6484–6491.
206. Jang, J.S.; Ji, S.M.; Bae, S.W.; Son, H.C.; Lee, J.S. Optimization of CdS/TiO₂ nano-bulk composite photocatalysts for hydrogen production from Na₂S/Na₂SO₃ aqueous electrolyte solution under visible light ($\lambda \geq 420$ nm). *J. Photochem. Photobiol. A* **2007**, *188*, 112–119.
207. Sabatier, P., Hydrogénations et déshydrogénations par catalyse. *Ber. Dtsch. Chem. Ges.* **1911**, *44* (3), 1984-2001.
208. Trasatti, S. Work function, electronegativity, and electrochemical behaviour of metals: III. Electrolytic hydrogen evolution in acid solutions. *J. Electroanal. Chem. Interfacial Electrochem.* **1972**, *39*, 163–184.
209. Nørskov, J. K.; Bligaard, T.; Logadottir, A.; Kitchin, J.; Chen, J. G.; Pandelov, S.; Stimming, U., Trends in the exchange current for hydrogen evolution. *J. Electrochem. Soc.* **2005**, *152* (3), J23-J26.
210. Bamwenda, G. R.; Tsubota, S.; Nakamura, T.; Haruta, M., Photoassisted hydrogen production from a water-ethanol solution: a comparison of activities of Au-TiO₂ and Pt-TiO₂. *J. Photochem. Photobiol., A* **1995**, *89* (2), 177-189.
211. Sheng, W.; Myint, M.; Chen, J.G.; Yan, Y. Correlating the hydrogen evolution reaction activity in alkaline electrolytes with the hydrogen binding energy on monometallic surfaces. *Energy Environ. Sci.* **2013**, *6*, 1509–1512.
212. Naldoni, A.; D'Arienzo, M.; Altomare, M.; Marelli, M.; Scotti, R.; Morazzoni, F.; Selli, E.; Dal Santo, V., Pt and Au/TiO₂ photocatalysts for methanol reforming: Role of metal nanoparticles in tuning charge trapping properties and photoefficiency. *Appl. Catal., B* **2013**, *130-131*, 239-248.

213. Park, H.; Reddy, D. A.; Kim, Y.; Lee, S.; Ma, R.; Kim, T. K., Synthesis of ultra-small palladium nanoparticles deposited on CdS nanorods by pulsed laser ablation in liquid: Role of metal nanocrystal size in the photocatalytic hydrogen production. *Chemistry* **2017**, *23* (53), 13112-13119.
214. Wenderich, K.; Mul, G., Methods, mechanism, and applications of photodeposition in photocatalysis: A review. *Chem. Rev.* **2016**, *116* (23), 14587-14619.
215. Pei, Z.; Weng, S.; Liu, P., Enhanced photocatalytic activity by bulk trapping and spatial separation of charge carriers: A case study of defect and facet mediated TiO₂. *Appl. Catal., B* **2016**, *180*, 463-470.
216. Saravanan, R.; Gracia, F.; Stephen, A., Basic principles, mechanism, and challenges of photocatalysis. In *Nanocomposites for visible light-induced photocatalysis*, Khan, M. M.; Pradhan, D.; Sohn, Y., Eds. Springer International Publishing: Cham, 2017; pp 19-40.
217. Al-Azri, Z. H. N.; Chen, W.-T.; Chan, A.; Jovic, V.; Ina, T.; Idriss, H.; Waterhouse, G. I. N., The roles of metal co-catalysts and reaction media in photocatalytic hydrogen production: Performance evaluation of M/TiO₂ photocatalysts (M = Pd, Pt, Au) in different alcohol–water mixtures. *J. Catal.* **2015**, *329*, 355-367.
218. Al-Azri, Z. H. N.; AlOufi, M.; Chan, A.; Waterhouse, G. I. N.; Idriss, H., Metal particle size effects on the photocatalytic hydrogen ion reduction. *ACS Catal.* **2019**, *9* (5), 3946-3958.
219. Bamwenda, G. R.; Tsubota, S.; Nakamura, T.; Haruta, M., The influence of the preparation methods on the catalytic activity of platinum and gold supported on TiO₂ for CO oxidation. *Catal. Lett.* **1997**, *44* (1/2), 83-87.
220. Kozlova, E. A.; Lyubina, T. P.; Nasalevich, M. A.; Vorontsov, A. V.; Miller, A. V.; Kaichev, V. V.; Parmon, V. N., Influence of the method of platinum deposition on activity and stability of Pt/TiO₂ photocatalysts in the photocatalytic oxidation of dimethyl methylphosphonate. *Catal. Commun.* **2011**, *12* (7), 597-601.
221. Marzun, G.; Streich, C.; Jendrzej, S.; Barcikowski, S.; Wagener, P., Adsorption of colloidal platinum nanoparticles to supports: charge transfer and effects of electrostatic and steric interactions. *Langmuir* **2014**, *30* (40), 11928-36.
222. Wang, C.-y.; Pagel, R.; Bahnemann, D. W.; Dohrmann, J. K., Quantum yield of formaldehyde formation in the presence of colloidal TiO₂-based photocatalysts: Effect of intermittent illumination, platinization, and deoxygenation. *J. Phys. Chem. B* **2004**, *108* (37), 14082-14092.
223. Haselmann, G. M.; Eder, D., Early-stage deactivation of platinum-loaded TiO₂ using in situ photodeposition during photocatalytic hydrogen evolution. *ACS Catal.* **2017**, *7* (7), 4668-4675.
224. Li, F. B.; Li, X. Z., The enhancement of photodegradation efficiency using Pt–TiO₂ catalyst. *Chemosphere* **2002**, *48* (10), 1103-1111.
225. Siuzdak, K.; Sawczak, M.; Klein, M.; Nowaczyk, G.; Jurga, S.; Cenia, A. Preparation of platinum modified titanium dioxide nanoparticles with the use of laser ablation in water. *Phys. Chem. Chem. Phys.* **2014**, *16*, 15199–15206.

226. Murcia, J. J.; Navío, J. A.; Hidalgo, M. C., Insights towards the influence of Pt features on the photocatalytic activity improvement of TiO₂ by platinisation. *Appl. Catal., B* **2012**, *126*, 76-85.
227. Farsinezhad, S.; Sharma, H.; Shankar, K. Interfacial band alignment for photocatalytic charge separation in TiO₂ nanotube arrays coated with CuPt nanoparticles. *Phys. Chem. Chem. Phys.* **2015**, *17*, 29723–29733.
228. Wang, C.; Yin, L.; Zhang, L.; Liu, N.; Lun, N.; Qi, Y., Platinum-nanoparticle-modified TiO₂ nanowires with enhanced photocatalytic property. *ACS Appl. Mater. Interfaces* **2010**, *2* (11), 3373-7.
229. Kang, J.-G.; Sohn, Y. Interfacial nature of Ag nanoparticles supported on TiO₂ photocatalysts. *J. Mater. Sci.* **2011**, *47*, 824–832.
230. Zhang, L.; Mohamed, H. H.; Dillert, R.; Bahnemann, D., Kinetics and mechanisms of charge transfer processes in photocatalytic systems: A review. *J. Photochem. Photobiol., C* **2012**, *13*, 263-276.
231. Mohamed, H. H.; Bahnemann, D. W., The role of electron transfer in photocatalysis: Fact and fictions. *Appl. Catal., B* **2012**, *128*, 91-104.
232. Wang, Z.; Li, C.; Domen, K., Recent developments in heterogeneous photocatalysts for solar-driven overall water splitting. *Chem. Soc. Rev.* **2019**, *48* (7), 2109-2125.
233. Wei, Z.; Janczarek, M.; Endo, M.; Wang, K.; Balcytis, A.; Nitta, A.; Mendez-Medrano, M.G.; Colbeau-Justin, C.; Juodkazis, S.; Ohtani, B.; et al. Noble metal-modified faceted anatase titania photocatalysts: Octahedron versus decahedron. *Appl. Catal. B* **2018**, *237*, 574–587.
234. Sreethawong, T.; Yoshikawa, S., Impact of Pt loading methods over mesoporous-assembled TiO₂-ZrO₂ mixed oxide nanocrystal on photocatalytic dye-sensitized H₂ production activity. *Mater. Res. Bull.* **2012**, *47* (6), 1385-1395.
235. Kraeutler, B.; Bard, A. J., Heterogeneous photocatalytic preparation of supported catalysts. Photodeposition of platinum on titanium dioxide powder and other substrates. *J. Am. Chem. Soc.* **1978**, *100* (13), 4317-4318.
236. Kumar, S.G.; Rao, K.S.R.K. Comparison of modification strategies towards enhanced charge carrier separation and photocatalytic degradation activity of metal oxide semiconductors (TiO₂, WO₃ and ZnO). *Appl. Surf. Sci.* **2017**, *391*, 124–148.
237. Chen, H. W.; Ku, Y.; Kuo, Y. L., Effect of Pt/TiO₂ characteristics on temporal behavior of o-cresol decomposition by visible light-induced photocatalysis. *Water Res.* **2007**, *41* (10), 2069-78.
238. Li, J.; Xu, J.; Dai, W.-L.; Fan, K., Dependence of Ag deposition methods on the photocatalytic activity and surface state of TiO₂ with twistlike helix structure. *J. Phys. Chem. C* **2009**, *113* (19), 8343-8349.
239. Elghniji, K.; Hentati, O.; Mlaik, N.; Mahfoudh, A.; Ksibi, M., Photocatalytic degradation of 4-chlorophenol under P-modified TiO₂/UV system: kinetics, intermediates, phytotoxicity and acute toxicity. *J. Environ. Sci. (China)* **2012**, *24* (3), 479-87.

240. Yoshida, H., Photocatalytic organic syntheses. In *Environmentally Benign Photocatalysts*, Anpo, M.; Kamat, P. V., Eds. Springer New York: New York, NY, 2010; pp 647-669.
241. Szczepanik, B., Photocatalytic degradation of organic contaminants over clay-TiO₂ nanocomposites: A review. *Appl. Clay Sci.* **2017**, *141*, 227-239.
242. Vasseghian, Y.; Khataee, A.; Dragoi, E.-N.; Moradi, M.; Nabavifard, S.; Oliveri Conti, G.; Mousavi Khaneghah, A. Pollutants degradation and power generation by photocatalytic fuel cells: A comprehensive review. *Arab. J. Chem.* **2020**, *13*, 8458–8480.
243. Benz, D.; Felter, K. M.; Koser, J.; Thoming, J.; Mul, G.; Grozema, F. C.; Hintzen, H. T.; Kreutzer, M. T.; van Ommen, J. R., Assessing the role of Pt clusters on TiO₂ (P25) on the photocatalytic degradation of Acid Blue 9 and Rhodamine B. *J. Phys. Chem. C* **2020**, *124* (15), 8269-8278.
244. Ajmal, A.; Majeed, I.; Malik, R. N.; Idriss, H.; Nadeem, M. A., Principles and mechanisms of photocatalytic dye degradation on TiO₂ based photocatalysts: a comparative overview. *RSC Advances* **2014**, *4* (70), 37003-37026.
245. Qourzal, S.; Barka, N.; Tamimi, M.; Assabbane, A.; Nounah, A.; Ihlal, A.; Ait-Ichou, Y., Sol–gel synthesis of TiO₂–SiO₂ photocatalyst for β-naphthol photodegradation. *Mater. Sci. Eng. C* **2009**, *29* (5), 1616-1620.
246. Antharjanam, S.; Philip, R.; Suresh, D., Photocatalytic degradation of wastewater pollutants: titanium dioxide mediated degradation of methyl orange and beta-naphthol orange. *Ann Chim* **2003**, *93* (9-10), 719-28.
247. Hashimoto, K.; Kawai, T.; Sakata, T. Photocatalytic reactions of hydrocarbons and fossil-fuels with water—Hydrogen production and oxidation. *J. Phys. Chem.* **1984**, *88*, 4083–4088.
248. Kim, J.; Choi, W., Hydrogen producing water treatment through solar photocatalysis. *Energy Environ. Sci.* **2010**, *3* (8), 1042.
249. Yuzawa, H.; Kumagai, J.; Yoshida, H. Reaction mechanism of aromatic ring amination of benzene and substituted benzenes by aqueous ammonia over platinum-loaded titanium oxide photocatalyst. *J. Phys. Chem. C* **2013**, *117*, 11047–11058.
250. Yuzawa, H.; Aoki, M.; Otake, K.; Hattori, T.; Itoh, H.; Yoshida, H., Reaction mechanism of aromatic ring hydroxylation by water over platinum-loaded titanium oxide photocatalyst. *J. Phys. Chem. C* **2012**, *116* (48), 25376-25387.
251. Yoshida, H.; Yuzawa, H.; Aoki, M.; Otake, K.; Itoh, H.; Hattori, T., Photocatalytic hydroxylation of aromatic ring by using water as an oxidant. *Chem. Commun.* **2008**, (38), 4634-6.
252. Mancuso, A.; Sacco, O.; Sannino, D.; Venditto, V.; Vaiano, V., One-step catalytic or photocatalytic oxidation of benzene to phenol: Possible alternative routes for phenol synthesis? *Catalysts* **2020**, *10* (12), 1424.
253. Kim, J.; Lee, J.; Choi, W., Synergic effect of simultaneous fluorination and platinization of TiO₂ surface on anoxic photocatalytic degradation of organic compounds. *Chem. Commun.* **2008**, (6), 756-8.

254. Sola, A. C.; Homs, N.; Ramírez de la Piscina, P., Photocatalytic H₂ production from ethanol_(aq) solutions: The effect of intermediate products. *Int. J. Hydrog. Energy* **2016**, *41* (43), 19629-19636.
255. Cho, Y.-J.; Kim, H.-i.; Lee, S.; Choi, W., Dual-functional photocatalysis using a ternary hybrid of TiO₂ modified with graphene oxide along with Pt and fluoride for H₂-producing water treatment. *J. Catal.* **2015**, *330*, 387-395.
256. Zhang, X.; Deng, J.; Yan, J.; Song, Y.; Mo, Z.; Qian, J.; Wu, X.; Yuan, S.; Li, H.; Xu, H., Cryo-mediated liquid-phase exfoliated 2D BP coupled with 2D C₃N₄ to photodegrade organic pollutants and simultaneously generate hydrogen. *Appl. Surf. Sci.* **2019**, *490*, 117-123.
257. Jiang, X.-H.; Wang, L.-C.; Yu, F.; Nie, Y.-C.; Xing, Q.-J.; Liu, X.; Pei, Y.; Zou, J.-P.; Dai, W.-L., Photodegradation of organic pollutants coupled with simultaneous photocatalytic evolution of hydrogen using quantum-dot-modified g-C₃N₄ catalysts under visible-light irradiation. *ACS Sustainable Chem. Eng.* **2018**, *6* (10), 12695-12705.
258. Mogyorósi, K.; Kmettykó, Á.; Czirbus, N.; Veréb, G.; Sipos, P.; Dombi, A., Comparison of the substrate dependent performance of Pt-, Au- and Ag-doped TiO₂ photocatalysts in H₂-production and in decomposition of various organics. *React. Kinet. Catal. Lett.* **2009**, *98* (2), 215-225.
259. Vaiano, V.; Iervolino, G., Photocatalytic removal of methyl orange azo dye with simultaneous hydrogen production using Ru-modified ZnO photocatalyst. *Catalysts* **2019**, *9* (11), 964.
260. Chu, K. H.; Ye, L.; Wang, W.; Wu, D.; Chan, D. K. L.; Zeng, C.; Yip, H. Y.; Yu, J. C.; Wong, P. K., Enhanced photocatalytic hydrogen production from aqueous sulfide/sulfite solution by ZnO_{0.6}S_{0.4} with simultaneous dye degradation under visible-light irradiation. *Chemosphere* **2017**, *183*, 219-228.
261. Patsoura, A.; Kondarides, D. I.; Verykios, X. E., Enhancement of photoinduced hydrogen production from irradiated Pt/TiO₂ suspensions with simultaneous degradation of azo-dyes. *Appl. Catal., B* **2006**, *64* (3-4), 171-179.
262. Wu, C.; Yin, M.; Zhang, R.; Li, Z.; Zou, Z.; Li, Z., Further studies of photodegradation and photocatalytic hydrogen production over Nafion-coated Pt/P25 sensitized by rhodamine B. *Int. J. Hydrog. Energy* **2020**, *45* (43), 22700-22710.
263. Mills, A.; Lee, S. K., Platinum group metals and their oxides in semiconductor photosensitisation. *Platinum Met. Rev.* **2003**, *47* (1), 2-12.
264. Montoya, J. F.; Velásquez, J. A.; Salvador, P., The direct–indirect kinetic model in photocatalysis: A reanalysis of phenol and formic acid degradation rate dependence on photon flow and concentration in TiO₂ aqueous dispersions. *Appl. Catal., B* **2009**, *88* (1-2), 50-58.
265. Monllor-Satoca, D.; Gómez, R.; González-Hidalgo, M.; Salvador, P., The “Direct–Indirect” model: An alternative kinetic approach in heterogeneous photocatalysis based on the degree of interaction of dissolved pollutant species with the semiconductor surface. *Catal. Today* **2007**, *129* (1-2), 247-255.
266. Kim, J.; Park, Y.; Park, H. Solar hydrogen production coupled with the degradation of a dye pollutant using TiO₂ modified with platinum and nafion. *Int. J. Photoenergy* **2014**, *2014*, 1-9

267. Howsam, M.; Jones, K. C., Sources of PAHs in the environment. In PAHs and related compounds, Neilson, A. H., Ed. Springer Berlin Heidelberg: Berlin, Heidelberg, 1998; pp 137-174.
268. Soana, F.; Sturini, M.; Cermenati, L.; Albini, A., Titanium dioxide photocatalyzed oxygenation of naphthalene and some of its derivatives. *J. Chem. Soc., Perkin Trans. 2* **2000**, (4), 699-704.
269. Soana, F.; Sturini, M.; Cermenati, L.; Albini, A. Titanium dioxide photocatalyzed oxygenation of naphthalene and some of its derivatives. *J. Chem. Soc. Perkin Trans.* **2000**, 699–704.
270. Hykrdová, L.; Jirkovský, J. r.; Mailhot, G.; Bolte, M., Fe(III) photoinduced and Q-TiO₂ photocatalysed degradation of naphthalene: comparison of kinetics and proposal of mechanism. *J. Photochem. Photobiol., A* **2002**, 151 (1), 181-193.
271. Lair, A.; Ferronato, C.; Chovelon, J.-M.; Herrmann, J.-M., Naphthalene degradation in water by heterogeneous photocatalysis: An investigation of the influence of inorganic anions. *J. Photochem. Photobiol., A* **2008**, 193 (2-3), 193-203.
272. Al-Madanat, O.; Curti, M.; Günnemann, C.; Alsalka, Y.; Dillert, R.; Bahnemann, D. W., TiO₂ photocatalysis: Impact of the platinum loading method on reductive and oxidative half-reactions. *Catal. Today* (under review).

Chapter Three: Photocatalytic H₂ Production from Naphthalene by Various TiO₂ Photocatalysts: Impact of Pt Loading and Formation of Intermediates

3.1 Foreword

Heterogeneous photocatalysis had been extensively studied for solar fuel production with simultaneous degradation of the organic pollutants. Several challenging issues still limit the achievement of dual-purpose photocatalysis technology. The study presented in this chapter is considered the basic building block for understanding the photocatalytic process of naphthalene under inert conditions. This chapter contains the article “*Photocatalytic H₂ Production from Naphthalene by Various TiO₂ Photocatalysts: Impact of Pt Loading and Formation of Intermediates*” by Osama Al-Madanat, Yamen AlSalka, Ralf Dillert, and Detlef W. Bahnemann. Reproduced with permission from Catalysts 2021 (11, 1, 107, DOI: 10.3390/catal11010107). Copyright 2021 MDPI. Herein, a series of naphthalene photocatalytic reforming experiments employing different systems of bare and platinized (0.5, 1.0, 5.0 wt%) Aeroxide P25 and Hombikat UV100 photocatalysts were performed to determine the best conditions for this reaction. The optimum Pt loading ratio on the surface of both photocatalysts was determined. Moreover, the electron paramagnetic resonance technique was employed to evaluate and understand the electron transfer process from the TiO₂ to Pt nanoparticles, in order to explain the different photocatalytic activities between the pristine and platinized P25/UV100, as well as, Pt-P25 and Pt-UV100. Besides that, the effect of the platinum nanoparticles and the formed organic intermediates on the H₂ formation and naphthalene conversion were also discussed.

3.2 Abstract

This work presents a comparative study of the efficiency of two commercial TiO₂ photocatalysts, Aeroxide P25 (ATiO₂) and Sachtleben Hombikat UV100 (HTiO₂), in H₂ production from an aqueous solution of naphthalene. The TiO₂ photocatalysts were platinized by the photodeposition method varying the platinum content of the suspension to 0.5, 1.0, and 5.0 wt%. A full physicochemical characterization for these materials was performed, showing no structural effects from the deposition method, and confirming a well dispersion of nanosized-Pt⁰ particles on the surface of both photocatalysts. Pristine ATiO₂ shows around 14% higher photocatalytic fractional conversion of naphthalene than

pristine HTiO₂ after 240 min of irradiation, while both materials exhibit negligible activity for H₂ formation. The 0.5 wt% Pt- HTiO₂ increases the photocatalytic fractional conversion of naphthalene from 71% to 82 % and produces 6 μmol of H₂. However, using a higher Pt content than the optimal platinization ratio of 0.5 wt% dramatically inhibits both processes. On the other hand, regardless of the fractional ratio of Pt, the platinization of ATiO₂ results in a decrease in the fractional conversion of naphthalene by 4 % to 33 % of the pristine value. Although the presence of Pt islands on the surface of the ATiO₂ is essential for the H₂ evolution, no dependency between the Pt ratio and the H₂ formation rate was observed since all the platinized materials show a similar H₂ formation of around 3 μmol. Based on the EPR results, the higher photocatalytic activity of the Pt-HTiO₂ is attributed to the efficient charge carrier separation and its larger surface area. The recyclability test confirms that the inhibition of the photocatalytic process is related to the deactivation of the photocatalyst surface by the adsorption of the photoformed intermediates. A strong relationship between the photocatalytic activity and the kind of the aromatic compounds was observed. The H₂ evolution and the photooxidation of the aromatic hydrocarbons exhibit higher photonic efficiencies than that of their corresponding hydroxylated compounds over the Pt-HTiO₂.

Keywords: naphthalene; photoreforming; Hombikat UV100; Aeroxide P25; H₂ production; EPR; charge carrier; Pt/TiO₂

3.3 Introduction

Achieving a fully sustainable energy system for the future involves the development of multiple and diverse technologies. One of these systems is the renewable energy carriers, such as molecular hydrogen (H₂), which possesses advantageous properties compared to petroleum and other fossil-derived fuels¹. It has the highest gravimetric heating density among all fuels, i.e. a heating value (HHV) of 142 MJ kg⁻¹², and it burns cleanly producing pure water³. The development of new, clean, and efficient technologies for H₂ production from renewable resources has gained increasing attention. Undoubtedly, efficient large-scale H₂ production from industrial wastewaters containing organic matter can contribute to the implementation of an H₂ economy^{4,5}.

Industrial effluents are often rich in persistent organic pollutants, such as polycyclic aromatic hydrocarbons (PAHs). PAHs originate chiefly from anthropogenic processes, especially from incomplete combustion of fossil fuels and from accidental spillages of

crude oil and refined fuels. The U.S. Environmental Protection Agency (EPA) classified PAHs as priority pollutants, due to their known human toxicity potential and their ubiquitous occurrence in the environment ^{6,7}. Among other PAHs, naphthalene is the most widespread PAH in the effluent streams of the petroleum and coal industries, which is definitely related to its relative higher water solubility in comparison to other PAHs ⁸. Over the years, processes have been developed for the removal of PAHs from contaminated waters including the ultrasonic process ⁹, adsorption ⁷, biodegradation ¹⁰, pulse radiolysis ¹¹, and heterogeneous photocatalysis ⁷. To date, TiO₂ has proven its efficacy in the photocatalytic oxidation of various PAHs and especially in the remediation of naphthalene ¹².

However, the development of methods for the conversion of these pollutants into chemical energy in the form of molecular hydrogen is a more attractive solution. In particular, solar photocatalysis is regarded as a promising and eco-friendly strategy for PAHs environmental remediation ⁷. Solar photocatalytic reforming of organic pollutants contained in wastewaters under anaerobic conditions may be a viable alternative to other renewable hydrogen technologies. Hydrogen production from wastewater is a rapidly growing field combining water decontamination and transformation of the chemical energy stored in pollutants to molecular hydrogen and carbon dioxide. Although photocatalytic aerobic oxidation has already proven to be an effective process for the naphthalene removal from aqueous solutions ^{7, 12, 13}, to our knowledge, very limited studies have been performed to investigate the photocatalytic oxidation of naphthalene under anaerobic conditions ¹⁴.

Heterogeneous photocatalysis, particularly TiO₂-based photocatalysis stands out amongst the most encouraging impetuses due to its high photo-reactivity, high photo-stability, low cost, and non-toxicity ^{15, 16}. However, the major drawbacks of TiO₂ are the inability of visible light absorption and the fast recombination of photoexcited electron/hole (e⁻/h⁺) pair ¹⁷. Aromatic hydrocarbon compounds have been rarely used in photocatalysis as sacrificial agents to enhance the H₂ production from the water splitting in the absence of O₂ ^{4, 14, 18, 19}. Nevertheless, the consumption of the photo-generated holes by these agents results in the accumulation of photo-generated electrons on the TiO₂ surface. Loading the surface of TiO₂ with noble metals, in particular, platinum (Pt) nanoparticles, plays an essential role in enhancing the photocatalytic conversion process ^{4, 20}. Interestingly, Pt nanoparticles on the surface of TiO₂ act as electron acceptors for the accumulated electrons,

enhancing the formation of molecular hydrogen by reducing the overpotential of proton reduction^{4, 21, 22}.

In our previous study¹⁴, the mechanistic pathways of the photoreforming of naphthalene on anatase TiO₂ were in-depth investigated by a novel feasible approach. However, in this study, we studied the effect of different parameters on the H₂ production by reforming of naphthalene in an aqueous medium under simulated solar light. Two different commercial TiO₂, Aeroxide P25 and Hombikat UV 100 have been used. These TiO₂ photocatalysts were platinized using a photodeposition method by varying the platinum content of the suspension. The difference in their activities was evaluated through the study of the charge carrier separation, H₂ production, and naphthalene conversion during the photocatalytic process. Moreover, the effect of the intermediate products during the photocatalytic process was also investigated.

3.4 Results and Discussion

3.4.1 Photocatalysts Characterization

The ICP-OES measurements in Table 1 show the actual content of Pt in TiO₂ samples. The results indicate an actual Pt content of all samples being approximately 10% lower than the nominal value. However, the values for each set of Pt percentage (0.50, 1.0, and 5.0 wt%) are nearly the same for different types of catalysts, and within the experimental error.

Table 3-1: Actual loaded Pt nanoparticles percentage, BET surface area, and crystallite size for the pristine and as-prepared platinized TiO₂.

<i>Photocatalyst</i>	<i>Measured Pt wt%</i>	<i>BET Surface Area g m⁻²</i>	<i>Crystallite Size^a nm</i>
HTiO ₂ (UV100)	-	295 ± 3	8.0 ± 0.7
0.5 wt% Pt-HTiO ₂	0.46 ± 0.02	290 ± 2	8.4 ± 1.1
1.0 wt% Pt-HTiO ₂	0.88 ± 0.03	287 ± 2	8.9 ± 2.8
5.0 wt% Pt-HTiO ₂	4.75 ± 0.07	278 ± 2	9.2 ± 2.1
ATiO ₂ (P25)	-	52.3 ± 0.8	17.5 ± 6.3
0.5 wt% Pt-ATiO ₂	0.45 ± 0.05	50.0 ± 0.2	18.5 ± 4.7
1.0 wt% Pt-ATiO ₂	0.90 ± 0.05	48.0 ± 0.3	19.3 ± 5.5
5.0 wt% Pt-ATiO ₂	4.50 ± 0.10	43.8 ± 1.2	20.6 ± 6.1

^aThe values are calculated based on the Scherrer equation.

The specific surface area (BET) values in Table 3-1 indicate that the pristine HTiO₂ possesses a larger specific surface area of 300 m² g⁻¹, compared to 52 m² g⁻¹ for the pristine ATiO₂, which is in good agreement with previous literature reports^{23, 24}. Apparently, the loading of platinum on the surface of both pristine photocatalysts slightly decreases the surface area by (5.0 - 10) %, which is consistent with the low loading amounts of platinum on the TiO₂ surface.

Figure 3-1 shows the XRD profiles of the pristine and platinumized HTiO₂ and ATiO₂, respectively. The diffraction patterns and peak positions of the modified and unmodified ATiO₂ (Figure 3-1a) possess well-defined characteristic peaks corresponding to a mixture of anatase-rutile phases (JCPDS card No. 21-1272 and 21-1276, respectively). The intensity ratio between 101 (anatase) and 110 (rutile) main diffraction peaks is around 84:16, respectively. On the other hand, Figure 3-1b shows that pristine and platinumized HTiO₂ samples fit pretty well with the XRD patterns of pure anatase TiO₂, which is in good agreement with JCPDS card No. 21-1272. The broadness of the HTiO₂ diffraction pattern peaks indicates less crystallinity and smaller average crystallite sizes (Table 3-1), which is in agreement with the high observed specific surface areas for the TiO₂^{24, 25}. Mean crystallite sizes were calculated from the main diffraction peaks based on the Scherrer equation²⁶.

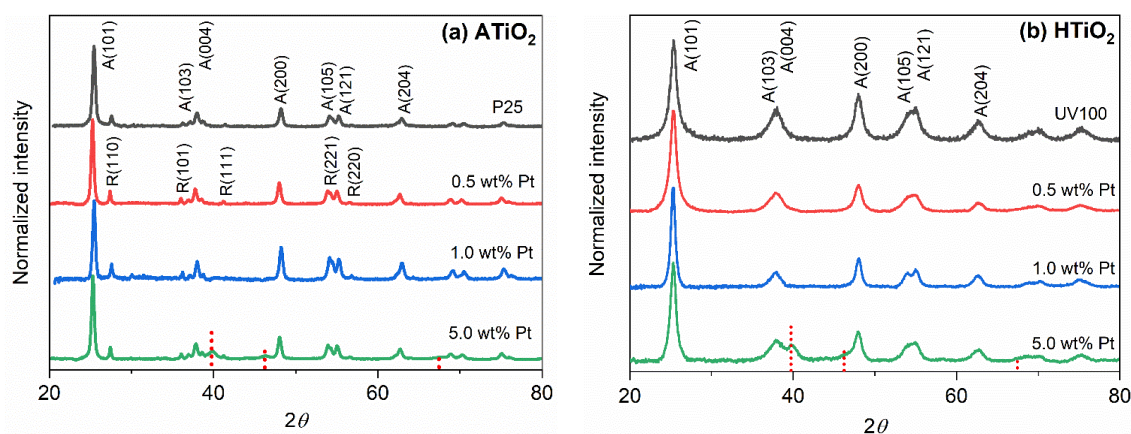


Figure 3-1: XRD patterns of pristine and different percentages of Pt loaded on (a) ATiO₂ and (b) HTiO₂ surfaces. A and R stand for anatase and rutile phases, respectively. The red lines at the bottom represent the Pt reference.

As revealed from Figure 3-1 and Table 3-1, the loading of Pt nanoparticles does not significantly change the XRD pattern position or features for all Pt-TiO₂ samples, indicating that the preparation method did not significantly change the phase content and the crystallinity of the TiO₂. Notably, the deposition of Pt did not generate any typical Pt

diffraction peaks, which might result from the uniform distribution and the low loading amount of Pt²⁷. However, in the 5.0 wt% Pt-loaded samples, two weak and broad peaks around 39.8° and 46.2° corresponding to 111 and 200 fcc platinum metal, respectively, have been observed.

The DR UV–vis spectra of pristine and platinized ATiO₂ and HTiO₂ samples were converted to their corresponding Tauc plots and shown in Figure 3-2. All the tested powders exhibit a similar optical bandgap of ~3.0 eV for ATiO₂ anatase-rutile polymorph (Figure 3-2a) and ~3.2 eV for the ATiO₂ anatase polymorph (Figure 3-2b)²⁸. The absorption spectra for Pt-TiO₂ samples indicate that the photodeposition method does not induce a substantial variation of the bandgap energy, however, a slight shift to the visible light region has been observed, due to the color change and high absorption of platinum clusters in the visible region²⁹. This optical characteristic of Pt-TiO₂ indicated that Pt nanoparticles do not exhibit localized surface plasmon absorption in the visible region, which can be attributed to a damping effect caused by d–d interband transitions²⁷.

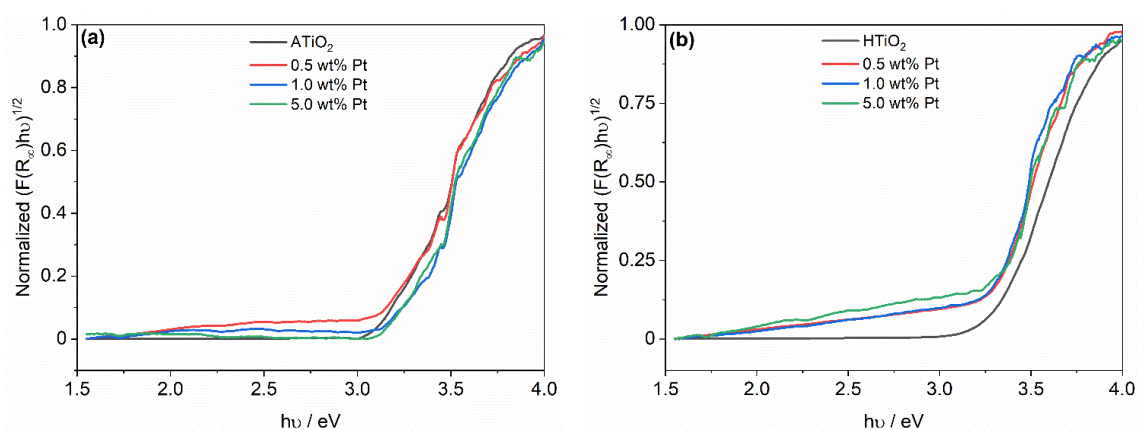


Figure 3-2: Normalized diffuse reflectance spectra (Tauc plot vs. photon energy) of pristine and platinized samples for (a) ATiO₂ and (b) HTiO₂.

The morphologies of the synthesized samples were investigated by high-resolution transmission electron microscopy (HRTEM). The micrographs of Figure 3-3 show the morphology of ATiO₂ and HTiO₂ photocatalysts before and after loading the Pt nanoparticles using the photodeposition method. The noticeable difference between the morphologies of ATiO₂ (Figure 3-3 a) and HTiO₂ (Figure 3-3 d) is related to the difference in their phase contents. HTiO₂ is pure anatase, while ATiO₂ contains also a rutile phase that possesses a larger crystallite size, altering the agglomeration abilities. As shown in Figure 3-3 (a-c) and (d-f), the loading of Pt nanoparticles does not have any significant effect on the particle size or shape of both materials. Pt-HTiO₂ shows highly agglomerated small

sub-particles, producing a higher specific surface area compared to Pt-ATiO₂. The nanoscale TiO₂ samples show sizes with different diameters of about 20–25 nm for Pt-ATiO₂ vs. 5–10 nm for Pt-HTiO₂, which is in agreement with the XDR results. Moreover, Figure 3-3 (c and f) show that the Pt nanoparticles are well dispersed over the whole oxide surface in both samples. The average grain size of Pt nanoparticles (Figure 3-3 g and h) formed during the photodeposition method was estimated from 100 metal deposits to be 3.4 ± 0.7 nm and 2.1 ± 0.5 nm for ATiO₂ and HTiO₂, respectively.

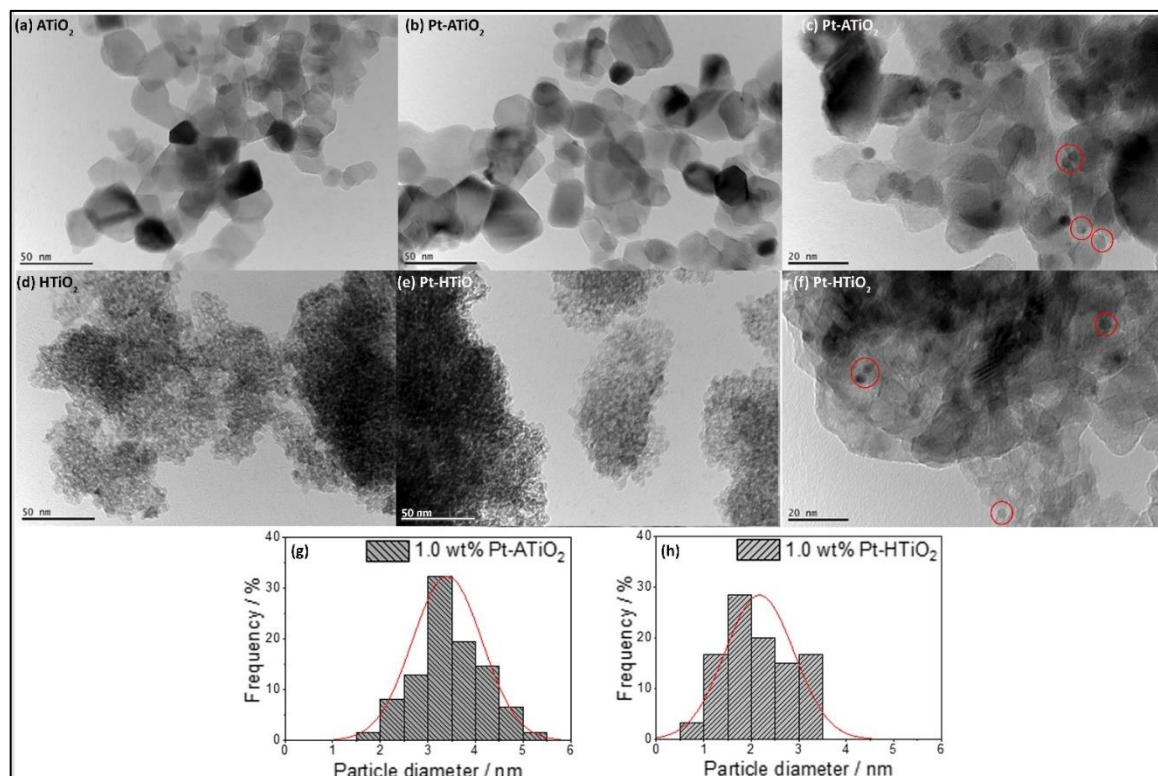


Figure 3-3: High-resolution transmission electron micrographs (HR-TEM) of pristine ATiO₂ (a), 1.0 wt% Pt-ATiO₂ (b, c), pristine HTiO₂ (d), and 1.0 wt% Pt-HTiO₂ (e, f). Pt particle diameter distribution images for 1.0 wt% Pt-ATiO₂ (g) and 1.0 wt% Pt-HTiO₂ (h).

3.4.2 Photocatalytic Reforming of Naphthalene

In this study, the same experimental conditions have been used to test the reforming of aqueous naphthalene solution employing different types of bare TiO₂ and platinized TiO₂ photocatalysts. It is worth to mention that no formation of molecular hydrogen was detected in the absence of light, or photocatalyst. Moreover, no activity for the H₂ evolution was observed during the illumination of pristine and platinized TiO₂ in the absence of naphthalene. This can be assigned to the fast recombination of the photogenerated charge carriers in the absence of a suitable hole scavenger, i.e., naphthalene, and the presence of an overpotential in the production of H₂ on the surfaces of the pristine photocatalysts²².

Figure 3-4 presents the photocatalytic hydrogen evolution over two different commercial TiO₂ photocatalysts, ATiO₂ and HTiO₂, in their pristine forms and after their loading with different amounts of platinum NPs (0.5, 1.0, and 5.0 wt%). As depicted in Figure 3-4 (a) and (b), in the presence of naphthalene, both pristine photocatalysts are not efficient for photocatalyzed H₂, due to the higher overpotential of proton reduction²⁰ and to the insufficient transfer capacities of the photogenerated electrons to the absorbed species due to their trapping on the surface of TiO₂ as Ti³⁺ sites.

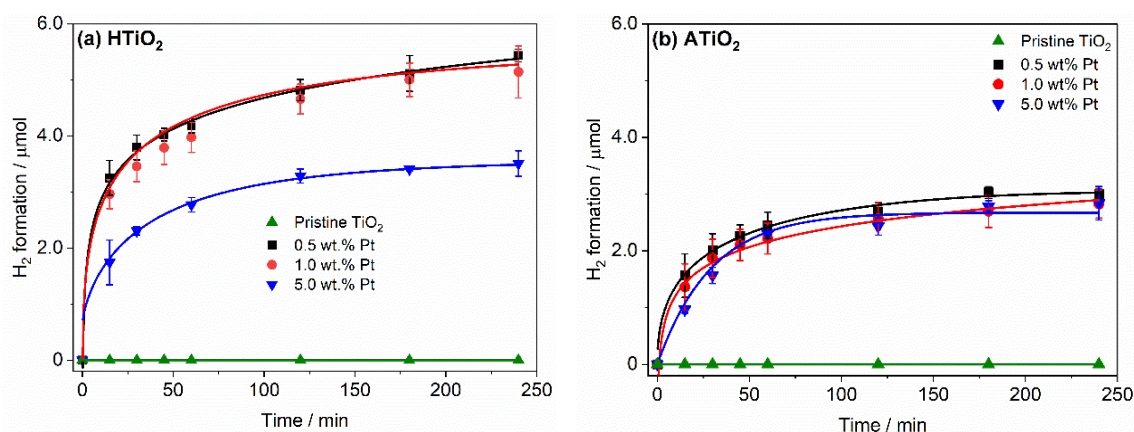


Figure 3-4: Comparison of molecular hydrogen formation during light-induced reforming of naphthalene in the presence of pristine TiO₂ and 0.5, 1.0, and 5.0 wt% Pt-TiO₂. (a) HTiO₂ and (b) ATiO₂ after 240-minute illumination using simulated solar light. Photocatalyst mass concentration, 1 g L⁻¹; 156 μM aqueous solution of naphthalene.

The presence of platinum NPs on the surface of both TiO₂ photocatalysts activates the reaction of molecular hydrogen formation by reduces the overpotential for its formation, and due to the formation of Schottky junction at the interfaces of a Pt–TiO₂ composite, which reduces the rate of the charge carrier recombination³⁰. Interestingly, Pt-HTiO₂ shows higher activity for H₂ production compared to Pt-ATiO₂ for all platinization ratios. Increasing the platinum deposition ratio on the surface of HTiO₂ from 0.5 to 1.0 wt% has no significant effect on the formation rate of molecular hydrogen. However, the 5.0 wt% platinization ratio showed around 40 % lower activity. On the other hand, the different Pt loading ratios on ATiO₂ revealed in the formation of the same amounts of molecular hydrogen, indicating the independence of the Pt content on the activity in the case of ATiO₂. Moreover, it is well known that the H₂ production is strongly dependent on the co-catalyst loading method, particle size, dispersion, and the oxidation state³³. Since the same platinization method has been used and the TEM and XRD results confirm a well dispersion of Pt⁰ NPs on the surfaces of both photocatalysts, we can exclude any effect of these factors.

Besides, the larger particle size of Pt on the surface of ATiO₂ could imply a smaller surface area of the co-catalyst comparing to that for Pt-HTiO₂, which could decrease the H₂ formation rate³⁴. If this is the case, we should observe an increase in the H₂ formation by increasing the Pt ratio from 0.5 to 1.0 wt% which compensates for this effect. However, this factor is excluded also, since the H₂ formation is almost the same.

On the other hand, we showed that upon increasing the fractional ratio of loaded Pt from 1.0 wt% to 5.0 wt%, the H₂ formation is reduced by 50%. The excessive loading amount of Pt on the surface of TiO₂ results in an increase of the opacity and, consequently, the light scattering of the suspension. This phenomenon reduces the number of photons absorbed by the TiO₂ particles and, thus, the number of charge carriers, thereby lowering the photocatalytic activity³⁵. Besides, the decrease of the photocatalytic activity of the 5.0 wt% Pt-HTiO₂ can be attributed to the formation of dense larger islands. In fact, the growth of Pt nanocrystals under a high concentration of Pt precursor would be readily accelerated to form thicker and large Pt islands during the photodeposition process^{36, 37}. These dense islands negatively affect H₂ formation due to the weak charge distribution between the platinum layers and the semiconductor³⁷. Chen et al.³⁸ demonstrated that the charge redistribution occurs at the interfacial region between TiO₂ and the first Pt layer while the charge depletion/accumulation becomes negligible beyond the third layer.

Concomitantly, the photocatalytic oxidation of naphthalene solution in the absence of molecular oxygen (inert condition) was investigated employing the previous photocatalysts under the same experimental conditions. While the photolysis of naphthalene decreased its initial concentration by ~33 %, the use of photocatalyst enhanced the conversion ratio to 70 % - 85 % over pristine and platinized photocatalysts as shown in Figure 3-5. Pristine ATiO₂ exhibited higher photocatalytic performance for naphthalene conversion than did the pristine HTiO₂. This observation was expected, and it could be mainly ascribed to the fact that the recombination rate of the photoexcited electron/hole (e⁻/h⁺) pair in pristine HTiO₂ is faster.

Anatase TiO₂ is generally reported as the most photochemically active phase of titania³⁹. Compared to rutile, the anatase phase exhibits a 10-fold greater rate of hole trapping⁴⁰, which decreases the recombination rates of electron-hole pairs. Recently, by the means of combining theory and experiment, Scanlon and co-workers⁴¹ suggested that the electron affinity of anatase is higher than that of rutile, leading to favor transfer the photogenerated

electrons from rutile to anatase. This behavior has been previously suggested by Hurum et al.⁴² who reported that Degussa P25 as a mixed phase of titania composed of small nanocrystallites of rutile dispersed within an anatase matrix possesses a higher activity than both pure phases. They affirmed that rutile acts as an antenna to extend the photoactivity into visible wavelengths and the stabilization of charge separation activates the catalyst, suppresses the recombination, and enhancing the photocatalytic activity.

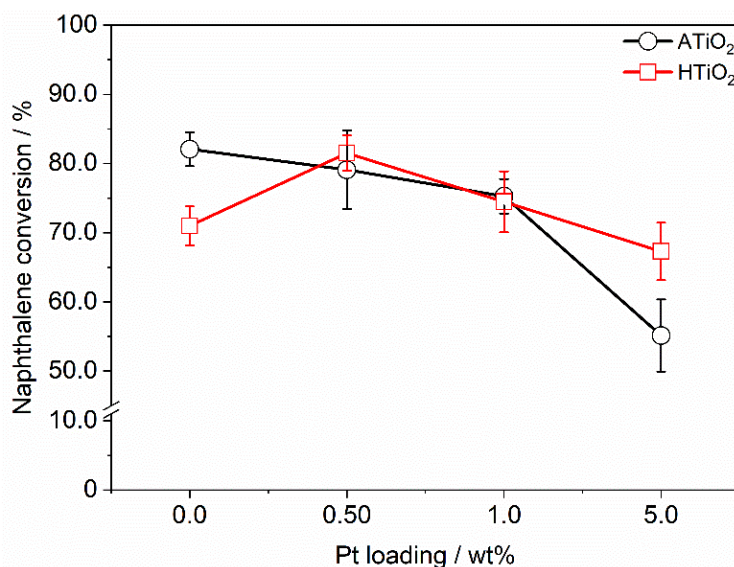


Figure 3-5: Naphthalene conversion in the presence of different photocatalysts. Conditions: [Naphthalene] = 0.156mM, [catalyst] = 1 g L⁻¹, V = 15 ml, T = 25 °C, 240 min illumination under simulated solar light ($I_0 = 3.31 \times 10^{-4} \text{ mol m}^{-2} \text{ s}^{-1}$).

Moreover, since the photocatalytic activity of the TiO₂ depends on its bulk and surface properties, it was suggested that the higher crystallinity leads to higher photocatalytic activity by reduces the charge carrier recombination⁴³. Considering that TiO₂ photocatalyst exhibit either a high crystallinity and a low surface area or versa vise⁴⁴. The XRD and TEM results in Figure 3-1 and Figure 3-3 shown that HTiO₂ consists of small particles (8 nm) with very low crystallinity than ATiO₂. Thus, the low surface area of the P25 should be accompanied by higher crystallinity, which enhancing the photocatalytic efficiency.

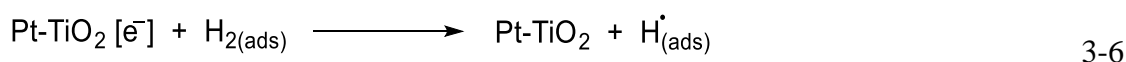
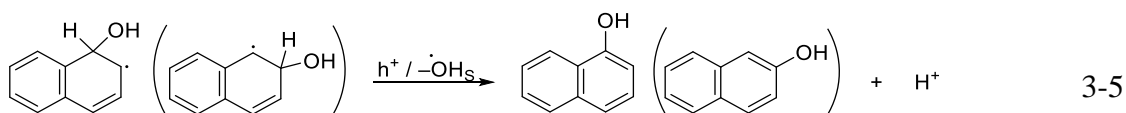
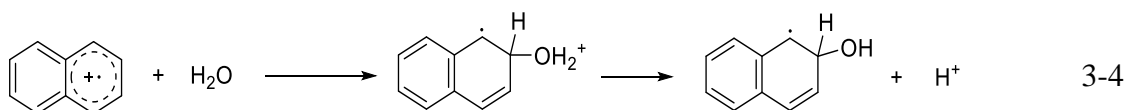
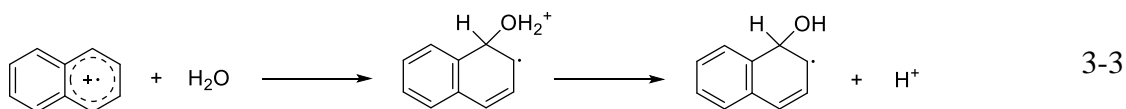
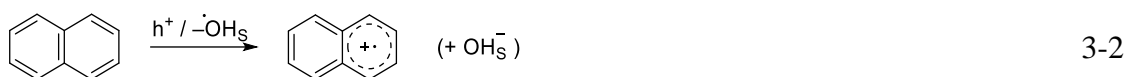
Interestingly, loading platinum NPs on the surface of TiO₂ has two different behaviors related to the nature of the photocatalyst. Figure 5 shows that the photocatalytic conversion of naphthalene was decreased by increasing the platinum loaded ratio on ATiO₂. In fact, increasing the platinum nanoparticles' content on the surface of pristine TiO₂ reduces the number of available active sites which plays a crucial role in the photooxidation of organic compounds⁴⁵. This result is in good agreement with the work of Sun et al.⁴⁶ reporting that

loading Degussa P25 with Pt resulted in a decrease of phenol decomposition and total carbon removal rates. The decrease of ATiO₂ activity after platinization suggests that Pt acts as a recombination center for the charge carrier. For such titania nanoparticles in aqueous media, Pt would not increase the efficiency of the charge carrier separation more than the separation already existing due to the presence of two mixed phases. A recent report by Benz et al.⁴⁷ demonstrated that upon the trapping of the photogenerated electrons by the Pt islands on the surface of P25 in the absence of O₂, Pt acts more as a recombination center regardless of its deposit ratio.

On contrary, the loading of platinum islands on the surface of HTiO₂ with a very small fraction (0.5 and 1.0 wt%) enhances the efficiency of the photocatalytic oxidation of naphthalene (Figure 3-5) compared to the use of pristine HTiO₂. Sun et al.⁴⁶ reported that the rates of phenol decomposition and the total carbon removal rose by a maximum factor of 1.5 when Hombikat TiO₂ was loaded with 1.0 wt% Pt. However, our data, as well as other reports^{46,48}, show that an optimum content of Pt (0.5 – 1.0 wt%.) on the surface of HTiO₂ should be considered, otherwise, increasing the Pt content reduces the efficiency of the photocatalytic process. In fact, the presence of hole scavengers (like naphthalene) can change the original equilibrium between the photogenerated holes and electrons. Platinum nanoparticles on the surface of TiO₂ act as electron scavengers, withdrawing the photogenerated holes out of the bulk TiO₂ because the formed Schottky barrier at Pt/TiO₂ interface serves as an efficient electron trap preventing the charge carrier recombination. This will enhance the charge carrier separation and prolong the lifespan of the photogenerated electrons⁴⁹. However, increasing the Pt loading more than the optimum value leads to make the space charge layer very narrow and the penetration depth of light exceeds the space charge layer. Thus, platinum nanoparticles can act as recombination centers, where the electron-hole pairs recombination process will be favorable^{48,50}. A more in-depth investigation of the Pt nanoparticles' effect on the dynamic charge carriers will be provided in *section 3.4.5*.

In our previous report, we paid attention to the products generated from the photocatalytic reforming of naphthalene discussing their formation pathways by using different chromatographic techniques and isotopic substitution studies¹⁴. The hydroxylation of the aromatic ring was found to be the principal process in the photocatalytic reforming of naphthalene, which mainly produces 1-naphthalenol and 2-naphthalenol among other hydroxylated by-products. The possible pathway explaining the formation of the two

naphthalenol's and molecular hydrogen is shown in Equations 3-1 to 3-7. The reforming of naphthalene is initiated by the excitation of the TiO₂, generating electrons and holes (Equation 3-1), which either recombine or react with species present in the surrounding electrolyte. Naphthalene's oxidation occurs by a direct hole transfer, or indirectly via its reaction with a surface trapped hole ($-\text{OH}_s^\bullet$) by single electron transfer producing a naphthalene cation radical (Equation 3-2). This carbocation radical reacts with water to form an OH adduct (Equations 3-3 and 3-4), which is subsequently oxidized by another hole forming naphthalen-1-ol or naphthalen-2-ol (Equation 3-5). On the other hand, the accumulated photogenerated electrons in the Pt nanoparticles reduce the adsorbed protons to hydrogen atoms (Equation 3-6), which upon dimerization yields H₂ (Equation 3-7).



In this context, we report in Figure 3-6 the detected amounts of these naphthalenols remaining in the reaction medium after 4 h of irradiation in the presence of all the synthesized Pt-TiO₂. Figure 3-6. shows that the accumulated amounts of 1-naphthalenol and 2-naphthalenol increased with increasing the Pt ratio on the surface of the different TiO₂ materials (ATiO₂ and HTiO₂). Platinization of the pristine TiO₂ enhance the formation of the naphthalenols products. While the relationship between the Pt content and the formation of naphthalenols is well established, there is an independency between their formation and the nature of TiO₂ when the same loading ratio was used.

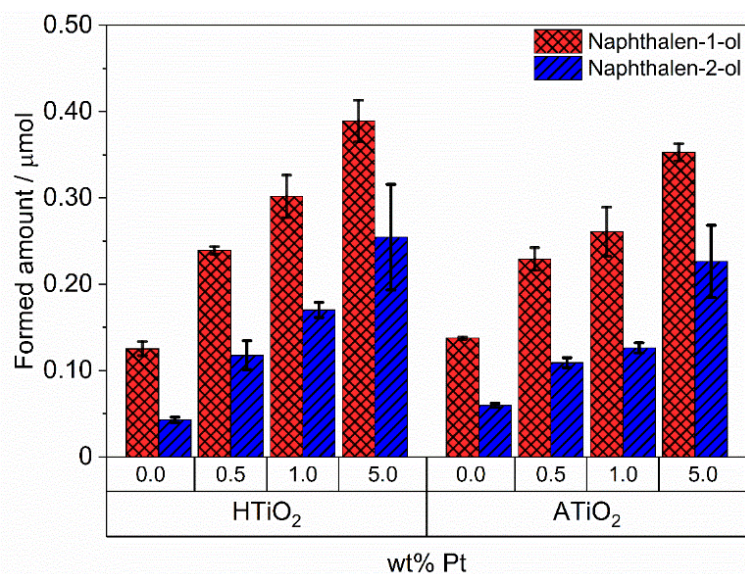


Figure 3-6: Photocatalytic formation of 1-naphthol and 2-naphthol during the reforming of naphthalene in aqueous suspensions of HTiO₂ and ATiO₂ loaded with various amounts of Pt.

Figures 3-4 and 3-6 confirm that the disappearance of the parent molecule naphthalene is accompanied by the formation of 1-naphthalenol and 2-naphthalenol besides the continuous formation of H₂. In such a photocatalytic system, the lower detected amount of these by-products that accompanied with higher conversion of the mother compound should be an indication for increasing the formation rate of the H₂ (Equation 3-8). However, this is not the case here, since we observed that all the synthesized Pt-ATiO₂ photocatalysts showed different photocatalytic activities towards the photooxidation of naphthalene and the formation of naphthalenols with almost the same amounts of evolved H₂. If we consider Equation 3-9 and the percentage of the total amount of naphthalenols to the converted naphthalene that is reported in Table 3-2, one can conclude that the formed amounts of H₂ for all the synthesis materials does not exceed 10-25% compared to the theoretical one. Thus, the concurrent decrease of the photocatalytic activity with the accumulation of the naphthalenols in the photocatalytic system by increasing the Pt ratio indicates the formation of other products. Such products can be strongly adsorbed on the surface of the photocatalysts and inhibiting the formation of H₂. It is reported that the photocatalytic oxidation of the aromatic compounds is initiated by the hydroxylation process producing different hydroxylated compounds as main products. This process is sometimes considered as the rate-determining step in the whole photocatalytic reaction under aerobic⁵¹⁻⁵³ and anaerobic conditions^{19, 54}. The strong adsorption of the surface phenoxy species and the coupling products on the available active sites^{16, 55-57}, deactivates the surface of the photocatalyst and negatively affects both redox half photocatalytic reactions. This can be

experimentally inferred by the decrease in the H₂ evolution rate after 30 min of irradiation with the simultaneous change in the photocatalyst color from light gray to faint brown. However, the color change is more pronounced in the case of Pt-A-TiO₂, which can be reflected in the higher adsorbed amount of these products.

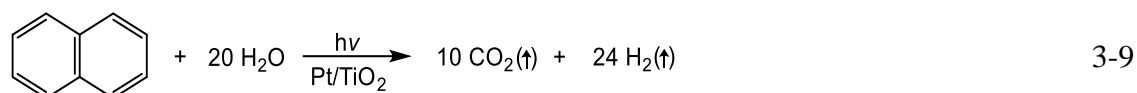
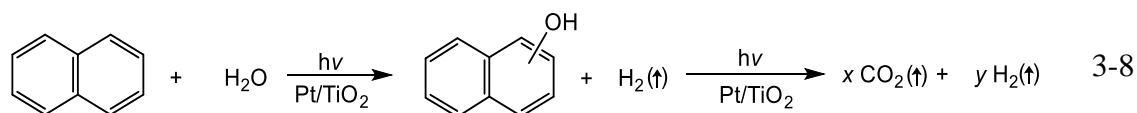


Table 3-2. Selectivity of total naphthalenols formation over different Pt-TiO₂ photocatalysts.

Property	HTiO ₂			ATiO ₂		
	0.5 wt% Pt	1.0 wt% Pt	5.0 wt% Pt	0.5 wt% Pt	1.0 wt% Pt	5.0 wt% Pt
Total naphthalenols	22.4	34.7	46.2	21.3	27.3	45.1
selectivity %	± 1.3	± 2.4	± 8.5	± 1.2	± 2.4	± 4.4

3.4.3 Stability of Pt Deposit

The recyclability of the photocatalyst can provide a good indication that there is no relationship between the leaching of the co-catalyst and the decreasing of the photocatalytic activity during the reforming of naphthalene. Therefore, three consecutive recycling runs on the 0.5 wt% Pt-HTiO₂ were performed. The used photocatalyst was collected, irradiated in the presence of molecular oxygen for 60 min to remove the adsorbed organic compounds, washed with water, centrifugated, and then finally dried at 100°C for 24 h.

As observed in Figure 3-7 (a, b), the reused photocatalyst exhibits good photocatalytic performance and stability over three cycles. Compared to the fresh photocatalyst, the naphthalene conversion efficiency remained almost the same, and a very slight decrease in molecular hydrogen formation was observed, which is considered within the experimental error.

Furthermore, in order to check whether metal leaching takes place during the photocatalytic process, the Pt content in the Pt-HTiO₂ was analyzed after each photocatalytic cycle by means of the ICP-OES technique. The amount was found 20-25 % lower than the original Pt ratio, mainly after the first cycle. In summary, one can conclude that 0.5 wt% Pt-UV100

is recyclable and stable. Therefore, the inhibition of H₂ formation and the naphthalene conversion during the photocatalytic process is not related to the leaching of the co-catalyst from the photocatalyst surface. These results support our hypothesis of the formation of stable photoformed products, which deactivate the photocatalyst surface.

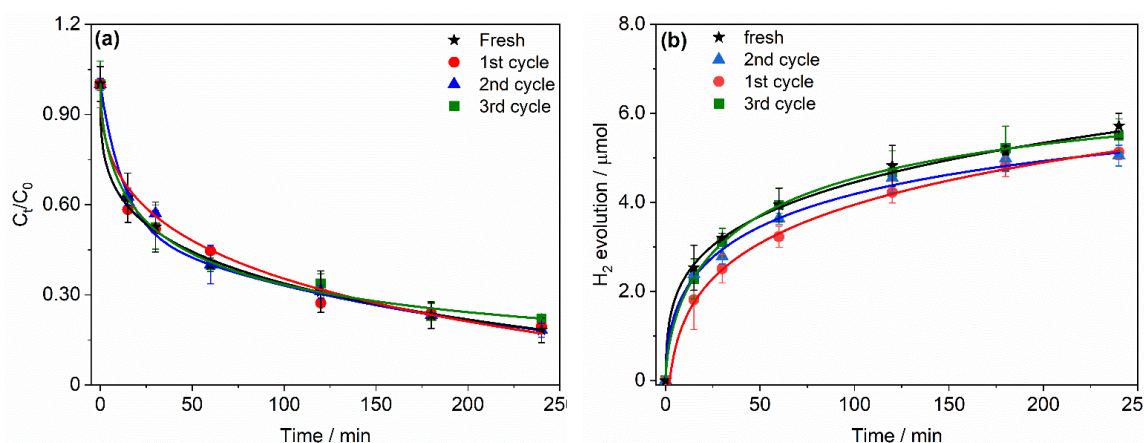


Figure 3-7: C_t/C_0 for naphthalene conversion (a) and molecular hydrogen formation (b) during the photocatalytic reforming of naphthalene using recycled 0.5 wt% Pt-HTiO₂ photocatalyst. Conditions: [Naphthalene] = 0.156mM, [catalyst] = 0.5 g L⁻¹, T = 25 °C, 240-minute illumination under simulated solar light.

Moreover, since the decrease of the Pt content during the recyclability experiments is not affecting the H₂ formation and the conversion of naphthalene. Thus, another important aspect can be concluded from these results: the 0.5 wt% of Pt loaded on HTiO₂ might not be the optimum loaded ratio. Although many previous studies have reported that 0.5 wt% is the optimum ratio of loaded Pt on the TiO₂⁴⁴, other reports have shown different values either higher⁴⁸ or lower^{19,20} than 0.5 wt% Pt. Therefore, a further investigation in the range lower than 0.5 wt. % is required to avoid an excess of the valuable Pt metal, thus, decreasing the cost of this photocatalyst in case of its practical application.

3.4.4 Effect of Naphthalene Oxidation Products on the H₂ Evolution

It is widely accepted that the formation of the by-products presumably causing inhibition of H₂ production during the photocatalytic reforming of the organic compounds^{57,58}. We examine the validity of this hypothesis by performing different photocatalytic experiments using naphthalene, 1-naphthalenol, and 2-naphthalenol under the same experimental conditions. The photooxidation profiles of the three compounds as a function of irradiation time are shown in Figure 3-8 (a). Apparently, the photooxidation of naphthalene is higher than that for both naphthalenol compounds. After 240 min of illumination, the conversion of naphthalene, naphthalen-1-ol, and naphthalen-2-ol were found to be 75 %, 63 %, and

52%, respectively. All the tested compounds showed a faster conversion rate in the initial stage of the reaction, which is attributed to the abundant availability of active sites on the surface of TiO₂⁵⁹. In this stage, naphthalene shows the longest period (60 min) with the faster conversion rate, while, the shorted period (15 min) with the slowest rate was observed for naphthalen-2-ol. The initial photonic efficiencies of the photooxidation of these compounds after 60 min of illumination were found to be 0.14 ± 0.01 %, 0.1 ± 0.02 %, and 0.08 ± 0.01 % for naphthalene, naphthalen-1-ol, and naphthalen-2-ol, respectively. A noticeable inhibition in the conversion rates was recorded after the first rapid period to reach a steady-state stage after 120 min. This behavior has been observed by King et al.⁶⁰, who reported that the initial stage was found to be the most rapid photodegradation rate for PAH removal in the presence and the absence of the photocatalyst.

On the other hand, a similar trend was observed for the photocatalytic H₂ formation profile shown in Figure 3-8 b. Naphthalene exhibits a two-fold higher formation amount of H₂ after irradiation for 240 min. One more time, the faster formation rate was observed during the first stage of the reaction, i.e during the first 60 min. Afterward, all the tested compounds exhibit almost a similar formation rate. The initial photonic efficiencies for the H₂ evolution in the first stage was found to be 0.51 ± 0.02 %, 0.28 ± 0.03 %, and 0.18 ± 0.02 % for naphthalene, naphthalen-1-ol, and naphthalen-2-ol, respectively.

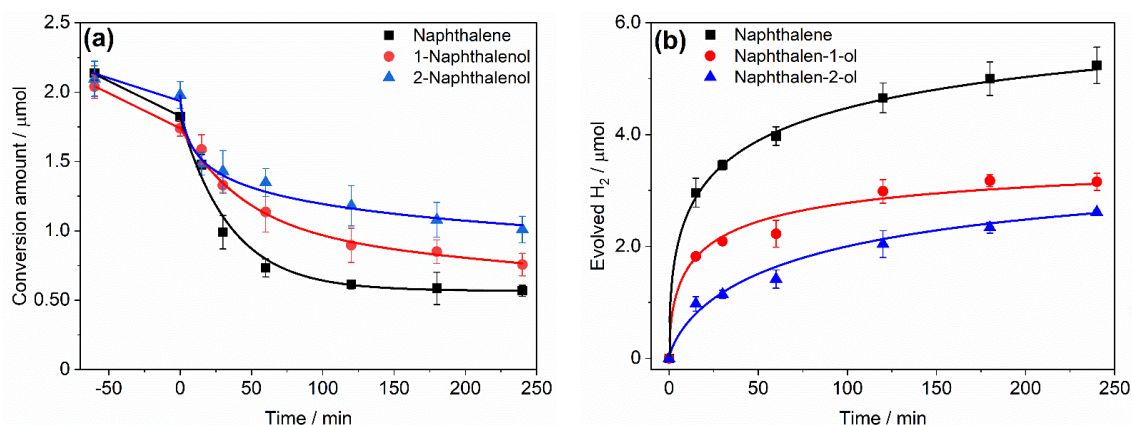


Figure 3-8: Photooxidation (a) and molecular hydrogen formation (b) during the photocatalytic reforming of naphthalene, naphthalen-1-ol, and naphthalen-2-ol as a function of illumination time. Conditions: [Naphthalene] = $2.1 \mu\text{mol}$, [naphthalenols] = $2.1 \mu\text{mol}$, [catalyst] = 1 g L^{-1} 1.0 wt% Pt-HTiO₂, $T = 25 \text{ }^\circ\text{C}$, illumination under simulated solar light.

We reported previously that naphthalene is oxidized into CO₂, H₂, and other by-products, such as naphthalenols, coupling, and hydroxylated compounds¹⁴. At the beginning of the photocatalyst process, the concentrations of these organic products are very low in the

system. Naphthalene is efficiently oxidized on the clean surface of the TiO₂ since there is no competition from these products to the surface of the photocatalyst. However, during the reaction, the formed intermediates are accumulated in the system and subsequently oxidized to other more polar compounds such as polyhydroxylated, quinones, and organic acid products^{14, 61, 62}. Such products have higher polarity comparing to naphthalene, therefore they can strongly adsorb to the surface of the photocatalyst, blocking the active sites on the catalyst surface. In general, the degradation of these compounds leaves recalcitrant carbonaceous residues on the photocatalyst surface as a result of incomplete degradation^{63, 64}, especially in the absence of O₂, which decreasing the photocatalytic activity of the TiO₂.

In this respect, it is noteworthy that the adsorption of the organic molecules is a very important factor in the photocatalytic process, however, in some cases, the strong adsorption of the organic compounds or intermediates may act as poison for the catalyst surface, which enhances the charge carrier recombination. The strong multilayer adsorption of organic molecules around the catalyst particles could lead to the excitation of these compounds by absorbing a significant amount of solar light rather than the photocatalyst. This could limit the interaction between the incoming light and the photocatalyst in the case of the indirect photooxidation mechanism, which reduces the photocatalytic efficiency^{65, 66}. In our case, the lack of naphthalen-2-ol photooxidation after less than 30 min of irradiation can be related to the adsorption of stable photoformed products on the surface of the photocatalyst that hinders the photocatalytic process. The photocatalytic degradation of 2-naphthol was investigated by Qourzal et al.⁶⁷ with and without replenishing the O₂ in the system and was found to be 100% and 58%, respectively. Our results suggest that the different kinds of organic pollutants have a significant influence on the photocatalytic H₂ production and the simultaneous photocatalytic degradation of the organic pollutant. In our case, the differences in the photonic efficiencies of the photooxidation and H₂ evolution can be related to the different photocatalytic behavior of these compounds. According to Denny et al.⁶⁸, increasing the number of hydroxyl groups in aliphatic compounds increases mineralization, however, this effect was not evident for the hydroxylated aromatic compounds. On the other hand, many reports have been shown that the photoreforming of aromatic hydrocarbons is more reactive than hydroxylated aromatic compounds¹⁸. Since the photocatalytic reforming of naphthalene is more efficient than both naphthalenols compounds under the same experimental conditions, our results thus confirm this

hypothesis. Therefore, based on the presented results, we can conclude that the photocatalytic process is highly dependent on the nature of the organic compound.

3.4.5 EPR Study

EPR spectroscopy is a suitable technique for studying charge carrier separation to predict the photocatalytic activity of different photocatalysts. All the EPR analyses (Figure 3-9) were carried out on 1.0 wt% Pt-ATiO₂ and 1.0 wt% Pt-HTiO₂ in the N₂ atmosphere to avoid the contribution from any other electron scavenger, i.e. molecular oxygen. Thus, to investigate the effect of the photocatalyst nature and the loaded PtNPs on the photogenerated electron and hole paramagnetic species, the signals from both photocatalysts were acquired before and after UV-Vis irradiation. Very weak signals observed for both catalysts in the dark can be related to formed oxygen vacancies during preparation. While under illumination, both photocatalysts exhibit two major features, i.e., the signals from the surface trapped holes at $g > 2.000$, and the signals from the trapping of electrons at $g < 2.00$, as shown in Figure 3-9 (a) and (b)^{69, 70}.

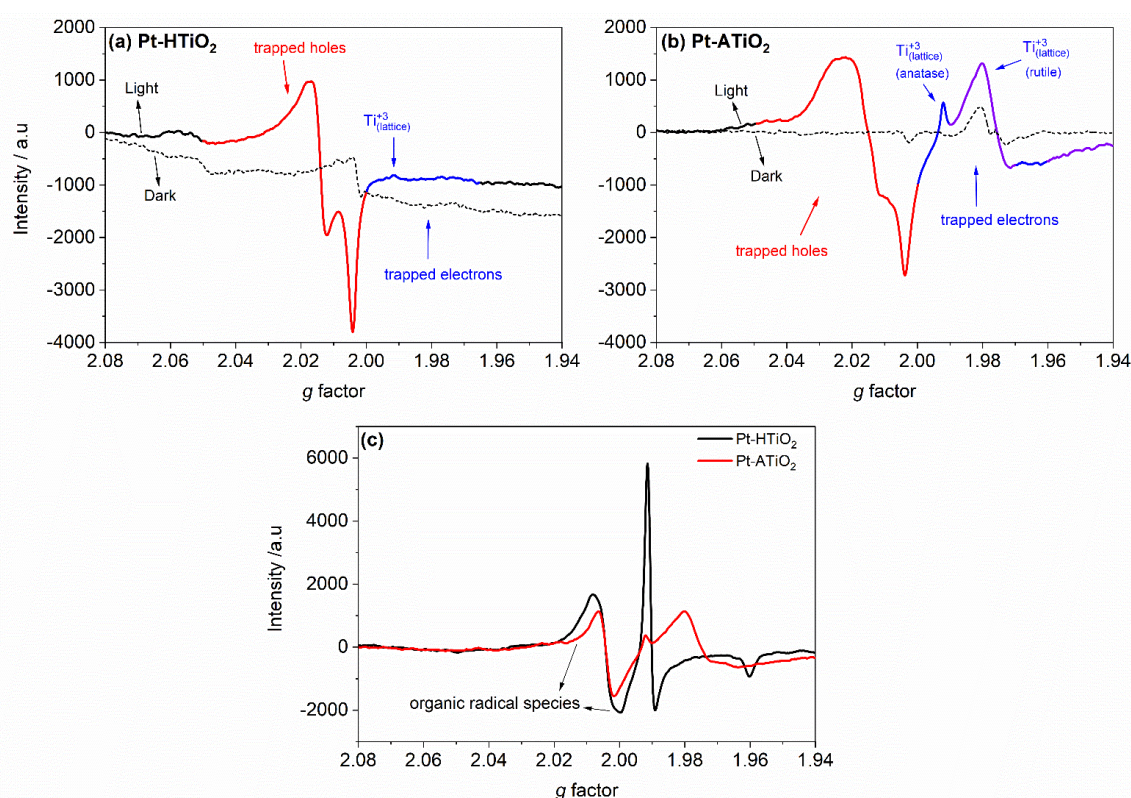


Figure 3-9: EPR spectra measured at 77 K in N₂ atmosphere for (a) 1.0 wt% Pt-HTiO₂, and (b) 1.0 wt% Pt-ATiO₂ in dark (dash line) and light (solid line). (c) The photogenerated signals for 1.0 wt% Pt-HTiO₂ (black line) and 1.0 wt% Pt-ATiO₂ (red line) in the presence of N₂-naphthalene vapor under illumination.

Irradiation of the platinized TiO₂ samples by the light of higher energy than the respective bandgap, lead to the formation the e⁻ - h⁺ pair, as shown in Equation 3-1. Both e⁻ and h⁺ can be trapped on the surface or interior of the lattice. The conduction band electrons can be trapped on the Pt islands and Ti⁺⁴ ions. In the second case, they form a paramagnetic Ti^{III} in the bulk or the surface^{71,72}. On another hand, the valance band trapped holes can be located on O⁻² as a O^{•-} either in the surface or subsurface^{70,72}. Shapovalov et al.⁷³ suggested that the holes can be delocalized over at least two surface oxygen atoms, and can be transferred between surface oxygen atoms and adsorbed species, thus, both •OH and O^{•-} species can be formed.

The hole trapping site in Figure 3-9(a) at g-tensor components g_x = 2.004, g_y = 2.015, and g_z = 2.019, represent the fingerprint of anatase oxygen site, while the small-signal at g_⊥ = 1.992 and the shoulder at g_∥ = 1.965 are assigned for the anatase lattice trapping electron site as Ti⁺³^{70,74}. On other hand, the trapped holes signals of Pt-ATiO₂ in Figure 3-9b at g-tensor components g_x = 2.003, g_y = 2.019, and g_z = 2.026 are not sufficiently resolved, which is considered a combination of trapped oxygen sites from anatase and rutile. However, the lattice trapped electron's EPR signals are well resolved. The Ti⁺³ signal from anatase can be observed clearly at the same g-tensor components assigned in Figure 3-9a, while the remaining signals at g_⊥ = 1.980 and g_∥ = 1.945 are characteristics for Ti⁺³ sites for trapped electrons in the rutile lattice^{69,74}.

Figure 3-9 (a, b) clearly shows around 20 % higher relative intensity of trapped holes in Pt-HTiO₂ (determined by double integration of the corresponding signal⁷⁵) than those in Pt-ATiO₂. On the other hand, Pt-ATiO₂ exhibits the strongest electron signals at both Ti⁺³ sites. Since no hole scavenger was used, the increase in the Ti³⁺ EPR signals can be a monitor of a potential increase in the charge carrier recombination during the photocatalytic processes, since the trapped electrons in the lattice will recombine with the photogenerated holes. These results indicate that Pt-HTiO₂ yields a better electron transfer to Pt islands than Pt-ATiO₂. Thus, an efficient charge carrier separation in the case of Pt-HTiO₂ is expected, which inhibits the electron-hole recombination and increases the photocatalytic efficiency.

Moreover, to investigate the different mechanisms of generating organic radicals by the photogenerated holes, experiments were performed in the presence of naphthalene as a hole scavenger. Upon the irradiation of both platinized TiO₂ samples, the photogenerated holes

react with naphthalene, forming the naphthalene radical cation via single-electron transfer (Equation 3-2) ¹⁴.

The EPR spectra in Figure 3-9c show that both photocatalysts generate similar signals having *g*-tensor components $g_x = 2.002$, $g_y = 2.006$, related to the formation of naphthalene radical cation ⁴², which formed as a result of the reaction between naphthalene and the photogenerated holes. Pt-HTiO₂ produces a relatively higher intense signal of such organic radicals and a stronger signal of the trapped electrons (Ti⁺³) compared to both signals produced from Pt-ATiO₂. This could be attributed to the higher amount of the trapped holes that are available to react with the adsorb naphthalene, due to the efficient charge carrier separation in the Pt-HTiO₂ photocatalyst. Interestingly, unlike Pt-HTiO₂, the intensity of the trapped electrons produced from Pt-ATiO₂ (Ti⁺³ anatase and rutile) does not change upon the introduction of naphthalene as a hole scavenger. The higher intensity of the formed organic radicals in Pt-HTiO₂ would be accompanied by a higher amount of the photogenerated electrons, which can be partially collected by PtNPs on the surface of Pt-HTiO₂ to catalyze the reduction of H⁺ ions to H₂, while the remaining electrons can be trapped as Ti⁺³.

Furthermore, the Ti_(lattice)⁺³ signals intensity in Pt-ATiO₂ is relatively low than the respective signal intensity in Pt-HTiO₂. This can be related to the rapid transfer of the photogenerated electrons from the ATiO₂ to the Pt islands. If so, we should observe a relatively higher signal from formed organic radicals. However, a relatively lower signal was observed, which can be attributed to faster recombination between photogenerated electrons and holes, results in a decrease in the amounts of evolved H₂ during the reforming of naphthalene. According to Sun et al. ⁴⁶, the interfacial contact between the two phases (rutile and anatase) in Pt-TiO₂ (P25) leads to the band bending, which increases the anatase conduction band energy within the space charge layer. Therefore, prohibiting the photogenerated electrons from migrating from anatase to rutile. On the other hand, the valance band bending results in the migration of the holes from the anatase to the rutile valance band ⁴¹. However, since the mobility and diffusivity of the electrons, as well as the electron flux in the rutile phase, is very low compared to anatase, the electrons flux from anatase to rutile, if happened, is negligible ^{41,46}. Therefore, trapped holes are accumulated in rutile particles, and electrons are left in the anatase, where oxidation and reduction mainly take place, respectively. However, the slow movement of the rutile electrons enhanced the probability of the electron–hole recombination, decreasing the rutile's

activity. Hence, it is suggested that the formed charge carriers in the rutile phase of P25 do not improve the photoactivity a lot, instead, it plays a role of charge carrier separation and provides sites for oxidation ⁷⁶.

3.5 Experimental

3.5.1 Materials

Titanium dioxide, Aeroxide P25 (ATiO₂) consist of anatase/rutile mixture was supplied from Evonik Corporation, USA. and Hombikat UV100 (HTiO₂) pure anatase phase was supplied by Sachtleben Chemie GmbH. Naphthalene ($\geq 99.0\%$), naphthalen-1-ol (97%), naphthalen-2-ol (99%), and chloroplatinic acid hexahydrate (H₂PtCl₆·6H₂O, 99.9%) were purchased from Sigma-Aldrich. Methanol HPLC gradient grade was purchased from Carl-Roth. All chemicals were used as received without any further purification, and their solutions were prepared with deionized water obtained from a Millipore Mill-Q system (18.2 M Ω .cm, 25 °C).

3.5.2 Preparation of the Pt-TiO₂ Photocatalysts.

Platinum-loaded TiO₂ samples were prepared by a photodeposition method according to our previous report ¹⁴. A 1.5 g of the commercially available TiO₂ (UV100 or P25) was dispersed into 150 mL of 10% aqueous methanol solution with the desired amount of platinum precursor (H₂PtCl₆, 0.1 M) corresponding to obtain 0.5, 1.0, and 5.0 wt% of Pt-TiO₂ nanoparticles. The suspension stirred for 1 h and then purging for another 1 h with argon. Afterward, it was top illuminated for 4 h with UV(A) light employing a Philips CLEO lamp inside a climatic chamber at 18°C. The solid was then collected by centrifugation, repeatedly washed one time with methanol, fourth with distilled water, and finally dried at 100 °C for 24 h.

3.5.3 Photocatalytic Experiments

The photocatalytic activity of the Pt-ATiO₂ and Pt- HTiO₂ were evaluated through the photocatalytic reforming of naphthalene, carried out in a batch mode using 20 mL glass vials tightly closed with a crimp cap and silicon septum. Due to the experiment limitation, the evaporation, and lower solubility of naphthalene during the preparation step ⁸, a fresh, saturated deaerated stock solution from it was prepared before each photocatalytic experiment. The estimated concentration of this solution is about 2.44×10^{-4} mol L⁻¹ at 25 °C, while, the specific concentration was determined by using the HPLC-UV technique.

In a typical experiment, 15 mg of the photocatalyst powder was suspended in a specific amount of deionized water. The vials were closed with the crimp septum and purged with argon for 30 min. Afterward, the desired volume from the naphthalene stock solution was injected inside the 15 mL-reaction vials using a pre-purged (with argon gas) needle syringe to have a final concentration of 20 mg L⁻¹ (1.56 × 10⁻⁴ mol L⁻¹ at 25 °C). Finally, the vials were left in the dark inside an orbital shaker for 1 h to reach the equilibrium adsorption. The orbital shaker was placed at a 30 cm distance below a 1000 W xenon lamp (Hönle UV Technology, Sol 1200) equipped with a filter to simulate the solar light. The temperature of the vials was controlled at 25 ± 2 °C by using a water bath. It is worth to mention that the reported concentrations of naphthalene in wastewater range between ng L⁻¹ to µg L⁻¹ ^{77, 78}, which are considered very low concentrations compared to those that were used in the photocatalytic experiments. Such a higher concentration was used to ensure proper repeatability in all experiments and to avoid the problem of naphthalene evaporation. Furthermore, almost a complete removal of naphthalene was observed by using a concentration lower than 20 ppm ⁷⁹, which will prevent a logical and practical comparison between the performance of both photocatalysts.

The photon flux density was measured from the spectral irradiance of the lamp in the wavelength range between 320 - 380 nm and was found to be $I_0 = 3.31 \times 10^{-4} \text{ mol m}^{-2} \text{ s}^{-1}$. The photonic efficiencies were calculated based on Equations 3-10 ²⁶.

$$\xi = \frac{\text{degradation or formation rate (mol s}^{-1}\text{)}}{\text{photon flux (mol m}^{-2} \text{ s}^{-1}\text{)}} = \frac{N_A hc V \Delta C}{I \lambda A \Delta t} \quad 3-10$$

where V is the suspension volume (0.015 l), $\Delta C/\Delta t$ is the formation rate (mol s⁻¹), A is the illuminated area (6.60 × 10⁻⁴ m²), I is the light intensity (Wm⁻²), λ is the corresponding wavelength (m), N_A is the Avogadro's constant (6.023 × 10²³ mol⁻¹), h is the Planck constant (6.636 × 10⁻³⁴ W s²) and c is the velocity of light (3.00 × 10⁸ m s⁻¹).

To quantify the photocatalytically evolved H₂, a 50 µL gas sample was periodically taken from the reaction headspace using a Valco gas-tight sampling syringe and injected into a Shimadzu 8A gas chromatograph (GC). The GC was equipped with a thermal conductivity detector (TCD) and a stainless- molecular sieve 5A GC column (Sigma-Aldrich, USA). The temperatures of the column, injector port, and TCD detector were maintained at 80°C, 120°C, and 120°C, respectively.

The concentration of naphthalene before and after the experiment was quantified using Merck L 6200A (Hitachi) High-Performance Liquid Chromatography (HPLC) system equipped with a Nucleosil 120 C18 (250 mm × 4.0 mm × 5.0 μm) column and a UV-VIS detector operated at 276 nm. The column temperature was maintained at 30 °C. The mobile phase was a mixture of methanol (A) and water (B) with a gradient mode [initial (40% A: 60% B); 17 min (85% A: 15% B) and hold for 4 min; 2 min (95% A: 5% B) and hold for 4 min; and finally, 1 min (40% A: 60% B) and hold for 3 min]. The flow rate was 1.0 mL min⁻¹ and the injection volume was 50 μl. The total run time was 32 min. A 1 mL from each reaction vial was taken at the end of the experiment, filtrated through 0.2 μm PTFE syringe filters to remove the TiO₂ particles, and then injected immediately in the HPLC to avoid the loss of naphthalene from the solution.

3.5.4 Catalyst Characterization

The synthesized photocatalysts were characterized by X-ray diffraction analysis (XRD) patterns using Bruker D8 Advance diffractometer (Bruker AXS GmbH) with a Bragg-Brentano geometry employing Cu K α radiation ($\lambda=1.54060$ Å). The patterns were recorded in the 2 θ range between 10° and 80° in steps of 0.039°. Brunauer – Emmett – Teller (BET) specific surface areas were measured by a FlowSorb II 2300 instrument equipped with a Micromeritics AutoMate 23. Prior to the measurements, all the synthesized platinumized TiO₂ samples were pre-degassed in a vacuum at 150 °C for 1 h. The specific surface area was measured in triplicates and determined through single-point standard BET surface area measurements. Diffuse reflectance (DR) UV-vis spectra were recorded with a Varian Cary 100 Bio Spectrophotometer (Agilent), equipped with a diffuse reflectance accessory. BaSO₄ was used as a baseline and blank for measuring the wavelength range from 200 to 800 nm. The actual percentage of Pt nanoparticles on the TiO₂ surface was determined by using Inductively coupled plasma - optical emission spectrometry (ICP-OES, Varian 715-ES, Varian). A 20 to 30 mg of the Pt-TiO₂ samples were digested at 150 °C for 3h in 5.00 mL aqua regia (3:1 HCl/HNO₃ mixture) until the acid nearly evaporated. Afterward, the digested samples re-dissolved in 10.00 mL of 3% HNO₃ and filtrated through a filter paper. The eluent was stored at 4 °C prior to the analysis. The 3% HNO₃ was used as a blank for all the analyses. The results are summarized in Table 3-1. Transmission Electron Microscopy (TEM) measurements were carried out on a Tecnai G2 F20 TMP (FEI) with an acceleration voltage of 200 kV field emission gun (FEG). The powdered specimen was dry fixed on a holey carbon film supported by a Cu grid.

3.5.5 EPR in Situ Experiments

Electron paramagnetic resonance (EPR) spin trapping technique was applied to study the dynamic of the charge carrier by monitoring the formation of paramagnetic intermediates upon irradiation of different platinized TiO₂ materials in situ using an X-band EPR MiniScope MS400 (Magnettech GmbH, Berlin, Germany) spectrometer. The experiments were carried out at 77 K using liquid nitrogen. The solid materials were charged inside an EPR quartz tube (260 mm × 4.0 mm × 0.5 mm), purged once with N₂, and other with N₂-naphthalene vapor mixture for 30 min each for separate measurements. The instrument was operated at 9.43 GHz field modulation and equipped with a UV spot-light (LC8, Hamamatsu, 200 W super-quiet mercury-xenon lamp). The acquisition parameters were as follows: center field: 337.07 mT, sweep time 30 s, range 30 mT, number of points: 4096, number of scans: 1, modulation amplitude: 0.15 mT, power: 10 mW, and gain: 5.

3.6 Conclusions

In summary, the presented results show that Pt-HTiO₂ exhibits a higher photocatalytic activity for H₂ evolution than Pt-ATiO₂ during the photoreforming of the naphthalene. However, both platinized photocatalysts show a similar activity towards the photooxidation of naphthalene. The 0.5 wt% fractional ratio of Pt nanoparticles on the surface of the HTiO₂ shows the higher photocatalytic activity toward the naphthalene conversion and H₂ evolution, while no relation was found between the H₂ evolution and the Pt content on the ATiO₂. In the presence of the hole scavenger naphthalene, Pt nanoparticles on the surface of HTiO₂ act as electron scavengers, enhancing hydrogen production rates, while on the surface of ATiO₂ they act as recombination centers for the photogenerated charge carrier. The photoreforming of naphthalene over Pt-HTiO₂ resulted in higher amounts of H₂ and conversion compared to their corresponding intermediates, naphthalen-1-ol and naphthalen-2-ol. The inhibition of the H₂ formation and naphthalene conversion rates during the photocatalysis process is ascribed to the adsorption of the formed intermediates on the surface of the TiO₂. Although this technique is considered as a promising process for hydrogen evolution in addition to the degradation of naphthalene, however, for the very low concentrations in real wastewater, other cheaper traditional removal techniques can be used.

3.7 Acknowledgments

Financial support from the Katholischer Akademischer Ausländer-Dienst (KAAD) and Graduiertenakademie at Gottfried Wilhelm Leibniz Universität Hannover are gratefully acknowledged for providing scholarships for Osama Al-Madanat to perform his Ph.D. Osama Al-Madanat wishes to thank Dr. Mariano Curti for the helpful assistance and discussion while preparing the manuscript. The publication of this article was funded by the Open Access Publishing Fund of Leibniz Universität Hannover.

3.8 Author Contributions

Conceptualization, methodology, formal analysis, investigation, writing—original draft preparation: **Osama Al-Madanat**. Writing—review and editing: **Osama Al-Madanat**, **Yamen AlSalka**, **Ralf Dillert**. Supervision: **Ralf Dillert**, **Detlef W. Bahnemann**.

3.9 References

1. Møller, K. T.; Jensen, T. R.; Akiba, E.; Li, H.-w., Hydrogen - A sustainable energy carrier. *Prog. Nat. Sci.* **2017**, *27* (1), 34-40.
2. Niaz, S.; Manzoor, T.; Pandith, A. H., Hydrogen storage: Materials, methods and perspectives. *Renew. Sust. Energ. Rev.* **2015**, *50*, 457-469.
3. Cavendish, H., XIII. Experiments on air. *Philos. Trans. R. Soc.* **1784**, *74*, 119-153.
4. Kennedy, J.; Bahruji, H.; Bowker, M.; Davies, P. R.; Bouleghlimat, E.; Issarapanacheewin, S., Hydrogen generation by photocatalytic reforming of potential biofuels: Polyols, cyclic alcohols, and saccharides. *J. Photochem. Photobiol. A.* **2018**, *356*, 451-456.
5. Fajrina, N.; Tahir, M., A critical review in strategies to improve photocatalytic water splitting towards hydrogen production. *Int. J. Hydrog. Energy* **2019**, *44* (2), 540-577.
6. Al Nasir, F.; Batarseh, M. I., Agricultural reuse of reclaimed water and uptake of organic compounds: pilot study at Mutah University wastewater treatment plant, Jordan. *Chemosphere* **2008**, *72* (8), 1203-14.
7. Rubio-Clemente, A.; Torres-Palma, R. A.; Penuela, G. A., Removal of polycyclic aromatic hydrocarbons in aqueous environment by chemical treatments: A review. *Sci. Total. Environ.* **2014**, *478*, 201-25.
8. Wauchope, R. D.; Getzen, F. W., Temperature dependence of solubilities in water and heats of fusion of solid aromatic-hydrocarbons. *J. Chem. Eng. Data* **1972**, *17* (1), 38-&.
9. Ghasemi, N.; Gbeddy, G.; Egodawatta, P.; Zare, F.; Goonetilleke, A., Removal of polycyclic aromatic hydrocarbons from wastewater using dual-mode ultrasound system. *Water Environ. J.* **2020**, *34* (S1), 425-434.

10. Kadri, T.; Rouissi, T.; Kaur Brar, S.; Cledon, M. Sarma, S.; Verma, M., Biodegradation of polycyclic aromatic hydrocarbons (PAHs) by fungal enzymes: A review. *J. Environ. Sci. (China)* **2017**, *51*, 52-74.
11. Chu, L. B.; Yu, S. Q.; Wang, J. L., Gamma radiolytic degradation of naphthalene in aqueous solution. *Radiat. Phys. Chem.* **2016**, *123*, 97-102.
12. Mondal, K.; Bhattacharyya, S.; Sharma, A., Photocatalytic degradation of naphthalene by electrospun mesoporous carbon-doped anatase TiO₂ nanofiber mats. *Ind. Eng. Chem. Res.* **2014**, *53* (49), 18900-18909.
13. Garcia-Martinez, M. J.; Canoira, L.; Blazquez, G.; Da Riva, I.; Alcantara, R.; Llamas, J. F., Continuous photodegradation of naphthalene in water catalyzed by TiO₂ supported on glass Raschig rings. *Chem. Eng. J.* **2005**, *110* (1-3), 123-128.
14. Al-Madanat, O.; Alsalka, Y.; Curti, M.; Dillert, R.; Bahnemann, D. W., Mechanistic insights into hydrogen evolution by photocatalytic reforming of naphthalene. *ACS Catal.* **2020**, *10* (13), 7398-7412.
15. AlSalka, Y.; Hakki, A.; Fleisch, M.; Bahnemann, D. W., Understanding the degradation pathways of oxalic acid in different photocatalytic systems: Towards simultaneous photocatalytic hydrogen evolution. *J. Photochem. Photobiol. A.* **2018**, *366*, 81-90.
16. Weon, S.; Kim, J.; Choi, W., Dual-components modified TiO₂ with Pt and fluoride as deactivation-resistant photocatalyst for the degradation of volatile organic compound. *Appl. Catal. B-Environ.* **2018**, *220*, 1-8.
17. Schneider, J.; Bahnemann, D. W., Undesired role of sacrificial reagents in photocatalysis. *J. Phy. Chem. Lett.* **2013**, *4* (20), 3479-3483.
18. Hashimoto, K.; Kawai, T.; Sakata, T., Photocatalytic reactions of hydrocarbons and fossil-fuels with Water - hydrogen-production and oxidation. *J. Phys. Chem.* **1984**, *88* (18), 4083-4088.
19. Yuzawa, H.; Aoki, M.; Otake, K.; Hattori, T.; Itoh, H.; Yoshida, H., Reaction mechanism of aromatic ring hydroxylation by water over platinum-loaded titanium oxide photocatalyst. *J. Phys. Chem. C* **2012**, *116* (48), 25376-25387.
20. AlSalka, Y.; Al-Madanat, O.; Curti, M.; Hakki, A.; Bahnemann, D. W., Photocatalytic H₂ evolution from oxalic acid: Effect of cocatalysts and carbon dioxide radical anion on the surface charge transfer mechanisms. *ACS Appl. Energy Mater.* **2020**, *3* (7), 6678-6691.
21. Kandiel, T. A.; Feldhoff, A.; Robben, L.; Dillert, R.; Bahnemann, D. W., Tailored titanium dioxide nanomaterials: Anatase nanoparticles and brookite nanorods as highly active photocatalysts. *Chem. Mater.* **2010**, *22* (6), 2050-2060.
22. Abdulrazzak, F. H.; Hussein, F. H.; Alkaim, A. F.; Ivanova, I.; Emeline, A. V.; Bahnemann, D. W., Sonochemical/hydration-dehydration synthesis of Pt-TiO₂ NPs/decorated carbon nanotubes with enhanced photocatalytic hydrogen production activity. *Photochem. Photobiol. Sci.* **2016**, *15* (11), 1347-1357.

23. Colon, G.; Hidalgo, M. C.; Navio, J. A., Photocatalytic deactivation of commercial TiO₂ samples during simultaneous photoreduction of Cr(VI) and photooxidation of salicylic acid. *J. Photochem. Photobiol. A* **2001**, *138* (1), 79-85.
24. Alonso-Tellez, A.; Masson, R.; Robert, D.; Keller, N.; Keller, V., Comparison of Hombikat UV100 and P25 TiO₂ performance in gas-phase photocatalytic oxidation reactions. *J. Photochem. Photobiol. A* **2012**, *250*, 58-65.
25. Abellan, M. N.; Dillert, R.; Gimenez, J.; Bahnemann, D., Evaluation of two types of TiO₂-based catalysts by photodegradation of DMSO in aqueous suspension. *J. Photochem. Photobiol. A* **2009**, *202* (2-3), 164-171.
26. AlSalka, Y.; Hakki, A.; Schneider, J.; Bahnemann, D. W., Co-catalyst-free photocatalytic hydrogen evolution on TiO₂: Synthesis of optimized photocatalyst through statistical material science. *Appl. Catal. B-Environ.* **2018**, *238*, 422-433.
27. Chen, Y.; Wang, Y.; Li, W.; Yang, Q.; Hou, Q.; Wei, L.; Liu, L.; Huang, F.; Ju, M., Enhancement of photocatalytic performance with the use of noble-metal-decorated TiO₂ nanocrystals as highly active catalysts for aerobic oxidation under visible-light irradiation. *Appl. Catal. B-Environ.* **2017**, *210*, 352-367.
28. Diebold, U., The surface science of titanium dioxide. *Surf. Sci. Rep.* **2003**, *48* (5-8), 53-229.
29. Kowalska, E.; Remita, H.; Colbeau-Justin, C.; Hupka, J.; Belloni, J., Modification of titanium dioxide with platinum ions and clusters: Application in photocatalysis. *J. Phys. Chem. C* **2008**, *112* (4), 1124-1131.
30. Kozlova, E. A.; Lyubina, T. P.; Nasalevich, M. A.; Vorontsov, A. V.; Miller, A. V.; Kaichev, V. V.; Parmon, V. N., Influence of the method of platinum deposition on activity and stability of Pt/TiO₂ photocatalysts in the photocatalytic oxidation of dimethyl methylphosphonate. *Catal. Commun.* **2011**, *12* (7), 597-601.
31. Kandiel, T. A.; Dillert, R.; Robben, L.; Bahnemann, D. W., Photonic efficiency and mechanism of photocatalytic molecular hydrogen production over platinumized titanium dioxide from aqueous methanol solutions. *Catal. Today* **2011**, *161* (1), 196-201.
32. Abdel-Azim, S. M.; Aboul-Gheit, A. K.; Ahmed, S. M.; El-Desouki, D. S.; Abdel-Mottaleb, M. S. A., Preparation and application of mesoporous nanotitania photocatalysts using different templates and PH media. *Int. J. Photoenergy* **2014**, *2014*, 1-11.
33. Wenderich, K.; Mul, G., Methods, mechanism, and applications of photodeposition in photocatalysis: A review. *Chem. Rev.* **2016**, *116* (23), 14587-14619.
34. Al-Azri, Z. H. N.; AlOufi, M.; Chan, A.; Waterhouse, G. I. N.; Idriss, H., Metal particle size effects on the photocatalytic hydrogen ion reduction. *ACS Catal.* **2019**, *9* (5), 3946-3958.
35. Li, H.; Yu, H.; Sun, L.; Zhai, J.; Han, X., A self-assembled 3D Pt/TiO₂ architecture for high-performance photocatalytic hydrogen production. *Nanoscale* **2015**, *7* (5), 1610-5.
36. Xing, J.; Li, Y. H.; Jiang, H. B.; Wang, Y.; Yang, H. G., The size and valence state effect of Pt on photocatalytic H₂ evolution over platinumized TiO₂ photocatalyst. *Int. J. Hydrog. Energy* **2014**, *39* (3), 1237-1242.

37. Wang, D.; Liu, Z. P.; Yang, W. M., Revealing the size effect of platinum cocatalyst for photocatalytic hydrogen evolution on TiO₂ support: A DFT study. *ACS Catal.* **2018**, *8* (8), 7270-7278.
38. Chen, H. R.; Li, P.; Umezawa, N.; Abe, H.; Ye, J. H.; Shiraishi, K.; Ohta, A.; Miyazaki, S., Bonding and electron energy-level alignment at metal/TiO₂ interfaces: A density functional theory study. *J. Phys. Chem. C* **2016**, *120* (10), 5549-5556.
39. Su, R.; Bechstein, R.; So, L.; Vang, R. T.; Sillassen, M.; Esbjornsson, B.; Palmqvist, A.; Besenbacher, F., How the anatase-to-rutile ratio influences the photoreactivity of TiO₂. *J. Phys. Chem. C* **2011**, *115* (49), 24287-24292.
40. Riegel, G.; Bolton, J. R., Photocatalytic efficiency variability in TiO₂ particles. *J. Phys. Chem.* **1995**, *99* (12), 4215-4224.
41. Scanlon, D. O.; Dunnill, C. W.; Buckeridge, J.; Shevlin, S. A.; Logsdail, A. J.; Woodley, S. M.; Catlow, C. R.; Powell, M. J.; Palgrave, R. G.; Parkin, I. P.; Watson, G. W.; Keal, T. W.; Sherwood, P.; Walsh, A.; Sokol, A. A., Band alignment of rutile and anatase TiO₂. *Nat. Mater.* **2013**, *12* (9), 798-801.
42. Hurum, D. C.; Agrios, A. G. Gray, K. A.; Rajh, T.; Thurnauer, M. C., Explaining the enhanced photocatalytic activity of Degussa P25 mixed-phase TiO₂ using EPR. *J. Phys. Chem. B* **2003**, *107* (19), 4545-4549.
43. Dahl, M.; Liu, Y.; Yin, Y., Composite titanium dioxide nanomaterials. *Chem. Rev.* **2014**, *114* (19), 9853-89.
44. Hufschmidt, D.; Bahemann, D.; Testa, J. J.; Emilio, C. A.; Litter, M. I., Enhancement of the photocatalytic activity of various TiO₂ materials by platinisation. *J. Photochem. Photobiol. A.* **2002**, *148* (1-3), 223-231.
45. Sakthivel, S.; Shankar, M. V.; Palanichamy, M.; Arabindoo, B.; Bahnemann, D. W.; Murugesan, V., Enhancement of photocatalytic activity by metal deposition: characterisation and photonic efficiency of Pt, Au and Pd deposited on TiO₂ catalyst. *Water Res.* **2004**, *38* (13), 3001-8.
46. Sun, B.; Vorontsov, A. V.; Smirniotis, P. G., Role of platinum deposited on TiO₂ in phenol photocatalytic oxidation. *Langmuir* **2003**, *19* (8), 3151-3156.
47. Benz, D.; Felter, K. M.; Koser, J.; Thoming, J.; Mul, G.; Grozema, F. C.; Hintzen, H. T.; Kreutzer, M. T.; van Ommen, J. R., Assessing the role of Pt Clusters on TiO₂ (P25) on the photocatalytic degradation of acid blue 9 and rhodamine B. *J. Phys. Chem. C* **2020**, *124* (15), 8269-8278.
48. Bamwenda, G. R.; Tsubota, S.; Nakamura, T.; Haruta, M., Photoassisted hydrogen production from a water-ethanol solution: a comparison of activities of Au-TiO₂ and Pt-TiO₂. *J. Photochem. Photobiol. A.* **1995**, *89* (2), 177-189.
49. Khan, M. R.; Chuan, T. W.; Yousuf, A.; Chowdhury, M. N. K.; Cheng, C. K., Schottky barrier and surface plasmonic resonance phenomena towards the photocatalytic reaction: study of their mechanisms to enhance photocatalytic activity. *Catal. Sci. Technol.* **2015**, *5* (5), 2522-2531.

50. Ola, O.; Maroto-Valer, M. M., Review of material design and reactor engineering on TiO₂ photocatalysis for CO₂ reduction. *J. Photochem. Photobiol. C.* **2015**, *24*, 16-42.
51. Bui, T. D.; Kimura, A.; Ikeda, S.; Matsumura, M., Determination of oxygen sources for oxidation of benzene on TiO₂ photocatalysts in aqueous solutions containing molecular oxygen. *J. Am. Chem. Soc.* **2010**, *132* (24), 8453-8.
52. Pang, X.; Chen, C.; Ji, H.; Che, Y.; Ma, W.; Zhao, J., Unraveling the photocatalytic mechanisms on TiO₂ surfaces using the oxygen-18 isotopic label technique. *Molecules* **2014**, *19* (10), 16291-311.
53. Augugliaro, V.; Bellardita, M.; Loddo, V.; Palmisano, G.; Palmisano, L.; Yurdakal, S., Overview on oxidation mechanisms of organic compounds by TiO₂ in heterogeneous photocatalysis. *J. Photochem. Photobiol. C.* **2012**, *13* (3), 224-245.
54. Montoya, J. F.; Ivanova, I.; Dillert, R.; Bahnemann, D. W.; Salvador, P.; Peral, J., Catalytic role of surface oxygens in TiO₂ photooxidation reactions: Aqueous benzene photooxidation with Ti¹⁸O₂ under anaerobic conditions. *J. Phys. Chem. Lett.* **2013**, *4* (9), 1415-22.
55. Bui, T. D.; Kimura, A.; Higashida, S.; Ikeda, S.; Mafsumura, M., Two routes for mineralizing benzene by TiO₂-photocatalyzed reaction. *Appl. Catal. B-Environ.* **2011**, *107* (1-2), 119-127.
56. Bui, T. D.; Kimura, A.; Ikeda, S.; Matsumura, M., Lowering of photocatalytic activity of TiO₂ particles during oxidative decomposition of benzene in aerated liquid. *Appl. Catal. B-Environ.* **2010**, *94* (1-2), 186-191.
57. Panagiotopoulou, P.; Karamerou, E. E.; Kondarides, D. I., Kinetics and mechanism of glycerol photo-oxidation and photo-reforming reactions in aqueous TiO₂ and Pt/TiO₂ suspensions. *Catal. Today* **2013**, *209*, 91-98.
58. Imizcoz, M.; Puga, A. V., Assessment of photocatalytic hydrogen production from biomass or wastewaters depending on the metal co-catalyst and its deposition method on TiO₂. *Catalysts* **2019**, *9* (7), 584.
59. Schneider, J.; Matsuoka, M.; Takeuchi, M.; Zhang, J.; Horiuchi, Y.; Anpo, M.; Bahnemann, D. W., Understanding TiO₂ photocatalysis: mechanisms and materials. *Chem. Rev.* **2014**, *114* (19), 9919-86.
60. King, S. M.; Leaf, P. A.; Olson, A. C.; Ray, P. Z.; Tarr, M. A., Photolytic and photocatalytic degradation of surface oil from the Deepwater Horizon spill. *Chemosphere* **2014**, *95*, 415-22.
61. Qourzal, S.; Assabane, A.; Ait-Ichou, Y., Synthesis of TiO₂ via hydrolysis of titanium tetraisopropoxide and its photocatalytic activity on a suspended mixture with activated carbon in the degradation of 2-naphthol. *J. Photochem. Photobiol. A.* **2004**, *163* (3), 317-321.
62. Brahmia, O.; Richard, C., Photochemical transformation of 1-naphthol in aerated aqueous solution. *Photochem. Photobiol. Sci.* **2005**, *4* (6), 454-8.
63. Weon, S.; Choi, W., TiO₂ nanotubes with open channels as deactivation-resistant photocatalyst for the degradation of volatile organic compounds. *Environ. Sci. Technol.* **2016**, *50* (5), 2556-63.

64. Theurich, J.; Bahnemann, D. W.; Vogel, R.; Ehamed, F. E.; Alhakimi, G.; Rajab, I., Photocatalytic degradation of naphthalene and anthracene: GC-MS analysis of the degradation pathway. *Res. Chem. Intermediat.* **1997**, *23* (3), 247-274.
65. Mills, A.; Davies, R. H.; Worsley, D., Water-purification by semiconductor photocatalysis. *Chem. Soc. Rev.* **1993**, *22* (6), 417-425.
66. Ajmal, A.; Majeed, I.; Malik, R. N.; Idriss, H.; Nadeem, M. A., Principles and mechanisms of photocatalytic dye degradation on TiO₂ based photocatalysts: a comparative overview. *RSC Adv.* **2014**, *4* (70), 37003-37026.
67. Qourzal, S.; Barka, N.; Tamimi, M.; Assabbane, A.; Ait-Ichou, Y., Photodegradation of 2-naphthol in water by artificial light illumination using TiO₂ photocatalyst: Identification of intermediates and the reaction pathway. *Appl. Catal. A-Gen.* **2008**, *334* (1-2), 386-393.
68. Denny, F.; Scott, J.; Chiang, K.; Teoh, W. Y.; Amal, R., Insight towards the role of platinum in the photocatalytic mineralisation of organic compounds. *J. Mol. Catal. A-Chem.* **2007**, *263* (1-2), 93-102.
69. Hurum, D. C.; Agrios, A. G.; Crist, S. E.; Gray, K. A.; Rajh, T.; Thurnauer, M. C., Probing reaction mechanisms in mixed phase TiO₂ by EPR. *J. Electron Spectrosc.* **2006**, *150* (2-3), 155-163.
70. Howe, R. F.; Gratzel, M., EPR study of hydrated anatase under UV irradiation. *J. Phys. Chem.* **1987**, *91* (14), 3906-3909.
71. Howe, R. F.; Gratzel, M., EPR observation of trapped electrons in colloidal titanium dioxide. *J. Phys. Chem.* **1985**, *89* (21), 4495-4499.
72. Kumar, C. P.; Gopal, N. O.; Wang, T. C.; Wong, M. S.; Ke, S. C., EPR investigation of TiO₂ nanoparticles with temperature-dependent properties. *J. Phys. Chem. B* **2006**, *110* (11), 5223-9.
73. Shapovalov, V.; Stefanovich, E. V.; Truong, T. N., Nature of the excited states of the rutile TiO₂(110) surface with adsorbed water. *Surf. Sci.* **2002**, *498* (1-2), L103-L108.
74. Nakaoka, Y.; Nosaka, Y., ESR Investigation into the effects of heat treatment and crystal structure on radicals produced over irradiated TiO₂ powder. *J. Photochem. Photobiol. A.* **1997**, *110* (3), 299-305.
75. Ke, S. C.; Wang, T. C.; Wong, M. S.; Gopal, N. O., Low temperature kinetics and energetics of the electron and hole traps in irradiated TiO₂ nanoparticles as revealed by EPR spectroscopy. *J. Phys. Chem. B* **2006**, *110* (24), 11628-34.
76. Connelly, K.; Wahab, A. K.; Idriss, H., Photoreaction of Au/TiO₂ for hydrogen production from renewables: a review on the synergistic effect between anatase and rutile phases of TiO₂. *Mater. Renew. Sustain. Energy* **2012**, *1* (1), 3.
77. Arizavi, A.; Mirbagheri, N. S.; Hosseini, Z.; Chen, P.; Sabbaghi, S., Efficient removal of naphthalene from aqueous solutions using a nanoporous kaolin/Fe₃O₄ composite. *Int. J. Environ. Sci. Technol.* **2020**, *17* (4), 1991-2002.

78. Nesterenko-Malkovskaya, A.; Kirzhner, F.; Zimmels, Y.; Armon, R., *Eichhornia crassipes* capability to remove naphthalene from wastewater in the absence of bacteria. *Chemosphere* **2012**, *87* (10), 1186-1191.
79. Al-Madanat, O.; Curti, M.; Günnemann, C.; Alsalka, Y.; Dillert, R.; Bahnemann, D. W., TiO₂ photocatalysis: Impact of the platinum loading method on reductive and oxidative half-reactions. *Catal. Today* (*under review*).

Chapter Four: TiO₂ Photocatalysis: Impact of the Platinum Loading Method on Reductive and Oxidative Half-Reactions

4.1 Foreword

The photocatalytic H₂ evolution reaction on the surface of the Pt-TiO₂ is driven by the capability of the Pt nanoparticles to scavenge the photogenerated electrons from the conduction band of the TiO₂ to act as cathodic sites for the reduction of the adsorbed protons. The trapping ability of Platinum nanoparticles in Pt-TiO₂ / organic pollutant-water systems is influenced by many structural factors, such as the Pt particle size, dispersion over the TiO₂ support, chemical state of Pt deposits, and the interaction between the metal and the support. In fact, these factors can be controlled and optimized by using a suitable preparation method. A fundamental understanding of the impact of these factors on the photocatalytic process still requires considerable investigation.

This chapter contains the article “*TiO₂ Photocatalysis: Impact of the Platinum Loading Method on Reductive and Oxidative Half-Reactions*” by Osama Al-Madanat, Mariano Curti, Carsten Günnemann, Yamen AlSalka, Ralf Dillert, and Detlef W. Bahnemann. Reproduced with permission from *Catalysis Today* 2021, 380, 3-15, (DOI: 10.1016/j.cattod.2021.07.013). Copyright 2021 Elsevier B.V.

In the previous chapter, the effects of different types of Pt-TiO₂ on the H₂ production by reforming of naphthalene were deeply investigated. In order to enhance the naphthalene photoreforming process, herein, platinum-loaded anatase TiO₂ photocatalysts were prepared using the photodeposition method and physical mixing of TiO₂ with Pt nanoparticles synthesized by laser ablation. Different analytical techniques were used to fully characterize both materials. The results of the photocatalytic experiments showed that the photodeposition method produced a higher active Pt-TiO₂ material. Although the smaller average Pt particle size in Pt-TiO₂ that was prepared by the photodeposition method could positively influence its properties, however, based on the transient absorption spectroscopy (TAS), and the electron paramagnetic resonance (EPR) experiments, it was found that the main factor governing the high activity of this material is the formation of a strong interaction between the Pt nanoparticles and the TiO₂ surface.

4.2 Abstract

Environmental pollution and shortage of energy resources are considered as the most serious threats faced by mankind. Heterogeneous photocatalysis has become one of the most frequently investigated technologies, thanks to its dual ability to convert solar energy into chemical energy and to perform environmental remediation. However, the low quantum efficiencies achieved so far by using TiO₂ photocatalysts represent a big challenge that needs to be overcome before their potential can be fully realized. Among other possibilities, the loading of noble metals (e.g. platinum) is a proven strategy to enhance the activity towards both, the photooxidation of organic pollutants and the evolution of molecular hydrogen via water reduction. However, the method in which Pt/TiO₂ is prepared appears to play a crucial role in tuning the photocatalytic activity.

In this work, platinum-loaded anatase TiO₂ photocatalysts were prepared using two alternative methods: photodeposition by reduction of PtCl₆²⁻ and physical mixing of TiO₂ with Pt nanoparticles synthesized by laser ablation. The effect of the Pt deposition method was evaluated for the photoreforming reaction of two organic substrates: naphthalene, and methanol. To explain the different activities, a full physicochemical characterization was performed for these samples, applying inductively coupled plasma - optical emission spectrometry (ICP-OES), X-ray diffraction (XRD), high resolution-transmission electron microscopy (HR-TEM), diffuse reflectance (DR) UV-vis spectroscopy, and Brunauer, Emmett and Teller adsorption (BET) methods. Moreover, the charge carrier dynamics in pristine and platinized TiO₂ were investigated by transient absorption spectroscopy (TAS), and by the electron paramagnetic resonance (EPR) technique, respectively.

The photodeposition of Pt leads to a significant decrease in the charge carrier recombination rates, which in turn led to an increased rate of the photocatalytic reactions. This effect was mainly attributed to the strong metal-semiconductor interaction resulting from the photodeposition process, aided by the preferential deposition on crystalline facets with strong reducing properties.

Keywords: Polycyclic aromatic hydrocarbons, preparation method, charge carrier dynamics, photoreforming, titania, H₂ production.

4.3 Introduction

Photocatalytic water splitting as a source for hydrogen (H₂) production is one of the most promising technologies for solar energy conversion and storage^{1, 2}. As a clean, inexhaustible, and renewable natural resource, solar energy emerges as the main option to overcome the dwindling energy resources and environmental deterioration^{1, 3}. Contrarily to fossil fuels, the photocatalytic production of hydrogen over semiconductor nanomaterials (e.g., TiO₂, WO₃, CdS) leads to a minimal environmental impact, with no atmospheric pollutants or particulates emitted during the production itself or the subsequent combustion of H₂^{4, 5}.

Among the various photocatalytic materials^{6, 7}, titanium dioxide is the most widely studied for water splitting reactions and environmental purification, because of its exceptional physicochemical characteristics, high oxidative power, and good photocatalytic performance in a wide range of reactions⁸⁻¹¹. However, the quantum efficiency of these processes remains extremely low¹², and therefore to reach practical applications three major obstacles must be overcome. Firstly, the rapid recombination of photogenerated charge carriers strongly limits the photocatalytic efficiency⁵. Secondly, the poor overlap of the absorption spectrum of TiO₂ with the solar emission spectrum results in a small fraction of photons being absorbed, mainly in the UV region. And thirdly, even in the presence of a sacrificial electron donor that promotes its formation, the quantum efficiency for H₂ production is negligible over pristine TiO₂, due to the large overpotential for the reduction of protons^{1, 13}.

Numerous strategies have been considered to improve the TiO₂'s photocatalytic performance, including sensitization with dyes, doping with metallic or non-metallic species, surface modification, and coupling with other materials^{2, 14}. Surface decoration with metals (especially Pt, Au, Ag, Cu) is able to simultaneously enhance charge carrier separation and to reduce the overpotential for H₂ evolution, which is known to greatly improve the H₂ production efficiency^{9, 15, 16}. According to the Schottky barrier model, such enhancement is attributed to the transfer of the photogenerated holes to the surface and the simultaneous migration of the electrons into the metal nanoparticles induced by the electric field in the space charge layer^{3, 11}. Amongst the metals that facilitate electron capture, Pt has been reported extensively as the most effective. Concomitantly, Pt is considered an excellent catalyst in dehydrogenation, oxidation in thermal catalysis, and hydrogenation

processes¹⁷. However, many structural factors seem to affect the activity of the resulting platinumized TiO₂, such as size^{15, 18}, dispersion¹⁹, chemical state of Pt deposits^{11, 19}, the interaction between the metal and the support^{20, 21}, and the preparation method^{14, 19, 22, 23}.

The most commonly adopted methods for the deposition of co-catalyst nanoparticles include photodeposition^{10, 22, 24}, deposition-precipitation²², chemical reduction^{9, 17}, impregnation²⁴, and physical mixing²², with photodeposition being the most commonly used^{2, 14}. Although one reason is that it tends to result in the most active materials, other beneficial features include the possibility of creating well-defined co-catalyst nanoparticles, with control over their geometrical distribution, size, and oxidation state, without the need for elevated temperatures or applied bias as other methods require^{1, 2, 12, 14, 22}.

Despite the positive features of the photodeposition technique, however, there is no clear consensus on why and when it results in high-performing materials. To shed light on this topic, herein we have prepared Pt-TiO₂ with two different methods: the classical photodeposition method, and the physical mixing method, where the Pt nanoparticles with a controlled shape and oxidation state were prepared via laser ablation. To differentiate their properties for both, the reductive and the oxidative photocatalytic half-reaction, we investigated the photoreforming of both naphthalene and methanol. Finally, by combining an extensive characterization of the materials with EPR and transient absorption spectroscopy, we offer a plausible explanation of the differences in the activity of the materials.

4.4 Experimental Section

4.4.1 Materials

Titanium dioxide (TiO₂, Hombikat UV100) was supplied by Sachtleben Chemie GmbH. Methanol (ROTISOLV® HPLC Gradient Grade, ≥ 99.9%) was supplied by Carl Roth GmbH, Germany. Naphthalene (≥ 99%), naphthalen-1-ol (97%), naphthalen-2-ol (99%), and chloroplatinic acid hexahydrate (H₂PtCl₆·6H₂O, 99.9%) were purchased from Sigma-Aldrich. All reagents were used as received. All solutions were prepared with deionized water obtained from a Millipore Mill-Q system (18.2 MΩ cm, 25 °C). Platinum nanoparticles (Pt NPs) were produced by Particular GmbH, Germany, using the pulsed laser ablation technique in deionized water, with high purity (99.99%) Pt plate as a target.

4.4.2 Preparation of the Photocatalysts

Platinum-loaded TiO₂ samples with a nominal 0.5% wt Pt fraction were prepared by two alternative methods. First, to prepare samples with the photodeposition method (Pt_{PD}-TiO₂), the TiO₂ powder (2.0 g) was dispersed in 200 mL of a 10% aqueous methanol solution with a 0.26 mmol L⁻¹ concentration in the platinum precursor (H₂PtCl₆). The suspension was stirred for 1 h prior to its purging for 1 h with argon. Afterward, the suspension was illuminated for 4 h with UV(A) light employing a Philips CLEO 15W lamp inside a climatic chamber to maintain the temperature at 18°C. The solid was separated by centrifugation, washed once with methanol and four times with distilled water, and finally dried at 100 °C for 24 h.

The synthesis procedure for platinum-loaded TiO₂ samples in which Pt NPs were prepared by laser ablation (Pt_{LA}-TiO₂) has been described by Marzun et al.²⁰. Briefly, after the preparation of the Pt nanoparticles colloid, the largest particles were separated by centrifugation (cut-off < 10 nm). After centrifugation, the Pt concentration in the colloid was determined by using ICP-OES. For the preparation of samples with nominal loadings of 0.5 and 1 wt%, the corresponding mass of the TiO₂ powder was mixed with the required volume of the Pt colloid and continuously stirred for one hour. Afterward, the platinum-loaded TiO₂ was recovered by centrifugation and dried at 70 °C overnight.

4.4.3 Photocatalysts Characterization

The actual loading of Pt NPs on the prepared photocatalysts was determined by using inductively coupled plasma - optical emission spectrometry (ICP-OES, Varian 715-ES, Varian). To this end, a mass of 20 to 30 mg of the Pt-TiO₂ samples was digested in 5.0 mL of aqua regia (3:1 HCl/HNO₃ mixture) at 150 °C for 3h, avoiding the complete evaporation. The digested samples were then diluted to 10.0 mL with 3% HNO₃, filtered, and the supernatant was stored at 4 °C prior to the analysis. Brunauer – Emmett – Teller (BET) specific surface areas were measured by a FlowSorb II 2300 instrument equipped with a Micromeritics AutoMate 23. All samples were pre-degassed in a vacuum at 150 °C for 1 h prior to the measurements. The specific surface areas were determined by means of single-point standard BET surface area measurements and measured by triplicate. X-ray diffraction (XRD) patterns were registered on a Bruker D8 Advance diffractometer (Bruker AXS GmbH) with a Bragg-Brentano geometry using Cu Ka radiation ($\lambda=1.54060 \text{ \AA}$). The patterns were recorded in the 2 θ range between 10° and 80° in steps of 0.039°. Diffuse reflectance (DR) UV-vis spectra were recorded with a Varian Cary 100 Bio

Spectrophotometer (Agilent), equipped with a diffuse reflectance accessory. BaSO₄ was used as a baseline and blank for measuring the wavelength range from 200 to 800 nm. Transmission Electron Microscopy (TEM) measurements were carried out on a JEOL JEM-2100F field-emission instrument, which was equipped with an EDX spectrometer of the type Oxford Instruments INCA-200 with an acceleration voltage of 200 kV from a field emission gun (FEG). The powdered specimen was dry-fixed (i.e. without using any solvent) on a holey carbon film supported by a Cu grid (Quantifoil, Multi A).

4.4.4 Transient Absorption Spectroscopy

The transient absorption spectroscopy (TAS) measurements were carried out in diffuse reflectance mode by means of an Applied Photophysics equipment employing an LKS80 nanosecond Laser Flash Photolysis Spectrometer with a pulsed Nd:YAG laser (Quantel, Brilliant B). Prior to the measurements, the powdered samples (contained in quartz cuvettes) were purged with N₂ or a mixture of nitrogen and methanol for 30 min. Excitation was performed at a wavelength of 355 nm with a pulse duration of 6 ns, with an average energy per pulse of 5 mJ cm⁻². The obtained transient signal, ΔJ, was detected upon measuring the absorbance value, Abs, of the reflected light before (J₀) and after the laser excitation (J) according to Equation 4-1. The transient signals were recorded up to 10 μs for each wavelength in the 660 to 400 nm range, at 20 nm steps.

$$\Delta J = 1 - 10^{-\text{Abs}} = \frac{J_0 - J}{J_0} \quad 4 - 1$$

4.4.5 Electron Paramagnetic Resonance

The electron paramagnetic resonance (EPR) technique was conducted in situ for pristine and platinized TiO₂ in order to detect and monitor the formation of the paramagnetic sites formed upon irradiation. The experiments were carried out at 77 K using liquid nitrogen. The equipment is an X-band EPR MiniScope MS400 (Magnettech GmbH, Germany) spectrometer operating at 9.43 GHz field modulation and equipped with a UV spot-light (LC8, Hamamatsu, 200 W super-quiet mercury-xenon lamp). The acquisition parameters were as follows: center field: 337.0 mT, field range 30 mT, sweep time 30 s, number of points: 4096, number of scans: 1, smooth 0.1 s, modulation amplitude: 0.15 mT, power: 10 mW, and gain: 5. The EPR signal was quantified by double integration of the signal, considered proportional to the amount of trapped charge carriers²⁵.

4.4.6 Photocatalytic Studies and Analytical Procedures

The photocatalytic activity of the synthesized platinumized TiO₂ was evaluated through the photocatalytic reforming of two different compounds, naphthalene, and methanol. In the first case, the experiments were carried out in batch mode, using 20 mL glass vials tightly closed with crimp caps and silicone septa. In a typical experiment, 15 mg of the photocatalyst powder was suspended in ca. 6 mL of deionized water inside a vial. The vial was then closed and purged with argon for 30 min. Afterward, the necessary volume from a deaerated stock naphthalene solution ($2.44 \times 10^{-4} \text{ mol L}^{-1}$) was injected inside the vial using a pre-purged syringe, to reach a final $1.00 \times 10^{-4} \text{ mol L}^{-1}$ (12.8 ppm) naphthalene concentration and a suspension volume of 15 mL. To establish the adsorption equilibrium, the vials were horizontally fixed and shook in the dark for 1 h inside an orbital shaker. Afterward, the orbital shaker was placed at a 30 cm distance below a solar simulator consisting of a 1000 W xenon lamp (Hönle UV Technology, Sol 1200) equipped with a filter to mimic the emission profile of sunlight. The temperature of the vials was maintained at $25 \pm 2 \text{ }^\circ\text{C}$ using a water bath. Photon flux density was determined by measuring the lamp irradiance in the wavelength range between 320 and 380 nm and was found to be $I_0 = 3.31 \times 10^{-4} \text{ mol m}^{-2} \text{ s}^{-1}$. Ignoring light losses due to reflection and scattering, $2.18 \times 10^{-7} \text{ mol}$ of photons entered the irradiated suspension per second. The photonic efficiencies were calculated based on Equations S4-1 and S4-2.

The concentration of naphthalene and its by-products were determined and monitored during the experiment by high-performance liquid chromatography (HPLC). HPLC analyses were performed using a Merck L 6200A (Hitachi) equipped with a UV-vis detector (Ecom system) operating at 276 nm. The column was a Nucleosil 120 C18 (250 mm \times 4.0 mm \times 5.0 μm), and the temperature was kept at 30 $^\circ\text{C}$. The oven temperature was 30 $^\circ\text{C}$ and the mobile phase was a mixture of methanol (A) and water (B) with a gradient mode as following: initial (40% A: 60% B); 17 min (85% A: 15% B) and hold for 4 min; 2 min (95% A: 5% B) and hold for 4 min; and finally, 1 min (40% A: 60% B) and hold for 3 min. The flow rate was 1.0 mL min⁻¹ and the injection volume was 50 μl , while the total run time was 32 min. Molecular hydrogen formation during the photo-induced degradation of naphthalene was quantified by using gas chromatography, with a Shimadzu GC-8A with thermal conductivity detector (GC-TCD), equipped with a stainless-steel molecular sieve 5A GC column (Sigma-Aldrich, USA). The temperatures of the column, TCD detector, and the injection port were kept at 80, 120, and 80 $^\circ\text{C}$, respectively. A 50 μL

gas sample was periodically taken from the headspace using a Valco gas-tight sampling syringe and injected into the GC.

For the photoreforming of methanol, 50 mg of platinized TiO₂ was suspended in 50 mL of a 10% (v/v) aqueous methanol solution inside a 65 mL cylindrical air-tight reactor with a quartz window (area = $5.03 \times 10^{-4} \text{ m}^2$). The reactor was connected to a HIDEN HPR-20 QIC gas analyzer equipped with a quadrupole mass spectrometer (QMS), to identify the evolved gases during the photocatalytic experiments. A continuous argon flow of 5 mL min^{-1} carried the headspace into the QMS system. In all experiments, the reaction suspension was purged with argon in the dark for 2 h to remove the dissolved O₂, and the temperature was maintained at 25 °C. Illumination was performed with an Osram XBO 1000-Watt xenon arc lamp as a solar simulator ($I_0^{320-385} = 1.55 \times 10^{-4} \text{ mol m}^{-2} \text{ s}^{-1}$). The amounts of formaldehyde and formic acid produced at the end of the irradiation period were determined by the Nash method²⁶ and High-Performance Ion Chromatography (HPIC) using a Dionex ICS-1000, respectively. The HPIC was equipped with a conductivity detector and an electro-regenerator suppressor. The temperature of the conductivity cell was kept constant at 35 °C during the analysis period. The column was an anion exchange resin (IonPac AS9-HC, L × I.D. 250 mm × 2 mm) and the sample eluted at a flow rate 0.3 mL min^{-1} with a mixture of alkaline solutions of $8 \times 10^{-3} \text{ mol L}^{-1} \text{ Na}_2\text{CO}_3$ and $1.5 \times 10^{-3} \text{ mol L}^{-1} \text{ NaHCO}_3$ for 90 min. Blank experiments showed no detectable gases evolution in the absence of either CH₃OH, irradiation, or Pt_{PD}-TiO₂ and Pt_{LA}-TiO₂ photocatalysts. Moreover, no signals for the formation of CH₂O or HCOOH were detected in the gas phase during all the photocatalytic experiments. The quantification of the QMS signals of H₂ and CO₂ was carried out by calibrating the QMS with standard argon-diluted H₂ and CO₂ (Linde Gas, Germany). The original signals of evolved gases during the experiments are shown in Figure S4-1 (a and b), while their integration is shown in the figures within the main text.

4.5 Results and Discussion

4.5.1 Photocatalysts Characterization

As a starting point in our analysis of the platinum deposition method, we performed a general characterization of samples prepared by two approaches: photodeposition from a Pt precursor, and physical mixing of TiO₂ with Pt NPs prepared by laser ablation. The X-ray diffraction (XRD) patterns of both types of samples, together with that of pristine TiO₂,

are shown in Figure 4-1. The three patterns display similar features, characteristic of nanocrystalline anatase TiO₂ photocatalysts, with broad reflections at the expected positions. This indicates small average crystallite sizes (Table 4-1) calculated from the main diffraction peak (101) based on the Scherrer equation. The loading of Pt at a 0.5 wt% fraction does not significantly change the patterns, showing that both preparation methods do not modify the phase or crystallite of TiO₂. Moreover, no reflections attributable to Pt were observed, as expected from its low mass fraction.

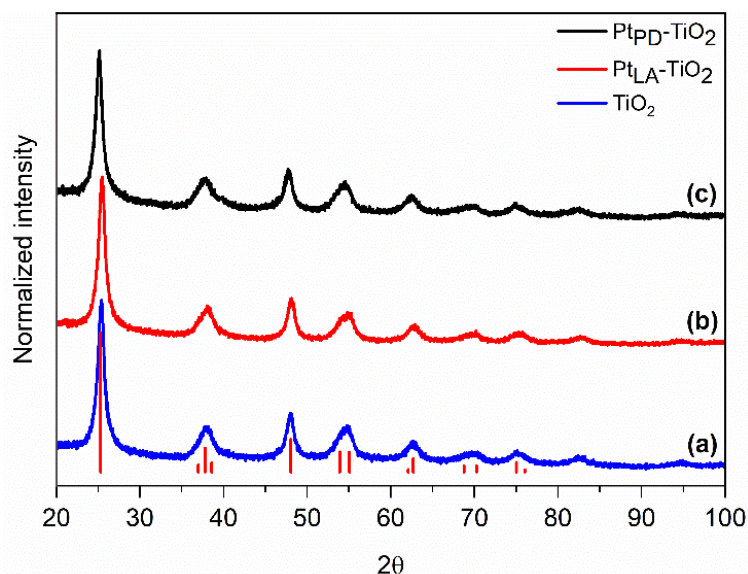


Figure 4-1: Normalized XRD pattern of (a) pristine TiO₂ (blue), (b) 0.5 wt% Pt_{LA}-TiO₂ (red), and (c) 0.5 wt% Pt_{PD}-TiO₂ (black). The red lines in the bottom represent the anatase reference.

Table 4-1: BET surface area and actual loaded Pt nanoparticles percentage for pristine and platinized TiO₂

Photocatalyst	Measured fraction of Pt wt%	BET surface area g m ⁻²	Average crystallite size ^a nm
TiO ₂ (UV100)	-	300 ± 3	8.1 ± 0.7
0.5 wt% Pt _{PD} -TiO ₂	0.46 ± 0.02	286 ± 2	8.4 ± 1.4
0.5 wt% Pt _{LA} -TiO ₂	0.43 ± 0.01	289 ± 3	8.2 ± 0.9
1.0 wt% Pt _{LA} -TiO ₂	0.88 ± 0.03	283 ± 2	8.5 ± 1.2

^a The values are calculated based on the Scherrer equation.

To confirm the presence of Pt NPs, and to determine their concentration, we performed ICP-OES after digesting the samples in aqua regia. The obtained values, shown in Table 4-1, indicate that the actual Pt content is slightly lower (~10%) than the nominal value for both employed methods. Within the experimental error, the values are the same irrespective of the preparation method. Moreover, as the nominal value is doubled, we observe that the measured Pt content increases in a similar trend.

Complementarily, we have determined the specific surface area of the samples through the BET method (Table 4-1). The TiO₂ material employed here, in pristine form, possesses a large specific surface area of 300 m² g⁻¹. This is consistent with the small crystallite size observed in XRD (Figure 4-1). The loading of platinum by the two methods leads to a decrease of around 5% in the specific surface area. We attribute this reduction to the surface coverage caused by the loading of Pt, noting that its small magnitude is consistent with the Pt fractions. A similar effect was reported by Sun et al.²⁷ during the platinization of Hombikat UV100 TiO₂. These authors observed an inverse proportional relation between the Pt fractional ratio and the surface area, which was explained by the agglomeration and clustering that occurred during the preparation process.

The diffuse reflectance UV–vis spectra of pristine and Pt-TiO₂ samples, transformed with the Kubelka – Munk function, are shown in Figure 4-2. All three spectra exhibit an absorption onset at 390 nm, in agreement with the optical band gap of 3.2 eV for the anatase TiO₂ polymorph⁸. Neither the photodeposition nor the physical mixing method induces a substantial variation of the bandgap. However, the Pt_{PD}-TiO₂ photocatalyst displays a small absorption increase in the visible region, as commonly observed in similar systems²⁸.

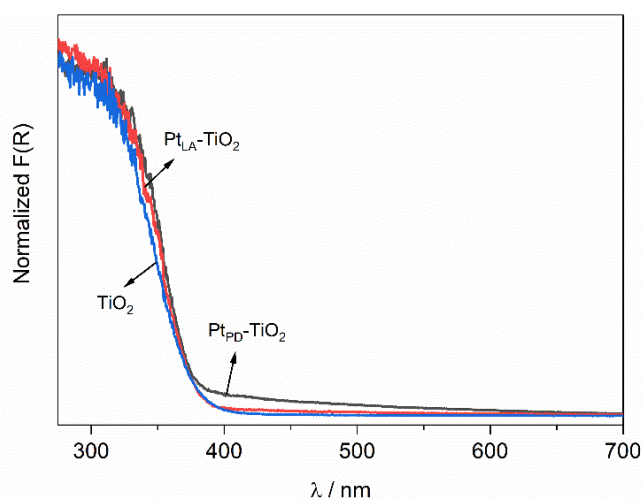


Figure 4-2: Normalized diffuse reflectance spectra (Kubelka–Munk function vs. wavelength) of pristine TiO₂ (blue line), 0.5 w% Pt_{LA}-TiO₂ (red), and 0.5 w% Pt_{PD}-TiO₂ (black).

We investigated the morphology of the Pt-TiO₂ samples prepared by the two methods by high-resolution transmission electron microscopy (HRTEM)-based energy-dispersive X-ray spectroscopy (EDXS) analysis. The micrographs of Figure 4-3 (a),(d) show the morphology of the TiO₂ nanoparticles, which display similar features irrespective of the Pt loading method. The crystallite diameters are in the range of 5-10 nm, while the selected

area electron diffraction (SAED) patterns (Figure S4-2) are consistent with the anatase phase. EDXS analysis confirms the homogeneous chemical composition with respect to titanium, oxygen, and platinum (Figure S4-3). Moreover, DF-HRTEM (Figure 4-3 (b, e)) and HAADF-STEM (Figure S4-4) elemental mapping images demonstrate highly dispersed Pt NPs over the oxide surface in both samples. However, a more uniform distribution was observed in the Pt_{PD}-TiO₂ catalyst. While this sample contains small Pt islands (Figure 4-3 a), suggesting a thin Pt layer on the surface of the TiO₂, spherical and larger Pt particles are observed on the surface of Pt_{LA}-TiO₂. The average particle size of Pt NPs formed during the photodeposition and laser ablation methods are estimated as 1.5 ± 0.6 nm and 2.6 ± 2.2 nm for a 100 deposit count (Figure 4-3 c,f), respectively. Moreover, EELS analysis confirms that the Pt particles formed by the laser ablation method are metallic Pt⁰ (Figure S4-5). By analogy with previous reports, we also expect the photodeposited sample to result in Pt⁰ nanoparticles²⁹⁻³¹.

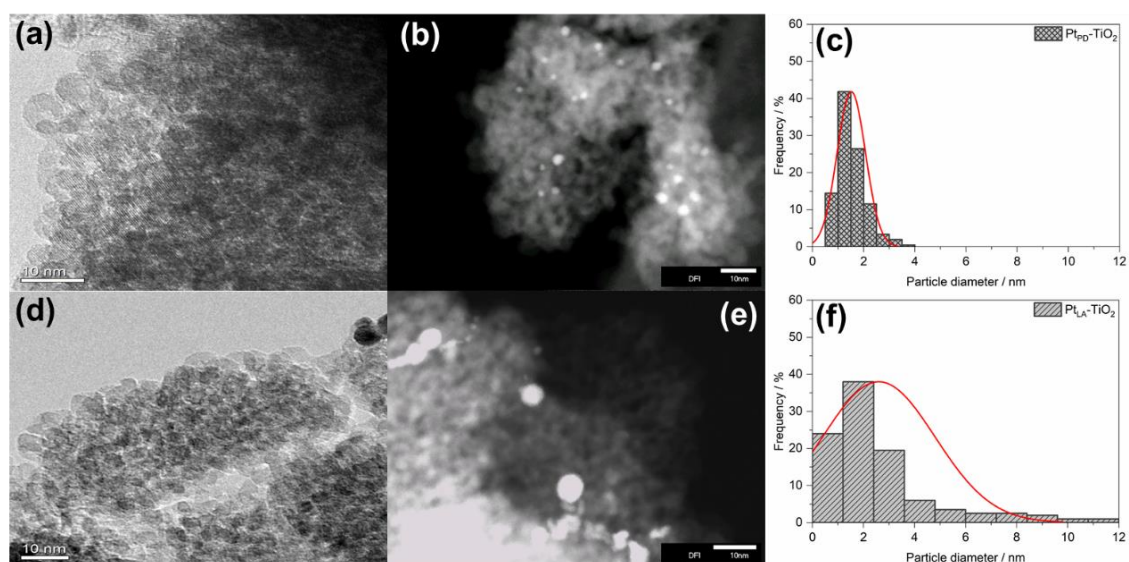


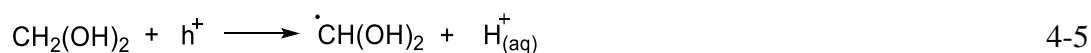
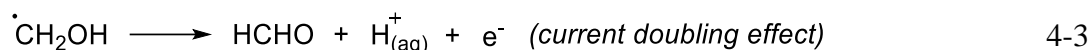
Figure 4-3. High-resolution transmission electron micrographs, high-angle annular dark-field scanning transmission electron micrographs (HAADF-STEM), and particle diameter distribution images for Pt_{PD}-TiO₂ (a, b, and c) and Pt_{LA}-TiO₂ (d, e, and f), respectively.

4.5.2 Photocatalytic Activity

To evaluate the effectiveness of the prepared Pt-TiO₂ samples we analyzed the photocatalytic reforming of two different sacrificial agents: methanol and naphthalene. This selection is based on the significantly different properties that they exhibit: while methanol strongly adsorbs on the TiO₂ surface^{9,32}, naphthalene interacts weakly with the surface of the TiO₂ through the formation of Ti⁴⁺⋯π-electron and/or OH_(surface)⋯π-electron type of complexes³³. Furthermore, naphthalene's oxidation is rather inefficient and involves a

large number of steps¹⁰, while methanol acts as a swift hole scavenger and is promptly mineralized. Moreover, its first oxidation step yields the hydroxymethyl radical, $\cdot\text{CH}_2\text{OH}$, which readily injects an electron into the conduction band of TiO₂⁴. This effect, known as current doubling, does not occur with naphthalene¹⁰.

Methanol is considered a good sacrificial electron donor. The main products of its reforming are acetaldehyde (HCHO), formic acid (HCOOH), and carbon dioxide (CO₂) from the oxidative pathway, and H₂ from the reduction side, as illustrated in Equations 4-1 to 4-10 and described in previous studies^{4,21}. In order to perform a long-term investigation, we employ here a high initial methanol concentration, to avoid its depletion and thus keep it as the majority donor species during the entire experiment.



The overall methanol decomposition reaction

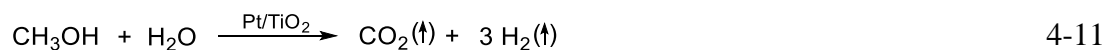


Figure 4-4 (a) shows the detected amounts of acetaldehyde and formic acid after 20 h of irradiation over each photocatalyst. Although acetaldehyde is readily oxidized to formic acid over TiO₂ (Equations 4-4 to 4-6), the higher concentration of methanol largely prevents this process by scavenging most holes, and thus the detected [acetaldehyde]:[formic acid] ratios are ~40 for pristine TiO₂ and ~80 for both platinized samples. Likewise, the time profiles for the formation of CO₂ (Figure 4-4 (b)) showed that both platinized photocatalysts formed relatively small amounts, while CO₂ formation was negligible in the

case of pristine TiO₂. However, both figures show that the Pt_{PD}-TiO₂ sample displays markedly faster oxidation kinetics for methanol than Pt_{LA}-TiO₂, producing approximately 3-fold higher amounts of acetaldehyde, formic acid, and CO₂ over the same time period. Looking at the production of H₂ (Figure 4-4 (c)), pristine TiO₂ formed a negligible amount in the absence of methanol. As discussed by Bahnemann et al.³⁴, H₂ is formed in substantial yields only in the presence of a co-catalyst such as Pt and a hole scavenger. Comparing the platinized materials, Pt_{PD}-TiO₂ displays a significantly better activity than Pt_{LA}-TiO₂. After 1 h illumination the photonic efficiencies for H₂ evolution are 15.6 % ± 0.3 % and 6.1 % ± 0.2 % for Pt_{PD}-TiO₂ and Pt_{LA}-TiO₂, respectively. A much lower value of 4.5 % was reported by Kandiel et al.⁴ for the H₂ formation after 1.5 h during the reforming of methanol over Pt-TiO₂ prepared by the photodeposition method.

A good comparison can be drawn with the work of Wang et al.²¹, who modified self-prepared colloidal TiO₂ with PtNPs by either the photodeposition or the physical mixing of colloidal Pt and TiO₂. They found that Pt-TiO₂ prepared by the photodeposition method is more efficient for photocatalytic oxidation of CH₃OH to HCHO. Similarly, it can be concluded here that platinization of the TiO₂ surface by the photodeposition technique provides a reliable procedure to improve the efficacy of the TiO₂, outperforming other preparation methods.

It is noteworthy that these experiments, performed over a relatively long period of time (>20 h), show no indication of an eventual decrease of the photocatalytic activity of either material, thus evincing their stability.

In addition, we note that the larger particle size of the Pt islands in Pt_{LA}-TiO₂ (Figure 4-3) may imply a smaller surface area of the co-catalyst. Therefore, to compensate for this effect, we have also considered for these reactions Pt_{LA}-TiO₂ samples with a nominal Pt loading of 1.0 wt%, often considered the optimal value^{14, 17, 22}. However, as shown in Figure S4-6 (a and b), this only results in a small increase in the production rate of each product, still far away from those observed for (0.5%) Pt_{PD}-TiO₂.

Complementarily, we performed similar experiments with the hole scavenger naphthalene. In our previous report¹⁰ we studied thoroughly the mechanism of photoreforming of naphthalene using the Pt_{PD}-TiO₂ photocatalyst. All by-products resulting from this process were also identified by using different chromatographic techniques, showing

that naphthalen-1-ol and naphthalen-2-ol are the major products of naphthalene photooxidation, according to Equations 4-12 to 4-17.

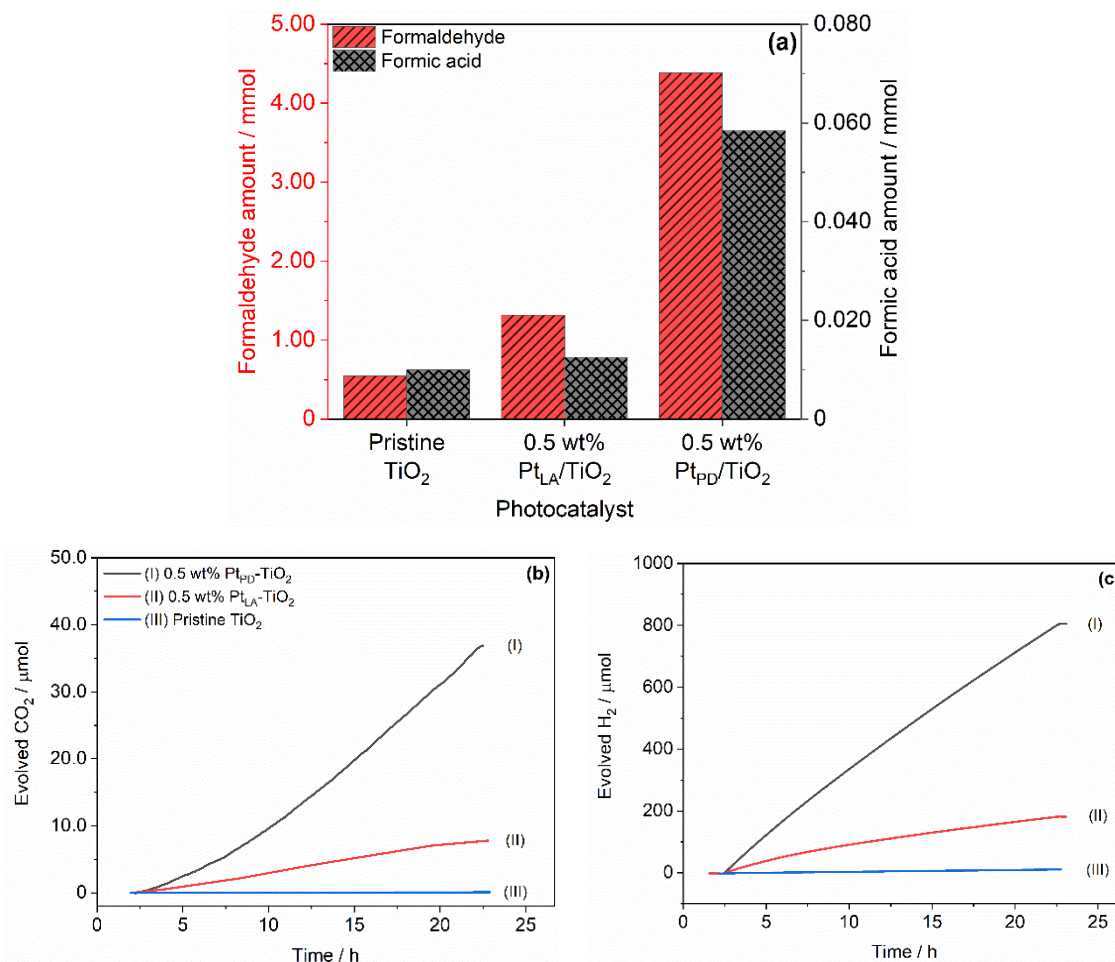
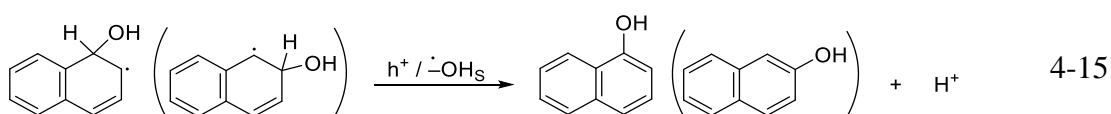
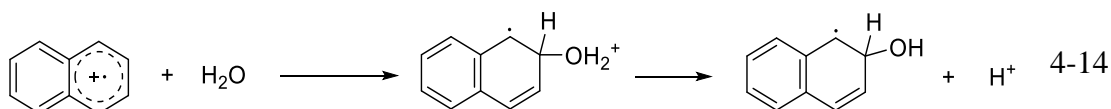
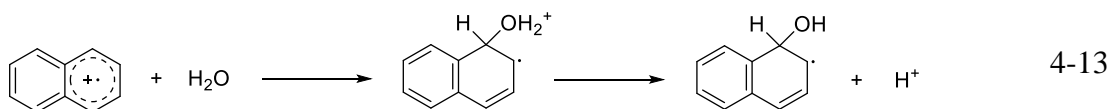
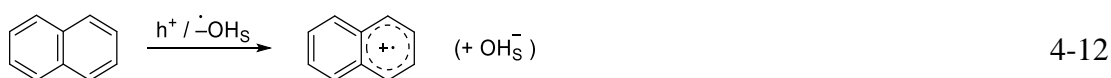


Figure 4-4. Amount of products from the photocatalytic reforming of 50 ml aqueous suspensions of 2.5 mol L⁻¹ methanol following 20 h of illumination over different photocatalysts. (a) the total amount of HCHO (red column) and HCOOH (black column), (b) and (c) evolved amounts of CO₂ and H₂, respectively



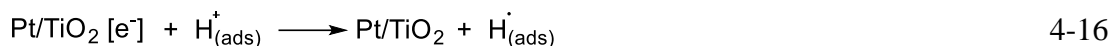


Figure 4-5 (a) shows the time profile for the naphthalene concentration during its photocatalytic reforming in the presence of pristine TiO₂, Pt_{PD}-TiO₂, and Pt_{LA}-TiO₂. The photonic efficiencies, calculated from the initial (1 h) removal rates, are 0.04 % ± 0.01 %, 0.12 % ± 0.01 %, and 0.11 % ± 0.01 %, respectively. Platinization of the TiO₂ resulted in an enhancement of the photocatalytic efficiency. However, in contrast with the methanol case, the preparation method has a minor effect on the photooxidation efficiency of naphthalene, with the Pt_{PD}-TiO₂ sample performing slightly better. On the other hand, both platinized samples achieve a ~90 % removal compared to ~60 % for pristine TiO₂ after 4h of irradiation.

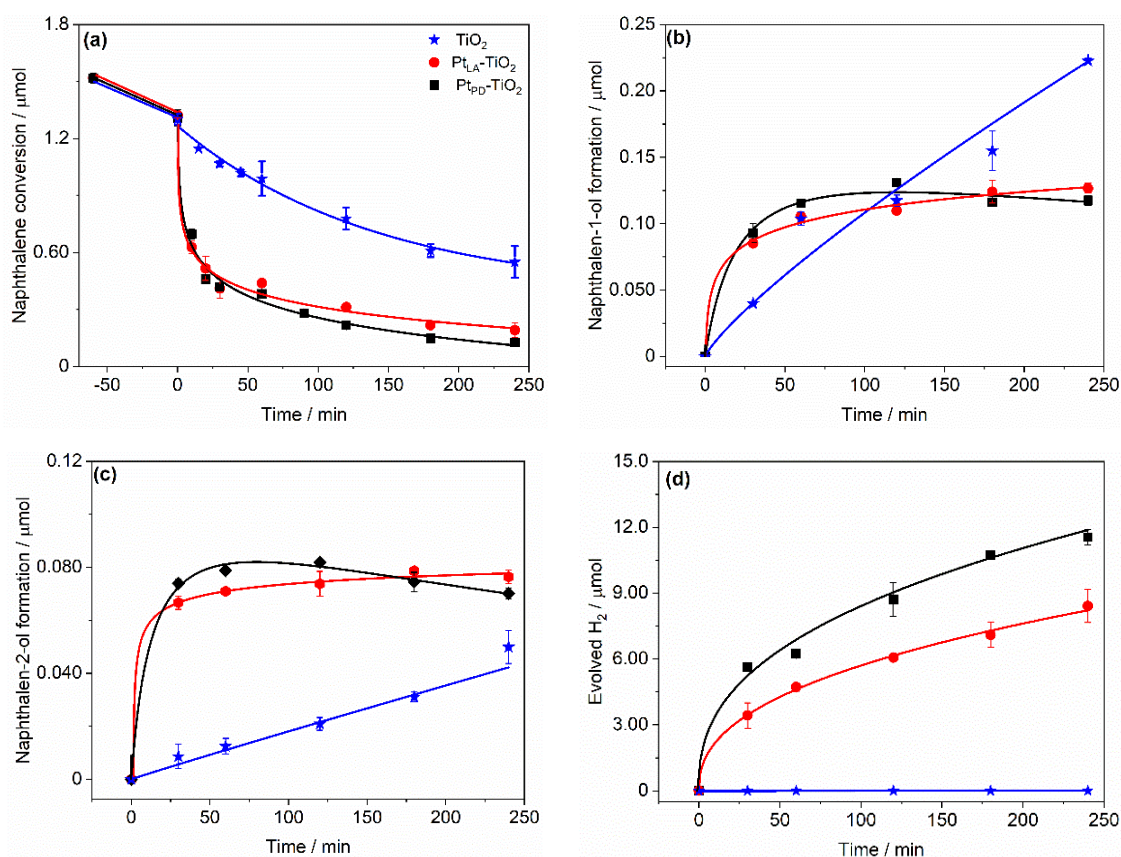


Figure 4-5: Kinetic profiles for (a) photooxidation of naphthalene, (b and c) formation of by-products during the reforming of naphthalene, and (d) production of H₂. Conditions: reaction volume, 15 mL; initial naphthalene concentration: 100 μmol L⁻¹; photocatalyst mass concentration 1 g L⁻¹; T = 25 °C; illumination with simulated solar light.

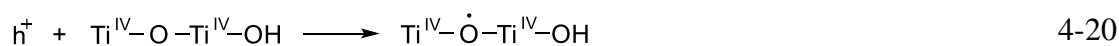
The main by-products of naphthalene photooxidation are naphthalen-1-ol and naphthalen-2-ol¹⁰, and we show the time profiles of their concentrations in Figure 4-5 (b

and c). Pristine TiO₂ showed a linear increase in the formation of both by-products with a higher selectivity for naphthalene-1-ol. The accumulation of both products in the system can be related to the inefficient photooxidation of naphthalene on the surface of pristine TiO₂ compared to the modified one. On the other hand, the overall shape of the kinetic profiles is similar for both platinized photocatalysts, with a fast accumulation in the first 25 minutes followed by a stabilization in the concentration of both naphthalene-1-ol and naphthalene-2-ol. The main difference is that, for the reaction over Pt_{PD}-TiO₂, naphthalenols concentrations reach maxima, and slowly decrease afterward, following the typical pattern of a reaction intermediate due to their increasingly faster consumption and slower production rates. The Pt_{LA}-TiO₂ sample displays slightly slower kinetics, with the concentration of both products still increasing after 4 h illumination.

The modification of the TiO₂ surface with platinum nanoparticles does not only promote the photooxidation of naphthalene but also enables H₂ evolution. Accordingly, the main difference between both platinized photocatalysts is observed in the reductive half-reaction. After 4 h of illumination, the amount of evolved H₂ is 40 % higher when using Pt_{PD}-TiO₂ than with Pt_{LA}-TiO₂, as shown in Figure 4-5 (d). The photonic efficiencies, calculated from the initial formation rates after 1 h, are 0.79 % ± 0.01 % and 0.60 % ± 0.02 %, respectively, which are within the typical ranges for heterogeneous photocatalytic processes³⁵.

4.5.3 EPR Investigation

Electronic paramagnetic resonance (EPR) spectroscopy is a powerful and sensitive technique to investigate charge carrier separation. Irradiation of anatase TiO₂ with photons of energy higher than 3.2 eV leads to the formation of electron-hole ($e^- - h^+$) pairs, as shown in Equation 4-1. Both e^- and h^+ are subsequently trapped either on the surface or in the bulk of the particles. Photogenerated electrons form paramagnetic Ti^{III}^{36, 37} (Equations 4-18 and 4-19), while holes are thought to be trapped in oxygen atoms, i.e. forming O^{•-} either in surface or subsurface positions (Equation 4-20)^{37, 38}.



Importantly, these species can be detected by EPR at liquid nitrogen temperatures (77 K), which allows studying the effect of the loaded PtNPs on the $e^- - h^+$ populations under irradiation conditions. For each sample, the signals were acquired before and after irradiation, after purging with either N₂ or N₂ - methanol. No significant signals were detected before irradiation in all samples (Figure S4-7). Upon irradiation, however, two groups of signals were registered in all cases (Figure S4-7), as is typical for hydrated anatase^{38, 39} (Figure S4-8). The region with g -tensor components > 2.000 ($g_x = 2.004$, $g_y = 2.015$, and $g_z = 2.019$) is attributed to trapped holes on or near the surface, while signals with g values < 2.000 are assigned to trapped electrons in the bulk, $Ti_{(bk)}^{III}$ ($g_{||}=1.992$ and $g_{\perp}=1.961$) and on the surface, $Ti_{(surf)}^{III}$ ($g_{||}=1.961$ and $g_{\perp}=1.94\sim 1.93$)^{37, 39, 40}.

Figure 4-6 (a) shows a comparison of the EPR signals for TiO₂, Pt_{LA}-TiO₂, and Pt_{PD}-TiO₂ after irradiation for 7 min under an inert atmosphere. The relative intensities of the electron and hole signals (determined by double integration⁴¹) show a clear and opposite trend: while pristine TiO₂ displays the strongest e^- signal and the weakest h^+ signal, the opposite is observed for Pt_{PD}-TiO₂, with the remaining sample (Pt_{LA}-TiO₂) showing an intermediate behavior.

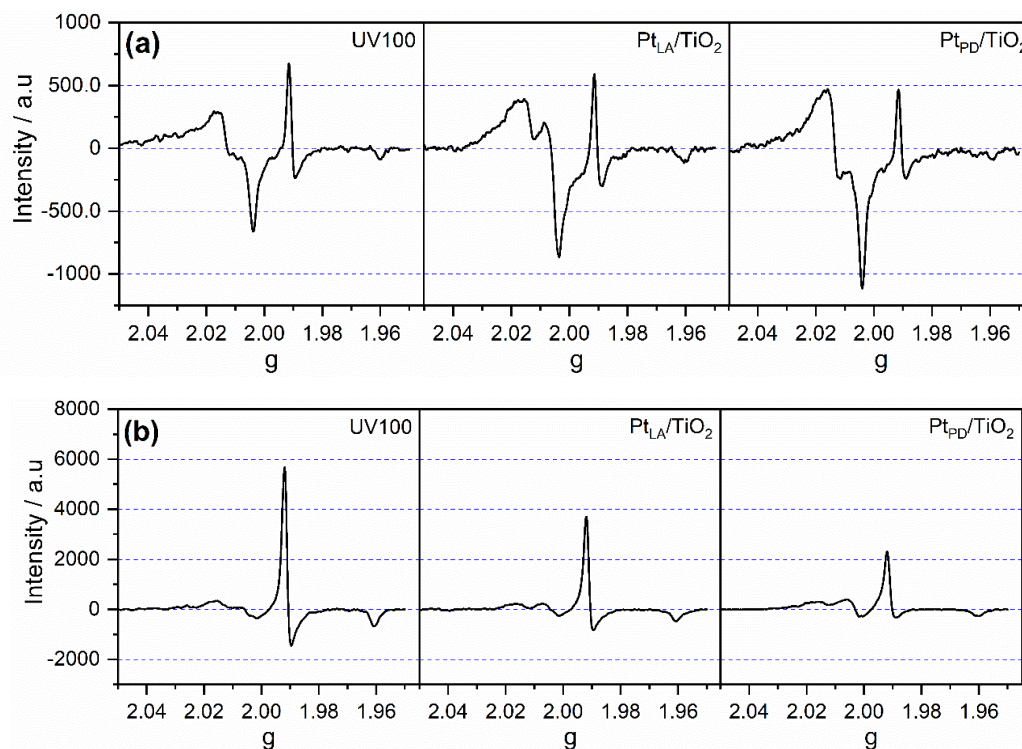


Figure 4-6. The photogenerated EPR signals of the trapped electrons and holes for pristine TiO₂, Pt_{PD}-TiO₂, and Pt_{LA}-TiO₂ at 77 K in (a) N₂ and (b) methanol conditions. Irradiation time: 7 minutes.

This result indicates that Pt_{PD}-TiO₂ yields an efficient electron transfer to Pt⁰, diminishing the number of paramagnetic Ti(III) centers, and, consequently, reducing the recombination rate (evinced as an increase in the signals related to holes). In comparison, the Pt_{LA}-TiO₂ sample shows a similar effect, although with a smaller magnitude (Figures S4-9). These results also evidence that not all the photogenerated electrons migrate to the Pt islands, with a significant number remaining trapped in the TiO₂ particles⁵ (Figures S4-7 a and S4-9 a).

In the presence of methanol (Figure 4-6 (b)), its reaction with holes gives rise to the latter's disappearance and the formation of the triplet signal of the $\cdot\text{CH}_2\text{OH}$ radical (g_x obscured by the Ti^{III} signal, $g_y = 2.004$, and $g_z = 2.018$)^{42, 43}. Simultaneously, stronger signals of the trapped electrons were recorded, attributed to the current doubling effect^{43, 44} caused by the injection of electrons of the $\cdot\text{CH}_2\text{OH}$ radical into TiO₂'s conduction band. As a consequence of the greater number of electrons available from current doubling, the signal of trapped electrons increases in the three samples in comparison with the experiments in the absence of methanol (cf. Figure 4-6 (a) and Figure S4-9). On the other hand, the relative intensities of the electron signals follow the same pattern in both conditions, with TiO₂ showing the strongest signal and Pt_{PD}-TiO₂ the weakest, confirming the rapid electron transfer to Pt in the latter sample.

In agreement with the photocatalytic experiments, this indicates that the photodeposition method yields samples which exhibit a better charge carrier separation than the physical mixing one.

4.5.4 Transient Absorption Spectroscopy

To analyze the charge carrier dynamics of pristine and platinized TiO₂ we employed diffuse reflectance transient absorption spectroscopy. Our measurements were performed in the wavelength range between 400 and 660 nm, where both trapped holes and electrons in TiO₂-based materials contribute signals to the transient absorption^{5, 45-48}. In general, photogenerated holes exhibit a transient absorption in the range 430 – 550 nm, while trapped electrons do so at around 650 nm⁴⁶⁻⁵⁰. In particular, Bahnemann et al.⁵¹ reported that in the absence of any hole scavenger, Pt-TiO₂ sols exhibit a broad absorption band with a maximum at 475 nm immediately after the laser pulse. The authors attributed this absorption to the positive holes that are trapped on the surface of the colloidal particles. The broadness of the band is related to the multiple possible electronic transitions from the valence band to the O⁻ trap and/or from the trap into the conduction band. On the other

hand, flashing a TiO₂ suspension that contained polyvinyl alcohol as a hole scavenger produces a broad absorption spectrum in the visible region, with a maximum at 630 nm attributed to long-lived photogenerated electrons. The shape of the absorption spectrum, as well as the lifetime of these long-lived electrons, depend strongly on the preparation method of the colloid.

Figure 4-7 (a) shows the transient absorption signals recorded at 520 nm for all studied materials in an inert atmosphere. We observe that the signal intensity right after the excitation is lower in the platinized samples. However, the decay rates of the transient signals for the platinized samples are slower than that for pristine TiO₂, which can be seen clearly in the inset Figure 4-7 (a). This can be attributed to the deceleration of the recombination process as a result of the migration of photogenerated electrons to the Pt islands⁴⁵.

A comparison between Pt_{PD}-TiO₂ and Pt_{LA}-TiO₂ shows that the initial intensity upon excitation is significantly higher in the former. This may be related not to a higher number of photogenerated charge carriers (because both materials show similar absorptions), but rather to a higher survival rate at the initial sampling time (i.e. after the first tens of nanoseconds). To perform a meaningful comparison, both decay curves were fitted employing second-order reaction kinetics, assuming bimolecular recombination of the electron-hole pairs^{46,49}. The rate constant (k , s⁻¹) for Pt_{PD}-TiO₂ and Pt_{LA}-TiO₂ are $(7.03 \times 10^5 \pm 0.23 \times 10^5 \text{ s}^{-1})$ and $(2.07 \times 10^7 \pm 0.76 \times 10^7 \text{ s}^{-1})$, respectively. The lower rate constant displayed by Pt_{PD}-TiO₂ indicates a slower recombination rate and increased lifespan of the electron-hole pairs, in agreement with the photocatalytic and EPR experiments^{47,48}.

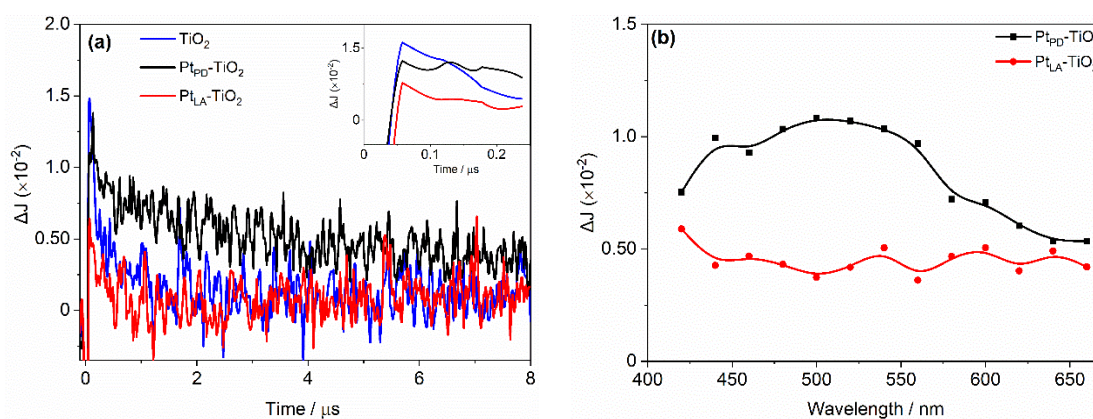


Figure 4-7. (a) Transient absorption signals observed at 520 nm in N₂ atmosphere for pristine and platinized TiO₂, and (b) Transient absorption spectra measured for Pt_{LA}-TiO₂ (●, red line) and Pt_{PD}-TiO₂ (■, black line) under N₂ atmosphere at 218 ns following the laser pulse.

Figure 4-7 (b) shows the transient absorption spectra for Pt_{PD}-TiO₂ and Pt_{LA}-TiO₂ in the N₂ atmosphere at 218 ns after the excitation with the laser pulse. Both materials exhibit a featureless, broad transient absorption. A broad absorption maximum is observed around 520 nm for Pt_{PD}-TiO₂. This suggests, unlike Pt_{LA}-TiO₂, a high number of holes trapped in the surface of Pt_{PD}-TiO₂⁴⁵, aided by the electron transfer to Pt. This observation is, again, in agreement with the EPR and the photocatalytic experiments results.

On the other hand, the addition of methanol shows an unexpected effect. Figure 4-8 shows the time profiles for the absorption at 660 nm, ascribed to photogenerated electrons. After a fast decay during the first 100 ns following excitation, all signals increase over time, approaching constant values towards 8 μs. This build-up of the transient is observed over the whole studied wavelength (400 – 660 nm).

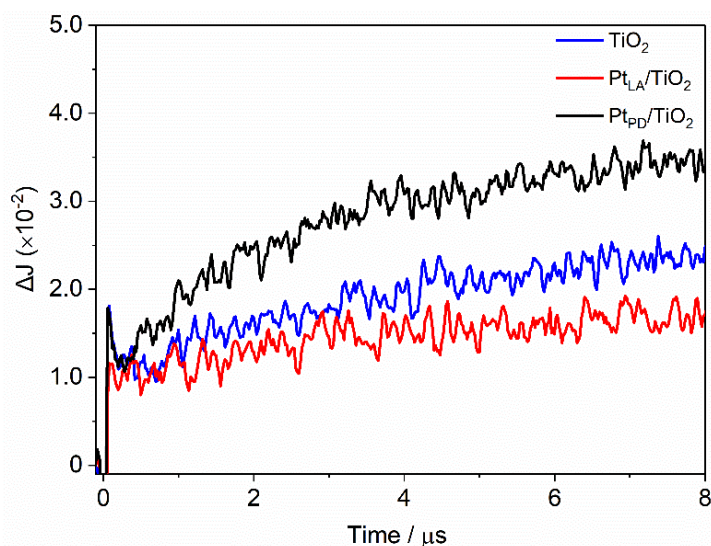


Figure 4-8. Transient absorption signals observed at 660 nm in N₂-methanol vapor atmosphere for pristine and platinized TiO₂.

The initial decay is ascribed to the reaction of the photogenerated holes with the adsorbed methanol that occurs during the laser flash. The slow build-up is attributed to the formation of Ti⁺³ as a result of the reaction of Ti⁺⁴ ions with photogenerated electrons formed by the laser excitation and from the current doubling effect that occurs after holes react with methanol to produce α -hydroxyl radicals (Equations 4-1 to 4-3), which in turn inject an electron into TiO₂^{4, 32, 34, 50}. Since the fractional ratio of Pt is very low on the surface of the TiO₂, which is not enough to accept all the electrons, a part of these electrons will react with any an electron acceptor in the system like Ti⁺³ leading to such observation. Similar behavior has been observed by Bahnemann et al.³⁴ for flash photolysis experiments on a

TiO₂ sol in presence of tetranitromethane (C(NO₂)₄, as electron scavenger) and thiocyanate (as a hole scavenger). A rapid build-up for the absorption signal at 500 nm was observed immediately after the flash-photolysis, related to the reaction of the photogenerated electrons with the C(NO₂)₄³⁴.

Although we expected that the Pt_{PD}-TiO₂ sample would display smaller signals related to electrons due to their migration to the Pt islands, it actually displays the stronger signals within the 8 μs window here studied. This indicates that (i)- under conditions of a high density of photogenerated electrons (due to current doubling and due to the relatively high intensity of the laser pulse), a significant number of them remain on the TiO₂ particles²⁸; and (ii)- that even under this conditions, the Pt_{PD}-TiO₂ sample still seems to yield a lower recombination rate, as evidenced by the higher number of trapped electrons.

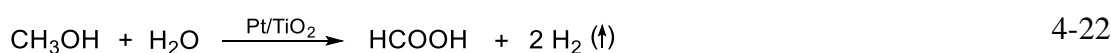
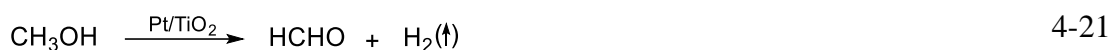
4.5.5 Comparison of the Deposition Methods

It is generally accepted that the incorporation of PtNPs on the surface of TiO₂ leads to an improvement in its photocatalytic activity through the formation of a Schottky barrier that induces electron transfer to Pt, thus enhancing charge carrier separation and partially inhibiting their recombination^{2, 11, 19, 52}. In fact, PtNPs have been attributed to the ability to extend the lifetime of trapped holes from picoseconds to the millisecond time scale^{5, 53}. Hence, our TAS experiments have been evincing this hypothesis, since we observed a slower transient signal decay for the Pt-TiO₂ photocatalysts. An elegant demonstration in a related system was done by Jakob et al.⁵⁴ who first formed (blue-colored) Ti(III) ions by irradiating TiO₂ particles in the absence of electron acceptors, and then showed their discoloration by bringing them into contact with gold nanoparticles. Our EPR results (Figure 4-6 and Figure S4-9) agree with these observations: in comparison with pristine TiO₂, the loading of Pt using either method results in a decrease of the signals related to Ti(III), and an increase of the signals related to trapped holes. Similar experiments were done by Anpo and Takeuchi,⁵⁵ who observed a strong decrease in the Ti(III) signals in the presence of Pt. Our comparison between Pt_{PD}-TiO₂ and Pt_{LA}-TiO₂ evinces a stronger charge transfer effect in the former, which is consistent with the photocatalytic experiments that show an overall better performance by these samples. Moreover, regardless of the platinization method, both platinized samples displayed an enhanced photooxidation efficiency of both naphthalene and methanol in comparison with pristine TiO₂. For instance, the removal of naphthalene after 4 h increased from 60 % in presence of pristine TiO₂ to ~90 % in the case of both platinized samples. Added to that, the accumulation of

naphthalenols in the pristine TiO₂ system evinces an ineffective photocatalytic process which can be related to the fast charge carrier recombination. Similarly, no CO₂ evolution was observed during the photooxidation of methanol over pristine TiO₂, whilst electron transfer to the Pt islands in platinized TiO₂ increased the lifetime of electron-hole pairs and thus allowed much faster methanol mineralization.

Although a full mass balance is outside the scope of this work, it is informative to compare the apparent stoichiometries. On the basis of the detected amounts of methanol's photooxidation products (CH₂O, HCOOH, and CO₂, Figure 4-4) and assuming that these are the only oxidative products, we can calculate the expected amount of H₂ from Equations 4-11, 4-21, and 4-22. Both in the case of Pt_{PD}-TiO₂ and Pt_{LA}-TiO₂, we observed a lower amount to that expected, with observed:expected ratios of ~ 0.2 and ~0.1, respectively. On one hand, this suggests that there are reductive reactions that are unaccounted for in the mechanism, but most importantly, it highlights the better selectivity for H₂ production for the Pt_{PD}-TiO₂ sample.

We performed a similar calculation for the naphthalene case. By neglecting the quantities of other undetectable products, the expected quantities of evolved H₂ were calculated from the quantity of photooxidized naphthalene, corrected by subtracting the formed amounts of naphthalenols and adsorbed naphthalene. The observed:expected ratio of H₂ formation was found to be ~0.5 and ~0.3 for the Pt_{PD}-TiO₂ and Pt_{LA}-TiO₂ samples, respectively. Thus, in a similar fashion to the methanol case, the ratios are considerably lower than one, but show a better selectivity for H₂ production in the Pt_{PD}-TiO₂ sample.



As mentioned above, the small ratios can be related to the formation of other reductive products. Generally speaking, the reduction potential of the TiO₂ conduction band (-0.5 V vs NHE at pH 7) ¹⁰ is suitable for the reduction of different kinds of organic compounds ⁵⁶. A recent report from Walenta et al. ⁵⁷ shows that CO forms on the surface of Pt-TiO₂ during the reforming of methanol, while Kandiel et al. ⁴ have observed the formation of 1,2-ethanediol as a byproduct. Several research groups reported as well the formation of other reductive products during the photocatalytic reforming of different alcohols ^{14, 18, 22}. In addition, the reduction of CO₂ during the photocatalytic process (to products like CH₄, CO, CH₃OH, CH₂O, and HCOOH ^{58, 59}) could be another source for consuming the

photogenerated electrons, which could also explain the relatively low formation of the CO₂ during the reforming of methanol.

In case of naphthalene, although the oxidative reactions (Figure 4-5 a and b) seem very similar in efficiency for the two photocatalysts, the production of H₂ is significantly more efficient for Pt_{PD}-TiO₂. This could be related to the competition with other reductive reactions.

It has been shown that reductive reactions over Pt-TiO₂ during the photoreforming of naphthalene lead to the formation of long-chain aliphatic alcohols and coupling products¹⁰. Similarly, it has been reported that cyclohexanol forms during the photocatalytic reforming of benzene on Pt-TiO₂⁶⁰. It is also possible that the reduction of these compounds is not direct but instead takes place via the hydrogen atoms adsorbed on Pt that formed upon the reduction of H₂O / H⁺^{34, 60, 61}. In either case, the consumption of these species ultimately leads to a deviation in the stoichiometry from the expected H₂ quantities.

A second benefit of using Pt is related to the high overpotential for hydrogen evolution over pristine TiO₂, which makes the presence of a co-catalyst a necessity for the reforming of organic compounds¹³. The photoreforming of both naphthalene and methanol, as studied here, confirms this notion: no hydrogen production was detected over pristine TiO₂.

Despite its ubiquity in photocatalytic studies, the optimization of the Pt deposition methodology over TiO₂ remains largely empirical¹⁴, with the photodeposition (PD) method usually^{9, 22} (but not always^{15, 23, 52}) displaying the best activity. An oft-cited reason for the appropriateness of the PD method is that it exclusively yields Pt⁰ islands¹⁴. In the present case, although we do observe an improved activity for Pt_{PD}-TiO₂ in comparison with Pt_{LA}-TiO₂, the oxidation state in the latter is shown to be Pt⁰ as well (Figure S4-5), so we can exclude it as a significant effect.

A further aspect that is thought to influence the activity of Pt as a co-catalyst is the particle size. From the geometrical point of view, it could be envisioned that smaller particles could lead to larger specific surface areas. Moreover, based on DFT+U calculations, Wang et al.⁶² proposed that quasi two-Pt-layer particles, corresponding to ~1 nm size, are the optimal for photocatalytic hydrogen evolution over anatase (101) due to a good balance between its electron transfer and surface catalysis capabilities. In the present case the measured particle sizes are only moderately different (1.5 ± 0.6 nm and 2.6 ± 2.2 nm respectively for Pt_{PD}-TiO₂ and Pt_{LA}-TiO₂, Figure 4-3), so we do not expect a strong effect from the surface area,

as illustrated by the methanol-reforming experiments using 1.0 wt% Pt_{LA}-TiO₂ (Figure S4-6). Although a size-dependent difference in the (photo-) catalytic properties of the resulting Pt-TiO₂ composites cannot be excluded, we note that the EPR experiments performed under inert conditions (i.e. in the absence of catalytic processes) display a marked decrease (increase) in the number of trapped electrons (holes) for Pt_{PD}-TiO₂ compared to Pt_{LA}-TiO₂, and thus we believe that the main factor behind its improved activity is not the properties of the Pt islands *per se*. Instead, an enhanced charge separation caused by electron transfer to Pt seems more important.

It is important to highlight that, in contrast with macroscopic crystals, nanocrystalline TiO₂ powders display a complex distribution of exposed facets. In particular, although often assumed to be composed mainly of (101) and (001) facets, surfaces of anatase nanoparticles have been shown to display large fractions of (100) or (111) facets⁶³. In addition, both computational modeling⁶⁴ and experimental studies⁶⁵ have shown that some surfaces are more adept than others for each hemi-reaction; in other words, while electrons seem to migrate to (101) facets, they avoid (001) facets, favoring reductions in the former and oxidation reactions in the latter. When preparing Pt_{LA}-TiO₂, it is expected that the Pt NPs physically bind to TiO₂ homogeneously across all surfaces. A similar situation can be envisioned for the initial step of the photodeposition method, where the Pt precursor (here, H₂PtCl₆) may adsorb uniformly. However, once photodeposition starts, the precursor reduction (and Pt⁰ deposition) will preferentially occur on those facets that facilitate electron transfer. This means that once formed, Pt islands will be in close contact with surfaces that have a strong tendency to give up electrons. On the contrary, since Pt⁰ in Pt_{LA}-TiO₂ is deposited non-specifically, a significant fraction of the islands may end up in contact with surfaces avoided by the photogenerated electrons, thus leading to an underutilization of the co-catalyst.

It is worth considering as well the clear differences in the photocatalytic efficiency observed for naphthalene and methanol. When comparing both platinized photocatalysts, we noticed low and very similar values of the photonic efficiencies for the reductive and oxidative processes during the reforming of naphthalene. In contrast, the photoreforming of methanol led to much higher efficiencies and clearly different behaviors between samples. In heterogeneous photocatalysis, the strength of the organic molecules' adsorption on the photocatalyst surface plays an important role, because the photogenerated oxidizing species may not migrate far from their formation centers^{66, 67}, and because it may fundamentally

change the hole-transfer mechanism⁶⁸. Therefore, the weak adsorption of naphthalene leads to a slow photooxidation rate. Moreover, we should note here that the observed time-dependent decrease in naphthalene concentration does not mean that these amounts are mineralized, but instead, they are mostly transformed into secondary pollutants, especially hydroxylated compounds^{10, 69}. We reported previously that the photocatalytic mineralization of naphthalene occurs by a multi-step process which forms a variety of by-products¹⁰. Many of these compounds adsorb strongly on the TiO₂ surface and poison it⁶⁹, and thus, decrease the photocatalytic activity. According to Hykrdová et al.⁷⁰, the formation of such compounds generates charge-transfer complexes with TiO₂, which reverse the charge transfer direction and increase the charge carrier recombination rate. All in all, this results in a situation where charge carriers are short-lived irrespective of the presence of Pt, and thus it can be argued that, given the relatively low irradiances employed here, the photon absorption frequency per nanoparticle is much slower than recombination.

On the other hand, methanol is well known as an efficient hole scavenger^{4, 5}, and leads to the formation of hydroxymethyl radicals that ultimately inject an electron to the conduction band of the TiO₂, yielding formaldehyde (Equations 4-1 to 4-3). The result is that electrons are very long-lived, and there is a non-negligible probability of a photon exciting a nanoparticle that contains a photogenerated electron. Under such conditions, the presence of Pt becomes critical, since it provides a sink for photogenerated electrons that allows them to avoid recombination.

Leaving aside the differences in photocatalytic activity, there are some practical differences in the deposition methods as well. The photodeposition method benefits from greater preparation simplicity, since in principle the equipment necessary for the subsequent photocatalytic reaction is sufficient to implement it. On the other hand, the Pt NPs used here for the physical mixing method, prepared by laser ablation, require specific equipment. On the positive side, the fact that these nanoparticles can be easily prepared in large quantities and pure form allows for detailed characterization analyses that are not possible with the photodeposited materials which required much more treatment.

4.6 Conclusions

We evaluated here the photocatalytic efficiency of platinized TiO₂ (Pt-TiO₂) samples for the photoreforming of two organic compounds: naphthalene and methanol. The main focus was on the preparation method of Pt-TiO₂: either by the commonly used photodeposition

method (PD), or by physical mixing with Pt nanoparticles prepared by laser ablation (LA). Pt_{PD}-TiO₂ exhibited a higher activity than Pt_{LA}-TiO₂ in the photooxidation of the organic compounds, and in turn, both platinized samples outperformed pristine TiO₂. A similar trend was observed for H₂ production, except that in this case, the pristine sample was unable to show any evolution. This observation is readily explained by recalling that the Pt islands strongly decrease the overpotential of H₂ evolution.

Complementary, electron paramagnetic resonance, and transient absorption spectroscopy measurements evinced that the interfacial transfer and trapping of photogenerated charges carrier are greatly influenced by the deposition of Pt and the method to do so. The amount of trapped photogenerated holes follow the order Pt_{PD}-TiO₂ > Pt_{LA}-TiO₂ > pristine TiO₂, while trapped photogenerated electrons show the opposite trend. This highlights the capability of the Pt deposits in Pt_{PD}-TiO₂ to act as an electron sink and reduce recombination.

Although the smaller average Pt particle size in Pt_{PD}-TiO₂ could positively influence its properties, based on the EPR and TAS experiments in the absence of electron or hole scavengers we propose that the main factor governing its high activity is the formation of a strong interaction between the Pt nanoparticles and the TiO₂ surface. This is maybe aided by the selective photodeposition of Pt nanoparticles on crystalline facets with a high tendency for electron transfer.

An important observation is that the magnitude of the enhancement generated by the photodeposition of Pt is highly dependent on the organic compound to be photoreformed. While the difference in activity between samples was relatively small for naphthalene, significantly different behaviors were observed for methanol. We ascribe this fact to the current-doubling effect of methanol, which largely increases the average number of photogenerated electrons per particle, and thus benefits more from the electron-capturing capabilities of Pt.

4.7 Supporting Information

4.7.1 Photonic Efficiency Determination

The photonic efficiencies ξ was calculated on the basis of equation (S1), where $\Delta C/\Delta t$ is the degradation (naphthalene) or formation (hydrogen) rate in units of mol s⁻¹, A is the illuminated area; for photocatalytic reforming of naphthalene is 6.60×10^{-4} m², and 5.03×10^{-4} m² for photoreforming of methanol, and I_0 the photon flux density in the wavelength range between 320 nm and 380 nm.

$$\xi = \frac{\text{degradation or formation initial rate (mol s}^{-1}\text{)}}{\text{photon flux (mol s}^{-1}\text{)}} = \frac{\Delta C}{\Delta t} \frac{1}{I_0 A} \quad \text{S4 - 1}$$

The photon flux density I_0 was determined from equation (S4-2), where I is the light intensity (W m⁻²), λ is the corresponding wavelength (m), N_A is Avogadro's constant (6.022×10^{23} mol⁻¹), h is Planck's constant (6.636×10^{-34} W s²) and c is the speed of light (3.00×10^8 m s⁻¹).

$$I_0 = \frac{I \lambda}{N_A h c} \quad \text{S4 - 2}$$

4.7.2 Photocatalytic Reforming of Methanol

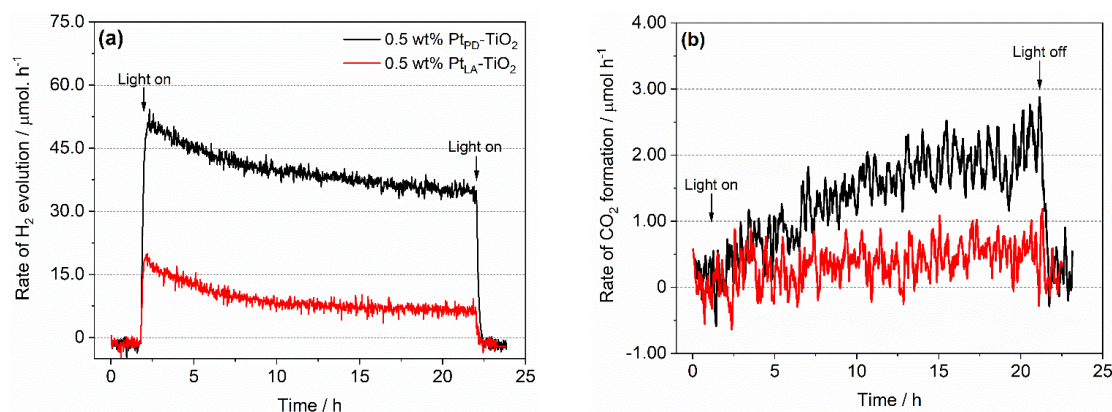


Figure S4-1. Photocatalytic H₂ (a) and CO₂ (b) evolution over Pt_{PD}-TiO₂ (black) and Pt_{LA}-TiO₂ (red) from 2.5M CH₃OH solution: 1.0 g L⁻¹ photocatalyst, 50 mL suspensions, T = 25 °C, light intensity I₂₅₀₋₄₅₀ = 30 mWcm⁻², and irradiation with an Osram XBO 1000-Watt xenon arc lamp as a solar simulator.

4.7.3 Transmission Electron Microscopy (TEM)

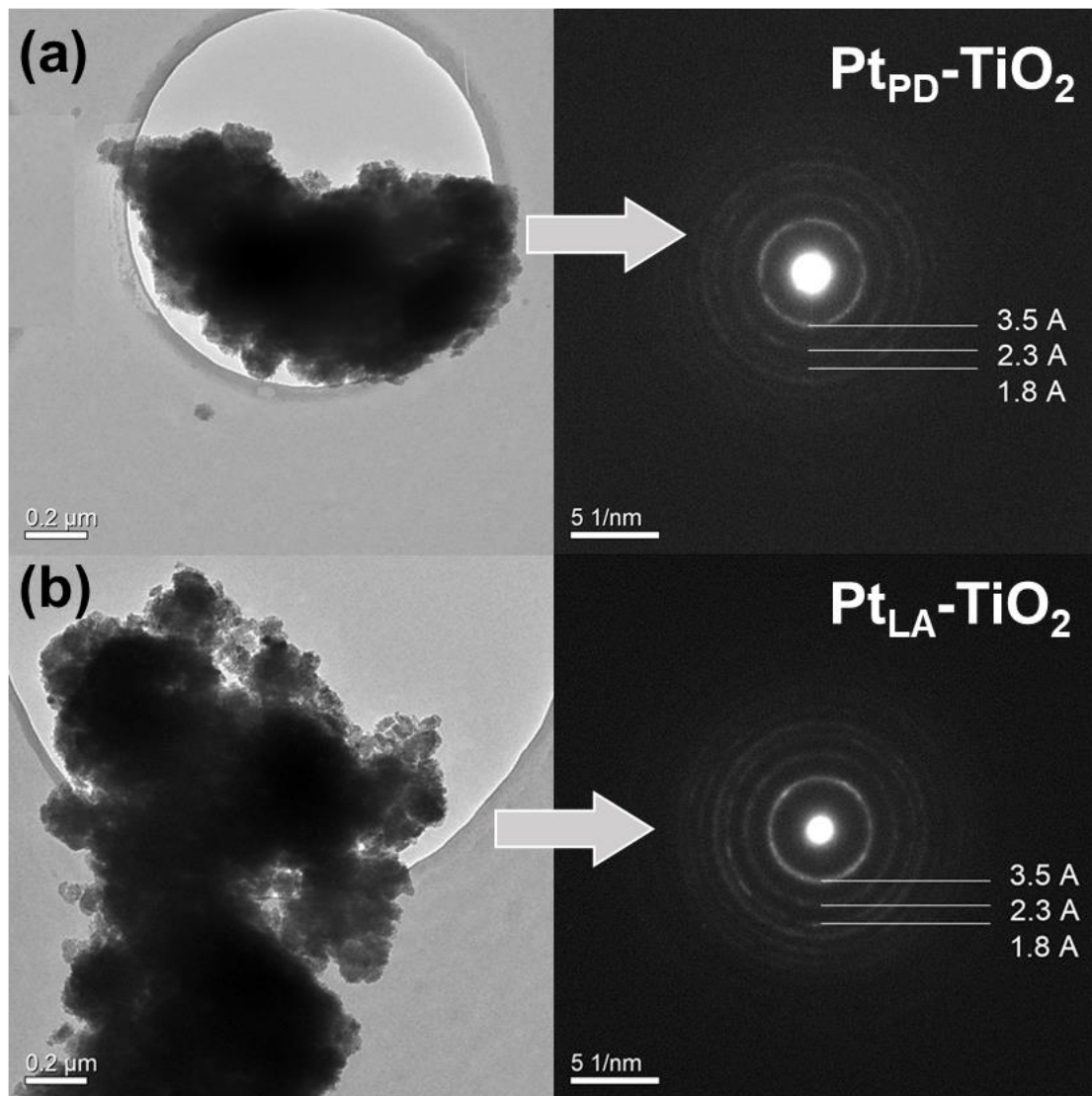


Figure S4-2. TEM images with the SAED patterns show the anatase phase for (a) Pt_{PD}-TiO₂ and (b) Pt_{LA}-TiO₂ nanoparticles.

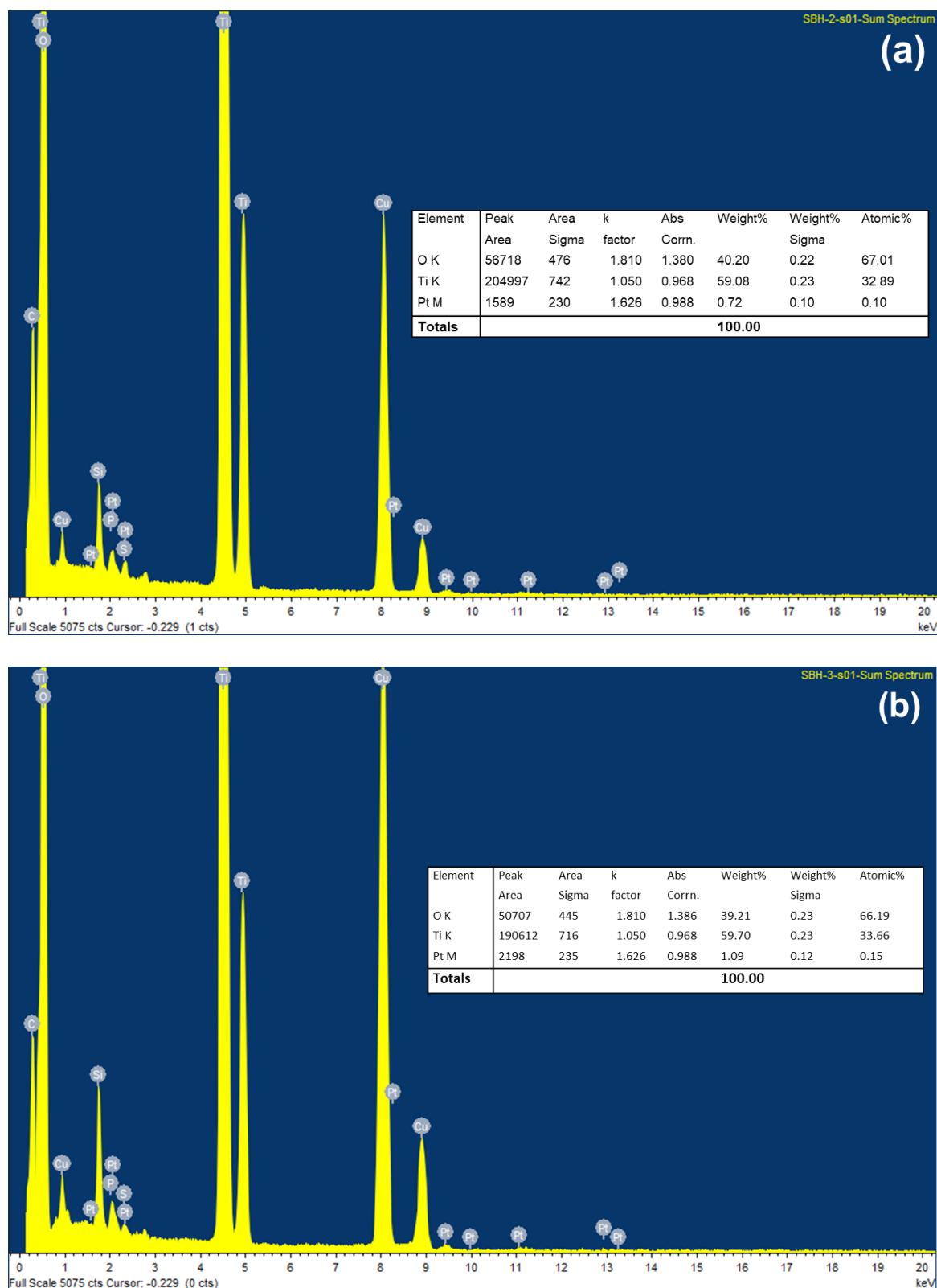


Figure S4-3. Energy dispersive X-ray spectroscopy (EDXS) of (a) Pt_{PD}-TiO₂ and (b) Pt_{LA}-TiO₂ nanoparticles

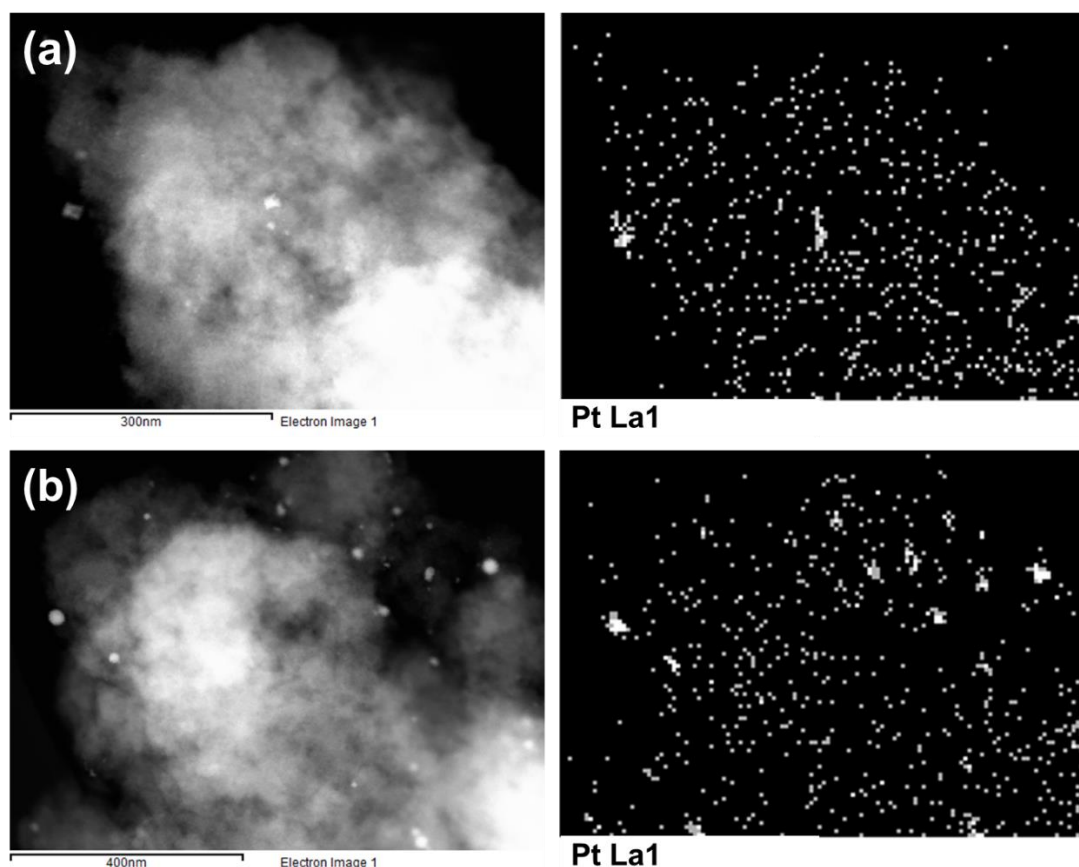


Figure S4-4. HAADF-STEM elemental mapping images of (a) Pt_{PD}-TiO₂ and (b) Pt_{LA}-TiO₂ nanoparticles

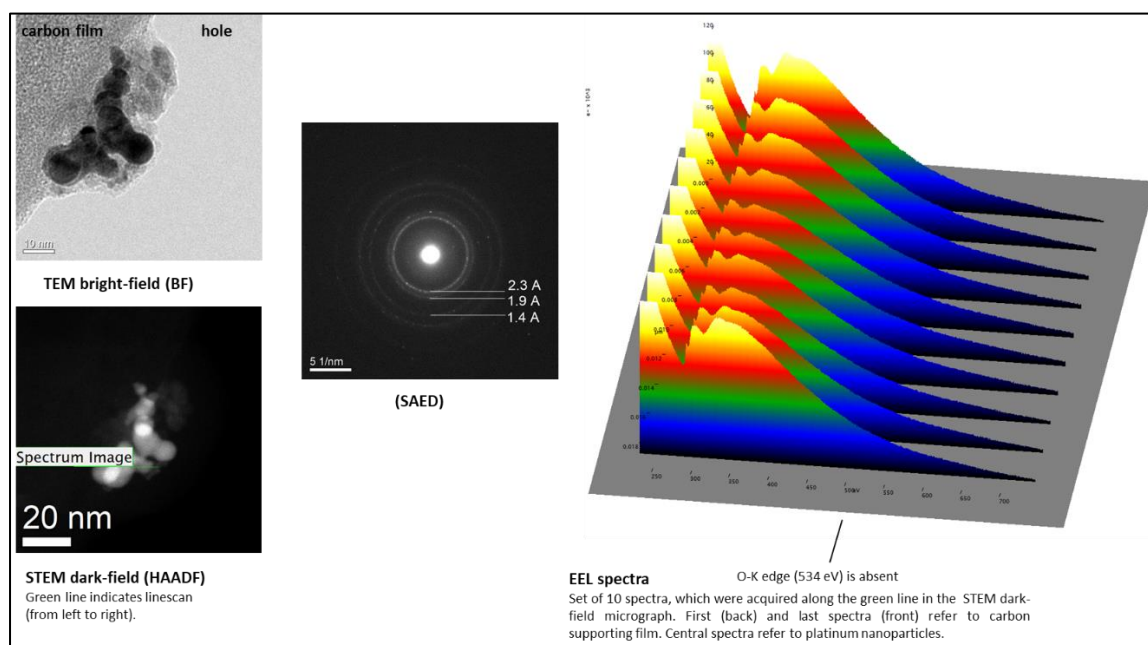


Figure S4-5. HAADF-STEM, SAED, and EELS analysis of Pt nanoparticles suspension produced by laser ablation method. Platinum $M_{4,5}$ ionization edge (2202 eV) is out of spectral range.

4.7.4 Photocatalytic Reforming of Methanol over 1.0 wt% Pt_{LA}-TiO₂

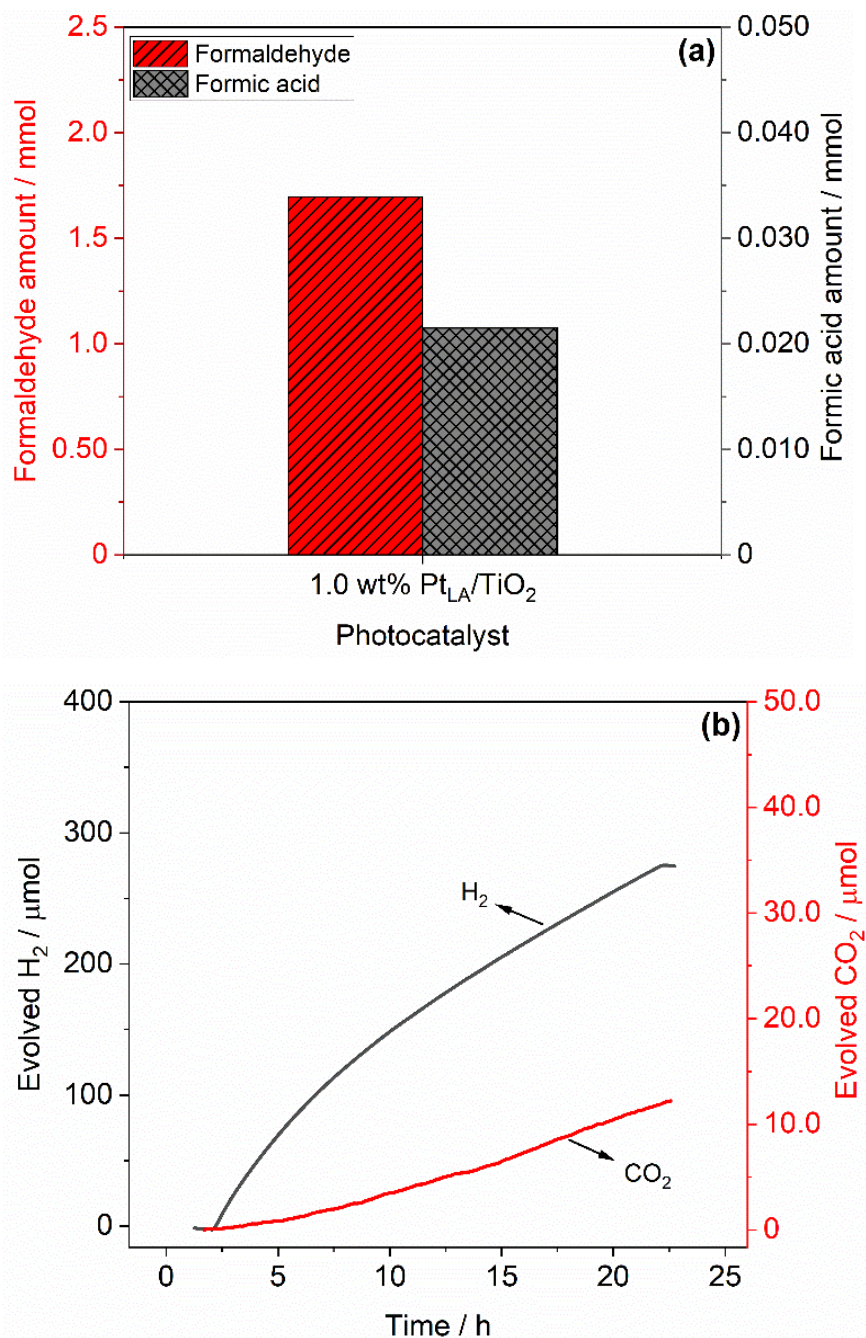


Figure S4-6. Amount of products from the photocatalytic reforming of 50 mL aqueous suspensions of 2.5 mol L⁻¹ methanol following 20 h of illumination over 1.0 wt% Pt_{LA}-TiO₂ photocatalyst. (a) the total amount of HCHO (red column) and HCOOH (black column), (b) evolved amounts of H₂ and CO₂.

4.7.5 EPR Investigation

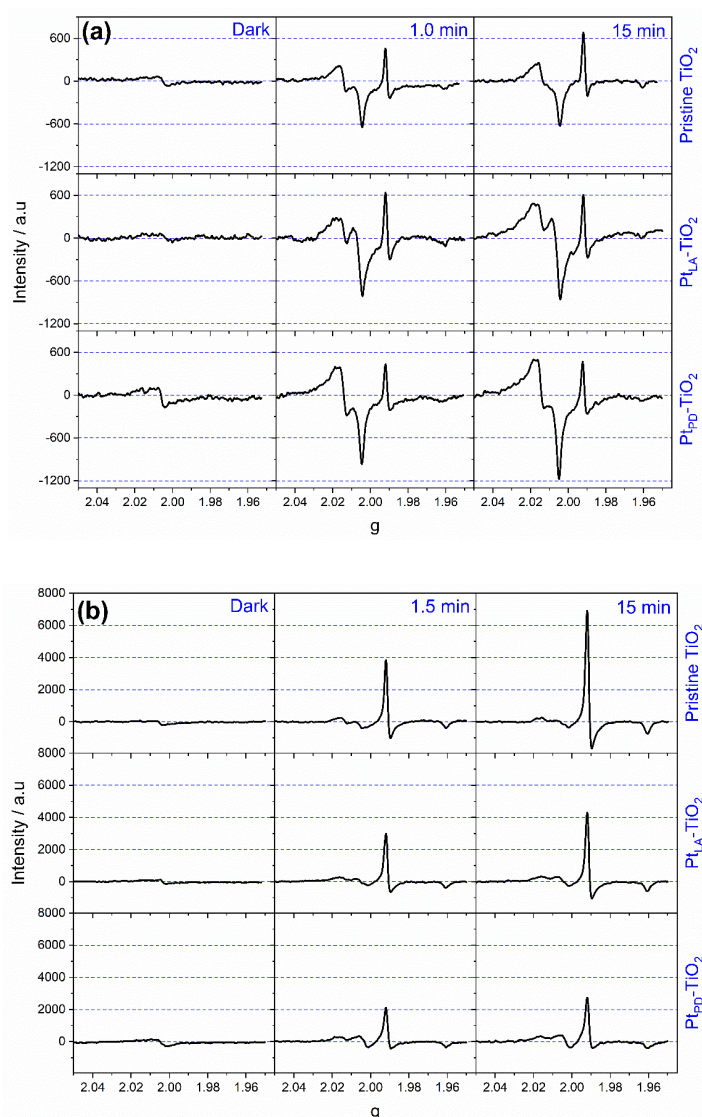


Figure S4-7. EPR spectra of pristine TiO₂, Pt_{LA}-TiO₂, and Pt_{PD}-TiO₂ samples in N₂ atmosphere (a) and N₂-methanol (b) atmospheres at different illumination interval time.

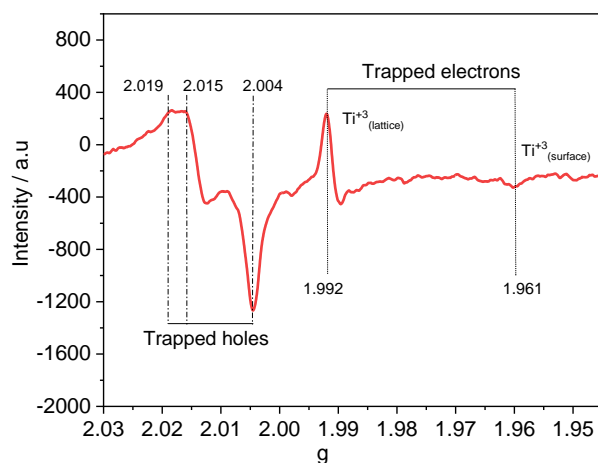


Figure S4-8. Typical in situ EPR signal of illuminated Pt-TiO₂ (anatase) under N₂ condition at 77 K.

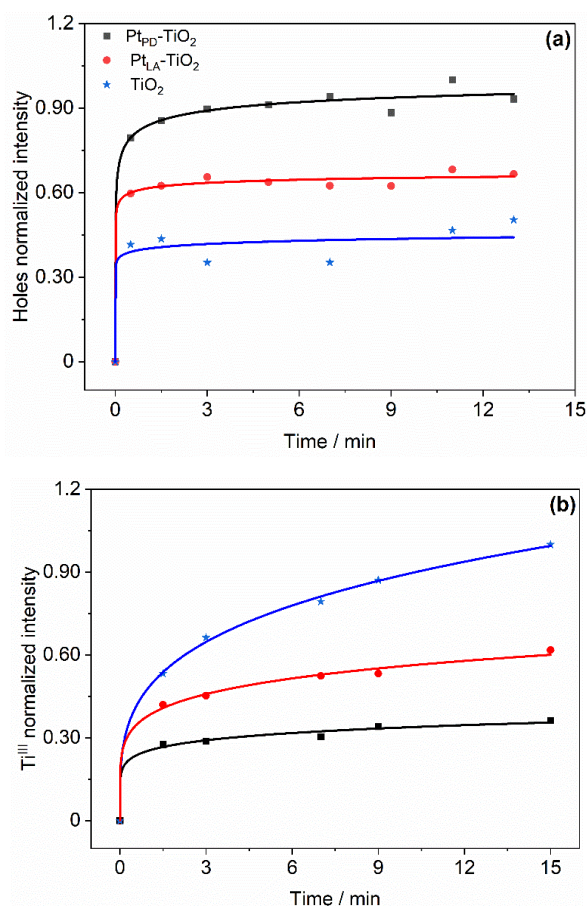


Figure S4-9. Growth of the ESR signal intensity of the trapped (a) holes in N₂ atmosphere and (b) electrons in N₂-methanol atmosphere, on pristine TiO₂ (★, blue), Pt_{PD}-TiO₂ (■, black) and Pt_{LA}-TiO₂ (●, red) during illumination, recorded at 77 K.

4.8 Acknowledgments

Financial support from the Katholischer Akademischer Ausländer-Dienst (KAAD) and Graduiertenakademie at Gottfried Wilhelm Leibniz Universität Hannover are gratefully acknowledged for providing scholarships for Osama Al-Madanat to perform his Ph.D. Mariano Curti is grateful to the DAAD together with the Ministerio de Educación, Cultura, Ciencia y Tecnología (Argentina) for his ALEARG scholarship. Yamen Alsalka gratefully acknowledges the financial support from the Deutscher Akademischer Austauschdienst (DAAD) and the Federal Foreign Office.

4.9 Author Contributions

Conceptualization, Software, Validation, Writing – Original Draft: **Osama Al-Madanat**. Methodology: **Osama Al-Madanat**, **Yamen Alsalka**. Investigation: **Osama Al-Madanat**, **Carsten Günnemann**. Writing – Original Draft: **Osama Al-Madanat**. Writing – Review

& Editing: **Osama Al-Madanat, Mariano Curti, Ralf Dillert.** Supervision: **Mariano Curti, Ralf Dillert, Detlef W. Bahnemann.**

4.10 References

1. Wang, Z.; Li, C.; Domen, K., Recent developments in heterogeneous photocatalysts for solar-driven overall water splitting. *Chem. Soc. Rev.* **2019**, *48* (7), 2109-2125.
2. Kumaravel, V.; Mathew, S.; Bartlett, J.; Pillai, S. C., Photocatalytic hydrogen production using metal doped TiO₂: A review of recent advances. *Appl. Catal., B* **2019**, *244*, 1021-1064.
3. Wang, H.; Zhang, L.; Chen, Z.; Hu, J.; Li, S.; Wang, Z.; Liu, J.; Wang, X., Semiconductor heterojunction photocatalysts: Design, construction, and photocatalytic performances. *Chem. Soc. Rev.* **2014**, *43* (15), 5234-44.
4. Kandiel, T. A.; Dillert, R.; Bahnemann, D. W., Enhanced photocatalytic production of molecular hydrogen on TiO₂ modified with Pt–polypyrrole nanocomposites. *Photochem. Photobiol. Sci.* **2009**, *8* (5), 683-690.
5. Schneider, J.; Matsuoka, M.; Takeuchi, M.; Zhang, J.; Horiuchi, Y.; Anpo, M.; Bahnemann, D. W., Understanding TiO₂ photocatalysis: Mechanisms and materials. *Chem. Rev.* **2014**, *114* (19), 9919-86.
6. AlSalka, Y.; Granone, L. I.; Ramadan, W.; Hakki, A.; Dillert, R.; Bahnemann, D. W., Iron-based photocatalytic and photoelectrocatalytic nano-structures: Facts, perspectives, and expectations. *Appl. Catal. B* **2019**, *244*, 1065-1095.
7. Ramadan, W.; Dillert, R.; Koch, J.; Tegenkamp, C.; Bahnemann, D. W., Changes in the solid-state properties of bismuth iron oxide during the photocatalytic reformation of formic acid. *Catal. Today* **2019**, *326*, 22-29.
8. Diebold, U., The surface science of titanium dioxide. *Surf. Sci. Rep.* **2003**, *48* (5-8), 53-229.
9. Naldoni, A.; D'Arienzo, M.; Altomare, M.; Marelli, M.; Scotti, R.; Morazzoni, F.; Selli, E.; Dal Santo, V., Pt and Au/TiO₂ photocatalysts for methanol reforming: Role of metal nanoparticles in tuning charge trapping properties and photoefficiency. *Appl. Catal., B* **2013**, *130*, 239-248.
10. Al-Madanat, O.; AlSalka, Y.; Curti, M.; Dillert, R.; Bahnemann, D. W., Mechanistic insights into hydrogen evolution by photocatalytic reforming of naphthalene. *ACS Catal.* **2020**, *10* (13), 7398-7412.
11. Li, F. B.; Li, X. Z., The enhancement of photodegradation efficiency using Pt–TiO₂ catalyst. *Chemosphere* **2002**, *48* (10), 1103-1111.
12. Wei, Z.; Janczarek, M.; Endo, M.; Wang, K.; Balcytis, A.; Nitta, A.; Mendez-Medrano, M. G.; Colbeau-Justin, C.; Juodkazis, S.; Ohtani, B.; Kowalska, E., Noble metal-modified faceted anatase titania photocatalysts: Octahedron versus decahedron. *Appl. Catal. B* **2018**, *237*, 574-587.
13. Linsebigler, A. L.; Lu, G. Q.; Yates, J. T., Photocatalysis on TiO₂ surfaces - principles, mechanisms, and selected results. *Chem. Rev.* **1995**, *95* (3), 735-758.

14. Wenderich, K.; Mul, G., Methods, mechanism, and applications of photodeposition in photocatalysis: A Review. *Chem Rev* **2016**, *116* (23), 14587-14619.
15. Park, H.; Reddy, D. A.; Kim, Y.; Lee, S.; Ma, R.; Kim, T. K., Synthesis of ultra-small palladium nanoparticles deposited on CdS nanorods by pulsed laser ablation in liquid: Role of metal nanocrystal size in the photocatalytic hydrogen production. *Chemistry* **2017**, *23* (53), 13112-13119.
16. AlSalka, Y.; Al-Madanat, O.; Curti, M.; Hakki, A.; Bahnemann, D. W., Photocatalytic H₂ evolution from oxalic acid: Effect of cocatalysts and carbon dioxide radical anion on the surface charge transfer mechanisms. *ACS Appl. Energy Mater.* **2020**, *3* (7), 6678-6691.
17. Wang, C.; Yin, L.; Zhang, L.; Liu, N.; Lun, N.; Qi, Y., Platinum-nanoparticle-modified TiO₂ nanowires with enhanced photocatalytic property. *ACS Appl. Mater. Interfaces* **2010**, *2* (11), 3373-7.
18. Al-Azri, Z. H. N.; AlOufi, M.; Chan, A.; Waterhouse, G. I. N.; Idriss, H., Metal particle size effects on the photocatalytic hydrogen ion reduction. *ACS Catal.* **2019**, *9* (5), 3946-3958.
19. Kozlova, E. A.; Lyubina, T. P.; Nasalevich, M. A.; Vorontsov, A. V.; Miller, A. V.; Kaichev, V. V.; Parmon, V. N., Influence of the method of platinum deposition on activity and stability of Pt/TiO₂ photocatalysts in the photocatalytic oxidation of dimethyl methylphosphonate. *Catal. Commun.* **2011**, *12* (7), 597-601.
20. Marzun, G.; Streich, C.; Jendrzey, S.; Barcikowski, S.; Wagener, P., Adsorption of colloidal platinum nanoparticles to supports: charge transfer and effects of electrostatic and steric interactions. *Langmuir* **2014**, *30* (40), 11928-36.
21. Wang, C.-y.; Pagel, R.; Bahnemann, D. W.; Dohrmann, J. K., Quantum yield of formaldehyde formation in the presence of colloidal TiO₂-based photocatalysts: Effect of intermittent illumination, platinization, and deoxygenation. *J. Phys. Chem. B* **2004**, *108* (37), 14082-14092.
22. Bamwenda, G. R.; Tsubota, S.; Nakamura, T.; Haruta, M., Photoassisted hydrogen production from a water-ethanol solution: A comparison of activities of Au-TiO₂ and Pt-TiO₂. *J. Photochem. Photobiol. A* **1995**, *89* (2), 177-189.
23. Siuzdak, K.; Sawczak, M.; Klein, M.; Nowaczyk, G.; Jurga, S.; Cenian, A., Preparation of platinum modified titanium dioxide nanoparticles with the use of laser ablation in water. *Phys. Chem. Chem. Phys.* **2014**, *16* (29), 15199-206.
24. Farsinezhad, S.; Sharma, H.; Shankar, K., Interfacial band alignment for photocatalytic charge separation in TiO₂ nanotube arrays coated with CuPt nanoparticles. *Phys. Chem. Chem. Phys.* **2015**, *17* (44), 29723-33.
25. Berger, T.; Diwald, O.; Knozinger, E.; Sterrer, M.; Yates, J. T., Jr., UV induced local heating effects in TiO₂ nanocrystals. *Phys. Chem. Chem. Phys.* **2006**, *8* (15), 1822-6.
26. Nash, T., The colorimetric estimation of formaldehyde by means of the Hantzsch reaction. *Biochem. J.* **1953**, *55* (3), 416-21.
27. Sun, B.; Vorontsov, A. V.; Smirniotis, P. G., Role of platinum deposited on TiO₂ in phenol photocatalytic oxidation. *Langmuir* **2003**, *19* (8), 3151-3156.

28. Kowalska, E.; Remita, H.; Colbeau-Justin, C.; Hupka, J.; Belloni, J., Modification of titanium dioxide with platinum ions and clusters: Application in photocatalysis. *J. Phys. Chem. C* **2008**, *112* (4), 1124-1131.
29. Scott, J.; Irawaty, W.; Low, G.; Amal, R., Enhancing the catalytic oxidation capacity of Pt/TiO₂ using a light pre-treatment approach. *Appl. Catal., B* **2015**, *164*, 10-17.
30. Lee, J.; Choi, W., Photocatalytic reactivity of surface platinized TiO₂: Substrate specificity and the effect of Pt oxidation state. *J. Phys. Chem. B* **2005**, *109* (15), 7399-406.
31. Jiang, Z.; Zhang, Z. Y.; Shangguan, W. F.; Isaacs, M. A.; Durndell, L. J.; Parlett, C. M. A.; Lee, A. F., Photodeposition as a facile route to tunable Pt photocatalysts for hydrogen production: On the role of methanol. *Catal. Sci. Technol.* **2016**, *6* (1), 81-88.
32. Schneider, J.; Bahnemann, D. W., Undesired role of sacrificial reagents in photocatalysis. *J. Phys. Chem. Lett.* **2013**, *4* (20), 3479-3483.
33. Nagao, M.; Suda, Y., Adsorption of benzene, toluene, and chlorobenzene on titanium-dioxide. *Langmuir* **1989**, *5* (1), 42-47.
34. Bahnemann, D.; Henglein, A.; Spanhel, L., Detection of the intermediates of colloidal TiO₂-catalyzed photoreactions. *Faraday Discuss.* **1984**, *78* (0), 151-163.
35. Loeb, S. K.; Alvarez, P. J. J.; Brame, J. A.; Cates, E. L.; Choi, W.; Crittenden, J.; Dionysiou, D. D.; Li, Q.; Li-Puma, G.; Quan, X.; Sedlak, D. L.; David Waite, T.; Westerhoff, P.; Kim, J. H., The technology horizon for photocatalytic water treatment: Sunrise or sunset? *Environ. Sci. Technol.* **2019**, *53* (6), 2937-2947.
36. Howe, R. F.; Gratzel, M., EPR observation of trapped electrons in colloidal titanium dioxide. *J. Phys. Chem.* **1985**, *89* (21), 4495-4499.
37. Kumar, C. P.; Gopal, N. O.; Wang, T. C.; Wong, M. S.; Ke, S. C., EPR investigation of TiO₂ nanoparticles with temperature-dependent properties. *J. Phys. Chem. B* **2006**, *110* (11), 5223-9.
38. Howe, R. F.; Gratzel, M., EPR study of hydrated anatase under UV irradiation. *J. Phys. Chem.* **1987**, *91* (14), 3906-3909.
39. Nakaoka, Y.; Nosaka, Y., ESR investigation into the effects of heat treatment and crystal structure on radicals produced over irradiated TiO₂ powder. *J. Photochem. Photobiol. A* **1997**, *110* (3), 299-305.
40. Berger, T.; Sterrer, M.; Diwald, O.; Knozinger, E.; Panayotov, D.; Thompson, T. L.; Yates, J. T., Jr., Light-induced charge separation in anatase TiO₂ particles. *J. Phys. Chem. B* **2005**, *109* (13), 6061-8.
41. Ke, S. C.; Wang, T. C.; Wong, M. S.; Gopal, N. O., Low temperature kinetics and energetics of the electron and hole traps in irradiated TiO₂ nanoparticles as revealed by EPR spectroscopy. *J. Phys. Chem. B* **2006**, *110* (24), 11628-34.
42. Micic, O. I.; Zhang, Y.; Cromack, K. R.; Trifunac, A. D.; Thurnauer, M. C., Trapped holes on titania colloids studied by electron paramagnetic resonance. *J. Phys. Chem.* **1993**, *97* (28), 7277-7283.

43. Dimitrijevic, N. M.; Shkrob, I. A.; Gosztola, D. J.; Rajh, T., Dynamics of interfacial charge transfer to formic acid, formaldehyde, and methanol on the surface of TiO₂ nanoparticles and its role in methane production. *J. Phys. Chem. C* **2012**, *116* (1), 878-885.
44. Hurum, D. C.; Agrios, A. G.; Gray, K. A.; Rajh, T.; Thurnauer, M. C., Explaining the enhanced photocatalytic activity of Degussa P25 mixed-phase TiO₂ using EPR. *J. Phys. Chem. B* **2003**, *107* (19), 4545-4549.
45. Bahnemann, D. W.; Hilgendorff, M.; Memming, R., Charge carrier dynamics at TiO₂ particles: Reactivity of free and trapped holes. *J. Phys. Chem. B* **1997**, *101* (21), 4265-4275.
46. Günnemann, C.; Curti, M.; Schneider, J.; Bahnemann, D. W., Dynamics of photoinduced bulk and surface reactions involving semiconductors characterized by time resolved spectroscopy techniques (2015–2018). In *Photochemistry*, The Royal Society of Chemistry: 2019; Vol. 47, pp 122-158.
47. Nunzi, F.; De Angelis, F.; Selloni, A., Ab initio simulation of the absorption spectra of photoexcited carriers in TiO₂ nanoparticles. *J. Phys. Chem. Lett.* **2016**, *7* (18), 3597-602.
48. Yoshihara, T.; Katoh, R.; Furube, A.; Tamaki, Y.; Murai, M.; Hara, K.; Murata, S.; Arakawa, H.; Tachiya, M., Identification of reactive species in photoexcited nanocrystalline TiO₂ films by wide-wavelength-range (400–2500 nm) transient absorption spectroscopy. *J. Phys. Chem. B* **2004**, *108* (12), 3817-3823.
49. Schneider, J.; Bahnemann, D., Strong transient absorption of trapped holes in anatase and rutile TiO₂ at high laser intensities. *J. Phys. Chem. C* **2018**, *122* (25), 13979-13985.
50. Qian, R.; Zong, H.; Schneider, J.; Zhou, G.; Zhao, T.; Li, Y.; Yang, J.; Bahnemann, D. W.; Pan, J. H., Charge carrier trapping, recombination and transfer during TiO₂ photocatalysis: An overview. *Catal. Today* **2019**, *335*, 78-90.
51. Bahnemann, D.; Henglein, A.; Lilie, J.; Spanhel, L., Flash photolysis observation of the absorption spectra of trapped positive holes and electrons in colloidal titanium dioxide. *J. Phys. Chem. B* **1984**, *88* (4), 709-711.
52. Li, J. X.; Xu, J. H.; Dai, W. L.; Fan, K. N., Dependence of Ag deposition methods on the photocatalytic activity and surface state of TiO₂ with twistlike helix structure. *J. Phys. Chem. C* **2009**, *113* (19), 8343-8349.
53. Kamat, P. V., Photoinduced transformations in semiconductor-metal nanocomposite assemblies. *Pure Appl. Chem.* **2002**, *74* (9), 1693-1706.
54. Jakob, M.; Levanon, H.; Kamat, P. V., Charge distribution between UV-irradiated TiO₂ and gold nanoparticles: Determination of shift in the fermi level. *Nano Lett.* **2003**, *3* (3), 353-358.
55. Anpo, M.; Takeuchi, M., The design and development of highly reactive titanium oxide photocatalysts operating under visible light irradiation. *J. Catal.* **2003**, *216* (1-2), 505-516.
56. Stroyuk, O. L.; Kuchmy, S. Y., Heterogeneous photocatalytic selective reductive transformations of organic compounds: A Review. *Theor. Exp. Chem.* **2020**, *56* (3), 143-173.
57. Walenta, C. A.; Courtois, C.; Kollmannsberger, S. L.; Eder, M.; Tschurl, M.; Heiz, U., Surface species in photocatalytic methanol reforming on Pt/TiO₂(110): Learning from surface science experiments for catalytically relevant conditions. *ACS Catal.* **2020**, *10* (7), 4080-4091.

58. Ola, O.; Maroto-Valer, M. M., Review of material design and reactor engineering on TiO₂ photocatalysis for CO₂ reduction. *J. Photoch. Photobio. C* **2015**, *24*, 16-42.
59. Karamian, E.; Sharifnia, S., On the general mechanism of photocatalytic reduction of CO₂. *J. CO₂ Util.* **2016**, *16*, 194-203.
60. Yuzawa, H.; Aoki, M.; Otake, K.; Hattori, T.; Itoh, H.; Yoshida, H., Reaction mechanism of aromatic ring hydroxylation by water over platinum-loaded titanium oxide photocatalyst. *J. Phys. Chem. C* **2012**, *116* (48), 25376-25387.
61. Joo, J. B.; Dillon, R.; Lee, I.; Yin, Y.; Bardeen, C. J.; Zaera, F., Promotion of atomic hydrogen recombination as an alternative to electron trapping for the role of metals in the photocatalytic production of H₂. *Proc. Natl. Acad. Sci. U S A* **2014**, *111* (22), 7942-7.
62. Wang, D.; Liu, Z. P.; Yang, W. M., Revealing the size effect of platinum cocatalyst for photocatalytic hydrogen evolution on TiO₂ support: A DFT study. *ACS Catal.* **2018**, *8* (8), 7270-7278.
63. Feldhoff, A.; Mendive, C.; Bredow, T.; Bahnemann, D., Direct measurement of size, three-dimensional shape, and specific surface area of anatase nanocrystals. *ChemPhysChem* **2007**, *8* (6), 805-9.
64. Selcuk, S.; Selloni, A., Facet-dependent trapping and dynamics of excess electrons at anatase TiO₂ surfaces and aqueous interfaces. *Nat. Mater.* **2016**, *15* (10), 1107-12.
65. Ohno, T.; Sarukawa, K.; Matsumura, M., Crystal faces of rutile and anatase TiO₂ particles and their roles in photocatalytic reactions. *New. J. Chem.* **2002**, *26* (9), 1167-1170.
66. Ajmal, A.; Majeed, I.; Malik, R. N.; Idriss, H.; Nadeem, M. A., Principles and mechanisms of photocatalytic dye degradation on TiO₂ based photocatalysts: a comparative overview. *RSC Adv.* **2014**, *4* (70), 37003-37026.
67. Hufschmidt, D.; Bahemann, D.; Testa, J. J.; Emilio, C. A.; Litter, M. I., Enhancement of the photocatalytic activity of various TiO₂ materials by platinisation. *J. Photochem. Photobiol. A* **2002**, *148* (1-3), 223-231.
68. Monllor-Satoca, D.; Gómez, R.; González-Hidalgo, M.; Salvador, P., The "Direct-Indirect" model: An alternative kinetic approach in heterogeneous photocatalysis based on the degree of interaction of dissolved pollutant species with the semiconductor surface. *Catal. Today* **2007**, *129* (1-2), 247-255.
69. Dass, S.; Muneer, M.; Gopidas, K. R., Photocatalytic degradation of wastewater pollutants. Titanium-dioxide-mediated oxidation of polynuclear aromatic hydrocarbons. *J. Photochem. Photobiol. A* **1994**, *77* (1), 83-88.
70. Hykrdova, L.; Jirkovsky, J.; Mailhot, G.; Bolte, M., Fe(III) photoinduced and Q-TiO₂ photocatalysed degradation of naphthalene: Comparison of kinetics and proposal of mechanism. *J. Photochem. Photobiol. A* **2002**, *151* (1-3), 181-193.

Chapter Five: Mechanistic Insights into Hydrogen Evolution by Photocatalytic Reforming of Naphthalene

5.1 Foreword

Yet, several kinds of photocatalytic materials are synthesized and studied for their potential application in H₂ formation, as well as the degradation of organic pollutants. Although the photocatalytic activity of these materials for a wide range of organic pollutants had been reported in the literature, it was rarely concerned to investigate and interpret the photocatalytic mechanisms of these compounds with a clear and precise scientific approach.

Following the chapter 3 and 4, it was found that the H₂ formation and naphthalene degradation are greatly enhanced in the presence of Pt-TiO₂. The experimental results presented in those chapters showing that: i) Hombikat UV100 is more active than Aeroxide P25; ii) a 0.5 wt% Pt ratio seems to be optimal for the reaction under investigation, and iii) the Pt-UV100 that was prepared by the photodeposition method exhibited a higher activity than the one prepared by the physical mixing method. Since photocatalyst optimization was studied previously, the main aim of this chapter is to investigate and elucidate the proposed mechanism and the possible pathways for photocatalytic oxidation of naphthalene and the H₂ formation under anaerobic conditions employing exclusively 0.5 wt% Pt-UV100 photocatalyst.

This chapter contains the article “*Mechanistic Insights into Hydrogen Evolution by Photocatalytic Reforming of Naphthalene*” by Osama Al-Madanat, Yamen AlSalka, Mariano Curti, Ralf Dillert, and Detlef W. Bahnemann. Reproduced with permission from *ACS Catalysis* 2020, 10 (13), 7398-7412 (DOI: 10.1021/acscatal.0c01713). Copyright 2020 American Chemical Society. Within the frames of this chapter, after analyzing and discussing the kinetic profiles of the photocatalytic H₂ formation and naphthalene oxidation, a deep analysis for the formed products was performed to determine the fate of naphthalene after its reaction with the photogenerated holes. It was found that the hydroxylation of the aromatic ring is the main path for the degradation of naphthalene. Different pathways for the photocatalytic oxidation of naphthalene were proposed on the basis of the possible reactive species that can be formed during the excitation of the Pt-TiO₂, i.e., free and trapped holes, free hydroxyl radical, and bridging oxygen radicals at the

TiO₂ surface. By performing several photocatalytic experiments employing: different scavengers, Ti¹⁸O₂, EPR-spin trapping technique, deuterium water, and naphthalene, the mechanism of the most proper pathway for the photocatalytic reforming of naphthalene was proposed.

5.2 Abstract

Heterogeneous photocatalysis has been widely considered, amongst other applications, for environmental remediation and hydrogen production. While these applications have been traditionally seen as well separated areas, recent examples have highlighted the possibility of coupling them. Here we demonstrate the simultaneous production of H₂ and naphthalene removal from aqueous solutions with (unoptimized) photonic efficiencies of 0.97% and 0.33%, respectively, over Pt-TiO₂ under simulated sunlight. Photocatalytic and spin trapping experiments in the presence of hydroxyl radical and hole scavengers evinced that only the photogenerated holes play a significant role in the oxidation of naphthalene. Isotopic labeling analyses showed that the evolved H₂ isotopologues match those of the solvent, and that deuterated water (but not deuterated naphthalene) decreases the reaction rate, suggesting its involvement in the rate-determining step. Moreover, the use of Ti¹⁸O₂ does not lead to the significant formation of ¹⁸O-enriched CO₂, suggesting that water is the source of the oxygen atoms. Ultimately, by considering the stable and transient reaction intermediates, we propose a plausible reaction pathway. Our work illustrates that environmental remediation can be effectively coupled to solar fuel production, providing a double purpose to photocatalytic reactions, while the mechanistic insights will be of utility for the further development of this strategy.

Keywords: Polycyclic aromatic hydrocarbons, persistent organic pollutants, photoreforming, titania, H₂ production, EPR, isotopic study, reaction mechanism

5.3 Introduction

Achieving a fully sustainable energy production system based on sunlight involves the development of multiple and diverse technologies. Although solar light represents a huge untapped potential, it is intermittent in nature, making the use of energy vectors an unavoidable requirement ¹. In this regard, the photocatalytic production of molecular hydrogen (H₂) in the solar-driven process is a promising strategy to store sunlight as chemical energy *via* photoinduced reduction of water ^{2,3}. As an energy vector, H₂ possesses the highest gravimetric gross calorific value among all fuels (142 MJ kg⁻¹), and burns

cleanly yielding only pure water⁴. Nonetheless, its photocatalytic production commonly requires the use of a sacrificial electron donor (SED) to push the oxidation half-reaction and achieve acceptable efficiencies^{2, 3}, in a process commonly called photocatalytic reforming of the SED. This entails, however, the consumption of compounds that may have a significant cost with respect to that of the produced H₂.

Lanterna and Scaiano have recently illustrated an interesting alternative⁵. These authors utilized water samples from Canadian rivers to perform a photocatalytic reaction where both the reduction and oxidation half-reactions were purposeful: while water was reduced to form H₂, the accompanying half-reaction was exploited to oxidize dissolved pollutants, thus simultaneously improving the water quality. This strategy increases the H₂ production efficiency with respect to pure water, avoids the use of potentially costly SEDs, and achieves the above-mentioned two-fold purpose. Another attractive dual-purpose system was described by Horiuchi et al.⁶ combining solar H₂ production with a plant factory. The use of plant biomass as SEDs aids the photocatalytic H₂ production, while the emitted CO₂ is useful for plant growth.

Industrial effluents are an attractive target to apply this approach. Although they commonly carry a broad range of pollutants, a particularly troublesome group is that of persistent organic pollutants such as polycyclic aromatic hydrocarbons (PAHs). These compounds, mainly distributed by the incomplete combustion of fossil fuels and by accidental oil spills, are ubiquitously found in the environment, have a great tendency to bioaccumulate, and, importantly, present a broad range of deleterious health effects^{7, 8}. Among the different PAHs, naphthalene is a particularly noxious member due to its relatively large solubility in water, which leads to increased bioavailability and ultimately to adverse effects in the environment and human health.

As for many other pollutants, oxidative processes based on photocatalysis have often been considered for the removal of PAHs. Nevertheless, while several studies have explored their photocatalytic oxidation in aerobic conditions (where the reduction half-reaction is the conversion of molecular oxygen to the superoxide radical anion)⁹⁻¹³, there are no reports on the remediation of PAHs with the simultaneous production of H₂. At the same time, reports on simpler aromatic compounds such as benzene and its derivatives have indeed shown that coupling their photocatalytic degradation to H₂ production could be a viable strategy¹⁴⁻¹⁶. In comparison to relatively simpler SEDs like methanol, however, the

involvement of the oxidation intermediates may play an important and undesired role¹⁷; to unravel these, mechanistic investigations on both the reductive and oxidative half-reactions are desired¹⁸.

In the present study, we report the investigation of the removal of naphthalene concurrently with the H₂ production reaction, using a platinumized TiO₂ photocatalyst under anaerobic irradiation with simulated sunlight. Moreover, we delve into the underlying mechanism and possible degradation pathways by monitoring the formation of organic intermediates, performing isotopic substitution experiments, and studying the reaction in the presence of active species scavengers and spin traps.

5.4 Experimental Section

5.4.1 Raw Materials

The commercial titanium dioxide (TiO₂) Hombikat UV100 was supplied by Sachtleben Chemie GmbH. Naphthalene (≥ 99%), naphthalen-1-ol (97%), naphthalen-2-ol (99%), 1,1'-binaphthalene (97%), naphthalene-1,4-dione (97%), 1,2,3,4-tetrahydro-1-naphthalenone (97%), 3,4-dihydronaphthalen-1(2H)-one (97%), 5-hydroxynaphthalene-1,4-dione (97%), dimethyl phthalate (99%), diethyl phthalate (99%), potassium iodide (99.5%), deuterium oxide (D₂O, 99.9 atom % D), 5,5-dimethyl-1-pyrroline N-oxide (DMPO, 97%), and chloroplatinic acid hexahydrate (H₂PtCl₆·6H₂O, 99.9%) were purchased from Sigma-Aldrich. Methanol (HPLC grade), acetone (GC grade), dichloromethane (GC grade), and ethyl acetate (GC grade) were purchased from Carl-Roth. All reagents were used as received without any further purification. All solutions were prepared with deionized water obtained from a Millipore Mill-Q system (18.2 MΩ cm, 25 °C).

5.4.2 Preparation and Characterization of the Photocatalysts

Platinum-loaded TiO₂ samples were prepared by a photodeposition method following the procedure of Melvin et al.¹⁹. The TiO₂ powder (1.5 g) was dispersed in 150 mL of a 10% aqueous methanol solution with 3.86 mL of 0.01M platinum precursor (H₂PtCl₆) and stirred for 1 h prior to its purging for 1 h with argon. The obtained suspension was then illuminated for 4 h with UV(A) light employing a Philips CLEO 15W lamp inside a climatic chamber with an adjusted temperature of 18°C. The solid was then collected by centrifugation, washed once with methanol and four times with distilled water, and finally dried at 100 °C for 24 h. Ti¹⁸O₂ was kindly provided by Dr. Juan Felipe Montoya and synthesized according to a previously reported procedure²⁰. The synthesized Ti¹⁸O₂ was mixed with the proper

volume of a platinum nanoparticles suspension prepared by laser ablation and kindly provided by Particular GmbH, Germany. Then it was stirred for 1h, and finally dried overnight to prepare 0.5 wt% Pt-Ti¹⁸O₂.

The synthesized platinized TiO₂ and pristine UV100 photocatalysts were characterized with the Brunauer–Emmett–Teller technique (Table S5-1), X-ray diffraction (XRD) (Figure S5-1), transmission electron microscopy (TEM) (Figure S5-2), and electron paramagnetic resonance spectroscopy (EPR) (Figure S5-3). A detailed discussion of the physicochemical characterization can be found in the supplementary information file.

5.4.3 Sample Preparation and Photocatalytic Experiments

Due to the low solubility of naphthalene in water ($2.44 \times 10^{-4} \text{ mol L}^{-1}$ at 25 °C²¹) and its high vapor pressure, special care was taken to prepare deaerated solutions of known concentrations, as summarized in Scheme S5-1. As a first step, a stock saturated and the deaerated solution was prepared in deionized water. In brief, 0.100 g of naphthalene was introduced in a double-jacket two-necked container with airtight screw caps, containing 200 mL of Milli-Q water. The mixture was purged with a gentle stream of argon for 1 h at room temperature. The temperature was then maintained at 40 °C by using a thermostatic water bath with continuous magnetic stirring for 2 h to increase the solubility of naphthalene ($4.30 \times 10^{-4} \text{ mol L}^{-1}$ at 40 °C²¹). Subsequently, the temperature was decreased and maintained at 25 °C with continuous stirring for 4 h. Afterward, the stirring was stopped, and the solution was left for 2 h to settle the undissolved naphthalene crystals. This procedure results in a solution with an estimated concentration of $2.44 \times 10^{-4} \text{ mol L}^{-1}$ (31ppm); the exact value was determined via HPLC-UV.

The photocatalytic experiments were carried out in batch mode. The photocatalytic H₂ evolution experiments were performed in 20 mL glass vials tightly closed with crimp caps and silicone septa. In a typical experiment, 15 mg of the photocatalyst powder was suspended in ca. ~9.5 mL of deionized water inside a vial. The vial was then closed with the crimp septum and purged with argon for 30 min. Afterward, the necessary volume from the stock naphthalene solution was injected inside the vial by using a pre-purged (with argon) needle and syringe, in order to reach a final $1.56 \times 10^{-4} \text{ mol L}^{-1}$ (20 ppm) naphthalene concentration. The total reaction volume was 15.0 mL, with a photocatalyst mass concentration of 1.0 g L⁻¹. Finally, the vials were horizontally fixed inside an orbital shaker and left in the dark for 1 h to establish the adsorption equilibrium. Afterward, the orbital

shaker was placed at a 30 cm distance below a solar simulator consisting of a 1000 W xenon lamp (Hönle UV Technology, Sol 1200) equipped with a filter to mimic the emission profile of sunlight. The temperature of the vials was maintained at 25 ± 2 °C by using a water bath. From the measurement of the lamp irradiance in the wavelength range between 320 nm and 380 nm at the irradiated area, the photon flux density was found to be $I_0 = 3.31 \times 10^{-4}$ mol m⁻² s⁻¹. Ignoring light losses due to reflection and scattering, 2.18×10^{-7} mole of photons entered the irradiated suspension per second.

The photocatalytic experiments in the presence of scavengers were performed under the same conditions, using a 20 mmol L⁻¹ concentration of either potassium iodide (KI) as the hole scavenger or tert-butyl alcohol (TBA) as the hydroxyl radical scavenger. For the radical trapping experiments, the necessary amount of the spin trapping agent 5,5-dimethyl-1-pyrroline N-oxide (DMPO, Aldrich) to achieve a 20 mmol L⁻¹ final concentration was also added. The suspensions were then transferred under an argon stream to a small quartz flat cell cuvette (FZK 160-7x0.3, Magnettech GmbH, Germany) designed for EPR analysis. The samples were irradiated at room temperature (~ 25 °C) directly in the EPR spectrometer microwave cavity, and the spectra were recorded before and during irradiation.

Identical experimental conditions were used for intermediates identification. However, a 250 mL borosilicate reactor was chosen to perform these experiments in a higher volume of the reaction suspension, to guarantee a detectable amount of these intermediates. All the photocatalytic tests were done by triplicate, yielding relative standard deviations (RSD) between 4% and 8%.

5.4.4 Mineralization Measurements

The extent of naphthalene mineralization was monitored by total organic carbon (TOC) measurements, using a Shimadzu TOC-5000A analyzer. Different concentrations of standard potassium hydrogen phthalate and sodium bicarbonate solutions were used for the calibration of the instruments before the analyses. The initial concentration was measured after the equilibrium adsorption of the naphthalene on the Pt-TiO₂ surface for 1h, and afterward, the TOC was recorded at regular intervals. All samples were filtrated with syringe filters (0.2 μm) and immediately analyzed, to minimize the volatilization of naphthalene.

A HIDEN HPR-20 QIC gas analyzer equipped with a quadrupole mass spectrometer (QMS) was used to identify the evolved gases during the photocatalytic tests. The

experiments were carried out in a 65 mL cylindrical air-tight reactor with a quartz window. A continuous flow of 5 mL min⁻¹ of argon carried the headspace into the QMS system. In all experiments, the aqueous suspension volume was 50 mL, while the temperature was kept constant at 25 ± 1 °C. Blank experiments showed no detectable gases evolution in the absence of either light, the photocatalyst or naphthalene. The same setup was employed for the isotopic substitution experiments. In this case, however, irradiation was performed in the vials in an identical way to the photocatalytic experiments, and then the headspace was swept into the QMS using a 0.75 mL min⁻¹ argon flow. The quantitative of the evolved gases was done by calibrating the QMS with standard argon-diluted H₂ (Linde Gas, Germany) and D₂ (Sigma-Aldrich).

5.4.5 Extraction Procedures

To ensure the complete extraction of stable intermediates, two complementary approaches were employed. In the liquid-liquid procedure, the irradiated suspension (250 mL) was transferred to a 500 mL separatory funnel and extracted with three 25 mL aliquots of dichloromethane. The organic layer was passed through a 0.45 mm filter paper containing anhydrous sodium sulfate to remove the TiO₂ particles and water. Finally, the organic layer was concentrated to 1 mL using a gentle stream of nitrogen.

In the solid-phase extraction procedure, the irradiated suspension was immediately filtered through 0.2 µm PTFE syringe filters to remove the TiO₂ particles, then transferred to a brown glass bottle. The extraction was performed within 24 hours to avoid any losses or degradation of the by-products, using packed cartridges (OASIS HLB, 6 mL/500 mg, from Waters® Ireland). The cartridges were connected to a solid-phase extraction apparatus (Supelco, USA) and preconditioned with 6 mL of methanol, 6 mL of ethyl acetate and 6 mL of acidified deionized water (pH 2.0) at a flow rate of 1 mL min⁻¹. Then a sample's aliquot of 200 mL (pH adjusted to 2.0 with 1 M HCl) was loaded into the cartridge and passed through it at a 3-4 mL min⁻¹ rate. Subsequently, the cartridge was pre-dried under low pressure for 5 min to remove the excess of water. Finally, the retained analytes were eluted using three 4 mL aliquots of ethyl acetate at a flow rate of 1 mL min⁻¹. The collected extract was passed through anhydrous sodium sulfate to remove any remaining water and then concentrated to around 0.5 mL using a gentle stream of nitrogen.

5.4.6 Analytical Methods

High-Performance Liquid Chromatography (HPLC) analyses were performed using an Ecom system equipped with a UV-vis detector operating at 276 nm and a Knauer Vertex Plus column packed with Eurospher II 100-5 C18 A material (length \times inner diameter 150 mm \times 4 mm with precolumn). The oven temperature was 30 °C and the mobile phase was a mixture of methanol and water. Different elution programs were applied for naphthalene and intermediates identification as described in Table S5-2.

The formation of short-chain organic acids was monitored via High-Performance Ion Chromatography (HPIC), using a Dionex ICS-1000 equipped with a conductivity detector and an electro-regenerator suppressor. The column was an anion exchange resin (IonPac AS9-HC, L \times I.D. 250 mm \times 2 mm) and the eluent was a mixture of alkaline solutions of 8×10^{-3} mol L⁻¹ Na₂CO₃ and 1.5×10^{-3} mol L⁻¹ NaHCO₃ with a flow rate of 0.3 mL min⁻¹. The temperature of the conductivity cell was kept constant at 35 °C during the analysis period (90 min).

Gas chromatography with thermal conductivity detection (GC-TCD) was used to quantify the photocatalytically evolved H₂. For this purpose, a 50 μ L gas sample was periodically taken from the headspace over the suspension using a Valco gas-tight sampling syringe equipped with a push-button valve. The gas sample was then injected into the injection port of a Shimadzu GC-8A, equipped with a stainless-steel molecular sieve 5A GC column (Sigma-Aldrich, USA). The temperature of the injection port and the TCD detector was maintained at 120 °C, while the column temperature was fixed at 80 °C.

The extracted reaction intermediates were analyzed by GC-MS using a GCMS-QP5050 (Shimadzu) coupled with AOC-5000 Plus autosampler and a capillary Agilent DB-5ms column (L \times I.D. \times film thickness 30 m \times 0.1 μ m \times 0.32 mm). The carrier gas was helium at a constant flow of 1.25 ml min⁻¹. The oven temperature was programmed at 70 °C for 3 min, followed by a raise to 180 °C at a rate of 10 °C min⁻¹, held for 2 min, and then a final raise at a rate of 20 °C min⁻¹ to 315 °C and held for 10 min. The injection port and the interface temperatures were set at 250 °C and 280 °C, respectively. The mass spectrometer was operated in the positive electron impact mode with ionization energy of 70 eV; the detection was performed in scan mode and peaks were identified according to the NIST library.

5.4.7 EPR in Situ Experiments

The electron paramagnetic resonance (EPR) spin-trapping technique was applied to detect and monitor the formation of paramagnetic intermediates. Such intermediates were detected upon in situ irradiation using an X-band EPR MiniScope MS400 (Magnettech GmbH, Germany) spectrometer operating at a 9.51 GHz field and equipped with a UV spot-light (LC8, Hamamatsu, 200 W super-quiet mercury-xenon lamp). The acquisition parameters were as follows: center field: 335.4086 mT, sweep time 15 s, number of points: 4096, number of scans: 1, modulation amplitude: 0.2 mT, power: 10 mW, gain: 5. The EPR spectra simulations were carried out using EasySpin²².

5.4.8 Transient Absorption Spectroscopy

The transient absorption spectroscopy (TAS) measurements were carried out in diffuse reflectance mode by means of an Applied Photophysics equipment, employing an LKS80 nanosecond Laser Flash Photolysis Spectrometer with a pulsed Nd:YAG laser (Quantel, Brilliant B). Samples were measured as aqueous slurries inside flat quartz cells. Prior to the measurements, the samples were purged with argon for 30 min. The excitation wavelength was 355 nm, with an average energy per pulse of 6 mJ cm⁻². The obtained transient signal is detected upon measuring the change in reflectance (ΔJ) before (J_0) and after the laser excitation (J), according to Equation 5-1.

$$\Delta J = \frac{J_0 - J}{J_0} \quad 5-1$$

5.5 Results and Discussion

5.5.1 Naphthalene Degradation and Photoreforming

We start our analysis by considering the requirements for the photocatalytic production of H₂ over bare and platinized Hombikat UV100 TiO₂ (from here on, UV100 or Pt-UV100, respectively). First, as expected from the known lack of water splitting activity of bare TiO₂²³, no H₂ is evolved in the absence of naphthalene. Similarly, there is no H₂ production in the absence of either light or a photocatalyst. However, the naphthalene concentration moderately decreases under irradiation in the absence of the photocatalyst (32% after 4 h), possibly due to the photolysis of the probe compound¹³. The direct photolysis of PAHs has been reported previously^{13,24}, and it is considered as one possible method for eliminating these compounds from the environment²⁵. For the photolysis to occur the absorption spectra of the organic molecules must overlap with the emission spectra of the source. In the present case only, a limited overlap occurs in the range 300-315nm (Figure S5-4), which

results in relatively slow photolysis of naphthalene. It has been reported that, upon irradiation, naphthalene undergoes oxidation to its radical cation^{24, 25}, which reacts with water or O₂ to mainly yield naphthol, quinone, and aldehyde²⁶. The detection of by-products in our system proved unsuccessful, most likely due to the low concentration and the sequential photooxidation of these products²⁷ in our system. The estimated photonic efficiency for the direct photolysis of naphthalene after 4 h irradiation is $2.3 \times 10^{-3} \%$. This value is low compared to that reported by Vialaton et al.²⁸ of $2.5 \times 10^{-1} \%$ for the photolysis of naphthalene under aerobic conditions at 313 nm irradiation. On the other hand, the absorption coefficient of TiO₂ is much higher in the range of the light source emission, and thus we expect that, when TiO₂ and naphthalene are both presents, most light is absorbed by TiO₂, significantly decreasing the photolysis rate.

The degradation of naphthalene is greatly enhanced in the presence of UV100 and Pt-UV100 (Figure 5-1). After irradiating the aqueous suspension for 4 h, the naphthalene concentration decreases by 71% and 86%, respectively. However, we only observe H₂ evolution in the presence of Pt-UV100. The lack of H₂ evolution over bare TiO₂ is a known issue, ascribed to the high overpotential for this reaction on the TiO₂ surface²⁹. In the present case, whilst photogenerated holes in TiO₂ may be consumed by naphthalene, the absence of molecular oxygen as the electron acceptor necessitates that the accompanying electrons either reduce one of the organic species present in the system or accumulate in the form of trivalent titanium (Ti³⁺) inside the photocatalyst³⁰.

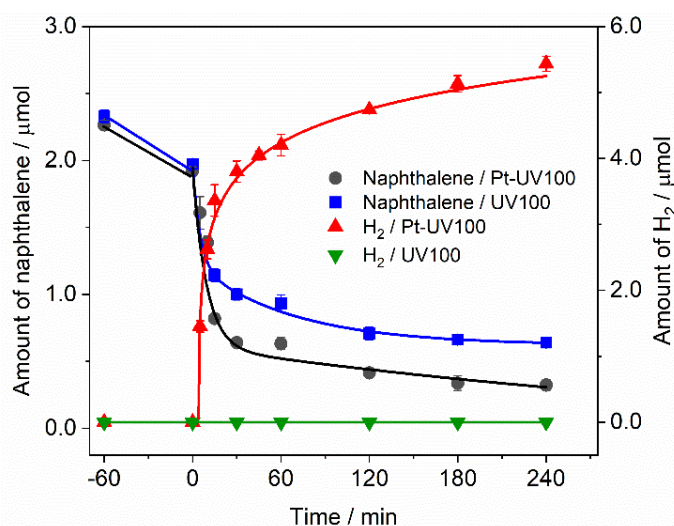


Figure 5-1: Kinetic profiles for the photocatalytic degradation of naphthalene and molecular hydrogen evolution over UV100 and Pt-UV100. Conditions: batch reactor, reaction volume = 15 mL; [Naphthalene] = $156 \mu\text{mol L}^{-1}$; [catalyst] = 1 g L^{-1} ; $T = 25 \text{ }^\circ\text{C}$; illumination under simulated solar light. Lines are guides for the eye.

Regarding the choice of the photocatalyst, we exclusively employ here the pure-anatase Hombikat UV100, either bare or loaded with 0.5 wt% of platinum (prepared by photodeposition). Although the photocatalyst optimization is out of the scope of this study, we mention that this selection is not arbitrary but is based on experimental results showing that i) UV100 is more active than Aeroxide P25; ii) the photodeposition method of Pt on TiO₂ surface results in a higher activity than other deposition methods such as physical mixing of titania with Pt nanoparticles, and iii) a 0.5 wt% Pt loading seems to be optimal for the reaction under investigation. We show the detailed characterization of UV100 and Pt-UV100 in the Supporting Information.

The analysis of the kinetic profiles reveals some interesting features. As shown in Figure 5-1, during the prior dark period around 14% of the initial naphthalene amount adsorbs on the surface of the photocatalysts. Although the compound is not expected to strongly interact with the TiO₂ surface, it is apparent that the high specific surface area of UV100 results in significant adsorption³¹. The adsorption kinetics of naphthalene on the surface of 0.5 w% Pt-UV100 are shown in Figure S5-5. We observe that the adsorption equilibrium is attained within 1h. The adsorbed amount at the equilibrium corresponds to a coverage of around 0.05 molecule nm⁻². A similar value for naphthalene on the surface TiO₂ (anatase) has been reported by Mahmoodi and Sargolzaei, with the difference that the dynamic equilibrium was established after 5 min in that case³². The adsorption of aromatic compounds on the TiO₂ surface was studied by Nagao and Suda³³, who suggested that the adsorption involves the formation of Ti⁺⁴··· π -electron and/or OH_(surface)··· π -electron type complexes.

Upon irradiation, we observe a rapid decrease of the naphthalene amount in the presence of both photocatalysts during the first 30 min of illumination. This decrease is found to be accompanied by rapid H₂ evolution only in the presence of Pt-UV100. After this initial 30 min period, the changes in the amounts of naphthalene, as well as evolved H₂, became significantly slower, suggesting the depredation of accumulated intermediates at the photocatalyst surface and the competition of naphthalene and intermediates for the holes during the photocatalytic process. This hypothesis of poisoning the photocatalyst surface is supported by the observation of a color change of the photocatalyst from light gray to brown after 1 h of illumination (Figure S5-6). This observation is in agreement with previous reports which have shown that the photocatalytic degradation of naphthalene and other aromatic compounds may yield intermediates, likely of polymeric nature, that deactivate

the catalyst surface^{34,35}. Additionally, we performed recycling experiments by collecting the photocatalyst and irradiating it in the presence of molecular oxygen for 1 h to remove the adsorbed organic compounds (Figure S5-6) for overcoming possible poisoning problems.

As illustrated in Figure 5-1, the loading of platinum nanoparticles on TiO₂ not only enables the evolution of H₂ possibly through the reduction of the overpotential for the electron transfer to the proton³⁶, but also promotes the degradation of naphthalene. We ascribe this observation to the charge separation effect caused by the Schottky barrier between TiO₂ and platinum, which results in a lower recombination rate of the photogenerated electron-hole pairs^{37,38}. On another hand, the reduction of the adsorbed protons on the surface of the TiO₂ by depletion of the photogenerated electrons could be another factor for enhancing the photocatalytic activity of the Pt/TiO₂ and lessening the charge carrier recombination. Since the reduced protons (i.e., hydrogen atoms) migrate to the Pt islands to combine yielding H₂ molecules, the degradation of the naphthalene is enhanced on the positively charged TiO₂ surface³⁹. Similarly, Sun et al.⁴⁰ have reported that the rates of light-induced phenol decomposition and total carbon removal increased by a factor of 1.5 when UV100 was loaded with 1 wt% Pt.

From the photocatalytic naphthalene reforming experiments over Pt-UV100, we determined the initial (< 30 min) photonic efficiencies, ξ , to be (0.97 ± 0.06) % for H₂ formation (3.8 μ mol / 30 min) and (0.33 ± 0.01) % for naphthalene degradation (1.3 μ mol / 30 min) after correction by subtracting the quantity of adsorbed naphthalene. The employed equations are detailed in the *Supporting Information section*. These are typical values for photocatalytic processes⁴¹, although much lower than those reported, for instance, for the photocatalytic reforming of methanol over Pt-UV100 (between 20 and 30 %) ⁴². Methanol, however, gives rise to current-doubling effects, that in conjunction with its well-known hole scavenging properties results in a highly efficient H₂ evolution.

We observe a considerably higher ξ for H₂ production than for naphthalene degradation. This suggests that H₂ is not only produced in association with the direct oxidation of naphthalene but also with the oxidation of organic intermediates, as will be discussed below. The 30 min period in which the ξ was determined is long enough to reach a significant conversion for naphthalene accompanied by the formation of reaction intermediates.

Besides the disappearance of naphthalene, it is of high importance for practical applications to evaluate the extent of complete mineralization of the reactant yielding CO_2 and H_2O . Therefore, we monitored the concentration of the total organic carbon (TOC) being present in the aqueous solution after the removal of the photocatalyst Pt-UV100. The TOC data points in Figure 5-2 showed a gradual decline to around 55 % after 4 h of irradiation.

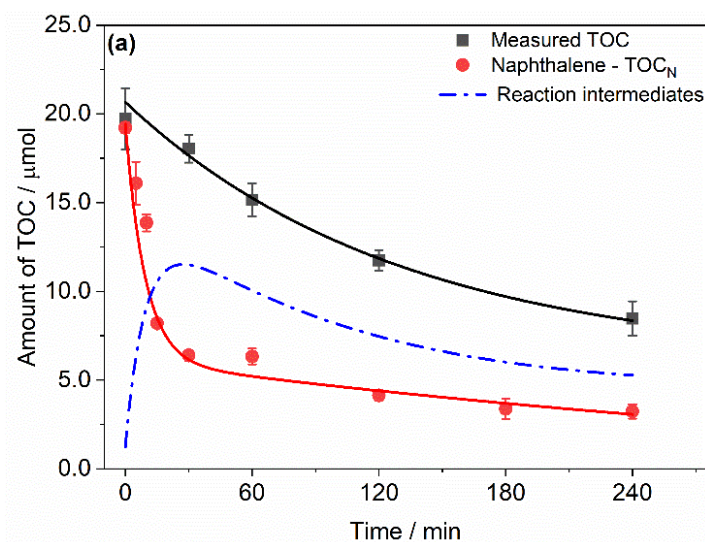


Figure 5-2. Kinetic profile for the relative amount of total organic carbon (TOC) during the photocatalytic reforming of naphthalene over Pt-UV100.

As mentioned above, the concentration of naphthalene decreases by 86 % in the same period of time, pointing to the formation of stable intermediates. By converting the amount of naphthalene to organic carbon, TOC_N , during the photocatalytic process in presence of the Pt-UV100 and subtracting its curve from that of measured TOC, we estimate the kinetic profile of all organic intermediates (Figure 5-2). This curve follows the expected profile for reaction intermediates, reaching a maximum at around 30 min and then progressively decreasing. We have identified these intermediates by various analytical techniques and describe the results in Section 3.2, together with a plausible reaction pathway. We note, however, that a decrease in the TOC amount could possibly reflect the adsorption of the by-products on the TiO_2 surface, instead of mineralization.

To rule out this possibility, we performed in-line monitoring of the reaction atmosphere by means of the quadrupole mass spectrometry (QMS) technique. Blank experiments showed no detectable evolution of gases in the absence of either irradiation, the photocatalyst, or naphthalene. Additionally, no significant signals were detected for the formation of CO , CH_4 , and other small alkanes and alkenes. We show the time course of the QMS signals for H_2 and CO_2 which are proportional to the amount of produced gases in Figure S5-7. We

note here that experimental limitations (namely, significant evaporation of naphthalene) prevent us from quantifying the absolute amounts of generated CO₂ and H₂. The following description is thus only qualitative. The observation of a CO₂ signal indeed indicates that complete mineralization of the reactant occurs. After a very short initial delay, CO₂ formation shows an increasing rate over time during the analyzed period. Contrarily, after a fast-initial growth, the H₂ QMS signal shows a marked decrease in its formation rate, in accordance with the results of Figure 5-1. On the other hand, the loss of naphthalene due to its large vapor pressure during these experimental runs, which were performed in an open system, prevents us to perform a direct comparison between the evolved amount of CO₂ and the decrease in the TOC. However, the brownish color of the recovered photocatalyst and its disappearance during the irradiation in the presence of O₂ could indicate that at least part of the TOC decrease is related to the adsorption of by-products on the TiO₂ surface.

5.5.2 Identification of Intermediates

We investigated the intermediates formed during the photocatalytic reforming of naphthalene over Pt-UV100 using a combination of chromatographic techniques. Firstly, we employed liquid-liquid and solid-liquid extraction procedures followed by gas chromatography-mass spectrometry (GC-MS) to obtain an overview of the stable intermediates. The identified by-products are shown in Chart 5-1 while the details of their detection (retention times, molecular ion peaks, and mass fragmentation patterns) are listed in Table S5-3. Among these compounds, we found that naphthalen-1-ol and naphthalen-2-ol are the main constituents after 4 h of irradiation (0.25 ± 0.01 and 0.13 ± 0.01 μmol , respectively). In contrast, we detected naphthalene-1,4-dione in a lower amount (0.030 ± 0.003 μmol), and only traces of the remaining compounds. Complementarily, we also analyzed the samples for short-chain organic acids using high-performance ion chromatography (HPIC). From these analyses, we determined the presence of formic acid and acetic acid in low concentrations (0.051 ± 0.008 and 0.029 ± 0.005 μmol , respectively).

Although these are, to the best of our knowledge, the first results concerning the photoreforming of naphthalene, we can perform a meaningful comparison with the intermediates previously observed during its aerobic photocatalytic oxidation, summarized in Table S5-4. Although there is some degree of coincidence, it is revealing that in the present case most detected intermediates correspond to earlier stages of the degradation process. This is consistent with the poisoning effect discussed above, that may limit the

extent of mineralization under anaerobic conditions. Similarly, we find short-chain acids, produced from ring cleavage reactions^{10, 12, 43} in very low concentrations.

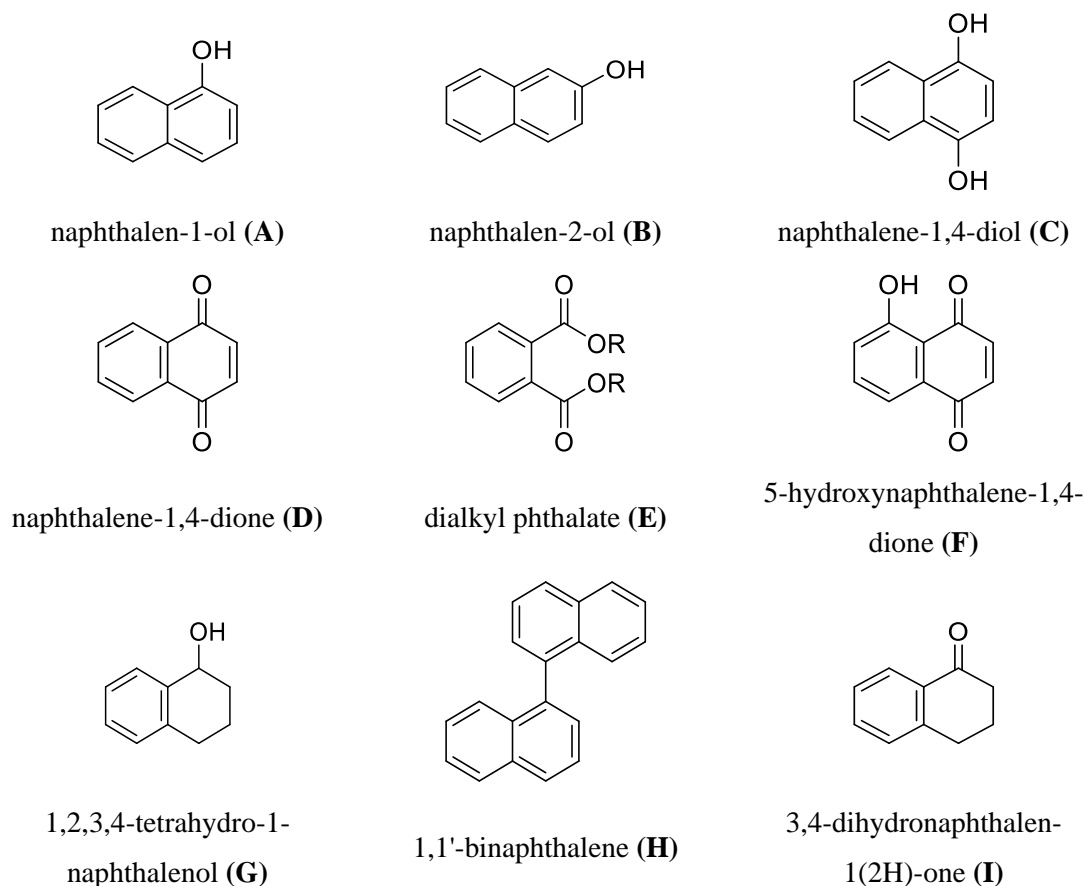


Chart 5-1: Detectable intermediates during the photocatalytic reforming of naphthalene using Pt-UV100.

Considering that naphthalen-1-ol and naphthalen-2-ol are the main detected intermediates, we now focus on the time dependence of their concentrations, as monitored by high-performance liquid chromatography (HPLC). The kinetic profiles, shown in Figure 5-3, closely match the degradation of naphthalene (Figure 5-1) with a high formation rate during the first 30 min, and a significant retarding at longer times. The detected amounts, however, are considerably smaller than those expected from the complete conversion of naphthalene. While, around 1.5 μmol of naphthalene was degraded after 4 h, only a combined amount of 0.39 μmol of naphthalen-1-ol and naphthalen-2-ol was formed. In the first stage of the reaction (Figure 5-3), the formation rate of these naphthalenols is larger than the rate of their consumption, thus, increased their amount in the medium.

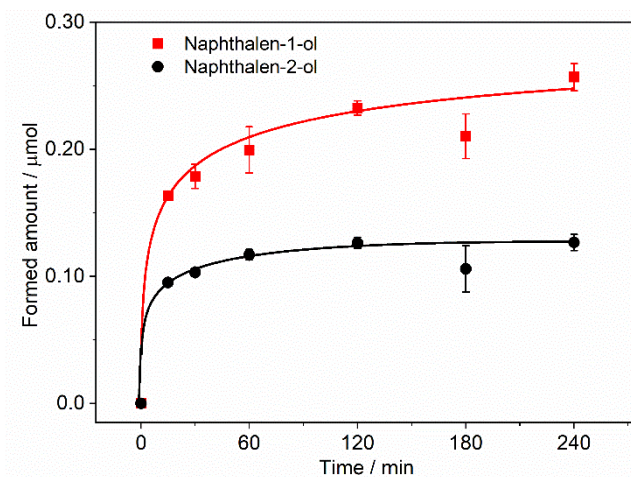


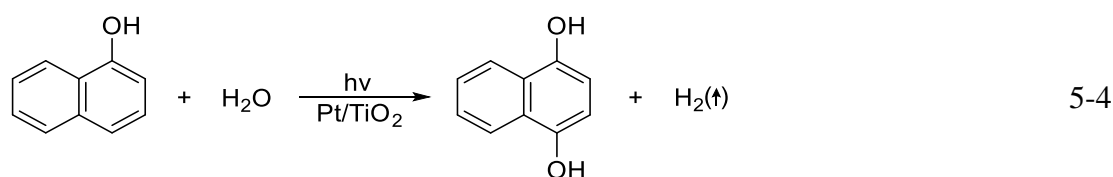
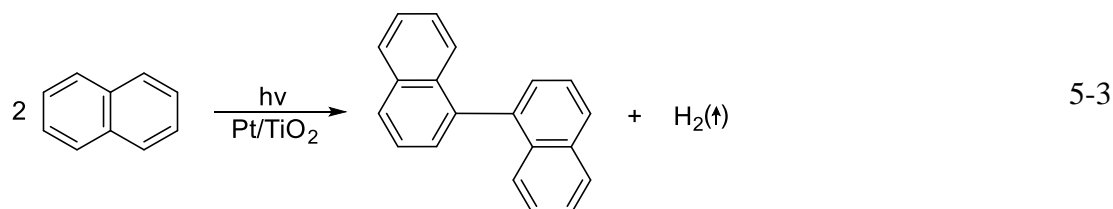
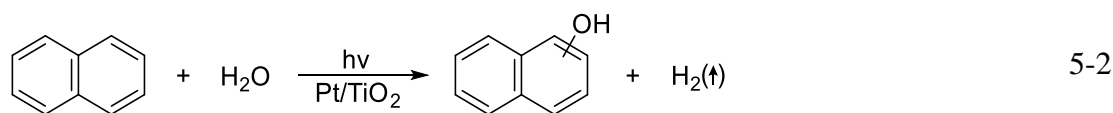
Figure 5-3. Kinetic profile for the formation of naphthalen-1-ol and naphthalen-2-ol during the photocatalytic reforming of naphthalene over Pt-UV100.

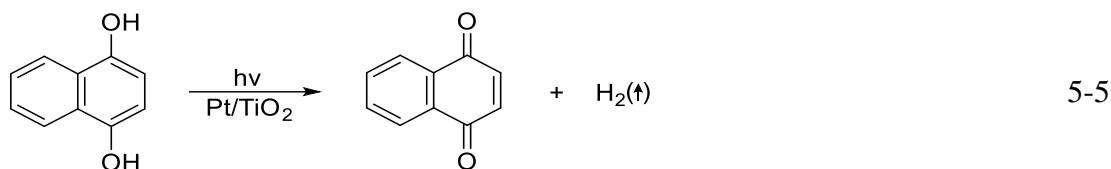
Subsequently, in the second stage, the formed amount becomes almost constant as both rates nearly equivalent. This may suggest the formation of a relatively large quantity of unidentified intermediates, consistent with the hypothesis of polymeric species poisoning the TiO_2 particles¹⁴, or alternatively strong adsorption of the naphthalenols over Pt-UV100. Regarding the latter, Mills et al. have suggested that the structurally similar phenol and 4-chlorophenol may indeed show strong binding to TiO_2 ⁴⁴.

A further interesting observation is that the concentration ratio of naphthalen-1-ol to naphthalen-2-ol is not unity but instead ranges from 1.7 to 2 throughout the reaction. We find a plausible explanation for this behavior on the basis of Dewar's molecular orbital theory⁴⁵ and the adsorption of naphthalene on the surface of the TiO_2 . Briefly, this theory predicts that the difference in the activation energy of two related aromatic substitution reactions is mainly determined by the difference in the so-called localization energies of the extended π -systems. Of relevance here, the localization energies have been quantified in the form of *Dewar's reactivity numbers*; a lower reactivity number corresponds to a faster aromatic substitution reaction, and vice versa. The reported values for the 1- and 2-positions in naphthalene are 1.81 and 2.12, respectively. Moreover, as determined from near edge x-ray absorption spectroscopy (NEXAFS), naphthalene molecules adsorb on the surface of rutile (110) in a flat-lying geometry with tilt angles about 24° , at relatively high altitudes that reach 3–4 Å from the substrate surface⁴⁶. Matsuura et al.⁴⁷ demonstrated that position 1 on the naphthalene molecule is more reactive for removing an electron than that of position 2 due to the higher charge density in this position. Thus, hydroxylation at position 1 results in a more stable product than hydroxylation at position 2, which has been

confirmed by Hückel-McLachlan molecular orbital calculations by Steenken⁴⁸ and experimentally by Hykrdova et al.³⁴ who reported the preferred formation of naphthalen-1-ol in the TiO₂ (heterogeneous) and Fe⁺³ (homogenous) systems. This becomes congruent with *Dewar's reactivity numbers* hypothesis and thus explains the preferential formation of naphthalen-1-ol. Considering these results, it can be concluded that the interaction of the naphthalene molecules with the TiO₂ surface does not significantly change its electronic distribution in naphthalene. Hence, the electronic density at the carbon atoms (C₁ > C₂ > C_{9,10}) of the naphthalene molecule governs the position of hydroxylation³⁴.

Although the mechanism for the formation of naphthalen-1-ol and naphthalen-2-ol will be discussed in *section 5.5.4*, we mention here that the overall reaction is given by Equation 5-2. Consequently, the expected H₂ to naphthalenols ratio is 1:1, thus being at odds with our observation of a >10:1 ratio, as deduced from Figure 5-1 and Figure 5-3. This discrepancy can be explained from two perspectives. On the one hand, there may be parallel channels by which naphthalene is degraded. One such example is given by Equation 5-3, that results in one of the detected intermediates, 1,1'-binaphthalene, and the formation of hydrogen. Additionally, the kinetic profile of naphthalenols in Figure 5-3 not only reflects their formation rate but also their simultaneous consumption rate by a photoreforming reaction, skewing the ratio towards higher H₂ values. This is illustrated by Equations 5-4 and 5-5, that result in the formation of two equivalents of H₂ via the successive transformation of naphthalene-1-ol into two of the detected intermediates, naphthalen-1,4-diol, and naphthalene-1,4-dione. Moreover, the strong binding of the naphthalenols to the TiO₂ surface could also explain their low observed amounts.





5.5.3 Mechanistic Study

5.5.3.1 Participation of the TiO₂ Surface as a Source of Oxygen Atoms

Recently, besides photogenerated holes and hydroxyl radicals as active species in photocatalytic processes, the role of bridging oxygen radicals at the TiO₂ surface (O_s) has been discussed^{14, 49, 50}. Holes could be trapped by bridging oxygen atoms on the TiO₂ surface ($\equiv\text{Ti}-\text{O}_s-\text{Ti}\equiv$) to produce the active species oxygen radical ($\equiv\text{Ti}-\text{O}_s^{\bullet}-\text{Ti}\equiv$), which ultimately can be incorporated into the reaction products, creating oxygen vacancies that are subsequently healed by water. Therefore, isotope labeling is a useful strategy to evaluate such mechanism, e.g. by using mass spectroscopy to monitor the isotopic composition of the evolved species. As we demonstrated in section 5.5.1, CO₂ was one of the final products during the photocatalytic reforming of naphthalene. Thus, if the bridging oxygens are the oxygen source for hydroxylation of naphthalene, in this case, we expect that the isotopic composition of the evolved CO₂ should (partially) reflect that of TiO₂. To investigate the participation of bridging oxygens, we performed the reaction over isotopically labeled Pt-Ti¹⁸O₂ and monitored different CO₂ isotopologues before and during the illumination by means of QMS.

Figure 5-4 illustrates the time evolution of the QMS signals of different CO₂ isotopologues and their fragments during the photocatalytic reforming of naphthalene over Pt-Ti¹⁸O₂. Before illumination, no changes in the background signals were observed for one hour, i.e., no catalytic reaction occurred between naphthalene and Pt-Ti¹⁸O₂ in the absence of light. Upon irradiation, only the signal of C¹⁶O₂ (m/z = 44) significantly increased, indicating the photocatalytic mineralization of naphthalene without the incorporation of oxygen atoms from the lattice. However, it should also be mentioned that oxides readily undergo lattice oxygen exchange with gaseous O₂, not only under UV irradiation but in dark conditions as well⁵¹. The absence of ¹⁸O-labelled CO₂ was also observed in batch reactor experiments where we increased the catalyst mass concentration 5-fold, collected the evolved gases in the headspace of the reaction vial and analyzed them via injection to the QMS to increase sensitivity.

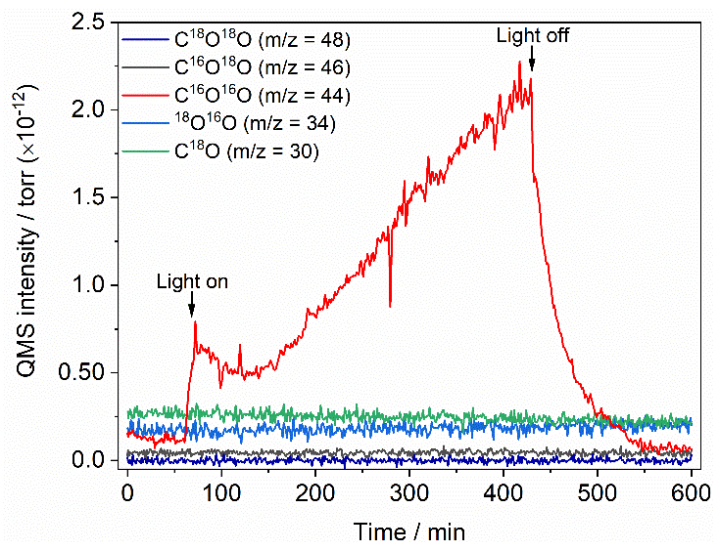


Figure 5-4. QMS signals for isotopologues of CO, CO₂, and O₂ from the reforming of naphthalene over Pt-Ti¹⁸O₂. Experimental conditions: reaction volume: 5 mL; [Naphthalene] = 230 μmol L⁻¹, light intensity I₂₅₀₋₄₅₀ = 30 mWcm⁻², [catalyst] = 2 g L⁻¹, T = 25 °C, and irradiation with an Osram XBO 1000-Watt xenon arc lamp as a solar simulator

Civis and co-workers⁵² studied the photocatalytic decomposition of formic acid on the surface of Ti¹⁸O₂ by the means of Fourier-transform infrared absorption spectroscopy, and found that the process does not lead to the evolution of either C¹⁶O¹⁸O nor C¹⁸O₂. On the contrary, Montoya and co-workers^{20, 50} did observe C¹⁶O¹⁸O evolution during the photocatalytic oxidation of benzene over Ti¹⁸O₂ in anaerobic conditions. Although we investigated the same kind of organic compounds, namely aromatic hydrocarbons, we believe that naphthalene could be photocatalytically oxidized by a different mechanism. This can be argued from several angles, first, we observe a significant production of 1,1'-binaphthalene, which cannot be accounted for by the bridging oxygen mechanism. Second, the one-electron standard redox potentials for the oxidation of benzene and naphthalene in acetonitrile are 2.65 and 1.85 V vs. NHE respectively⁵³. Thus, neglecting the slight variation in aqueous solution, the one-electron oxidation of naphthalene by its direct reaction with holes (valence band potential: 2.68 V vs. NHE at pH 7)⁵⁴ is thermodynamically favored with respect to the same reaction for benzene. Hence, as long as the reaction does not fall into the Marcus inverted region, it will be significantly faster. The observation by Fox et al. of increasing photocatalytic oxidation rates for substituted naphthalenes as the exergonicity increased supports this notion⁵⁵. Accordingly, abstraction of an electron from naphthalene by the valence band hole, which has a more positive potential, is likely to take place. And third, as shown in Figure 5-1 naphthalene adsorbed significantly on the TiO₂ surface, unlike benzene⁵⁶. Indeed, temperature programmed

desorption measurements over rutile single crystals have shown a significantly stronger binding by naphthalene⁴⁶. Notably, the direct-indirect hole transfer model (DT-IT) of Salvador et al.⁵⁷, proposes that the specific pathway depends on the degree of electronic interaction of the dissolved molecules with the semiconductor surface. The relatively strong interaction of naphthalene with TiO₂ leads us to conjecture that, although both mechanisms may be operative, in contrast with benzene, the direct transfer of holes to naphthalene is favored with respect to the indirect, bridging oxygen mediated transfer⁵⁶. Therefore, according to what we presented above; we propose that naphthalenols are the product of naphthyl radical cation formation followed by its reaction with water. More experimental evidences supporting this argument will be presented in the following sections.

5.5.3.2 Scavengers and Electron Paramagnetic Resonance (EPR) Spin-Trapping Technique

To determine the involvement of different active species in the photoreforming of naphthalene, we performed the reaction in the presence of two scavengers: potassium iodide (KI), which acts as a hole scavenger⁵⁸, and 2-methylpropan-2-ol ((CH₃)₃COH, TBA), a known hydroxyl radical ([•]OH) scavenger⁵⁹. As shown in Figure 5-5 (a), the photocatalytic conversion of naphthalene is completely inhibited in the presence of KI, with a degradation rate identical to that of the photolytic process.

In contrast, the addition of TBA does not appreciably affect the photocatalytic process, yielding a kinetic profile virtually identical to that in the absence of scavengers. These results suggest that free hydroxyl radicals ([•]OH_{free}) present, have a minor contribution in the process. In contrast, the use of a hole scavenger leads to a halt in the photocatalytic process, confirming that naphthalene's disappearance is initiated by an oxidative half-reaction. Miller and Olejnik²⁵, as well as Beltran et al.⁶⁰, showed that neither TBA nor bicarbonate ions, respectively, affect the degradation rate of different PAH compounds in the presence of hydroxyl radicals in homogeneous systems. Therefore, they concluded that the photooxidation of these compounds was initiated via the formation of a radical cation, without involving free hydroxyl radicals. Accordingly, our results are in good agreement with their findings, despite the difference between both types of systems.

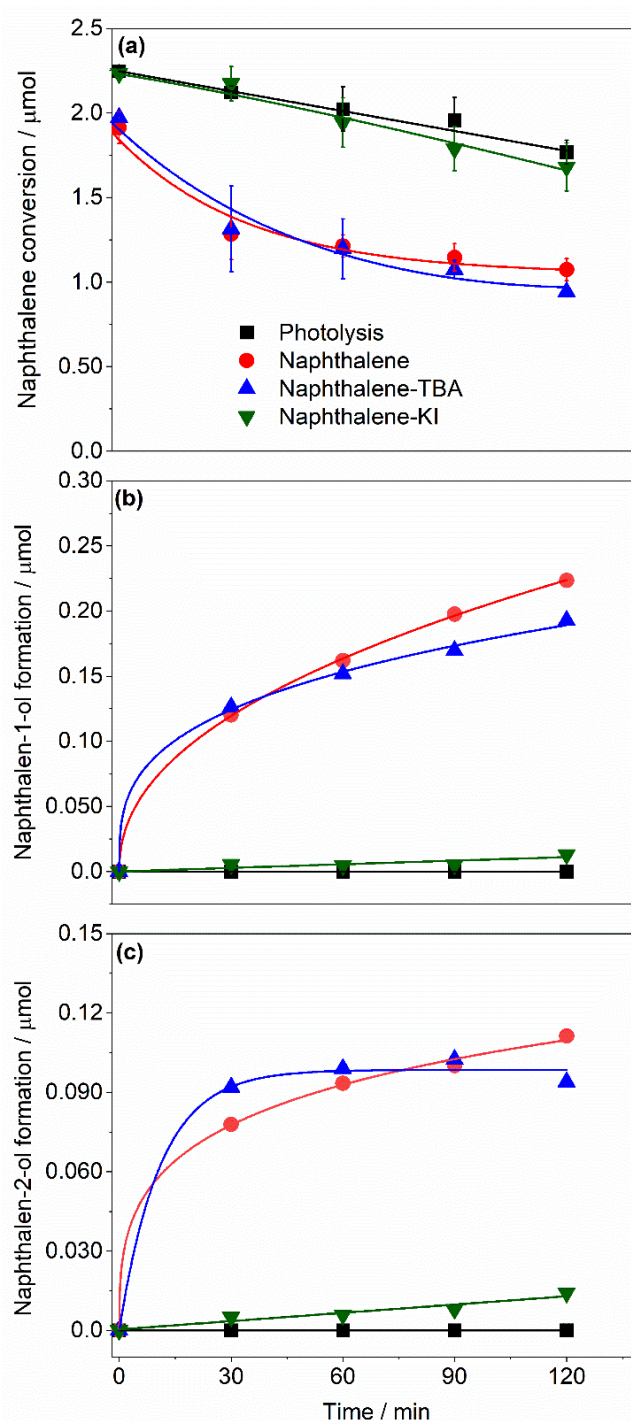


Figure 5-5. Kinetic profiles for the disappearance of naphthalene (a), the formation of naphthalen-1-ol (b), and the formation of naphthalen-2-ol (c) during the photocatalytic reforming of naphthalene in the presence of different scavengers over Pt-UV100. [catalyst] = 1 g L⁻¹; 156 μmol L⁻¹ aqueous solution of naphthalene; 20 mmol/L of KI and TBA; UV illumination. The initial amount of naphthalene for all reactions was considered after 1 h dark adsorption. Lines are guides for the eye.

Complementarily, we monitored the formation of naphthalen-1-ol and naphthalen-2-ol during these experiments, as shown in Figure 5-5 (b) and (c). Their kinetic profiles are consistent with those of naphthalene degradation: while the addition of TBA does not

significantly affect the formation of naphthalenols, the addition of KI hinders naphthalene degradation almost completely due to the consumption of holes by this scavenger, highlighting their role in the photoreforming process. This result is not only important from the mechanistic point of view, but also for potential applications, since the simultaneous presence of hole-scavenging species in industrial effluents may completely inhibit naphthalene reforming.

The involvement of $\cdot\text{OH}_{\text{free}}$ in photocatalytic reactions is the subject of a long-standing debate. Salvador has provided strong arguments against the oxidative formation of $\cdot\text{OH}_{\text{free}}$ on the grounds of thermodynamic and kinetic arguments, stating that their observation in photocatalytic systems must respond to the reduction of molecular oxygen⁶¹. However, recent works have challenged this idea, suggesting that the irradiation of anatase TiO_2 does lead to the formation of $\cdot\text{OH}_{\text{free}}$, although this is not the case for the rutile polymorph⁶². We thus employed electron paramagnetic resonance (EPR) spectroscopy to obtain additional insights regarding the role of $\cdot\text{OH}_{\text{free}}$ in our system. To this end, we performed in-situ naphthalene photoreforming experiments in the presence of either TBA or KI, and the spin trap 5,5-dimethyl-1-pyrroline N-oxide (DMPO). As expected, under dark conditions no radicals are detected. Upon irradiation, however, the tested samples under all conditions lead to the appearance of a signal attributable to the DMPO-OH adduct (four lines with relative intensities of 1:2:2:1), Figure 5-6.

The simulation of the EPR spectrum (Figure S5-8) yields the spin Hamiltonian parameters $a_{\text{N}} = 1.453$ mT, $a_{\text{H}} = 1.494$ mT and $g = 2.0059$, in accordance with previously reported values for this adduct^{63, 64}. Notably, we observe the production of the $\cdot\text{OH}$ adduct in the absence of molecular oxygen, providing evidence in favor of their formation from the oxidation of water⁶⁵. Additionally, we could detect neither organic radicals nor their DMPO adducts, likely due to a relatively low concentration of naphthalene and its intermediate radicals inside the EPR cell, together with a large multiplicity for the hyperfine splitting of the adducts. A similar conclusion was reached by Steenken et al.⁴⁸ who could not detect any signal from organic radicals during the reaction of naphthalene (and some of its derivatives) with both $\cdot\text{OH}$ and $\text{SO}_4\cdot^-$ in aqueous solution, both in the presence and the absence of spin trapping agents.

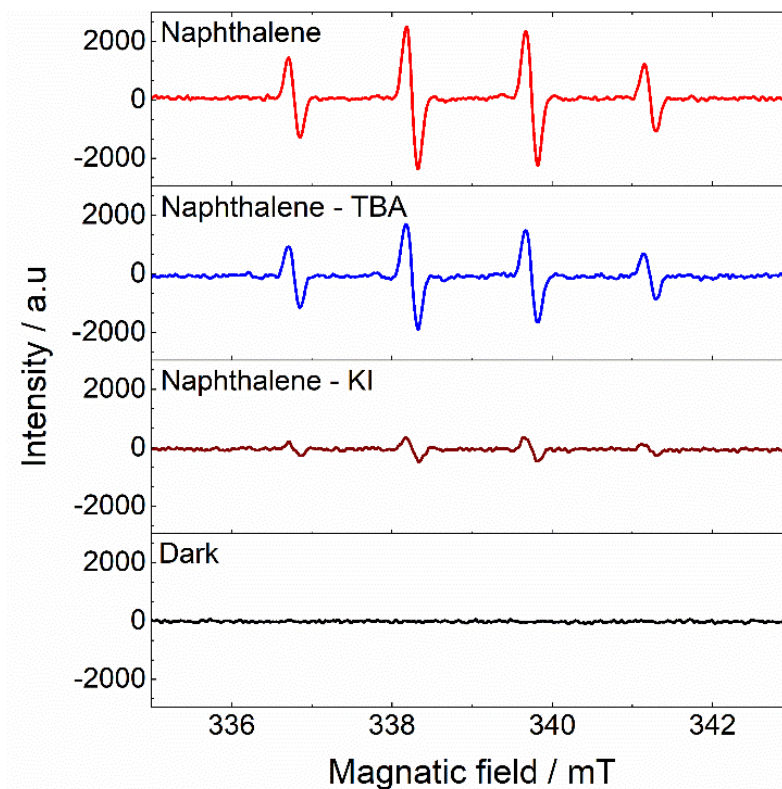


Figure 5-6. EPR spectra were recorded during the photocatalytic reforming of naphthalene after 15 seconds in the presence of DMPO, DMPO-TBA, and DMPO-KI. [catalyst] = 1 g/L; 156 $\mu\text{mol/L}$ aqueous solution of naphthalene; 20 mmol/L of KI and TBA; irradiation using UV(A); microwave frequency: 9.51 GHz.

By performing the same experiment (i.e., aqueous DMPO with Pt-UV100) either in the absence or presence of naphthalene, we obtained similar signals (Figure S9), showing that, under these conditions, naphthalene is not a strong $\cdot\text{OH}$ scavenger. In the presence of TBA, however, the adduct signal shows a decrease of 35 % (Figure 5-6) and vanished within 90 sec comparing to more than 240 sec in its absence (Figure S5-10), confirming TBA's $\cdot\text{OH}$ scavenging properties. Nevertheless, this lower quantity of available $\cdot\text{OH}$ radicals does not impact on naphthalene's degradation (Figure 5-5), providing evidence against a degradation mechanism initiated by the attack of $\cdot\text{OH}_{\text{free}}$.

The addition of KI to the system, on the other hand, practically nullifies the adduct formation, as could be expected from the efficient hole consumption by this scavenger. Regarding the role of holes, although we can confirm their importance, we cannot distinguish between a direct hole (h^+) transfer to naphthalene or its indirect oxidation via surface-trapped holes ($-\text{OH}_\text{s}^\cdot$).

Moreover, by means of an electrochemical degradation process, Li and Goel⁶⁶ showed that naphthalene degradation was not affected by the presence of acetone and methanol as an

$\cdot\text{OH}$ competitor, suggesting that naphthalene degradation occurred as a result of direct electron transfer. Thus, they excluded the indirect oxidation via the $\cdot\text{OH}$. We applied a simple model by Luo et al.⁶⁷ to determine the Gibbs free energy (ΔG°) for the single electron transfer reaction from benzene, naphthalene, and anthracene to $\cdot\text{OH}$ to produce the corresponding radical cation and hydroxide ions. The calculated values are +24.6, +1.7, and -21.5 kcal mol⁻¹, respectively. It is thus apparent that by increasing the number of aromatic rings in the organic compound the reaction becomes more spontaneous. Hence, naphthalene has a higher tendency to react with $\cdot\text{OH}$ forming a radical cation, rather than an adduct, as is the case for benzene.

5.5.3.3 Diffuse Reflectance Transient Absorption Spectroscopy

To evaluate the formation of short-lived species during the reaction, we turned to diffuse reflectance transient absorption spectroscopy. Figure 5-7 shows the spectra obtained 300 ns after the laser excitation (355 nm, 6 mJ pulse⁻¹) of anaerobic Pt-TiO₂ slurries in the presence of (a) a (1:1) water/acetonitrile mixture and (b) naphthalene in the same solvent.

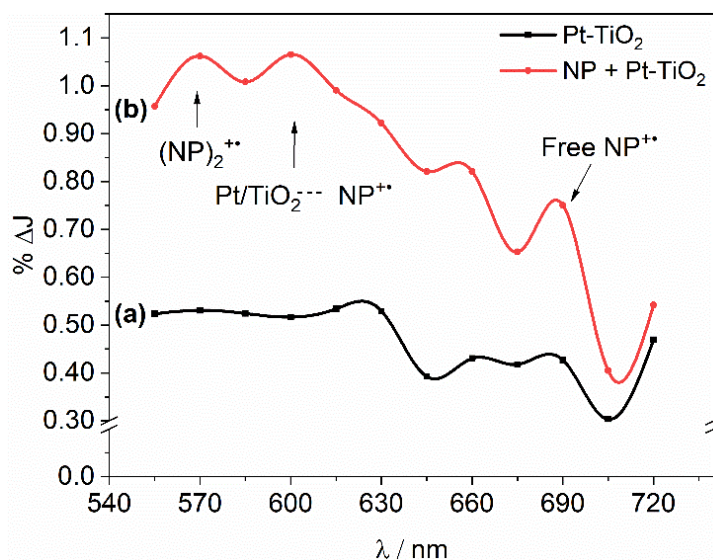


Figure 5-7. Diffuse reflectance transient absorption spectroscopy spectra obtained 300 ns after the laser excitation (355 nm, 6 mJ pulse⁻¹) of anaerobic Pt-TiO₂ slurries in the presence of (a) a (1:1) water/acetonitrile mixture and (b) naphthalene (NP) in the same solvent.

In the absence of naphthalene, excitation of Pt-TiO₂ leads to a relatively featureless transient spectrum, slightly increasing at short wavelengths. Since Pt acts as an electron sink, this signal can be readily attributed to trapped holes, with an absorption maximum reported at around 430 nm⁶⁸. On the contrary, in the presence of naphthalene, we could identify at least two distinct bands: a very broad one between 540 and 670 nm, and a narrow

band at 685 nm. Since in this case, where both a hole scavenger (naphthalene) and an electron scavenger (Pt nanoparticles) are present, these bands can be ascribed to transient species related to naphthalene. Indeed, an absorption band at 685 nm has been attributed to the naphthalene radical cation in homogeneous photolysis experiments^{48,69}. Moreover, due to its high reactivity, the radical cation can readily react with a second naphthalene molecule, giving rise to a naphthalene dimer radical cation which shows an absorption centered at 580 nm⁶⁹. In addition, we also note that electronic interactions between polyaromatic radical cations and the TiO₂ surface have been attributed to the occurrence of new absorption bands, red-shifted with respect to the free species⁷⁰. Taking this into consideration, we attribute the broad transient spectrum of Figure 5-7 to a convolution of the signals of the free naphthalene radical cation, the radical cation of its dimer, and the same ions interacting with the TiO₂ surface.

5.5.3.4 Origin of the Evolved Molecular Hydrogen

In order to identify the origin of the evolved H₂, we performed isotopic substitution studies on the photoreforming of naphthalene, using in-line monitoring of H₂, HD, and D₂ via quadrupole mass spectrometry (QMS), as shown in Figure S5-11.

The first evident effect of replacing H₂O by D₂O is a progressive decrease in the total amount of evolved gases as the D₂O fraction increases Figure 5-8.

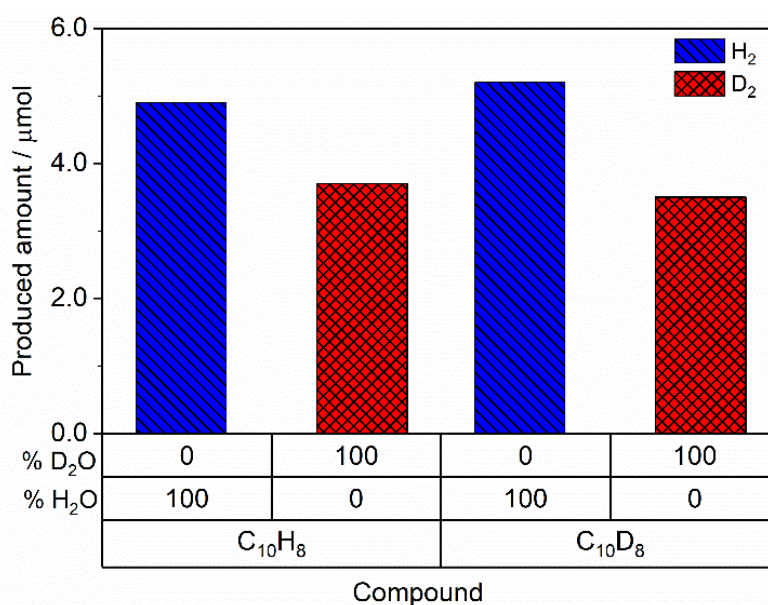


Figure 5-8. Isotopic distribution of the evolved gases (H₂, and D₂) from the photocatalytic reforming of aqueous naphthalene and deuterated naphthalene over Pt-UV100 employing D₂O and H₂O. Conditions: reaction volume, 15 mL; [Naphthalene] = 235 μmol L⁻¹; [catalyst] = 1 g L⁻¹; T = 25 °C; illumination with simulated solar light.

Considering the two extreme cases, pure H₂O and pure D₂O, the ratio between the amounts of evolved gases after 4h is ~1.3. Although we observed a smaller effect, similar behavior has been observed for the photocatalytic reforming of formaldehyde⁷¹ and benzene¹⁴ over platinumized TiO₂ and interpreted on the basis of a hindered production of ·OH radicals when using D₂O, which limited the rate of the reaction. In the present case, however, we rule out that these radicals play an important role in naphthalene's decomposition (Figure 5-6). In our interpretation, therefore, the observed kinetic isotope effect responds to a rate-determining step related to proton reduction^{72, 73}, although further experiments are necessary to ascertain this hypothesis.

With respect to the identity of the evolved gases, it is remarkable that neither H₂ nor HD are detected when using 100% D₂O. We note that similar results have been previously interpreted as proof that water (and not the SED) is the source of H₂ in the photocatalytic reforming of methanol²³. However, proton exchange reactions in aqueous media are extremely fast, and thus it is also possible that the hydrogen atoms originate from the sacrificial donor. Since the solvent's isotopic species are present in an overwhelming majority, the exchange reaction could mask the real origin of the atoms. On the other hand, recent reports have shown that in some photocatalytic systems the production of H₂ from SEDs can be sufficiently fast and spatially localized to avoid proton exchange, leading to isotopic compositions of the gases matching those of the sacrificial donor⁷⁴. From our analysis, we can conclude that such effects are not operative in the present system.

In the experiments performed with intermediate fractions of H₂O and D₂O (Figure S5-12), we observe, as expected from these arguments, a mixture of gases that approximately follows the isotopic composition of the solvent. The distributions, however, are skewed towards protium-rich gases (i.e. primarily H₂, and in second term HD), due to the above-mentioned preferential protium reduction. A clear illustration of this effect is given by the 50% H₂O – 50% D₂O composition, which yields H₂ and HD in almost a similar amount, but no D₂.

Additionally, we studied the effect of using fully deuterated naphthalene, Figure 5-8. In agreement with the previous experiments, the ratio between the amounts of evolved gases after 4h is 1.4. The photoreforming of deuterated naphthalene in H₂O leads to the exclusive formation of H₂. In D₂O, obviously, only D₂ is formed. Interestingly, the total amount of evolved gases in both solvents coincides, within experimental error, with the amounts

observed using non-deuterated naphthalene. This suggests that, in contrast with water, hydrogen abstraction from naphthalene is not involved in the rate-determining step of the reaction. Similar conclusions have been drawn for the photocatalytic reforming of aqueous benzene over platinized TiO₂¹⁴.

5.5.4 Mechanism of the Photocatalytic Reforming of Naphthalene

We now unify the acquired knowledge into a plausible mechanism for the photocatalytic reforming of naphthalene, summarized in Scheme 5-1. Considering that naphthalene only absorbs light of wavelengths shorter than 315 nm (Figure S5-4)⁹, the use of simulated sunlight leads to the exclusive excitation of TiO₂, with the concomitant generation of electron-hole pairs (Equation 5-6). From the EPR experiments and the associated photocatalytic runs in the presence of scavengers, we postulate that $\cdot\text{OH}_{\text{free}}$ radicals do not play an important role in the initial reaction of naphthalene. Naphthalene's degradation, thus, is initiated either by a direct hole transfer or indirectly via its reaction with surface trapped holes ($-\text{OH}_s$). This reaction can in principle follow two pathways: either a single electron transfer (SET) leading to the production of a radical cation (Equation 5-7), or a hydrogen abstraction reaction, leading to a naphthyl radical (Equation 5-8). If the latter were to occur, however, we would expect a strong effect from the presence of $\cdot\text{OH}_{\text{free}}$, since they would promptly react with the naphthyl radicals to yield naphthalenol (Equation 5-9). Instead, we propose the formation of the naphthalene radical cation (Equation 5-7), as we supported by the transient absorption spectroscopy experiments. This carbocation radical swiftly reacts with water to form an OH adduct (Equation 5-10)^{75, 76}, in coincidence with the reported reactions of benzene with both persulfate and Pt-TiO₂ in aqueous media^{77, 78}. The adduct itself reacts in either a further oxidation step (Equation 5-11), or a hydrogen abstraction by a hydrogen atom via a special type of "current doubling" (Equation 5-12) to form (as exemplified) naphthalen-1-ol (**A**), or naphthalene-2-ol (**B**). In this stage, we excluded the current doubling mechanism from either the naphthalene radical cation or the naphthalene radical for several reasons. The large difference between the oxidation potential of single electron transfer (1.85 V vs NHE) for naphthalene comparing with the conduction band (-0.5 V vs NHE)⁷⁹ of the TiO₂ does not allow the naphthyl radical cation to inject its unpaired electron in the conduction band of the TiO₂. Moreover, the ionization energy of the naphthalene radical cation is much larger than that for naphthalene (around 8.0 eV⁸⁰), which requires a much higher potential to transfer the unpaired electron⁸¹. This is in line with the observations of Hykaway et al.⁸² who reported that naphthalene did not

show any current doubling effect during its oxidation to a carbocation radical on the surface of the TiO₂ electrode.

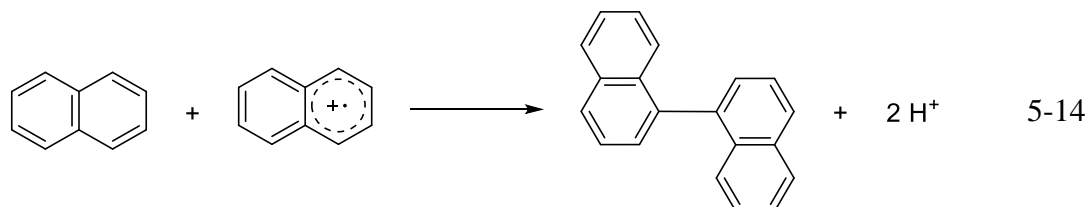
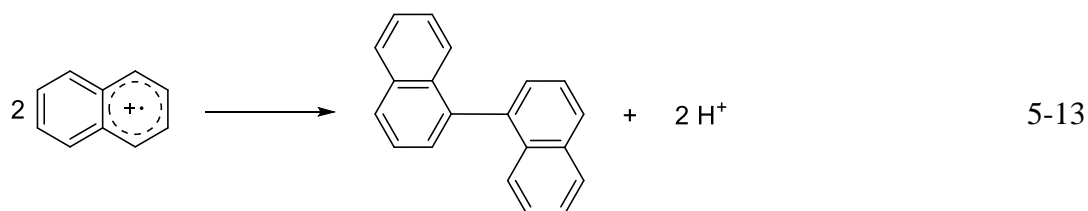
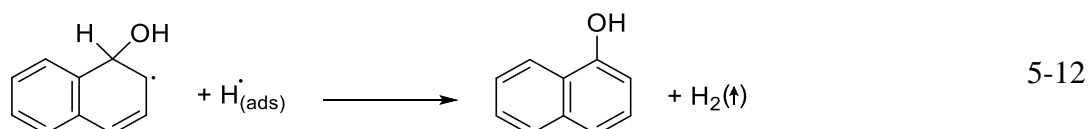
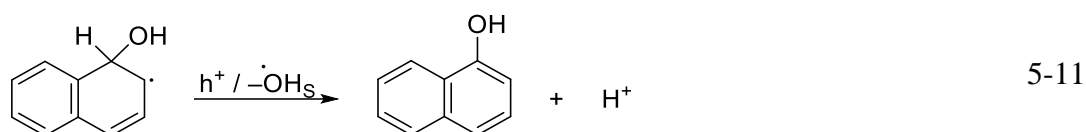
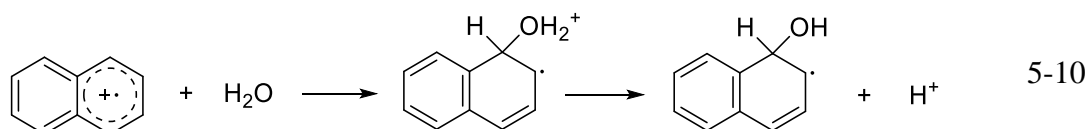
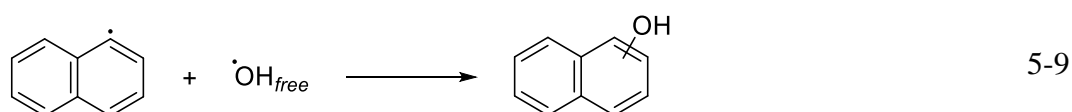
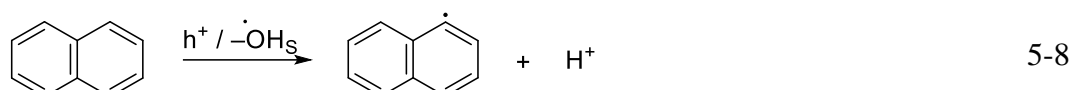
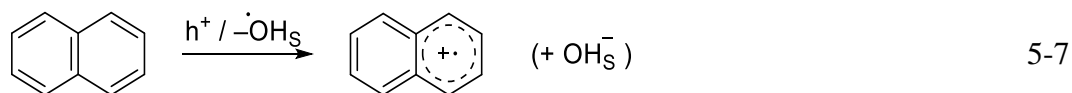
Moreover, by using isotopically labeled TiO₂ we conclude that the surface oxygen atoms are not incorporated in the naphthalenols, thus leaving water as the source of oxygen in the products. We note that this mechanism is conceptually equivalent to that proposed by Yoshida et al.¹⁴ for the photocatalytic reforming of benzene, although we consider here the TiO₂ surface only implicitly.

The only non-oxygenated intermediated we observed during the photooxidation of naphthalene over Pt-UV100 is 1,1'-binaphthalene (**H**). Its formation can be explained by the coupling of two naphthyl radical cations accompanied by proton release (Equation 5-13), or of one radical cation with the mother compound (Equation 5-14) The equivalent compound biphenyl has previously been observed in the anaerobic photocatalytic oxidation of benzene by Hashimoto et al.⁷⁷. Thus, the formation of this compound supports the SET mechanism.

The naphthalenols are susceptible to be further oxidized, by a similar mechanism, to different diols, of which we only observed naphthalene-1,4-diol (**C**) in significant amounts. In turn, the diols can be readily oxidized to form the respective naphthoquinones, such as the detected naphthalene-1,4-dione (**D**). A new hydroxylation step yields another of the detected intermediates, 5-hydroxynaphthalene-1,4-dione (**F**)¹². Alternatively, **D** can after successive oxidation steps, undergo a ring cleavage reaction to produce phthalic acid (**K**), which upon alkylation with alkyl radicals (**R**[•]) can produce the detected dialkylphthalates (**E**). The formation of the esters could be aided by the production of carboxylate radicals in the first step of the photo-Kolbe reaction⁸³, and their subsequent coupling with alkyl radicals (Equations 5-15 and 5-16)⁸⁴. In fact, Zhang et al.¹¹ found that phthalate esters are the main intermediates during the photooxidation of phenanthrene over TiO₂ suspensions. Moreover, this reaction has been reported in the literature during the degradation of different PAHs in homogeneous systems^{85, 86}. The ring-opening reactions and further oxidations eventually lead to short-chain carboxylic acids, of which we observed formic and acetic acids. Their decarboxylation via a photo-Kolbe reaction⁸⁷ can thus be the source of the alkyl radicals.

As noted above, we detected the 1,4-diol (**C**), but not the 1,2- isomer. The reactivity of such diols is however very high. In the case of the anaerobic degradation of benzene, it has been

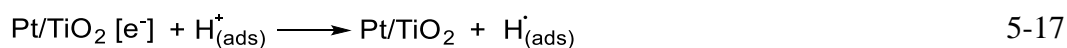
reported that the equivalent diol undergoes a rapid ring cleavage reaction to yield muconic acid, which upon successive oxidation yields CO_2 ⁷⁷. We thus interpret the absence of the 1,2-diol as proof of its high reactivity, instead of its lack of formation. A similar argument applies to naphthalene-1,2-dione (**J**).

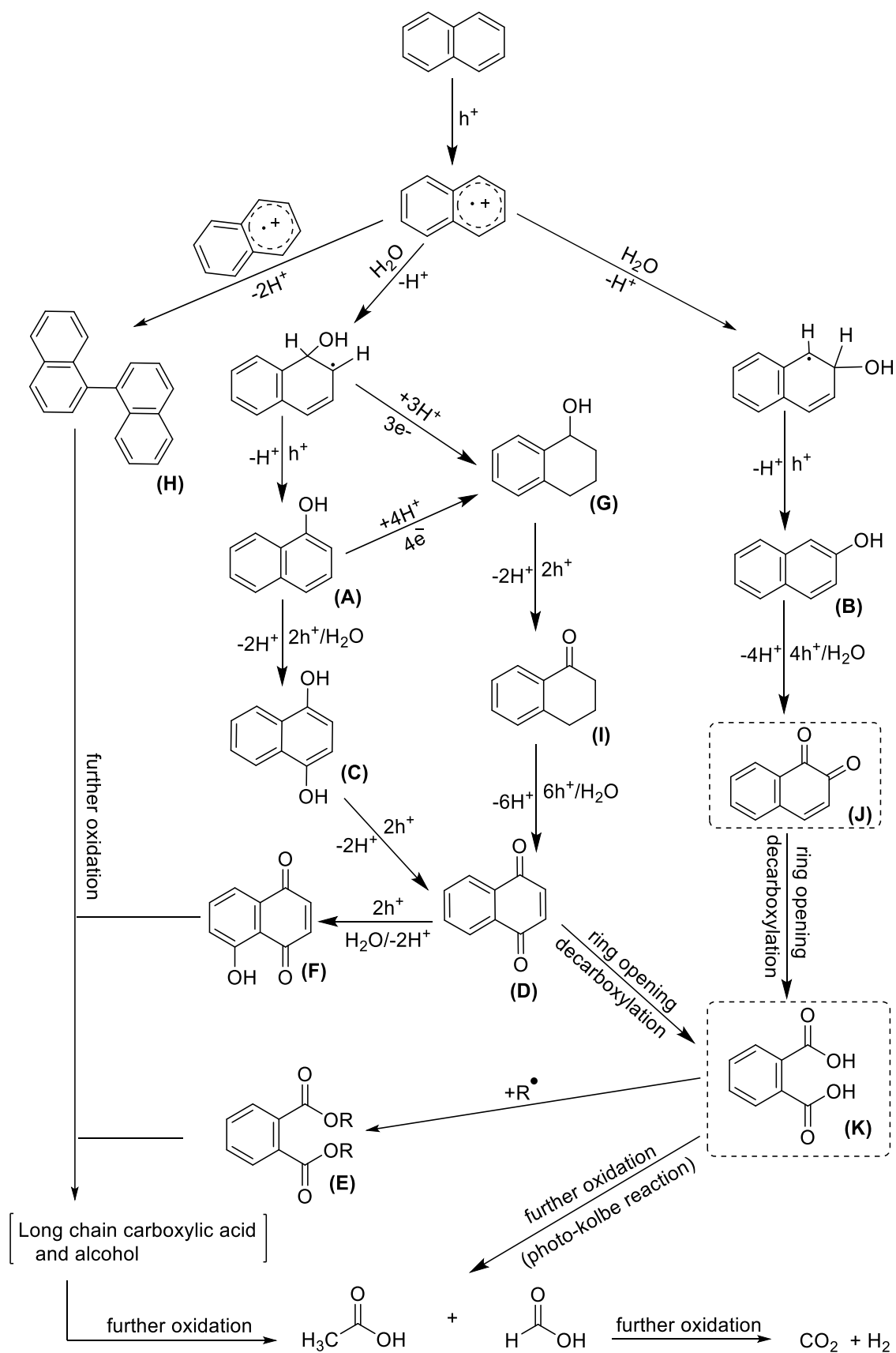


Looking at the reductive side, the photogenerated electrons have a strong tendency to accumulate in the platinum particles. Once there, they can reduce protons to hydrogen atoms (Equation 17), which, upon dimerization, form H_2 (Equation 18). Notably, although the successive oxidation of naphthalene may yield protons (e.g. Equations 10 and 11), the

fast exchange reaction with water (Equation 19) implies that the origin of the protons that eventually are reduced may be indistinguishable.

In the same way, as the organic intermediates can compete with naphthalene for holes, they can also compete for the photogenerated electrons. This explains the observation of partially reduced compounds, such as 1,2,3,4-tetrahydro-1-naphthalenol (**G**) and 1,2,3,4-tetrahydro-1-naphthalenone (**I**). Additionally, the reduction may not be direct, but rather related to the hydrogen atoms produced by Equation 12. For instance, Yoshida et al. have shown their direct involvement in the photoreforming of benzene ¹⁴.





Scheme 5-1 Proposed mechanism for the photocatalytic reforming of naphthalene over Pt-UV100 under simulated sunlight. Note: Compounds inside dashed square were not detected during the by-product's identification.

5.6 Conclusions

We have studied the photocatalytic degradation of naphthalene, the most abundant polycyclic aromatic hydrocarbon in water, coupled with the production of molecular hydrogen, a potential energy vector for a sunlight-based economy. Although the photocatalyst TiO₂ initiates the degradation of naphthalene in anaerobic conditions under simulated sunlight irradiation, the evolution of molecular hydrogen requires the presence of a platinum co-catalyst. By applying a combination of chromatographic and mass spectroscopic techniques, we have performed close monitoring of the stable reaction intermediates, finding that 1- and 2-naphthalenol, acetic acid, and formic acid are the ones present in largest concentrations in the solution, while H₂ and CO₂ are the only gaseous products. Many possible pathways for photoinduced reforming of naphthalene involving different reactive species on the surface of photoexcited Pt/TiO₂ have been tested. The use of Ti¹⁸O₂ did not lead to a significant evolution of ¹⁸O-enriched CO₂, suggesting that lattice oxygen atoms are not incorporated into this product. In addition, experiments using solvents with variable H₂O - D₂O compositions and deuterated naphthalene led to an isotopic composition of the evolved hydrogen matching those of the solvent, and not that of naphthalene. By analyzing the reaction rates, we further determined that water (but not naphthalene) appears to be involved in the rate-determining step of the reaction. Furthermore, by performing photocatalytic experiments in the presence of a hole and hydroxyl radical scavengers, we determined that only the former plays a significant role in the oxidation of naphthalene. Complementary spin trapping experiments using electron paramagnetic resonance spectroscopy confirm this notion. Moreover, transient absorption spectroscopy allowed us to detect the radical cations of naphthalene and its dimer as short-lived species in the nanosecond time scale, in addition to their interaction with the Pt/TiO₂ surface. On the basis of the results, the most probable reaction route is the formation of naphthalene radical cation via SET from naphthalene, scavenging the photogenerated hole in the Pt/TiO₂ surface. This carbocation radical swiftly reacts with water to form an OH adduct which furtherly oxidized by another hole to produce the hydroxylated naphthalene. Concomitantly, the photogenerated electrons reduced the proton originated mainly from water to molecular hydrogen.

5.7 Supporting Information

5.7.1 Material Characterization

5.7.1.1 BET Surface Area

Brunauer – Emmett – Teller (BET) specific surface areas were measured by a FlowSorb II 2300 instrument equipped with a Micromeritics AutoMate 23. All the studied samples (pristine and platinized TiO₂) were pre-degassed in a vacuum at 150 °C for 1 h. The specific surface area was measured in triplicates and determined by means of single-point standard BET surface area measurements.

The results are summarized in Table S5-1. Pristine UV100 possess a large specific surface area, close to 300 m² g⁻¹. While the deposition of platinum leads to a slight decrease, it is only of 2.8%, a figure consistent with its small loading on the TiO₂ surface.

Table S5-1. BET surface area measurement for pristine Hombikat TiO₂ (UV100) and 0.5 wt% Pt-UV100

Catalyst	UV100	0.5 wt% Pt-UV100
Average Specific surface area (n=3) m ² g ⁻¹	295.0	286.6
Standard deviation	1.2	1.6

5.7.1.2 X-Ray Diffraction (XRD)

X-ray diffraction (XRD) patterns were registered on a Bruker D8 Advance diffractometer (Bruker AXS GmbH) with a Bragg-Brentano geometry using Cu K α radiation ($\lambda=1.54060$ Å). The patterns were recorded in the 2 θ range between 10° and 80° in steps of 0.039°. The obtained diffraction data were compared with reference patterns for anatase TiO₂ in the ICDD database (black lines).

Figure S5-1 shows the obtained patterns for UV100 and Pt-UV100. They show similar features, with all reflections corresponding exclusively to the anatase phase of TiO₂. Furthermore, the broadness of such reflections indicates small average crystallite sizes, in agreement with the high observed specific surface areas. The deposition of Pt does not significantly change the XRD pattern.

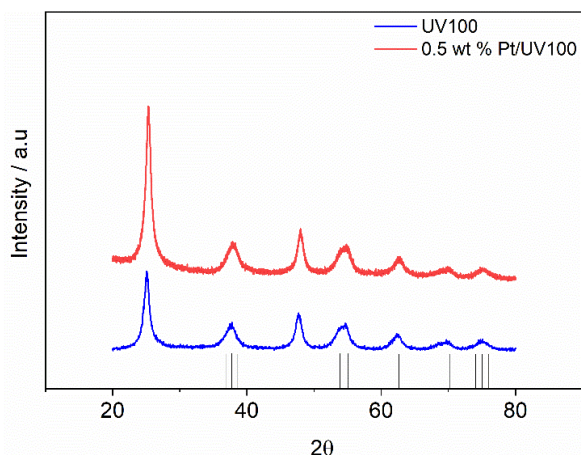


Figure S5-1. XRD patterns of pristine UV100 and 0.5 wt% Pt-UV100

5.7.1.3 Transmission Electron Microscopy (TEM)

Transmission Electron Microscopy (TEM) measurements were carried out on a JEOL JEM-2100F field-emission instrument, which was equipped with an EDX spectrometer of the type Oxford Instruments INCA-200 with an acceleration voltage of 200 kV from a field emission gun (FEG). The powdered specimen was dry-fixed (i.e. without using any solvent) on a holey carbon film supported by a Cu grid (Quantifoil, Multi A).

As shown in Figure S5-2, the nanoscaled TiO₂ material shows agglomerates in the μm range, and crystalline domains with diameters of about 5-10 nm, inconsistency with the XRD results. The Pt nanoparticles on the surface of UV100 show sizes of about 1-3 nm.

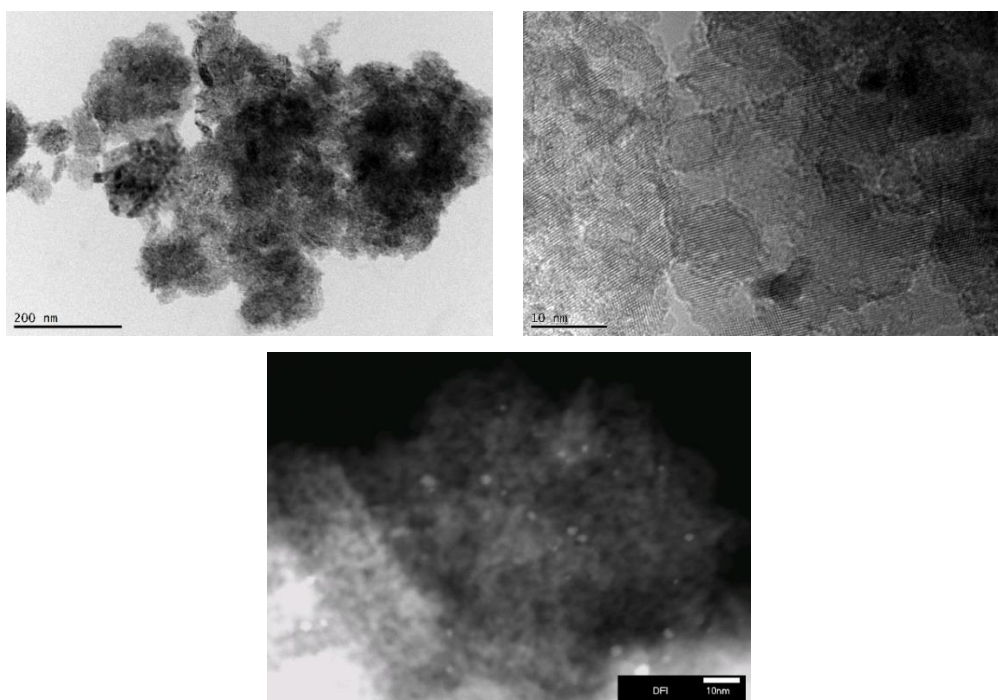


Figure S2. TEM images of 0.5 wt% Pt-UV100 nanoparticles at different magnifications.

5.7.1.4 Electron Paramagnetic Resonance (EPR) Technique

The electron paramagnetic resonance (EPR) technique was conducted in situ for pristine and platinumized TiO₂ in order to detect and monitor the formation of the paramagnetic sites formed upon irradiation. The experiments were carried out at 77 K using liquid nitrogen. The equipment is an X-band EPR MiniScope MS400 (Magnettech GmbH, Germany) spectrometer operating at 9.51 GHz field modulation and equipped with a UV spot-light (LC8, Hamamatsu, 200 W super-quiet mercury-xenon lamp). The acquisition parameters were as follows: center field: 335.4086 mT, sweep time 15 s, number of points: 4096, number of scans: 1, modulation amplitude: 0.2 mT, power: 10 mW, gain: 5. The photocatalysts were contained in a clean quartz tube and degassed for 1h using a gentle stream of N₂ gas prior the experiment. As shown in Figure S5-3, no EPR signal was detected in dark conditions for pristine UV100, while a small signal at $g = 2.004$ was detected for Pt-UV100 attributed to oxygen vacancies that formed during its synthesis^{88, 89}. While, after illumination for 15 min significant signals were detected for trapped electrons and holes⁹⁰⁻⁹³ in both catalysts. Remarkably, the signal intensity of trapped holes in Pt-UV100 was found to be higher than that for UV100. Double integration of the hole signals show that Pt-UV100 exhibits a ~20% higher amount of trapped holes compared to UV100. While, the signal intensity of trapped electrons (Ti³⁺) in UV100 was found to be two-fold higher than that for Pt/UV100. Platinum nanoparticles on the surface of UV100 act as electron sinks, decreasing the recombination process⁹³ and thus enhancing signals attributed to holes.

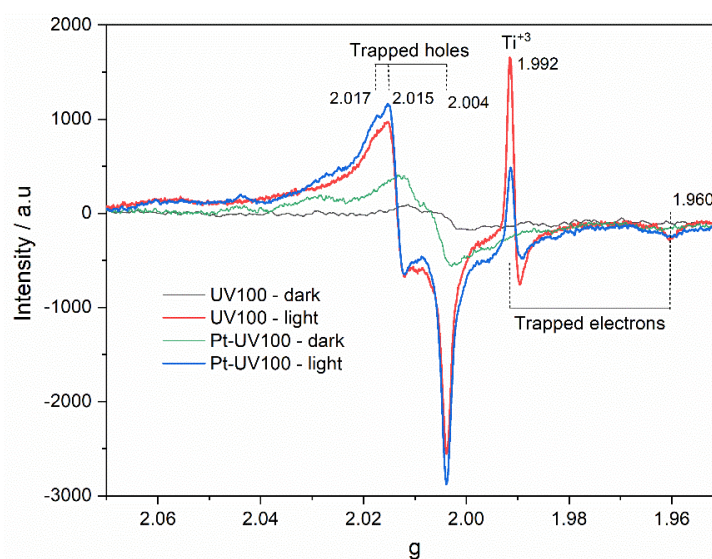
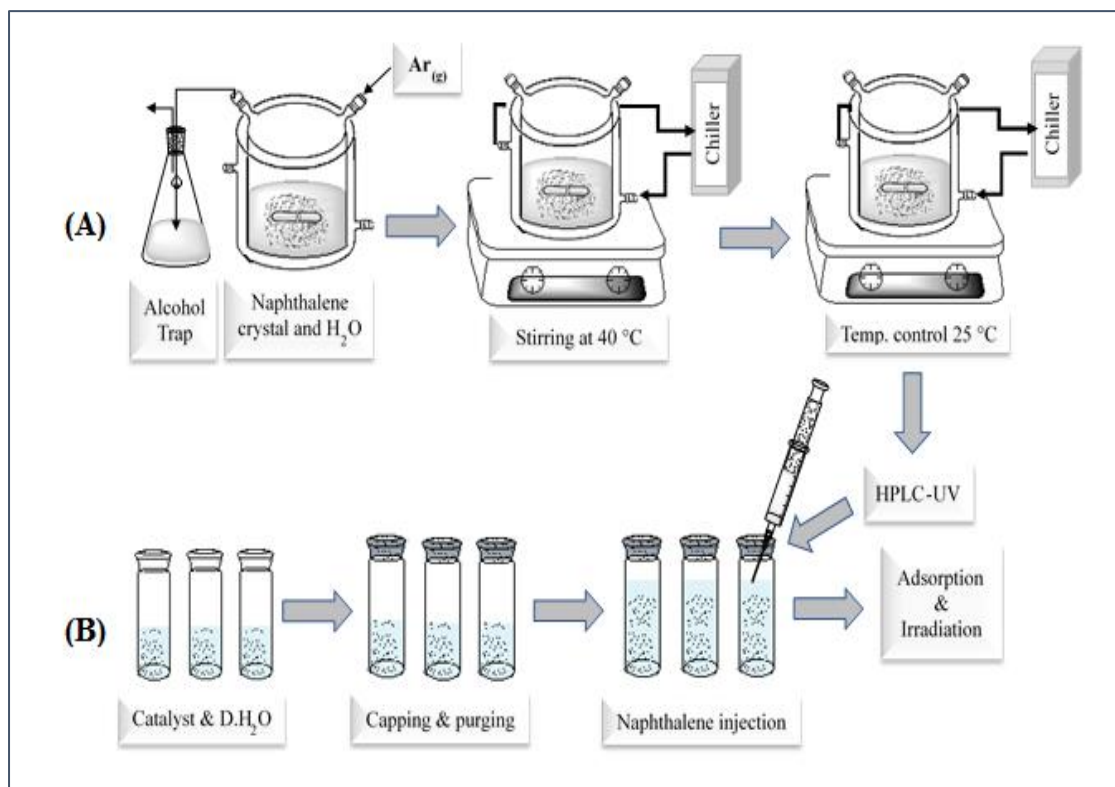


Figure S5-3. In situ EPR spectra for pristine and Pt/UV100 in the dark (black and green, respectively), and after 15 min illumination (red and blue, respectively).

5.7.2 Sample Preparation and Photocatalytic Experiments

5.7.2.1 Samples Preparation



Scheme S5-1. Stock solution preparation (A), and sample preparation for the photocatalytic H₂ evolution and naphthalene oxidation experiments (B).

5.7.2.2 Photonic Efficiency Determination

The determination of the photonic efficiencies ξ was carried out on the basis of Equation (S5-1), where $\Delta C/\Delta t$ is the degradation (naphthalene) or formation (hydrogen) rate in units of mol s⁻¹, A is the illuminated area (6.60×10^{-4} m²), and I_0 the photon flux density, equal to 3.31×10^{-4} mol m⁻² s⁻¹ in the wavelength range between 320 nm and 380 nm.

$$\xi = \frac{\text{degradation or formation initial rate (mol s}^{-1}\text{)}}{\text{photon flux (mol s}^{-1}\text{)}} = \frac{\Delta C}{\Delta t} \frac{1}{I_0 A} \quad \text{S5 - 1}$$

The photon flux density I_0 was determined from Equation (S5-2), where I is the light intensity (W m⁻²), λ is the corresponding wavelength (m), N_A is Avogadro's constant (6.022×10^{23} mol⁻¹), h is Planck's constant (6.636×10^{-34} W s²) and c is the speed of light (3.00×10^8 m s⁻¹).

$$I_0 = \frac{I \lambda}{N_A h c} \quad \text{S5 - 2}$$

5.7.2.3 Initial Photonic Efficiencies, ξ , for Naphthalene Degradation:

Time (min)	Naphthalene amount (μmol)
Initial conc. before ads.	2.26
0 (after ads.)	1.92
30	0.639

Δ amount of naphthalene after 30 min = $1.92 - 0.639 = 1.28 \mu\text{mol}$.

$$\% \xi = \frac{\text{degradation or formation initial rate (mol s}^{-1}\text{)}}{\text{photon flux (mol s}^{-1}\text{)}} * 100\%$$

$$= \left(\frac{1.28 \times 10^{-6} \text{ mol}}{1800 \text{ s}} \left(\frac{1}{3.31 \times 10^{-4} \text{ mol m}^{-2} \text{ s}^{-1} * 6.60 \times 10^{-4} \text{ m}^2} \right) \right) * 100\%$$

$$\% \xi = 0.33$$

5.7.2.4 Naphthalene Absorption and Solar Simulator Emission Spectra

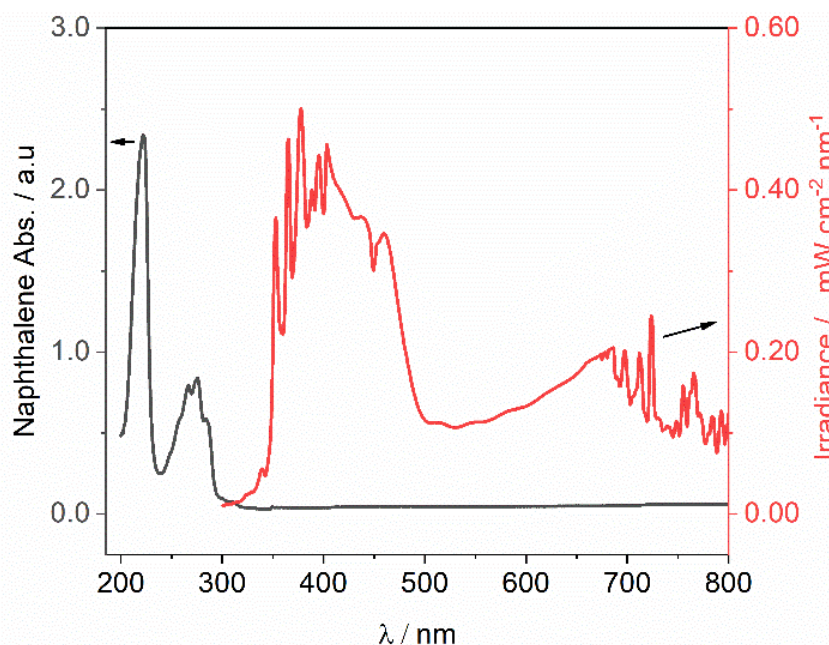


Figure S5-4. UV-vis absorption spectra for a $156 \mu\text{mol L}^{-1}$ naphthalene solution (black line) and solar irradiance spectral (red line).

5.7.2.5 Dark Adsorption

The adsorption experiments were carried out in a borosilicate air-tight reactor, while the temperature was kept constant at 25 ± 1 °C. In a typical experiment, 100 mg of the photocatalyst powder was suspended in 100 mL of naphthalene solution ($156 \mu\text{mol L}^{-1}$). Afterward, the suspension was mixed at low speed using a magnetic stirring, and the concentration of naphthalene was monitored at regular intervals using the HPLC. All samples were filtrated with syringe filters ($0.2 \mu\text{m}$) and immediately analyzed, to minimize the volatilization of naphthalene. However, we should note that the equilibrium amount of naphthalene in the gas phase did not consider in this experiment.

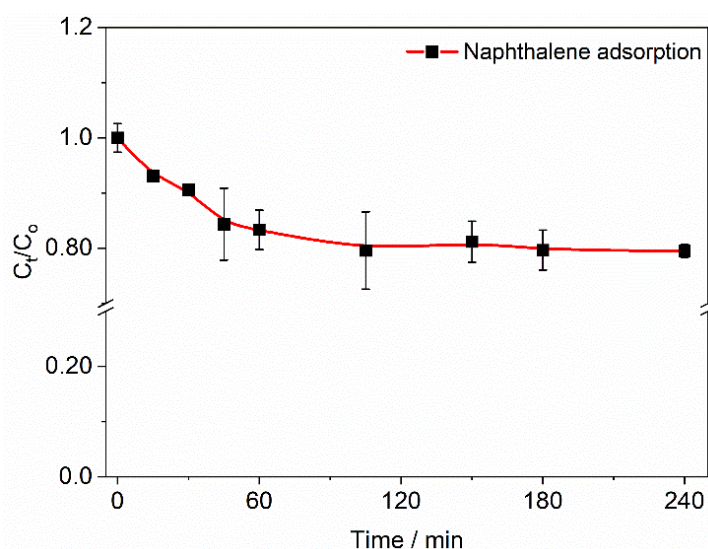


Figure S5-5. Adsorption kinetics of naphthalene on the surface of 0.5 w% Pt-UVI100. Conditions: double jacket reactor, reaction volume = 100 mL; $[\text{Naphthalene}] = 156 \mu\text{mol L}^{-1}$; $[\text{catalyst}] = 1 \text{ g L}^{-1}$; $T = 25$ °C. Lines are guides for the eye.

5.7.2.6 Photocatalyst Reusability

As detailed in the main text, the photocatalytic degradation of naphthalene in anaerobic conditions leads to the formation of colored intermediates. Figure S5-6 shows the color of a suspension after irradiation for 4 h, which has turned to a brown color due to the formation of such intermediates. Interestingly, by irradiating for 1 h under aerobic conditions these intermediates can be promptly removed, turning the suspension color back to white. The reused photocatalyst exhibits photocatalytic performance and stability over three cycles. Compared to the fresh photocatalyst, the naphthalene conversion efficiency and molecular hydrogen formation remained almost the same (~90%).

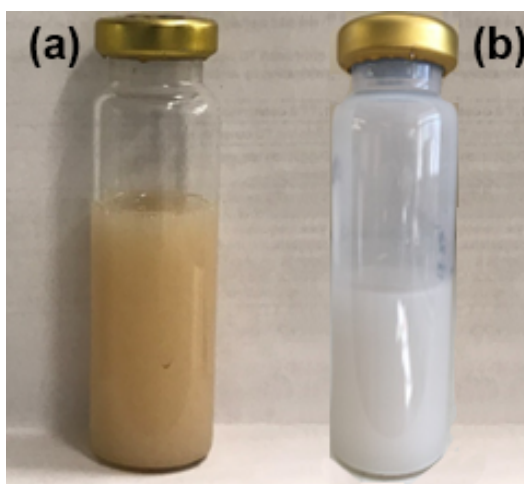


Figure S5-6: Photography of a reaction vial used for the photocatalytic degradation of naphthalene, (a) after irradiation for 4 h under anaerobic conditions (left), and (b) a picture of the same sample after the subsequent irradiation in aerobic conditions for 1 h (right).

5.7.3 Analytical Methods

Table S5-2. Conditions for the HPLC separations.

Naphthalene identification				By-products identification			
Time min	Methanol %	Water %	Flow rate mL min ⁻¹	Time min	Methanol %	Water %	Flow rate mL min ⁻¹
Initial	70	30	1.00	Initial	10	90	0.8
6.00	70	30	1.00	20	65	30	0.8
-	-	-	-	30	65	30	0.8
-	-	-	-	35	95	5	1.00
-	-	-	-	40	10	90	0.8

5.7.4 Photocatalytic CO₂ and H₂ Evolution During the Reforming of Naphthalene using Quadrupole Mass Spectroscopy.

The photocatalytic reforming of the naphthalene has been carried out using a quadrupole mass spectrometer (QMS) for gas analysis (Hiden HPR-20), to figure out the mineralization of naphthalene. Figure S5-7 shows the QMS signal for Photocatalytic CO₂ (blue) and H₂ (red) evolution. Both H₂ and CO₂ signals are immediately produced upon illumination. After a very short initial delay, CO₂ formation shows an increasing rate over time during the analyzed period. Contrarily, after a fast-initial growth, the H₂ signal shows a marked decrease in its formation rate, in accordance with the results of Figure 5-1 in the main article. The differing behaviors can be explained by considering that, while H₂ can be readily produced from naphthalene, the formation of CO₂ implies its mineralization, for which several oxidation steps are needed. Consequently, CO₂ formation will benefit from

the accumulation and successive oxidation of organic intermediates, and thus its formation rate is expected to be delayed with respect to that of H₂, causing a longer period in which its formation rate increases. Similar behavior has been reported for the reforming of short-chain alcohols over platinumized TiO₂ ⁹⁴.

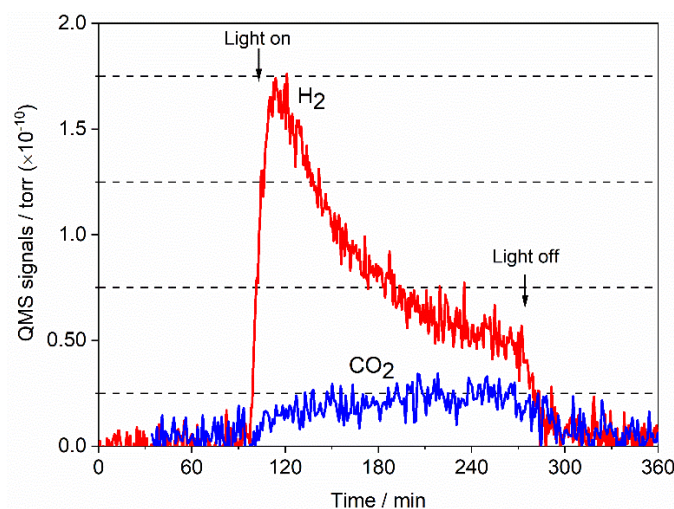


Figure S5-7: QMS signal for photocatalytic CO₂ (black) and H₂ (red) evolution from the reforming of naphthalene over Pt-UV100 employing an. Experimental conditions: double jacket reactor with quartz window, [Naphthalene] = 156 μmol L⁻¹, light intensity I₂₅₀₋₄₅₀ = 30 mWcm⁻², [catalyst] = 1 g L⁻¹, T = 25 °C, and irradiation with an Osram XBO 1000-Watt xenon arc lamp as a solar simulator.

5.7.5 Intermediates Identification

Table S5-3. Retention time and ions peaks for the detected compounds by GC-MS during the photocatalytic reforming of naphthalene over 0.5 wt% Pt-UV100.

#	Retention time / min	Name	Ion peaks
1	5.175	Naphthalene	64, 75, 101, 102, 128
2	7.642	1,2,3,4-tetrahydro-1-naphthalenone	105, 115, 129, 120, 130, 134
3	7.917	3,4-dihydronaphthalen-1(2H)-one	90, 118, 131, 146
4	8.442	Naphthalene-1,4-dione	76, 102, 104, 130, 158
5	8.900	Dimethylphthalate	76, 90, 104, 118, 132, 163
6	9.417	Naphthalene-1,4-diol	104, 131, 160
7	9.717	Naphthalen-1-ol	72, 89, 101, 115, 116, 144
8	9.875	Naphthalen-2-ol	72, 89, 101, 115, 144
9	10.692	Diethylphthalate	93, 104, 105, 121, 132, 149, 176, 177, 222
10	13.983	5-hydroxynaphthalene-1,4-dione	92, 118, 120, 146, 174
11	18.658	1,1'-binaphthalene	113, 126, 150, 226, 239, 250, 252, 253, 254

Table S5-4: Identified intermediates during the photocatalytic oxidation of naphthalene in the presence of molecular oxygen from previous studies. Compounds highlighted in bold are those also found in the present study (in the absence of oxygen).

Catalyst	Light source	Intermediate	Ref.
TiO ₂	UV	Naphthalen-1-ol, naphthalen-2-ol, x-hydroxynaphthalene-1,4-dione, naphthalene-1,4-dione , coumarin, 1,2-benzenedicarboxaldehyde, phthalic acid, 2,3-dihydro-2,3-epoxy-1,4-naphthalenedione, (<i>E</i>)-2-(3-oxoprop-1-en-1-yl)benzaldehyde, and (<i>Z</i>)-2-(3-oxoprop-1-en-1-yl)benzaldehyde.	12
WO ₃ -MWCNT	570 W Xe	Naphthalen-1-ol, naphthalene-1,4-dione, and phthalic acid.	95
TiO ₂	UV	Naphthalen-1-ol, naphthalen-2-ol, 5-hydroxynaphthalene-1,4-dione , Phthalide, Cinnamaldehyde, naphthalene-1,4-dione , 1,2-benzenedicarboxaldehyde, and 2-carboxycinnamaldehyde.	96
Q-TiO ₂	125 W Hg	Naphthalen-1-ol, naphthalen-2-ol , naphthalene-1,2-dione, naphthalene-1,4-dione , and 2-(3-oxoprop-1-en-1-yl)benzaldehyde	34
TiO ₂	UV	Naphthalen-1-ol , 1,2-benzenedicarboxaldehyde, 2 <i>H</i> -chromen-2-one, and 2-hydroxynaphthalene-1,4-dione.	97
GO-Ag ₃ PO ₄	300 W Xe	Naphthalen-1-ol, naphthalene-1,4-diol, naphthalene-1,4-dione, phthalic acid, and dialkyl ester.	98
p-Co ₃ O ₄ /n-Bi ₂ O ₂ CO ₃	500W Xe	Naphthalen-1-ol, naphthalene-1,4-dione , phthalic acid, 2-hydroxybenzaldehyde, hydroquinone, acetic acid , oxalic acid, 2,3-dihydroxybenzaldehyde, and methanol.	10

5.7.6 Mechanistic Study

5.7.6.1 EPR Spectra

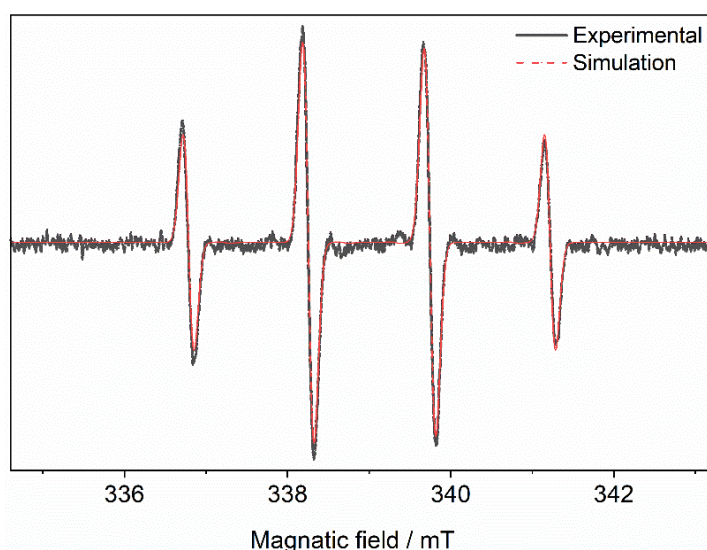


Figure S5-8: Experimental (black) and simulated (red) EPR spectra measured after 15 sec of continuous irradiation in the presence of the spin trapping agent DMPO. Catalyst mass concentration, 1 mg mL⁻¹; naphthalene concentration, 156 μmol L⁻¹; DMPO concentration, 20 mM. The simulation represents the EPR signal of the DMPO–OH adduct ($a_N = 1.453$ mT, $a_H = 1.494$ mT; $g = 2.0059$) in H₂O.

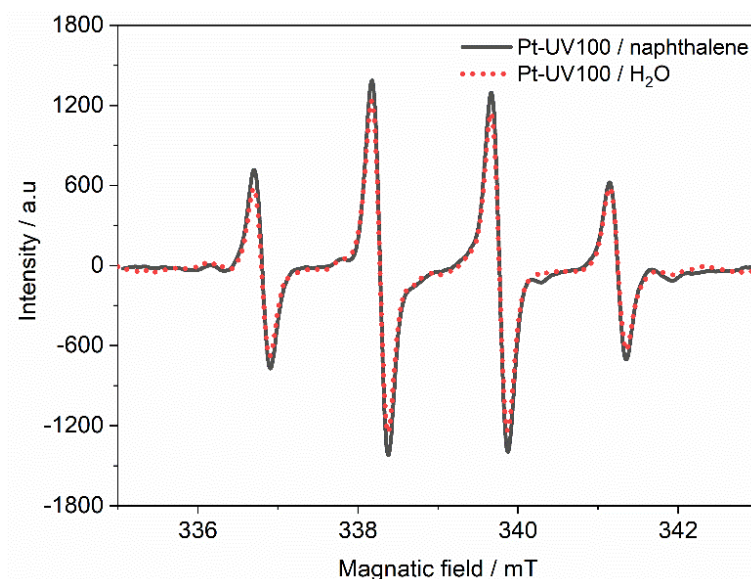


Figure S5-9: EPR spectra measured after 1 min of continuous irradiation in the presence of the spin trapping agent DMPO in the presence (solid line, black) and absence (dot line, red) of naphthalene. Catalyst mass concentration, 1 mg mL^{-1} ; naphthalene concentration, $156 \text{ }\mu\text{mol L}^{-1}$; DMPO concentration, $20 \text{ }\mu\text{mol L}^{-1}$,

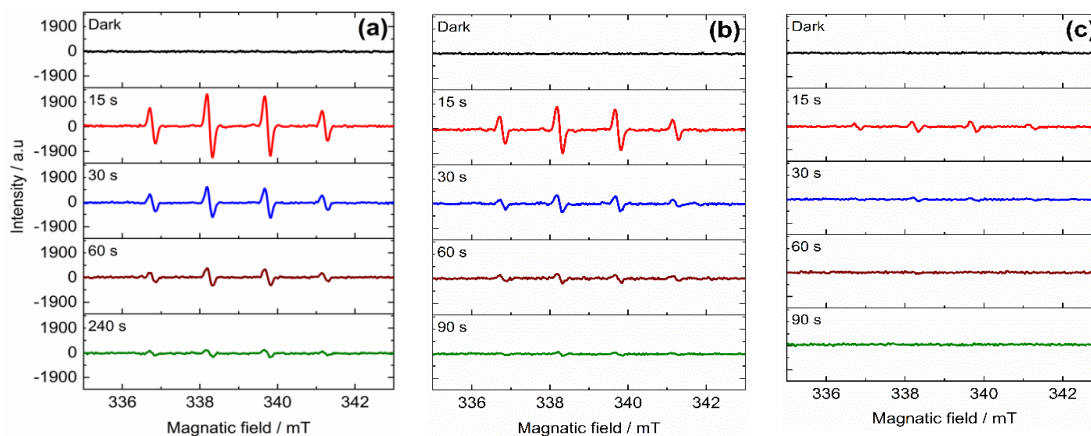


Figure S5-10: EPR spectra recorded during the photocatalytic reforming of naphthalene in the presence of (a) DMPO (b) DMPO and TBA, and (c) DMPO and KI. Photocatalyst mass concentration, 1 g/L ; $156 \text{ }\mu\text{mol L}^{-1}$ aqueous solution of naphthalene; irradiation using UV(A); microwave frequency: 9.51 GHz .

5.7.6.2 Isotopic Labeling Analyses

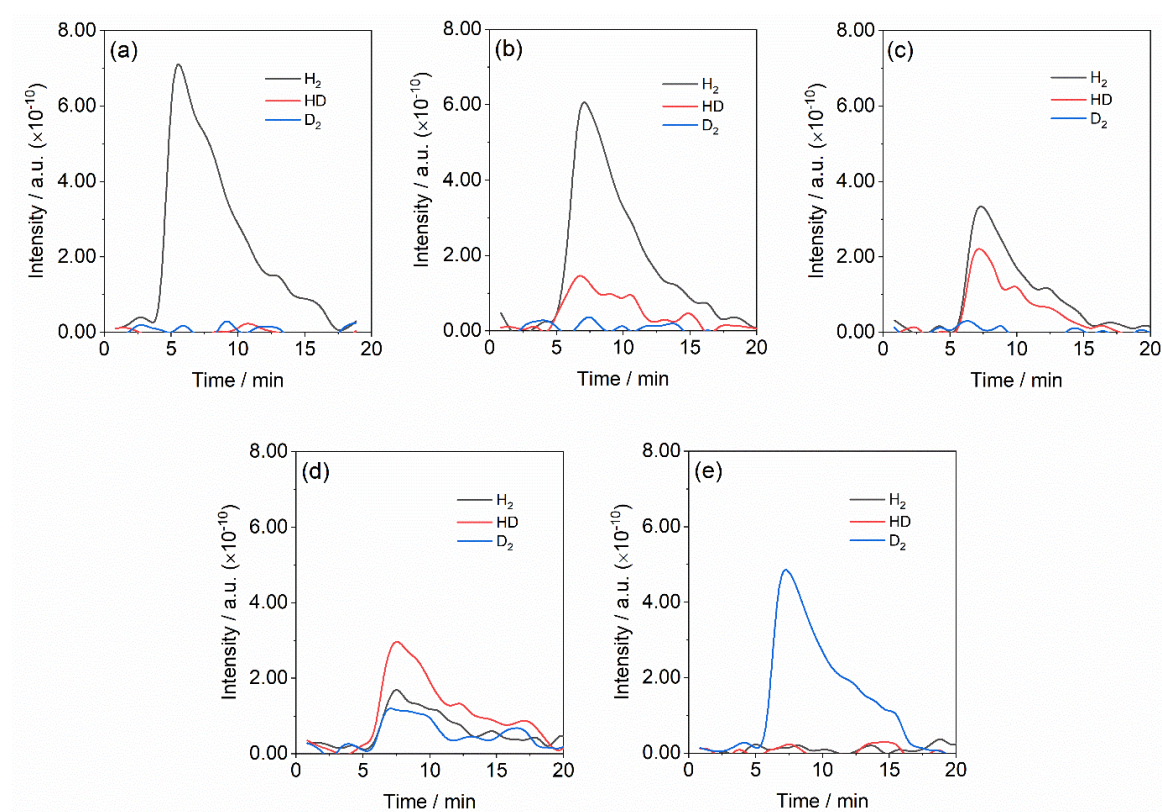


Figure S5-11. Quadrupole Mass Spectroscopy (QMS) signals for the photocatalytic H_2 , HD, and D_2 formation in different H_2O/D_2O mixtures over 0.5 wt% Pt-UV100 during the reforming of naphthalene. (a) 100% H_2O / 0% D_2O , (b) 75% H_2O / 25% D_2O , (c) 50% H_2O / 50% D_2O , (d) 25% H_2O / 75% D_2O , (e) 0% H_2O / 100% D_2O .

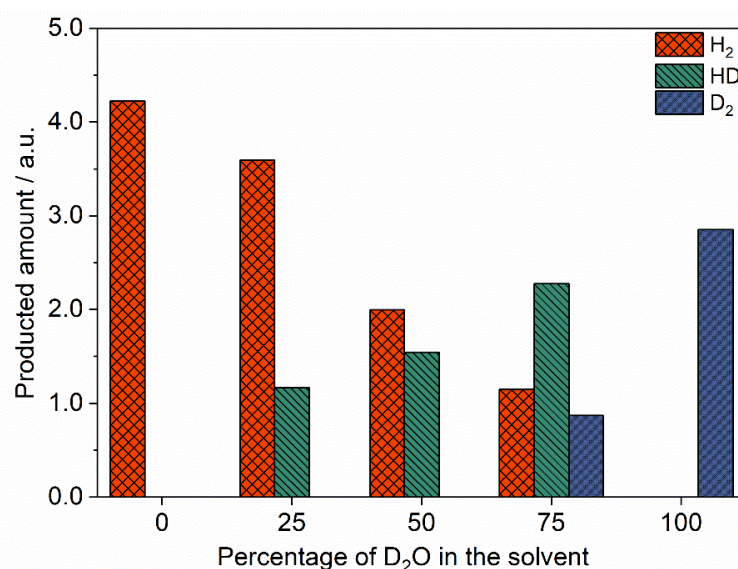


Figure S5-12: Isotopic distribution of the evolved gases (H_2 , HD, and D_2) from the photocatalytic reforming of aqueous naphthalene over Pt-UV100 a) employing different D_2O/H_2O compositions. Conditions: reaction volume, 15 mL; [Naphthalene] = 235 $\mu\text{mol L}^{-1}$; [catalyst] = 1 g L^{-1} ; $T = 25$ $^{\circ}\text{C}$; illumination with simulated solar light. Note: Since the setup was operated at the same sensitivity factor for all gases, the observed signals are directly comparable.

5.8 Acknowledgments

Financial support from the Katholischer Akademischer Ausländer-Dienst (KAAD) is gratefully acknowledged for providing a scholarship for Osama Al-Madanat to perform his Ph.D. Yamen Alsalka gratefully acknowledges the financial support from the Deutscher Akademischer Austauschdienst (DAAD) and the Federal Foreign Office. Mariano Curti is grateful to the DAAD together with the Ministerio de Educación, Cultura, Ciencia y Tecnología (Argentina) for his ALEARG scholarship. Osama Al-Madanat wishes to thank Dr. Samia Ben Hammouda for the helpful discussion while preparing the manuscript. The authors thank Mr. Carsten Günnemann for helping with the transient absorption spectroscopy analysis. This work was supported by Saint-Petersburg State University via a research grant ID 32706707. Financial support from the Global Research Laboratory Program (2014 K1 A1 A2041044), Korea Government (MSIP) through NFR is gratefully acknowledged.

5.9 Author Contributions

Conceptualization, Software, Validation, Writing – Original Draft: **Osama Al-Madanat**. Methodology: **Osama Al-Madanat, Yamen Alsalka**. Investigation: **Osama Al-Madanat**. Writing – Review & Editing: **Osama Al-Madanat, Mariano Curti, Yamen Alsalka, Ralf Dillert**. Supervision: **Ralf Dillert, Detlef W. Bahnemann**.

5.10 References

1. Møller, K. T.; Jensen, T. R.; Akiba, E.; Li, H.-w., Hydrogen - a Sustainable Energy Carrier. *Prog. Nat. Sci. Mater. Int.* **2017**, *27* (1), 34-40.
2. Kennedy, J.; Bahruji, H.; Bowker, M.; Davies, P. R.; Bouleghlimat, E.; Issarapanacheewin, S., Hydrogen Generation by Photocatalytic Reforming of Potential Biofuels: Polyols, Cyclic Alcohols, and Saccharides. *J. Photochem. Photobiol. A* **2018**, *356*, 451-456.
3. Fajrina, N.; Tahir, M., A Critical Review in Strategies to Improve Photocatalytic Water Splitting Towards Hydrogen Production. *Int. J. Hydrogen Energy* **2019**, *44* (2), 540-577.
4. Niaz, S.; Manzoor, T.; Pandith, A. H., Hydrogen Storage: Materials, Methods and Perspectives. *Renew. Sust. Energ. Rev.* **2015**, *50*, 457-469.
5. Lanterna, A. E.; Scaiano, J. C., Photoinduced Hydrogen Fuel Production and Water Decontamination Technologies. Orthogonal Strategies with a Parallel Future? *ACS Energy Lett.* **2017**, *2* (8), 1909-1910.

- Horiuchi, Y.; Fukuda, H.; Matsuoka, M.; Anpo, M., Integration of Artificial Photosynthesis (Photocatalysis) and Natural Photosynthesis for the Environmentally Harmonious Production of H₂ from H₂O Involving Biomass and Vegetables. In *Plant Factory Using Artificial Light*, Anpo, M.; Fukuda, H.; Wada, T., Eds. Elsevier: 2019; pp 383-393.
- Mastral, A. M.; Callén, M. S., A Review on Polycyclic Aromatic Hydrocarbon (PAH) Emissions from Energy Generation. *Environ. Sci. Technol.* **2000**, *34* (15), 3051-3057.
- Drwal, E.; Rak, A.; Gregoraszczyk, E. L., Review: Polycyclic Aromatic Hydrocarbons (PAHs)-Action on Placental Function and Health Risks in Future Life of Newborns. *Toxicology* **2019**, *411*, 133-142.
- Mondal, K.; Bhattacharyya, S.; Sharma, A., Photocatalytic Degradation of Naphthalene by Electrospun Mesoporous Carbon-Doped Anatase TiO₂ Nanofiber Mats. *Ind. Eng. Chem. Res* **2014**, *53* (49), 18900-18909.
- Guo, Y.; Dai, Y.; Zhao, W.; Li, H.; Xu, B.; Sun, C., Highly Efficient Photocatalytic Degradation of Naphthalene by Co₃O₄/Bi₂O₂CO₃ under Visible Light: A Novel P–N Heterojunction Nanocomposite with Nanocrystals/Lotus-Leaf-Like Nanosheets Structure. *Appl Catal B-Environ* **2018**, *237*, 273-287.
- Zhang, Y.; Wong, J. W.; Liu, P.; Yuan, M., Heterogeneous Photocatalytic Degradation of Phenanthrene in Surfactant Solution Containing TiO₂ Particles. *J. Hazard. Mater.* **2011**, *191* (1-3), 136-143.
- Theurich, J.; Bahnemann, D. W.; Vogel, R.; Ehamed, F. E.; Alhakimi, G.; Rajab, I., Photocatalytic Degradation of Naphthalene and Anthracene: GC-MS Analysis of the Degradation Pathway. *Res. Chem. Intermediat.* **1997**, *23* (3), 247-274.
- Rubio-Clemente, A.; Torres-Palma, R. A.; Penuela, G. A., Removal of Polycyclic Aromatic Hydrocarbons in Aqueous Environment by Chemical Treatments: A Review. *Sci. Total Environ.* **2014**, *478*, 201-25.
- Yuzawa, H.; Aoki, M.; Otake, K.; Hattori, T.; Itoh, H.; Yoshida, H., Reaction Mechanism of Aromatic Ring Hydroxylation by Water over Platinum-Loaded Titanium Oxide Photocatalyst. *J. Phys. Chem. C* **2012**, *116* (48), 25376-25387.
- Kim, J.; Choi, W., Hydrogen Producing Water Treatment through Solar Photocatalysis. *Energ. Environ. Sci.* **2010**, *3* (8), 1042-1045.
- Kim, J.; Monllor-Satoca, D.; Choi, W., Simultaneous Production of Hydrogen with the Degradation of Organic Pollutants Using TiO₂ Photocatalyst Modified with Dual Surface Components. *Energ Environ Sci* **2012**, *5* (6), 7647-7656.
- Schneider, J.; Bahnemann, D. W., Undesired Role of Sacrificial Reagents in Photocatalysis. *J. Phys. Chem. Lett.* **2013**, *4* (20), 3479-3483.
- Kamat, P. V.; Jin, S., Semiconductor Photocatalysis: “Tell Us the Complete Story!”. *ACS Energy Lett.* **2018**, *3* (3), 622-623.

19. Melvin, A. A.; Illath, K.; Das, T.; Raja, T.; Bhattacharyya, S.; Gopinath, C. S., M–Au/TiO₂ (M = Ag, Pd, and Pt) Nanophotocatalyst for Overall Solar Water Splitting: Role of Interfaces. *Nanoscale* **2015**, *7* (32), 13477-13488.
20. Montoya, J. F.; Ivanova, I.; Dillert, R.; Bahnemann, D. W.; Salvador, P.; Peral, J., Catalytic Role of Surface Oxygens in TiO₂ Photooxidation Reactions: Aqueous Benzene Photooxidation with Ti¹⁸O₂ under Anaerobic Conditions. *J. Phys. Chem. Lett.* **2013**, *4* (9), 1415-22.
21. Wauchope, R. D.; Getzen, F. W., Temperature Dependence of Solubilities in Water and Heats of Fusion of Solid Aromatic Hydrocarbons. *J. Chem. Eng. Data* **1972**, *17* (1), 38-41.
22. Stoll, S.; Schweiger, A., Easyspin, a Comprehensive Software Package for Spectral Simulation and Analysis in EPR. *J. Magn. Reson.* **2006**, *178* (1), 42-55.
23. Kandiel, T. A.; Ivanova, I.; Bahnemann, D. W., Long-Term Investigation of the Photocatalytic Hydrogen Production on Platinized TiO₂: An Isotopic Study. *Energy Environ. Sci.* **2014**, *7* (4), 1420.
24. Fasnacht, M. P.; Blough, N. V., Mechanisms of the Aqueous Photodegradation of Polycyclic Aromatic Hydrocarbons. *Environ. Sci. Technol.* **2003**, *37* (24), 5767-72.
25. Miller, J. S.; Olejnik, D., Photolysis of Polycyclic Aromatic Hydrocarbons in Water. *Water Research* **2001**, *35* (1), 233-243.
26. McConkey, B. J.; Hewitt, L. M.; Dixon, D. G.; Greenberg, B. M., Natural Sunlight Induced Photooxidation of Naphthalene in Aqueous Solution. *Water Air Soil Poll.* **2002**, *136* (1-4), 347-359.
27. Sioda, R. E.; Frankowska, B.; Lesiak, E. B., Electro-Oxidation of Certain Naphthalene Derivatives. *Monatsh. Chem.* **2008**, *139* (5), 513-519.
28. Vialaton, D.; Richard, C.; Baglio, D.; Paya-Perez, A. B., Mechanism of the Photochemical Transformation of Naphthalene in Water. *J. Photochem. Photobiol. A* **1999**, *123* (1-3), 15-19.
29. AlSalka, Y.; Hakki, A.; Schneider, J.; Bahnemann, D. W., Co-Catalyst-Free Photocatalytic Hydrogen Evolution on TiO₂: Synthesis of Optimized Photocatalyst through Statistical Material Science. *Appl. Catal. B-Environ* **2018**, *238*, 422-433.
30. Schneider, J.; Matsuoka, M.; Takeuchi, M.; Zhang, J.; Horiuchi, Y.; Anpo, M.; Bahnemann, D. W., Understanding TiO₂ Photocatalysis: Mechanisms and Materials. *Chem. Rev.* **2014**, *114* (19), 9919-86.
31. Bhatkhande, D. S.; Pangarkar, V. G.; Beenackers, A. A. C. M., Photocatalytic Degradation for Environmental Applications - a Review. *J. Chem. Technol. Biot.* **2002**, *77* (1), 102-116.

32. Mahmoodi, V.; Sargolzaei, J., Optimization of Photocatalytic Degradation of Naphthalene Using Nano-TiO₂/UV System: Statistical Analysis by a Response Surface Methodology. *Desalin. water treat.* **2014**, *52* (34-36), 6664-6672.
33. Nagao, M.; Suda, Y., Adsorption of Benzene, Toluene, and Chlorobenzene on Titanium-Dioxide. *Langmuir* **1989**, *5* (1), 42-47.
34. Hykrdová, L.; Jirkovský, J. r.; Mailhot, G.; Bolte, M., Fe(III) Photoinduced and Q-TiO₂ Photocatalysed Degradation of Naphthalene: Comparison of Kinetics and Proposal of Mechanism. *J. Photochem. Photobiol. A* **2002**, *151* (1), 181-193.
35. Weon, S.; Kim, J.; Choi, W., Dual-Components Modified TiO₂ with Pt and Fluoride as Deactivation-Resistant Photocatalyst for the Degradation of Volatile Organic Compound. *Appl Catal B-Environ* **2018**, *220*, 1-8.
36. Linsebigler, A. L.; Lu, G. Q.; Yates, J. T., Photocatalysis on TiO₂ Surfaces - Principles, Mechanisms, and Selected Results. *Chem. Rev.* **1995**, *95* (3), 735-758.
37. Khan, M. R.; Chuan, T. W.; Yousuf, A.; Chowdhury, M. N. K.; Cheng, C. K., Schottky Barrier and Surface Plasmonic Resonance Phenomena Towards the Photocatalytic Reaction: Study of Their Mechanisms to Enhance Photocatalytic Activity. *Catal. Sci. Technol.* **2015**, *5* (5), 2522-2531.
38. Wang, C.-y.; Pagel, R.; Bahnemann, D. W.; Dohrmann, J. K., Quantum Yield of Formaldehyde Formation in the Presence of Colloidal TiO₂-Based Photocatalysts: Effect of Intermittent Illumination, Platinization, and Deoxygenation. *J. Phys. Chem. B* **2004**, *108* (37), 14082-14092.
39. Joo, J. B.; Dillon, R.; Lee, I.; Yin, Y.; Bardeen, C. J.; Zaera, F., Promotion of Atomic Hydrogen Recombination as an Alternative to Electron Trapping for the Role of Metals in the Photocatalytic Production of H₂. *Proc. Natl. Acad. Sci. U S A* **2014**, *111* (22), 7942-7.
40. Sun, B.; Vorontsov, A. V.; Smirniotis, P. G., Role of Platinum Deposited on TiO₂ in Phenol Photocatalytic Oxidation. *Langmuir* **2003**, *19* (8), 3151-3156.
41. Loeb, S. K.; Alvarez, P. J. J.; Brame, J. A.; Cates, E. L.; Choi, W.; Crittenden, J.; Dionysiou, D. D.; Li, Q.; Li-Puma, G.; Quan, X.; Sedlak, D. L.; David Waite, T.; Westerhoff, P.; Kim, J. H., The Technology Horizon for Photocatalytic Water Treatment: Sunrise or Sunset? *Environ. Sci. Technol.* **2019**, *53* (6), 2937-2947.
42. Kandiel, T. A.; Dillert, R.; Robben, L.; Bahnemann, D. W., Photonic Efficiency and Mechanism of Photocatalytic Molecular Hydrogen Production over Platinized Titanium Dioxide from Aqueous Methanol Solutions. *Catal. Today* **2011**, *161* (1), 196-201.
43. Guo, Z.; Ma, R.; Li, G., Degradation of Phenol by Nanomaterial TiO₂ in Wastewater. *Chem. Eng. J.* **2006**, *119* (1), 55-59.

44. Mills, A.; O'Rourke, C.; Moore, K., Powder Semiconductor Photocatalysis in Aqueous Solution: An Overview of Kinetics-Based Reaction Mechanisms. *J. Photochem. Photobiol. A* **2015**, *310*, 66-105.
45. Dewar, M. J. S., A Molecular Orbital Theory of Organic Chemistry. VI.1 Aromatic Substitution and Addition. *J. Am. Chem. Soc.* **1952**, *74* (13), 3357-3363.
46. Reiß, S.; Krumm, H.; Niklewski, A.; Staemmler, V.; Wöll, C., The Adsorption of Acenes on Rutile TiO₂(110): A Multi-Technique Investigation. *J. Chem. Phys.* **2002**, *116* (17), 7704-7713.
47. Matsuura, A.; Nishinaga, T.; Komatsu, K., Structural Studies on the Radical Cations of Benzene, Naphthalene, Biphenylene, and Anthracene Fully Annelated with Bicyclo[2.2.2]octene Frameworks. *J. Am. Chem. Soc.* **2000**, *122* (41), 10007-10016.
48. Steenken, S.; Warren, C. J.; Gilbert, B. C., Generation of Radical-Cations from Naphthalene and Some Derivatives, Both by Photoionization and Reaction with SO⁴⁻: Formation and Reactions Studied by Laser Flash Photolysis. *J. Chem. Soc., Perkin Trans. 2* **1990**, (2), 335-342.
49. Melchers, S.; Schneider, J.; Bahnemann, D. W., Isotopic Studies on the Degradation of Acetaldehyde on Anatase Surfaces. *Catal. Today* **2020**, *340*, 318-322.
50. Montoya, J. F.; Bahnemann, D. W.; Peral, J.; Salvador, P., Catalytic Role of TiO₂ Terminal Oxygen Atoms in Liquid-Phase Photocatalytic Reactions: Oxidation of Aromatic Compounds in Anhydrous Acetonitrile. *Chem. phys. chem.* **2014**, *15* (11), 2311-20.
51. Pichat, P.; Courbon, H.; Enriquez, R.; Tan, T. T. Y.; Amal, R., Light-Induced Isotopic Exchange between O₂ and Semiconductor Oxides, a Characterization Method That Deserves Not to Be Overlooked. *Res. Chem. Intermed.* **2007**, *33* (3-5), 239-250.
52. Civiš, S.; Ferus, M.; Zukalová, M.; Kubát, P.; Kavan, L., Photochemistry and Gas-Phase FTIR Spectroscopy of Formic Acid Interaction with Anatase Ti¹⁸O₂ Nanoparticles. *J. Phys. Chem. C* **2012**, *116* (20), 11200-11205.
53. Pysh, E. S.; Yang, N. C., Polarographic Oxidation Potentials of Aromatic Compounds. *J. Am. Chem. Soc.* **1963**, *85* (14), 2124-&.
54. Rothenberger, G.; Fitzmaurice, D.; Graetzel, M., Spectroscopy of Conduction Band Electrons in Transparent Metal Oxide Semiconductor Films: Optical Determination of the Flatband Potential of Colloidal Titanium Dioxide Films. *J. Phys. Chem.* **1992**, *96* (14), 5983-5986.
55. Fox, M. A.; Chen, C. C.; Younathan, J. N. N., Oxidative Cleavage of Substituted Naphthalenes Induced by Irradiated Semiconductor Powders. *J Org Chem* **1984**, *49* (11), 1969-1974.
56. Montoya, J. F.; Atitar, M. F.; Bahnemann, D. W.; Peral, J.; Salvador, P., Comprehensive Kinetic and Mechanistic Analysis of TiO₂ Photocatalytic Reactions

- According to the Direct–Indirect Model: (II) Experimental Validation. *J. Phys. Chem. C* **2014**, *118* (26), 14276-14290.
57. Monllor-Satoca, D.; Gómez, R.; González-Hidalgo, M.; Salvador, P., The “Direct–Indirect” Model: An Alternative Kinetic Approach in Heterogeneous Photocatalysis Based on the Degree of Interaction of Dissolved Pollutant Species with the Semiconductor Surface. *Catal. Today* **2007**, *129* (1-2), 247-255.
 58. Raza, W.; Bahnemann, D.; Muneer, M., A Green Approach for Degradation of Organic Pollutants Using Rare Earth Metal Doped Bismuth Oxide. *Catal. Today* **2018**, *300*, 89-98.
 59. Chen, Y.; Wang, Y. N.; Li, W. Z.; Yang, Q.; Hou, Q. D.; Wei, L. H.; Liu, L.; Huang, F.; Ju, M. T., Enhancement of Photocatalytic Performance with the Use of Noble-Metal-Decorated TiO₂ Nanocrystals as Highly Active Catalysts for Aerobic Oxidation under Visible-Light Irradiation. *Appl Catal B-Environ* **2017**, *210*, 352-367.
 60. Beltran, F. J.; Ovejero, G.; Garciaaraya, J. F.; Rivas, J., Oxidation of Polynuclear Aromatic-Hydrocarbons in Water .2. UV-Radiation and Ozonation in the Presence of UV-Radiation. *Ind. Eng. Chem. Res* **1995**, *34* (5), 1607-1615.
 61. Salvador, P., On the Nature of Photogenerated Radical Species Active in the Oxidative Degradation of Dissolved Pollutants with TiO₂ Aqueous Suspensions: A Revision in the Light of the Electronic Structure of Adsorbed Water. *J. Phys. Chem. C* **2007**, *111* (45), 17038-17043.
 62. Nosaka, Y.; Nosaka, A., Understanding Hydroxyl Radical (•OH) Generation Processes in Photocatalysis. *ACS Energy Lett.* **2016**, *1* (2), 356-359.
 63. Belhadj, H.; Melchers, S.; Robertson, P. K. J.; Bahnemann, D. W., Pathways of the Photocatalytic Reaction of Acetate in H₂O and D₂O: A Combined EPR and ATR-FTIR Study. *J. Catal.* **2016**, *344*, 831-840.
 64. Dvoranova, D.; Barbierikova, Z.; Brezova, V., Radical Intermediates in Photoinduced Reactions on TiO₂ (an EPR Spin Trapping Study). *Molecules* **2014**, *19* (11), 17279-304.
 65. Shibata, H.; Ogura, Y.; Sawa, Y.; Kono, Y., Hydroxyl Radical Generation Depending on O₂ or H₂O by a Photocatalyzed Reaction in an Aqueous Suspension of Titanium Dioxide. *Biosci Biotechnol Biochem* **1998**, *62* (12), 2306-11.
 66. Li, L.; Goel, R. K., Role of Hydroxyl Radical During Electrolytic Degradation of Contaminants. *J. Hazard. Mater.* **2010**, *181* (1-3), 521-5.
 67. Luo, S.; Wei, Z.; Spinney, R.; Villamena, F. A.; Dionysiou, D. D.; Chen, D.; Tang, C. J.; Chai, L.; Xiao, R., Quantitative Structure-Activity Relationships for Reactivities of Sulfate and Hydroxyl Radicals with Aromatic Contaminants through Single-Electron Transfer Pathway. *J. Hazard. Mater.* **2018**, *344*, 1165-1173.

68. Bahnemann, D. W.; Hilgendorff, M.; Memming, R., Charge Carrier Dynamics at TiO₂ Particles: Reactivity of Free and Trapped Holes. *J. Phys. Chem. B* **1997**, *101* (21), 4265-4275.
69. Gschwind, R.; Haselbach, E., Laserflash-Photolysis of The p-Chloranil/Naphthalene System: Characterization of the Naphthalene Radical Cation in a Fluid Medium. *Helvetica Chimica Acta* **1979**, *62* (4), 941-955.
70. Tachikawa, T.; Tojo, S.; Fujitsuka, M.; Majima, T., Photocatalytic One-Electron Oxidation of Biphenyl Derivatives Strongly Coupled with the TiO₂ Surface. *Langmuir* **2004**, *20* (7), 2753-9.
71. Belhadj, H.; Hamid, S.; Robertson, P. K. J.; Bahnemann, D. W., Mechanisms of Simultaneous Hydrogen Production and Formaldehyde Oxidation in H₂O and D₂O over Platinized TiO₂. *Acs Catal* **2017**, *7* (7), 4753-4758.
72. Post, B.; Hiskey, C. F., Electrokinetics of Hydrogen Evolution.^{1,2} II. Deuterium Overvoltage on Mercury. *J. Am. Chem. Soc.* **1951**, *73* (1), 161-164.
73. Yates, J. T.; McKee, D. W., Kinetic Isotope Effect in the Heterogeneous Reaction of Graphite with H₂O (D₂O). *J. Chem. Phys.* **1981**, *75* (6), 2711-2714.
74. Zhao, G.; Busser, G. W.; Froese, C.; Hu, B.; Bonke, S. A.; Schnegg, A.; Ai, Y.; Wei, D.; Wang, X.; Peng, B.; Muhler, M., Anaerobic Alcohol Conversion to Carbonyl Compounds over Nanoscaled Rh-Doped SrTiO₃ under Visible Light. *J. Phys. Chem. Lett.* **2019**, *10* (9), 2075-2080.
75. Neta, P.; Madhavan, V.; Zemel, H.; Fessenden, R. W., Rate Constants and Mechanism of Reaction of Sulfate Radical Anion with Aromatic Compounds. *J. Am. Chem. Soc.* **1977**, *99* (1), 163-164.
76. Jenks, W., Photocatalytic Reaction Pathways - Effects of Molecular Structure, Catalyst, and Wavelength. In *Photocatalysis and Water Purification: From Fundamentals to Recent Applications*, Pichat, P., Ed. Wiley-VCH Verlag GmbH & Co.: 2013; pp 25-51.
77. Hashimoto, K.; Kawai, T.; Sakata, T., Photocatalytic Reactions of Hydrocarbons and Fossil Fuels with Water. Hydrogen Production and Oxidation. *J. Phys. Chem.* **1984**, *88* (18), 4083.
78. Eberhardt, M. K., Reaction of Benzene Radical Cation with Water. Evidence for the Reversibility of Hydroxyl Radical Addition to Benzene. *J. Am. Chem. Soc.* **1981**, *103* (13), 3876-3878.
79. Arimi, A.; Gunnemann, C.; Curti, M.; Bahnemann, D. W., Regarding the Nature of Charge Carriers Formed by UV or Visible Light Excitation of Carbon-Modified Titanium Dioxide. *Catalysts* **2019**, *9* (8).
80. Xu, B.; Stein, T.; Ablikim, U.; Jiang, L.; Hendrix, J.; Head-Gordon, M.; Ahmed, M., Probing Solvation and Reactivity in Ionized Polycyclic Aromatic Hydrocarbon-Water

- Clusters with Photoionization Mass Spectrometry and Electronic Structure Calculations. *Faraday Discuss* **2019**, 217 (0), 414-433.
81. Sioda, R. E.; Frankowska, B., Reactivity of Electrochemically Generated Radical Cations of Alkyl-naphthalenes Interpreted by AM1 Calculations. *Tetrahedron Lett* **2005**, 46 (16), 2747-2749.
82. Hykaway, N.; Sears, W. M.; Morisaki, H.; Morrison, S. R., Current-Doubling Reactions on Titanium Dioxide Photoanodes. *J. Phys. Chem.* **1986**, 90 (25), 6663-6667.
83. Kraeutler, B.; Jaeger, C. D.; Bard, A. J., Direct Observation of Radical Intermediates in the Photo-Kolbe Reaction - Heterogeneous Photocatalytic Radical Formation by Electron Spin Resonance. *J. Am. Chem. Soc.* **1978**, 100 (15), 4903-4905.
84. Svadkovskaya, G. E.; Voitkevich, S. A., Electrolytic Condensation of Carboxylic Acids. *Russ Chem Rev* **1960**, 29 (3), 161-180.
85. Zeng, Y.; Hong, P. K. A.; Wavrek, D. A., Integrated Chemical-Biological Treatment of Benzo[a]Pyrene. *Environ. Sci. Technol.* **2000**, 34 (5), 854-862.
86. Zhao, S.; Jia, H.; Nulaji, G.; Gao, H.; Wang, F.; Wang, C., Photolysis of Polycyclic Aromatic Hydrocarbons (PAHs) on Fe³⁺-Montmorillonite Surface under Visible Light: Degradation Kinetics, Mechanism, and Toxicity Assessments. *Chemosphere* **2017**, 184, 1346-1354.
87. Kraeutler, B.; Bard, A. J., Photoelectrosynthesis of Ethane from Acetate Ion at an N-Type Titanium Dioxide Electrode. The Photo-Kolbe Reaction. *J. Am. Chem. Soc.* **1977**, 99 (23), 7729-7731.
88. Livraghi, S.; Chiesa, M.; Paganini, M. C.; Giamello, E., On the nature of reduced states in titanium dioxide as monitored by electron paramagnetic resonance. I: The anatase case. *J Phys Chem C* **2011**, 115 (51), 25413-25421.
89. Serwicka, E.; Schlierkamp, M. W.; Schindler, R. N., Localization of conduction band electrons in polycrystalline TiO₂ studied by ESR. In *Z. Naturforsch. A*, 1981; Vol. 36, p 226.
90. Howe, R. F.; Gratzel, M., EPR study of hydrated anatase under UV irradiation. *J. Phys. Chem* **1987**, 91 (14), 3906-3909.
91. Hurum, D. C.; Agrios, A. G.; Gray, K. A.; Rajh, T.; Thurnauer, M. C., Explaining the enhanced photocatalytic activity of degussa P25 mixed-phase TiO₂ using EPR. *J. Phys. Chem. B* **2003**, 107 (19), 4545-4549.
92. Nakaoka, Y.; Nosaka, Y., ESR investigation into the effects of heat treatment and crystal structure on radicals produced over irradiated TiO₂ powder. *J. Photochem. Photobiol., A* **1997**, 110 (3), 299-305.

93. Nie, J.; Schneider, J.; Sieland, F.; Zhou, L.; Xia, S.; Bahnemann, D. W., New insights into the surface plasmon resonance (SPR) driven photocatalytic H₂ production of Au–TiO₂. *RSC Adv* **2018**, 8 (46), 25881-25887.
94. Patsoura, A.; Kondarides, D.; Verykios, X., Photocatalytic degradation of organic pollutants with simultaneous production of hydrogen. *Catal. Today* **2007**, 124, 94-102.
95. Farhadian, M.; Sangpour, P.; Hosseinzadeh, G., Preparation and photocatalytic activity of WO₃–MWCNT nanocomposite for degradation of naphthalene under visible light irradiation. *RSC Adv* **2016**, 6 (45), 39063-39073.
96. Lair, A.; Ferronato, C.; Chovelon, J.-M.; Herrmann, J.-M., Naphthalene degradation in water by heterogeneous photocatalysis: An investigation of the influence of inorganic anions. *J. Photochem. Photobiol., A* **2008**, 193 (2-3), 193-203.
97. Woo, O. T.; Chung, W. K.; Wong, K. H.; Chow, A. T.; Wong, P. K., Photocatalytic oxidation of polycyclic aromatic hydrocarbons: intermediates identification and toxicity testing. *J. Hazard. Mater.* **2009**, 168 (2-3), 1192-9.
98. Yang, X.; Cai, H.; Bao, M.; Yu, J.; Lu, J.; Li, Y., Insight into the highly efficient degradation of PAHs in water over graphene oxide/Ag₃PO₄ composites under visible light irradiation. *Chem. Eng. J.* **2018**, 334, 355-376.

Chapter Six: Summarizing Discussion and Conclusions

6.1 Foreword

In this thesis, the photocatalytic degradation of a polycyclic aromatic hydrocarbon (PAH) in water, coupled with the production of molecular hydrogen as a potential energy vector for a sunlight-based economy, was studied employing TiO₂-based photocatalysts under solar irradiation. Although the photocatalytic degradation of PAHs in water and air has been frequently investigated in aerobic conditions, the photocatalytic reforming of these compounds yielding molecular hydrogen was investigated for the first time. Naphthalene as the simplest PAH compound and frequently detected pollutant in the aquatic environment had been chosen as a model compound to perform all the photocatalytic experiments.

This Chapter will begin with discussing the H₂ formation and photooxidation of naphthalene during its photocatalytic reforming over two different commercial TiO₂ photocatalysts, namely, Evonik Aeroxide P25 and Sachtleben Hombikat UV100, loaded with Pt nanoparticles, irradiated by a solar simulator. Hereby, the impact of several factors such as the type of TiO₂, the platinization method, and intermediates formation on the efficiency of the charge carrier transfer, H₂ formation, and naphthalene photooxidation will be the bases of the discussion. Finally, the most proper proposed mechanism of the photoreforming of naphthalene will be elucidated in a systematic and thorough discussion based on the results of different chromatographic and spectroscopic techniques.

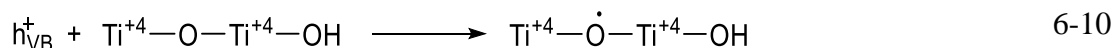
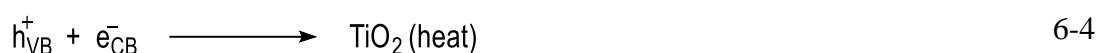
6.2 Photocatalytic Reforming of Naphthalene

The investigation described in Chapter 3 addresses the photoreforming of naphthalene in the absence and presence of different commercial types of bare and platinized TiO₂ photocatalysts. As mentioned previously in that chapter, different types of TiO₂ exhibit different photocatalytic activities. Thus, the catalysts not only have to be used and optimized for their activity but they must also be investigated for which reactions or substrates they are most suitable. This step, indeed, is the basic building block for understanding the photocatalytic process of naphthalene under inert conditions. To this end, the most reported active commercial types of TiO₂, namely, Evonik Aeroxide P25 (84% anatase: 16% rutile, specific surface area of 52 m² g⁻¹) and Sachtleben Hombikat UV100 (100% anatase, specific surface area of 300 m² g⁻¹), were employed for evaluating the H₂

production during photooxidation of an aqueous solution of naphthalene under the same experimental conditions. Both pristine photocatalysts were loaded with different fractional ratios of platinum nanoparticles (PtNPs) via the photodeposition method.

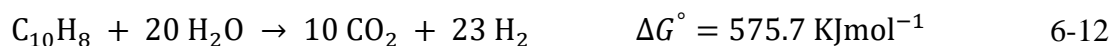
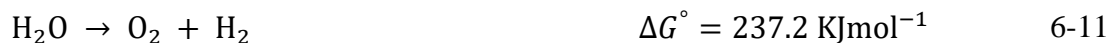
6.2.1 H₂ Evolution

It is generally accepted that bandgap excitation of TiO₂ results in the photogeneration of charge carriers (Equation 6-1). Both species, the electron and hole, rapidly migrate and are trapped to the surface (Equations 6-2 and 6-3) where they recombine (Equations 6-4 to 6-6) or initiate the oxidation and reduction reactions occurring at the TiO₂/ electrolyte interface^{1,2}. In the presence of a suitable co-catalyst, such as Pt, the electrons migrate from the TiO₂ surface to the Pt metal site (Equation 6-7). A part of these electrons is involved in the reduction reaction and/or another fraction is trapped on the surface of the TiO₂ as Ti⁺³ (Equations 6-8 and 6-9). On the other hand, the holes are trapped firstly inside the TiO₂ nanoparticle and then slowly migrate to the surface where they induce oxidation reactions (Equation 6-10)².



Before starting the photocatalytic reforming of naphthalene over the TiO₂ materials, the requirements for this process were evaluated. Indeed, all pristine and as-prepared platinumized materials did not show any activity for H₂ evolution from naphthalene in the absence of

light. The cleavage of water to produce H₂ and O₂, as well as the decomposition of naphthalene over TiO₂ requires an input of energy due to the positive Gibbs energy for both reactions (Equations 6-11 and 6-12)^{3,4}.

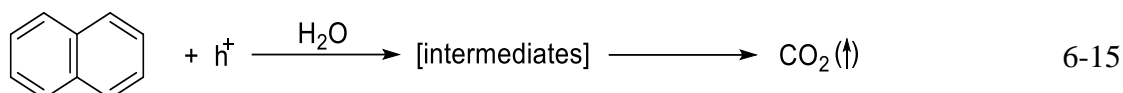
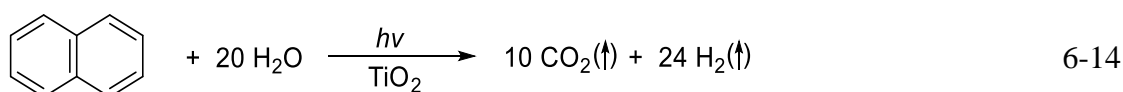
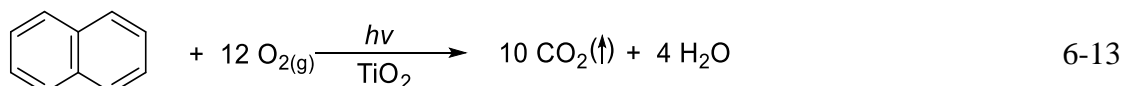


Therefore, to overcome this lack, the energy of light is used, evincing the importance of converting light energy into chemical energy. Besides that, no H₂ evolution was observed during the illumination of pristine and platinized TiO₂ in the absence of naphthalene. This can be assigned for many reasons: (i) The fast recombination of the photogenerated charge carriers in the absence of a suitable hole scavenger, i.e., naphthalene. (ii) The presence of an overpotential in the production of H₂ on the surfaces of the pristine photocatalysts. (iii) The fast backward recombination of H₂ and O₂ yielding water, which could easily take place and compete with the water-splitting⁵. In fact, the lack of H₂ production during water splitting over different types of Pt-TiO₂ under UV or visible light illumination has been reported previously^{6,7}. Galinska and Walendziewski⁸ did not observe any H₂ production by using Pt-TiO₂ under UV illumination without the addition of a sacrificial reagent⁸. Similarly, Kandiel et al.⁷ have been reported that Pt-P25 and Pt-UV100 are inactive to photocatalyze H₂ evolution from pure water in the absence of methanol.

Moreover, the naphthalene concentration moderately decreases under irradiation in the absence of the photocatalyst (32% after 4 h), possibly due to the photolysis of the naphthalene. The direct photolysis of PAHs has been reported previously⁹, and it is considered as one possible method for eliminating these compounds from the environment¹⁰. The estimated photonic efficiency for the direct photolysis of naphthalene after 4 h irradiation is 2.3×10^{-3} %. This value is low compared to that reported by Vialaton et al.¹¹ of 2.5×10^{-1} % for the photolysis of naphthalene under aerobic conditions at 313 nm irradiation, which can be related to the presence of molecular oxygen that enhances the photodegradation of the PAHs⁹.

The general stoichiometry of the photocatalytic degradation of naphthalene in the presence of molecular oxygen is represented by Equation 6-13. As shown in this equation, typical photocatalytic oxidation (mineralization) converts the hydrogen bound to organic carbons to hydrogen bound in water since this is the most thermodynamically stable form. It is also

possible in the absence of O_2 to achieve a partial conversion instead of the complete mineralization of organic compounds. This reaction which can be driven by solar photocatalysis yields H_2 from the degradation of naphthalene (Equation 6-14). On the surface of the excited TiO_2 , the adsorbed naphthalene are oxidized by the photogenerated holes to CO_2 (Equation 6-15), whereas, the present protons are reduced to H_2 by the photogenerated electrons (Equation 6-16).



However, in this study, as can be seen in Figure 6-1, both pristine photocatalysts (UV100 and P25) had not shown activity for H_2 evolution, although the energy of the photogenerated electrons in the conduction band of both rutile ($E_{CB} = -0.11$ V at pH 0) and anatase ($E_{CB} = -0.32$ V at pH 0)¹² is sufficient to form H_2 by reducing water.

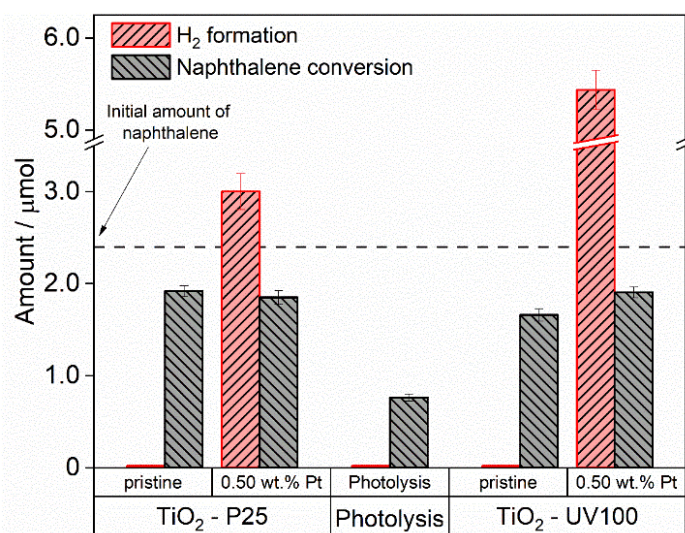


Figure 6-1: Molecular hydrogen formation (red columns) and naphthalene conversion (black square symbols) during light-induced reforming of naphthalene in the presence of pristine and platinized TiO_2 (P25 and UV100), after 240-minutes of illumination using simulated solar light.

Photocatalyst mass concentration, 1 g L⁻¹; volume 15 mL, and 156 μM aqueous solution of naphthalene.

The lack of H₂ evolution over bare TiO₂ is a known issue, ascribed to the fast recombination of charge carriers and the high overpotential for this reaction on the TiO₂ surface⁶. In the present case, whilst the photogenerated holes in TiO₂ may be consumed by naphthalene (Equation 6-15), the absence of molecular oxygen as the electron acceptor necessitates that the accompanying electrons either reduce one of the organic species present in the system or they accumulate in the form of trivalent titanium (Ti³⁺) inside the photocatalyst due to their insufficient transfer capacity to an absorbed species¹. Transient absorption spectroscopy (TAS) data revealed that the generated electrons were trapped as blue Ti³⁺ ions instead of reducing H⁺ upon the consumption of holes by the electron donor^{6,13}. The presence of platinum NPs on the surface of both TiO₂ photocatalysts activates the reduction of adsorbed protons to molecular hydrogen. The reduction of the overpotential of H₂ evolution and the formation of a Schottky junction at the Pt–TiO₂ interface is considered the main driving force for this reaction¹⁴. Considering that, Pt NPs have lower the Fermi level compared to that of TiO₂. When TiO₂ and Pt are connected, photogenerated electrons can migrate from TiO₂ to the PtNPs through the interface until a thermodynamic equilibrium is achieved¹. A Schottky barrier is defined as the barrier against the flow of electrons from the metal to the n-type semiconductor, i.e., TiO₂. During the irradiation, this thermodynamic equilibrium will be disturbed, permitting the photogenerated electrons to continuously flow from the CB of TiO₂ to the metal NPs¹. Generally, it has been known that such a Schottky barrier facilitates electron trapping by the metal, providing better charge separation. Thus, the trapped electrons have a longer lifetime to promote the reduction reactions of the adsorbed protons to H₂¹⁵. It should be noted that Patsoura et al.¹⁶ conducted similar experiments over pristine TiO₂ at pH 6 and 10 using an azo-dye (Acid Orange 7) as a hole scavenger. Even after 20 h illumination, the authors did not observe hydrogen production, although decolorization of the solution was achieved in less than 15 min. This indicates the necessity of the presence of a suitable electrocatalyst (here: Pt) for the photoinduced H₂ production from dye-containing solutions. However, it is known that other noble metals, such as Pd, Au, and Ag are suitable hydrogen evolution reaction catalysts, too.

Interestingly, as can be seen in Figure 6-1, after 0.5 wt% platinum deposition on the TiO₂ surface, the photocatalytic activities for H₂ evolution increase for all the platinized samples

as a result of the improved charge separation efficiency. Pt-UV100 shows higher activity for H₂ production compared to Pt-P25. The difference in H₂ formation between Pt-UV100 and Pt-P25 could be explained by the enormous variation in the specific surface areas of these two catalysts, i.e., 300 m² g⁻¹ vs. 50 m² g⁻¹, respectively. The larger the surface area, the higher the adsorption of the pollutant molecules due to the higher number of active sites (Ti⁴⁺) on the TiO₂ surface. This leads to a rise in the rate of electron transfer to Pt nanoparticles and decreases the internal mass transfer limitation of the pollutant to the active sites, thus promoting the H₂ formation⁷. Kandiel et al.⁷ explained the higher H₂ formation rate over Pt-UV100 during the reforming of aqueous methanol solutions to the higher BET surface area of UV100 as compared to Pt-P25. However, in general, the differences in the photocatalytic activity between the materials depend on various properties, such as surface area, particle size, optical properties, crystallinity, structure, and many other factors, and cannot be interpreted based on a single property³.

The differences in the structure between the UV100 and P25 could be another reason for enhancing the UV100 activity. It has been reported that UV100 exhibits a mesoporous structure, whereas P25 is completely non-porous. This mesoporous TiO₂ structure, resulting from the compactly packed nanoparticles, which form a uniform agglomerate, enables efficient charge separation through interparticle charge transfer, thus enhancing the photocatalytic activity^{7,17}.

A further aspect that is thought to influence the activity of Pt as a co-catalyst is the particle size. As shown in Chapter 3, the average grain size of Pt nanoparticles on the surfaces of Pt-P25 and Pt-UV100 formed by the photodeposition method was found to be 3.4 ± 0.7 nm and 2.1 ± 0.5 nm, respectively. Considering that the mass density of Pt is 21.45 g cm⁻³, and assuming the spherical shape of the Pt particle, the average mass of the Pt particle on the surface of P25 and UV100 is 4.41 × 10⁻¹⁹ and 1.04 × 10⁻¹⁹ g, respectively. Therefore, each gram of 0.5 wt.% Pt-P25 and 0.5 wt% Pt-UV100 contain 1.13 × 10¹⁶ and 4.81 × 10¹⁶ Pt islands, respectively. From the geometrical point of view, it could be envisioned that smaller Pt particles could lead to larger specific surface areas. Moreover, based on DFT+U calculations, Wang et al.¹⁸ proposed that quasi two-Pt-layer particles, corresponding to ~1 nm size, are the optimal for photocatalytic hydrogen evolution over anatase (101) due to a good balance between its electron transfer and surface catalysis capabilities. In the present case, the smaller Pt particle sizes on the surface of UV100 form a higher surface area of the

spread Pt, which increases the probability of electron transfer to the Pt particle, thus, increasing the H₂ formation.

6.2.2 Naphthalene Conversion

It is well known that both reductive and oxidative processes occur simultaneously in a photocatalytic system. As mentioned earlier in Chapter 1, it is very imperative to evaluate the fate of both the charge carrier components, i.e., the hole and electron, during the photocatalytic reforming process. The previous section had shown that electrons participate in the reduction of the protons to molecular hydrogen during the photocatalytic reforming of naphthalene over Pt-P25 and Pt-UV100, whereas the photogenerated holes are responsible for the most of primary oxidation processes. This section provides more information regarding the fate of naphthalene after reaction with the photogenerated holes.

As can be seen in Figure 6-1, the degradation of naphthalene is greatly enhanced in the presence of all the photocatalysts (pristine and platinized P25 and UV100) comparing to the photolysis process. After irradiating the aqueous suspension for 4 h, the naphthalene concentration decreases by 70% - 86%. Similar results have been reported by Lair et al.¹⁹, who found that the conversion of naphthalene is greatly enhanced in the presence of TiO₂ under irradiation, where it increased linearly when increasing the TiO₂ loading to reach a maximum at about 2.5 gL⁻¹.

In the presented study, pristine TiO₂-P25 exhibited higher photocatalytic performance for naphthalene conversion compared to pristine TiO₂-UV100. This observation was expected, and it could be mainly ascribed to the fact that the recombination rate of the photoexcited electron-hole pair in pristine TiO₂-UV100 is faster compared to the mixed phases TiO₂-P25²⁰. Scanlon and co-workers²¹ demonstrated that the electron affinity of anatase is higher than rutile. Thus, the photogenerated conduction band electrons will flow from rutile to anatase due to the existence of a band alignment of ~0.4 eV between them, which significantly lowers the effective bandgap of composite materials, and facilitate an efficient electron-hole separation. The authors considered this alignment as a driving force for the increased photoactivity. Previously, many investigations have been reported the better photoactivity of pristine TiO₂-P25 comparing to TiO₂-UV100 for photooxidation of aromatic compounds such as phenol²² and 4-chlorophenol²³, and salicylic acid²⁴ in an aqueous medium.

Interestingly, loading platinum NPs on the surface of TiO₂ has exhibited two different behaviors related to the nature of the photocatalysts. As shown in Figure 6-1, loading platinum NPs on the surfaces of TiO₂-P25 decreased the photooxidation of naphthalene (~ 10 %) in comparison to pristine material. In the case of TiO₂-UV100, an enhancement of naphthalene photooxidation was observed after loading the PtNPs, which is attributed to a reduction in the charge carrier recombination. Anatase is generally regarded as the most photochemically active phase of titania, presumably due to many reasons e.g., the wide bandgap, higher charge carrier mobility, combined effect of lower rates of recombination, and higher surface adsorptive capacity. The presence of a small amount of Pt as a co-catalyst enhances the charge carrier separation through collecting the photogenerated electrons and thereby avoiding the electron-hole recombination¹⁸. In the case of Pt-P25, the co-catalyst Pt seemingly could not increase the efficiency of the charge carrier separation more than the separation already exists in the mixed-phases TiO₂-P25. The decrease of TiO₂-P25 activity after platinization suggests that Pt acts as a recombination center for the charge carrier, thus, a very small amount of the photogenerated electrons can be involved in the H₂ formation. The presented results in this thesis are in good agreement with the investigation of Sun et al.²² who reported that loading Degussa P25 with Pt resulted in a decrease of phenol conversion and the total carbon removal rates, whereas these rates rise by a maximum factor of 1.5 when Hombikat TiO₂ was loaded with 1.0 wt% Pt.

The electron paramagnetic spectroscopy (EPR) investigations for the dynamic of the charge carrier in Pt-UV100 and Pt-P25 have supported the photocatalytic results. As can be seen clearly in Figure 6-2 a, Pt-UV100 exhibits an approximately 20 % higher amount of trapped holes than Pt-P25 in the N₂ atmosphere and under irradiation. Whereas Pt-P25 exhibits the strongest electron signals at Ti⁺³ sites. The Ti⁺³ site is formed from the Ti⁺⁴ site at which the photogenerated electrons are trapped (Equations 6-8 and 6-9). Since no hole scavenger was used, the increase in the Ti⁺³ signal is related to a higher amount of trapped electrons in the lattice of Pt-P25.

Anpo and Takeuchi²⁵ have proved the transfer of the photogenerated electrons from TiO₂ to Pt NPs by the mean of electron spin resonance signals of Ti⁺³. By increasing the irradiation time in the absence of the Pt NPs, the Ti⁺³ signals increased, while their presence decreased the amount of Ti⁺³. These results clearly indicate that the photogenerated electrons in the Pt NPs loaded TiO₂ quickly migrate from TiO₂ to Pt NPs, so that few Ti⁺³ sites could be observed. Thus, the trapped electrons on the Pt NPs enhance the reduction of

protons to H_2 . In the present case, the presence of high trapped electron sites (Ti^{+3}) on the surface of Pt-P25 will increase the probability to recombine the trapped electrons with the trapped photogenerated holes. On the other hand, the very small signal of Ti^{3+} and the higher amount of trapped holes in the case of Pt-UV100 indicates a better electron transfer to Pt islands than Pt-P25. Therefore, an efficient charge carrier separation in the case of Pt-UV100 is expected, which inhibits the electron-hole recombination and increases the photocatalytic efficiency. This hypothesis was proved after the addition of the hole scavenger naphthalene to the system. The data presented in Chapter 5 shows that the reaction of naphthalene with the photogenerated hole produces a naphthyl radical cation, according to Equation 6-17.

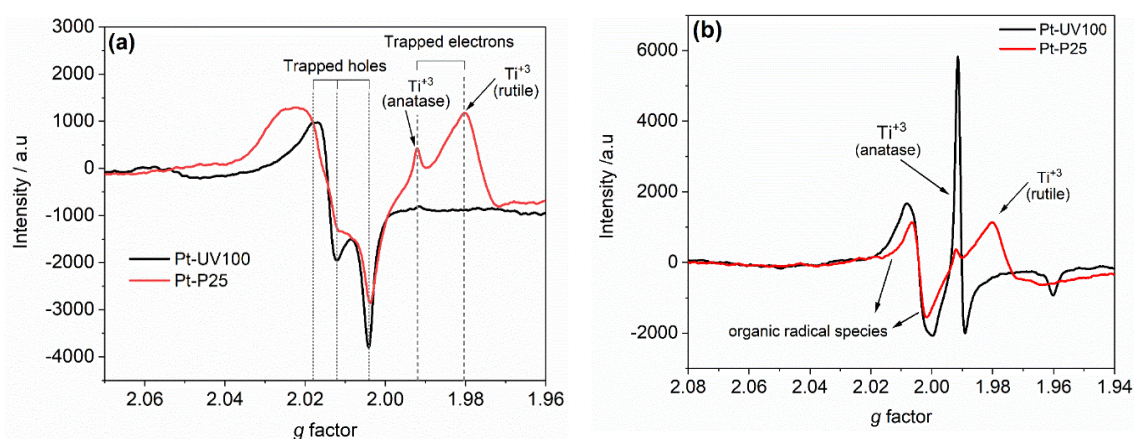


Figure 6-2: EPR spectra measured at 77 K under irradiation for Pt-UV100 (black line) and Pt-P25 (red line) in: (a) N_2 atmosphere, and (b) N_2 -naphthalene vapor under illumination.

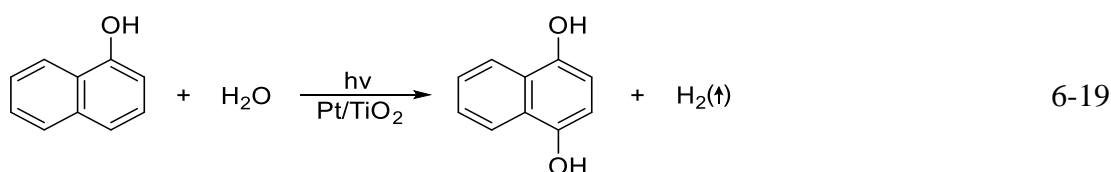
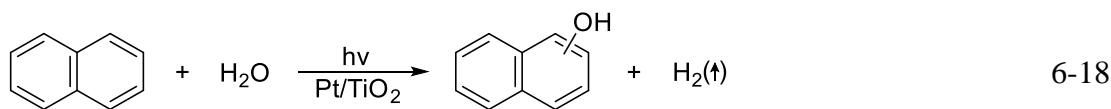


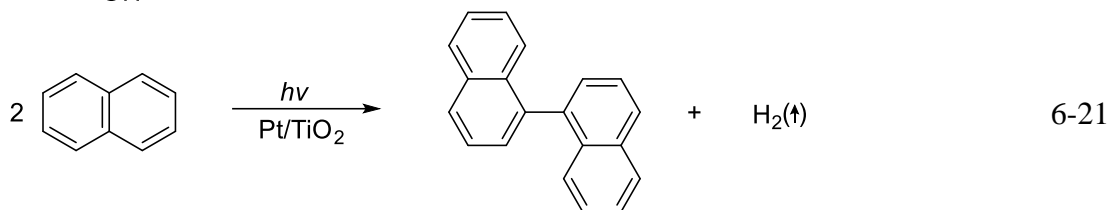
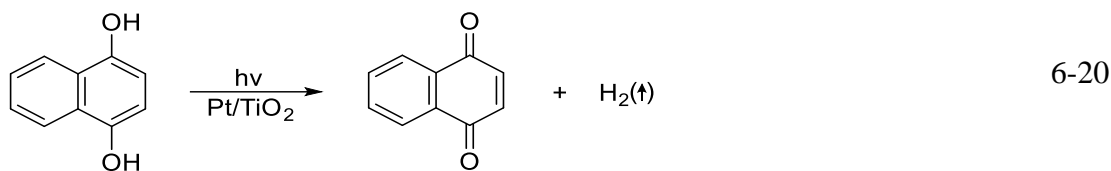
Although both photocatalysts generate similar EPR signals at g -tensor components $g_x = 2.002$, and $g_y = 2.006$ (Figure 6-2 b) due to the formation of the naphthalene radical cation²⁰, Pt-UV100 produced a relatively higher intense signal of this organic radical and a stronger signal of the trapped electrons (Ti^{+3}) compared to both signals produced from Pt-P25. This can be attributed to the higher amount of the trapped holes that are available to react with the adsorbed naphthalene. Interestingly, unlike Pt-UV100, the intensity of the trapped electrons produced from Pt-P25 (Ti^{+3} anatase and rutile) did not relatively change upon the introduction of naphthalene as a hole scavenger. The higher intensity of the formed organic radicals in Pt-UV100 would be accompanied by a higher amount of the photogenerated electrons, which can be partially collected by PtNPs on the surface of Pt-

UV100 to catalyze the reduction of H^+ ions to H_2 , while the remaining electrons can be trapped as Ti^{+3} .

Thus, according to the previously presented results, 0.5 wt% Pt-UV100 had exhibited the highest photocatalytic activity under solar radiation toward the H_2 formation and naphthalene conversion compared to all other pristine and platinumized photocatalysts. Therefore, this photocatalyst was used to perform further investigations to determine the fate of naphthalene after reaction with the photogenerated holes during its photoreforming.

The analyses of the reaction suspension using a combination of chromatographic techniques that were mentioned in *Chapter 5, section 5.3.2*, have shown that the hydroxylation of the aromatic ring was found to be the main process in the photocatalytic oxidation of naphthalene. Several hydroxylated compounds had been identified after 4 h of irradiation, mainly, naphthalen-1-ol, naphthalen-2-ol, naphthalene-1,4-diol, and naphthalene-1,4-dione, etc., besides the formation of the coupling compound 1,1'-binaphthalene (Equations 6-18 to 6-21) and formic acid and acetic acid in low concentrations. Among these compounds, naphthalen-1-ol and naphthalen-2-ol had been found to be the main intermediates. On the other hand, the gas-phase analysis showed that CO_2 and H_2 are the only gases produced. It has been reported that such organic compounds are formed by the reaction of the aromatic compound with the electrophilic oxygen species that are photocatalytically derived from water ²⁶. Several research groups had reported the formation of different hydroxylated compounds besides the H_2 and CO_2 gases during the photocatalytic reforming of benzene over titania ²⁷. Yuzawa et al. found that the photocatalytic reaction of benzene with water over Pt- TiO_2 in an anaerobic system produced phenol, biphenol, and cyclohexanol ²⁸. The detection of such hydroxylated compounds in the present case reveals that the most detected intermediates correspond to earlier stages of the degradation process, which suggests a limited extent of mineralization under anaerobic conditions.





6.2.3 Kinetic of the Photocatalytic Reforming of Naphthalene

The photocatalytic reforming of naphthalene and as well other multi-carbons compounds is complex and involves many reductions and oxidations steps ¹⁹. The analysis of the detailed kinetic profiles of the photocatalytic reforming of naphthalene over Pt-UV100 reveals some interesting features. In the present work, the converted amount of naphthalene and the H₂ evolution vs time did not follow a first-order model, indicating that there is more than one limiting step in the reaction mechanism, which is expected considering its several intermediates and their different photooxidation processes ^{29, 30}.

As can be seen in Figure 6-3, the reduction of about 14% of the initial naphthalene amount in the dark before the illumination evinces that it can adsorb on the surface of the photocatalysts. Although naphthalene is not expected to interact strongly with the TiO₂ surface, apparently the high specific surface area of UV100 results in significant adsorption. The adsorbed amount at the equilibrium corresponds to a coverage of about 0.05 molecule nm⁻². A similar value for naphthalene on the surface TiO₂ (anatase) was reported by Mahmoodi and Sargolzaei, with the difference that the dynamic equilibrium was established after 5 min in that case ³¹. The adsorption of aromatic compounds on the TiO₂ surface was studied by Nagao and Suda ³², who suggested that the adsorption involves the formation of Ti⁺⁴···π-electron and/or OH_(surface)···π-electron type complexes.

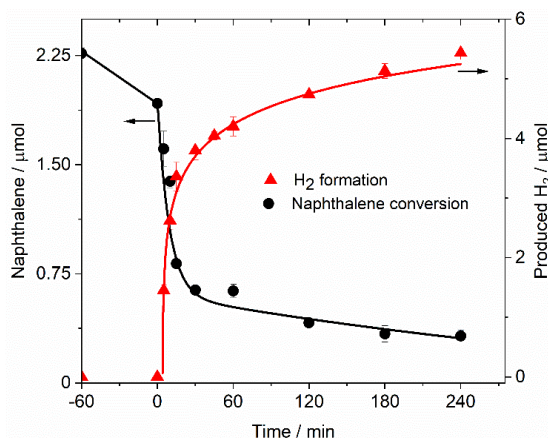


Figure 6-3: Kinetic profiles for the photocatalytic degradation of naphthalene and molecular hydrogen evolution over Pt-UV100. Conditions: batch reactor, reaction volume = 15 mL; [Naphthalene] = 156 $\mu\text{mol L}^{-1}$; [catalyst] = 1 g L^{-1} ; $T = 25\text{ }^{\circ}\text{C}$; illumination under simulated solar light. Lines are guides for the eye.

Indeed, upon irradiation, the kinetic profiles of the photoreforming of naphthalene (Figure 6-3) can be divided into two stages: a very rapid decrease in naphthalene amount accompanied by rapid H_2 evolution in the presence of Pt-UV100 during the first 30 min of illumination. The initial photonic efficiencies were $0.97 \pm 0.06\%$ for H_2 formation and $0.33 \pm 0.01\%$ for naphthalene degradation. Actually, these values represent around 70% of the total H_2 formation and naphthalene conversion during 4h of illumination. After this initial 30 min period, the changes in the amounts of naphthalene, as well as evolved H_2 , became significantly slower. The photonic efficiencies after 4h of illumination were found to be $0.17 \pm 0.03\%$ for H_2 formation and $0.05 \pm 0.002\%$ for naphthalene degradation. The accompanying degradation of 4-chlorophenol with H_2 formation under the anoxic condition exhibited similar behavior, too³³. The authors have observed high rates for H_2 evolution and 4-chlorophenol conversion over Pt-TiO₂ within the first hour, which were highly inhibited after this period. In the case of naphthalene in this study, the photonic efficiency for H_2 formation was found to be higher than those reported for different aromatic compounds over Pt-TiO₂, such as hydroquinone (0.05%), 4-chlorophenol (0.003%), 4-chlorobenzoic acid (0.002%), and bisphenol A (0.019%)³⁴.

In the second stage, the inhibition of the H_2 formation and naphthalene conversion suggests the depreation of the holes by the accumulated intermediates at the photocatalyst surface and the competition of naphthalene and its intermediates for these holes during the photocatalytic process. This hypothesis of “poisoning of the photocatalyst surface” is supported by the observation of a color change of the photocatalyst from light gray to brown after 1 h of illumination. This observation is in agreement with previous reports which had

shown that the photocatalytic degradation of naphthalene and other aromatic compounds may yield intermediates, likely of polymeric nature, that deactivate the catalyst surface³⁵. Furthermore, besides the disappearance of naphthalene, it is of high importance to evaluate the extent of complete mineralization of the reactant yielding CO₂ and H₂O. As shown in Chapter 5, the total organic carbon (TOC) being present in the aqueous solution showed a gradual decline to around 55 % after 4 h of irradiation. Moreover, as shown in Figure 6-3 above, the amount of naphthalene decreases by 86 % in the same period of time. This variance can be ascribed to the formation of stable intermediates adsorbed on the TiO₂ surface, instead of mineralization.

As mentioned in Chapter 3, the validity of the poisoning of the photocatalyst surface has been confirmed by performing different photocatalytic experiments using naphthalene and its main products, i.e., 1-naphthalenol, and 2-naphthalenol, under the same experimental conditions. As can be seen in Figure 6-4, the kinetic profiles for the photoreforming of 1-naphthalenol, and 2-naphthalenol have shown a similarity to the naphthalene profile, however, higher conversion and H₂ formation rates were observed in the naphthalene system. After 240 min of illumination, the conversion of naphthalene, naphthalen-1-ol, and naphthalen-2-ol were found to be 75%, 63%, and 52%, respectively.

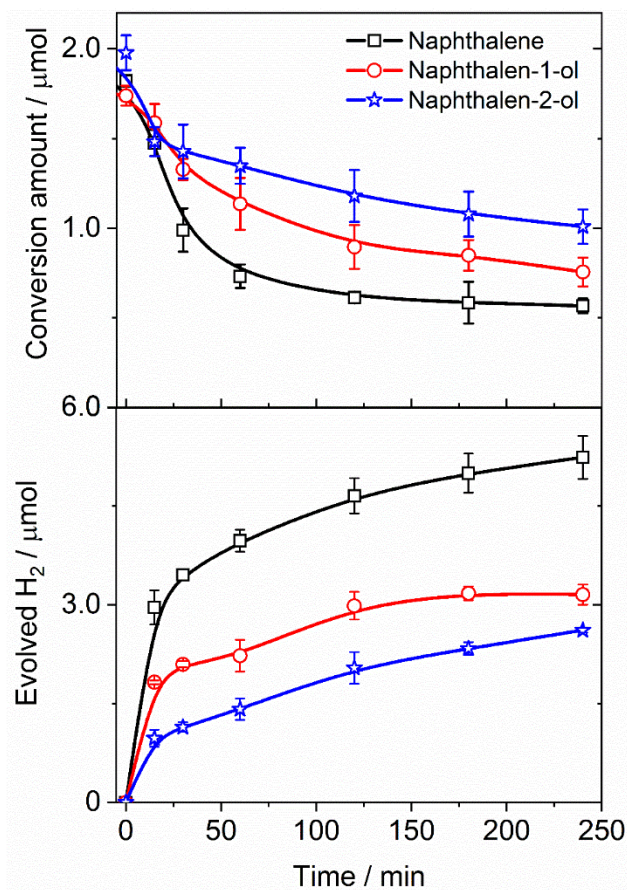


Figure 6-4: Photooxidation and molecular hydrogen formation during the photocatalytic reforming of naphthalene, naphthalen-1-ol, and naphthalen-2-ol as a function of illumination time. Conditions: organic compounds amount = 2.1 μmol , [catalyst] = 1 g L⁻¹ 1.0 wt% Pt-HTiO₂, T = 25 °C, illumination under simulated solar light.

All the tested compounds showed a faster conversion rate at 15 to 30 minutes of illumination, afterward, a noticeable inhibition in both rates. The fast rates in the first stages can be attributed to the abundant availability of active sites on the surface of TiO₂¹. This behavior has been observed by King et al.³⁶, who reported that the initial stage has the most rapid photodegradation rate for PAH removal in the presence and the absence of the photocatalyst. The initial photonic efficiencies of the H₂ formation and photooxidation of these compounds after 60 min of illumination were found to be 0.51 ± 0.02 %, and 0.14 ± 0.01 % for naphthalene, 0.28 ± 0.03 %, and 0.1 ± 0.02 % for naphthalen-1-ol, and 0.18 ± 0.02 % and 0.08 ± 0.01 % for naphthalen-2-ol, respectively.

Considering the kinetic profile of naphthalene degradation, at the beginning of the photocatalysis process, the concentrations of these organic products are very low in the system. Thus, naphthalene is efficiently oxidized on the clean surface of the TiO₂ since there is no competition from these products on the surface of the photocatalyst. However,

during the reaction, the formed intermediates are accumulated in the system and subsequently oxidized to other more polar compounds such as polyhydroxylated, quinones, and organic acid^{37, 38}. Such products have a higher polarity comparing to naphthalene. Therefore, they can strongly adsorb to the surface of the photocatalyst, blocking the active sites on this surface. In general, the degradation of these compounds leaves recalcitrant carbonaceous residues on the photocatalyst surface as a result of incomplete degradation³⁹, especially in the absence of O₂, which decreases the photocatalytic activity of the TiO₂.

In this respect, it is noteworthy that the adsorption of the organic molecules is a very important factor in the photocatalytic process, however, in some cases, the strong adsorption of the organic compounds or their intermediates may act as a poison for the catalyst surface, which enhances the charge carrier recombination. The strong multilayer adsorption of organic molecules around the catalyst particles could limit the interaction between the incoming light and the photocatalyst in the case of the indirect photooxidation mechanism, which will reduce the photocatalytic efficiency⁴⁰. In the presented case, the lack of naphthalen-2-ol photooxidation after less than 30 min of irradiation can be related to the adsorption of stable photoformed products on the surface of the photocatalyst that hinders the photocatalytic process. The photocatalytic degradation of 2-naphthol was investigated by Qourzal et al.⁴¹ with and without replenishing the O₂ in the system and was found to be 100 % and 58 %, respectively. Since the photocatalytic reforming of naphthalene is more efficient than the reforming of both naphthalenols compounds under the same experimental conditions, this confirms the negative impact of the reaction intermediates on the reforming process.

Furthermore, although the full mass balance of the photocatalytic reforming of naphthalene is outside the scope of this work, it is informative to compare the apparent stoichiometries of the kinetic profiles of naphthalene photoreforming and the relative amount of TOC during its reforming over Pt-TiO₂ that were presented in Chapter 5. Considering that 55% (11.2 μmol) of TOC is removed from the medium, and neglecting the quantities of the adsorbed intermediates on the surface of the photocatalyst, this amount of TOC is corresponding to totally mineralized 1.1 μmol of naphthalene. According to Equation 6-14, the expected quantities of evolved H₂ formed from this amount of naphthalene is 26.4 μmol. However, as shown in Figure 6-3 the evolved amount of H₂ during the reforming of naphthalene was found to be only 5.6 μmol. Thus, the “observed: expected” ratio of H₂ formation was found to be ~0.2, which is considerably lower than one. Accordingly, this

ratio suggests that there are reductive reactions that compete with the proton reduction which are unaccounted for in the mechanism. In fact, as mentioned in Chapter 5, different reduction products have been identified during the analysis of naphthalene intermediates in low concentrations, such as 1,2,3,4-tetrahydro-1-naphthalenol, 3,4-dihydronaphthalen-1(2H)-one, and long chains of aliphatic acids.

Generally speaking, the reduction potential of the TiO₂ conduction band (-0.5 V vs NHE at pH 7)³⁸ is suitable for the reduction of different kinds of organic compounds. A recent report from Walenta et al.⁴² shows that CO is formed on the surface of Pt-TiO₂ during the reforming of organic compounds. Moreover, as mentioned in Chapter 5, the photooxidation of naphthalene leads to produce different phenoxy and hydroxylated compounds. These compounds could be reduced on the TiO₂ surface, since their reduction potentials are suitable to be reduced by the TiO₂. In this context, the reduction potentials of 1-naphthoxyl radical, 2-naphthoxyl radical, and 1,4 naphthoquinone were determined to be 0.59 V, 0.69 V⁴³, and 0.49 V⁴⁴ versus NHE, respectively. Similarly, it has been reported that cyclohexanol is formed during the photocatalytic reforming of benzene on Pt-TiO₂²⁸. It is also possible that the reduction of these compounds is not a direct process, but instead, it takes place via the hydrogen atoms adsorbed on Pt that are formed upon the reduction of H₂O / H⁺^{28, 45}. In either case, the consumption of these species ultimately leads to a deviation in the stoichiometry from the expected H₂ quantities.

The investigations presented in *Chapters 2, 3, and 4* reveal several factors affecting the photocatalytic reforming of naphthalene. Actually, the H₂ formation, as well as the photooxidation rates and the efficiency of the photocatalytic process are highly dependent on several parameters that govern the photocatalytic process. Several studies had highlighted many factors such as the nature and the concentration of the photocatalyst, the concentration of the substrate, nature of the substrate, the by-products formation^{4, 16}, and the structure and the properties of the co-catalyst^{14, 46-48}. Some of these factors were already discussed previously in this Chapter such as the nature of the photocatalyst and the by-product formation, while in the following sections, the impact of the fractional ratio of Pt nanoparticles and its loading methods on the H₂ formation during the photooxidation of naphthalene is discussed.

6.3 Effect of Platinum Ratio in Different Types of Commercial TiO₂

It is well known that the most popular and recommended way to enhance the photoactivity of the photocatalyst is the loading of metal co-catalyst. As mentioned in the second section of this chapter, the loading of Pt on the surface of the TiO₂-P25 and TiO₂-UV100 photocatalyzed the H₂ formation during the photoreforming of naphthalene. On the other hand, although the photoactivity of the TiO₂-UV100 was enhanced after the loading, a reduction in the TiO₂-P25 photoactivity was observed. To further prove the role of Pt on the surface of these catalysts in the photoreforming of naphthalene, different fractional ratios of Pt were deposited on the surfaces of materials and employed in the photocatalytic process.

As shown in Chapter 3 section 3.4.2, the increase of the platinum content on the surface of TiO₂-UV100 over the optimum ratio (0.5–1.0 wt%.) had shown a negative effect on the formation rate of molecular hydrogen and naphthalene conversion. In the case of P25, naphthalene conversion was also decreased with increasing the Pt content, however, the same H₂ amount was photocatalyzed over all the platinized P25 materials. The data presented in Chapter 3, as well as other reports^{22, 46}, show that an optimum content of Pt on the surface of TiO₂ should be considered, otherwise, increasing the Pt content will reduce the efficiency of the photocatalytic process. Actually, the presence of hole scavengers (like naphthalene) can change the original equilibrium between the photogenerated holes and electrons. Platinum nanoparticles on the surface of TiO₂ act as electron scavengers, withdrawing the photogenerated holes out of the bulk TiO₂. However, increasing the Pt loading more than the optimum value makes the space charge layer very narrow, and then, the penetration depth of light exceeds the space charge layer. Thus, platinum nanoparticles can act as recombination centers, where the electron-hole recombination process will be favorable^{22, 46}.

Apparently, Pt on the surface of TiO₂-P25 is a hot spot for the recombination of the charge carriers. The only benefit of Pt NPs on the TiO₂-P25 surface is to enable the H₂ formation by reducing the overpotential of its formation. Benz et al.⁴⁹ recently discussed this point. They demonstrated that the fate of the charge carriers is strongly affected by the deposition of Pt nanoparticles. In the absence of O₂, the photogenerated electrons trapped by the Pt islands on the surface of P25 will not be consumed by the reduction reactions, but easily recombine with the holes in TiO₂. In the presented study, regardless of the Pt deposit ratio,

its behavior on the surface of P25 may result from the overloading that exceeds the optimum ratio. By increasing the Pt content on the surface of pristine TiO₂, the Pt nanoparticles themselves will absorb light and consequently blocking it to reach the TiO₂ surface, thus negatively influencing its photocatalytic activity. Besides, this will reduce the number of available active sites which plays a crucial role in the photooxidation of organic compounds⁵⁰. The effect of this factor can be clearly observed on the Pt-P25 as shown in Figure 6-5. The measured BET surface area of pristine P25 and UV100 was found to be $52 \pm 0.8 \text{ m}^2 \text{ g}^{-1}$ and $295 \pm 3 \text{ m}^2 \text{ g}^{-1}$, respectively. The deposition of Pt NPS results in a decrease in the surface area, however, a more pronounced effect was observed in the case of P25.

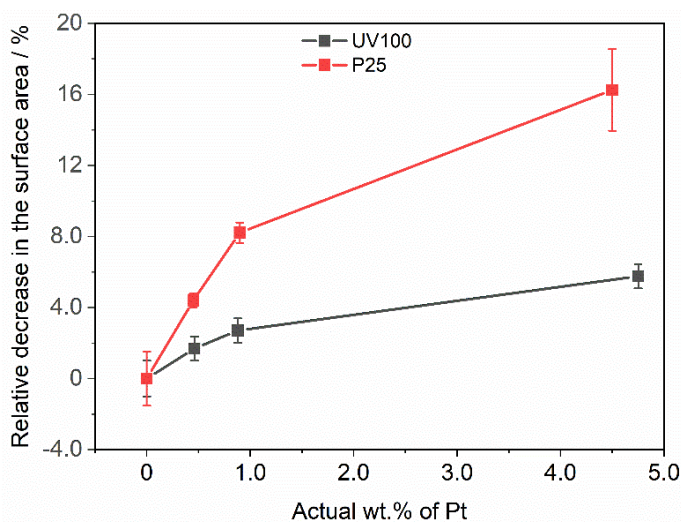


Figure 6-5: The relative decrease in the BET surface area of P25 and UV100 after platinization.

Alkaim et al. studied the H₂ formation in the EDTA system using self-prepared TiO₂ loaded with different ratios (0.1 – 1.0 wt.%) of PtNPs. They found that increasing the Pt content from 0.1 wt.% to 0.3 wt.% leads to an increase in the H₂ formation rate. Further increase of the Pt content resulted in decreasing the H₂ formation rate, which was attributed to the fact that Pt can act as a recombination site at a high loading ratio, and alteration of the light absorption capacity because of the gray coloration of the Pt-loaded TiO₂ nanoparticles. A similar photocatalytic activity dependency on the content of Pt loading on the surface of TiO₂ has been reported previously for biomass reforming⁵¹.

6.4 Impact of the Platinization Method

As discussed in Chapter 4, surface decoration of TiO₂ nanoparticles by metal such as Au, Ag, Cu, and especially Pt is an outstanding technique to revamp the electronic properties

of TiO₂ without affecting its original crystallinity, thus, enhancing the photocatalytic activity and enriching the H₂ production efficiency⁵². Different co-catalyst loading methods have been successfully applied⁴⁷, however, the structure and the properties of the co-catalyst were found to play a critical role in achieving superior photoactivity⁵³. The size⁵⁴, dispersion¹⁴, chemical state of Pt deposits⁵⁵, and the interaction between the Pt and the TiO₂⁵⁶ seem to affect the activity of the resulting Pt-TiO₂. However, all these factors can be optimized by using proper preparation methods⁴⁶⁻⁴⁸. The most commonly adopted methods for the deposition of co-catalyst nanoparticles include photodeposition^{46, 57}, deposition-precipitation⁴⁶, chemical reduction⁵², impregnation⁵⁷, and physical mixing⁴⁶, with photodeposition being the most commonly used⁴⁷.

As mentioned in Chapter 4, 0.5 wt.% Pt-TiO₂ (UV100) had been prepared by two different methods to differentiate between their impact on both, the reductive and the oxidative photocatalytic half-reaction during the reforming of naphthalene. These methods are the classical photodeposition method (Pt_{PD}-TiO₂), and the physical mixing method (Pt_{LA}-TiO₂).

As can be seen in Figure 6-6, both platinized photocatalysts (Pt_{PD}-TiO₂, Pt_{LA}-TiO₂) exhibited similar kinetic and achieved a ~90 % removal of naphthalene, thus, the preparation method has a minor effect on the photooxidation efficiency of naphthalene. The main difference between both platinized photocatalysts is observed in the reductive half-reaction. After 4 h of illumination, the amount of evolved H₂ is 40 % higher when using Pt_{PD}-TiO₂ than with Pt_{LA}-TiO₂. The photonic efficiencies, calculated from the initial formation rates after 1 h, are 0.79 % ± 0.01 % and 0.60 % ± 0.02 %, respectively, which are within the typical ranges for heterogeneous photocatalytic processes⁵⁸. Since the difference in the photocatalytic activity between the prepared Pt-TiO₂ samples was not appropriate to be evaluated through the photooxidation of naphthalene, methanol was used as another hole scavenger. This selection is based on the significantly different properties that methanol and naphthalene exhibit: while methanol strongly adsorbs on the TiO₂ surface^{52, 59}, naphthalene -as mentioned before- interacts weakly with the surface of the TiO₂. Furthermore, total oxidation of naphthalene is rather inefficient and involves a large number of reactions³⁸, while methanol acts as a swift hole scavenger and is promptly mineralized. Moreover, its first oxidation step yields the hydroxymethyl radical, ·CH₂OH, which readily injects an electron into the conduction band of TiO₂⁶⁰. This effect, known as current doubling, does not occur with naphthalene³⁸.

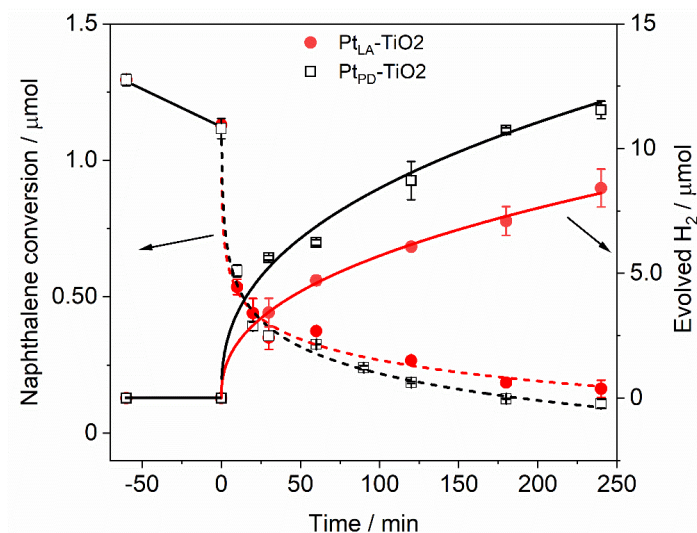
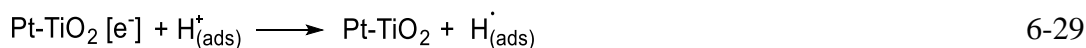
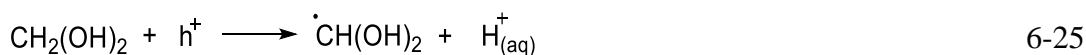
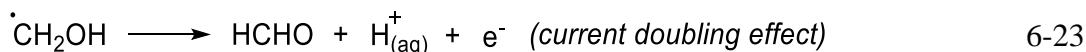
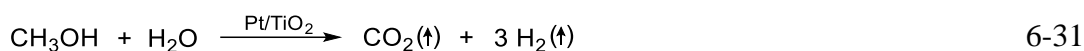


Figure 6-6: Kinetic profiles for photooxidation of naphthalene (---, dash line) and production of H₂ reforming (—, solid line) during the reforming of naphthalene over Pt_{LA}-TiO₂ (●, red circle) and Pt_{PD}-TiO₂ (□, black square). Conditions: reaction volume, 15 mL; initial naphthalene concentration: 100 μmol L⁻¹; photocatalyst mass concentration 1 g L⁻¹; T = 25 °C; illumination with simulated solar light.

Methanol is considered a good sacrificial electron donor. The main products of its reforming are acetaldehyde (HCHO), formic acid (HCOOH), and carbon dioxide (CO₂) from the oxidative pathway, and H₂ from the reduction side (Equations 6-22 to 6-31)^{56, 60}.



The overall methanol decomposition reaction



In the presented work, Pt_{PD}-TiO₂ displays a significantly better activity toward the H₂ formation during the reforming of methanol than Pt_{LA}-TiO₂. After 1 h illumination the photonic efficiencies for H₂ evolution are 15.6 % ± 0.3 % and 6.1 % ± 0.2% for Pt_{PD}-TiO₂ and Pt_{LA}-TiO₂, respectively. Looking at the oxidative products, both figures show that the Pt_{PD}-TiO₂ sample displays markedly faster oxidation kinetics for methanol than Pt_{LA}-TiO₂. As shown in Figure 6-7, both half-redox reactions of Pt_{PD}-TiO₂ producing approximately 3-fold higher amounts of H₂, acetaldehyde, formic acid, over the same time period compared to that of Pt_{LA}-TiO₂.

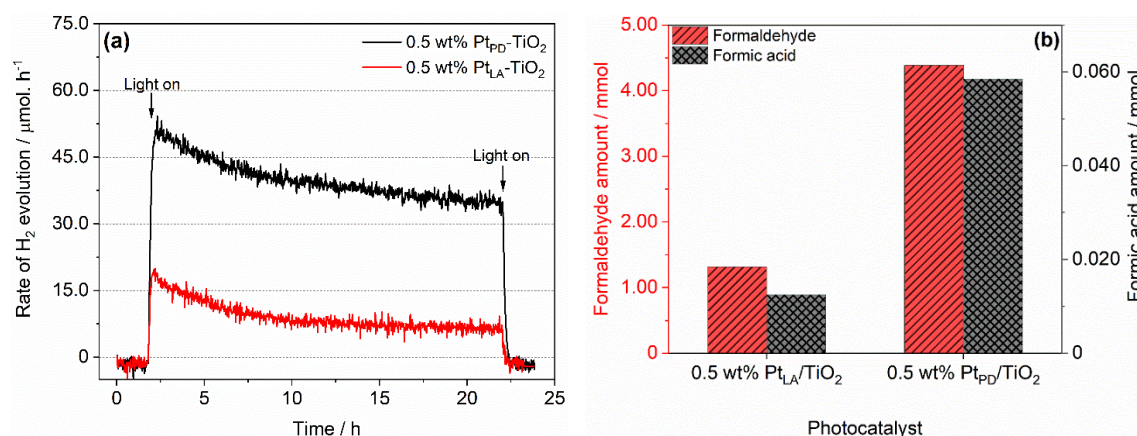


Figure 6-7: (a) Photocatalytic H₂ evolution over Pt_{PD}-TiO₂ (black) and Pt_{LA}-TiO₂ (red), and (b) total amount of HCHO (red column) and HCOOH (black column) from 10% CH₃OH–H₂O solution: 1.0 g L⁻¹ photocatalyst, 50 mL suspensions, T = 25 °C, light intensity I₂₅₀₋₄₅₀ = 30 mWcm⁻², and irradiation with an Osram XBO 1000-Watt xenon arc lamp as a solar simulator.

The general characterizations presented in Chapter 4, section 4.3.1, did not show any fundamental difference between both photocatalysts to interpret and explain the reasons behind their different efficiency, especially for H₂ production. Thus, study the dynamic of the charge carriers by using EPR and TAS techniques provides useful information regarding the efficiency of these materials.

The in-situ EPR signals of each photocatalyst were acquired before and after irradiation, after purging with either N₂ or N₂-methanol. As can be seen in Figure 6-8, in the N₂ atmosphere, the relative intensities of the electron and hole signals (determined by double integration) show a clear and opposite trend: while Pt_{PD}-TiO₂ displays the strongest h⁺ signal and the weakest e⁻ signal, the opposite is observed for Pt_{LA}-TiO₂.

These results indicate that $\text{Pt}_{\text{PD}}\text{-TiO}_2$ yields an efficient electron transfer to Pt ⁵², diminishing the number of paramagnetic Ti^{3+} centers reducing the recombination rate (evinced by an increase in the signals related to the holes). However, the extrapolated results from Figure 6-8 evidence that not all the photogenerated electrons migrate to the Pt islands, but a significant number of these electrons remain trapped in the TiO_2 particles as Ti^{3+} ions. The same behavior was observed by Anpo and Takeuchi ²⁵, the Ti^{III} ESR signal intensity increase linearly with the illumination time by irradiation of the bare TiO_2 , while almost no change in the intensity with the Pt loaded one, indicating the fast transfer of the photogenerated electrons from the TiO_2 to the Pt islands.

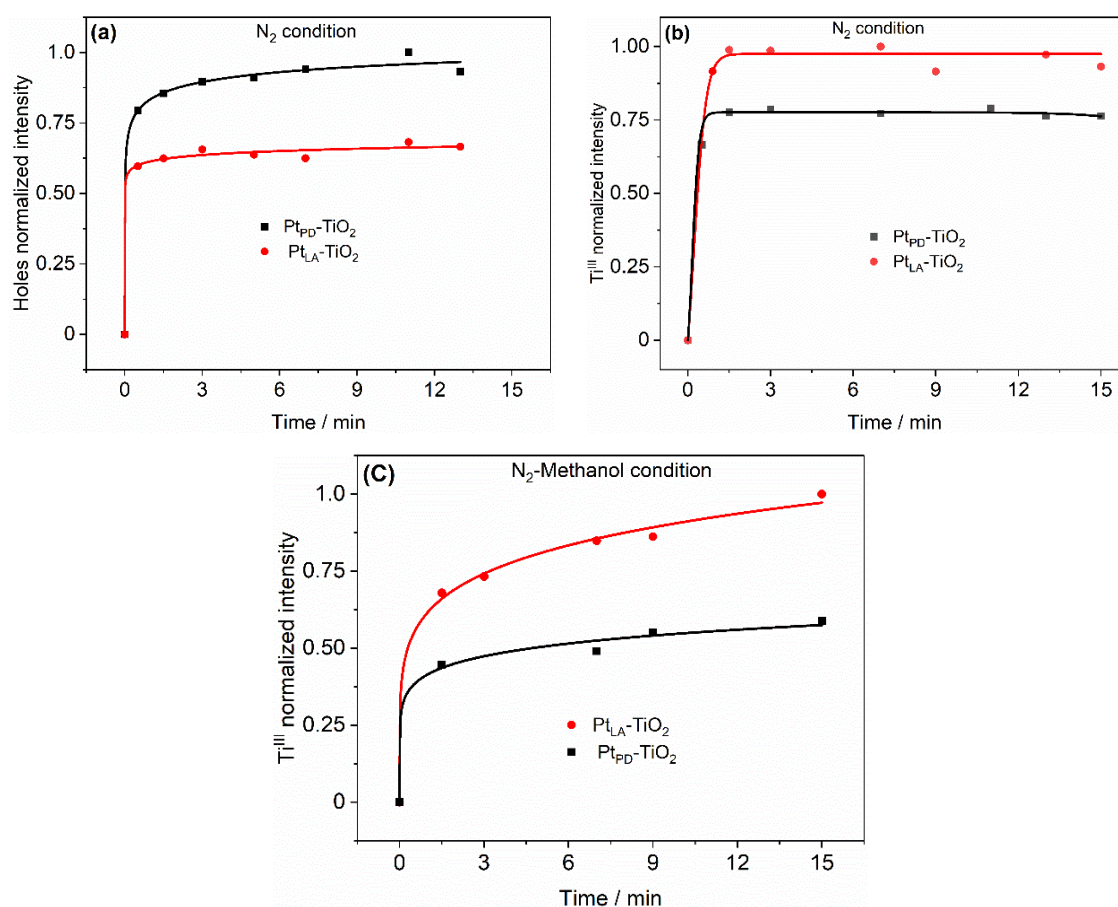


Figure 6-8: Growth of the EPR signal intensity of the trapped (a) holes (b) electrons in N_2 atmosphere, and (c) electrons in N_2 -methanol atmosphere, $\text{Pt}_{\text{PD}}\text{-TiO}_2$ (■, black) and $\text{Pt}_{\text{LA}}\text{-TiO}_2$ (●, red) during illumination, recorded at 77 K.

On the other hand, in the presence of the hole scavenger methanol (Figure 6-8), the electron signal in $\text{Pt}_{\text{PD}}\text{-TiO}_2$ is weaker than $\text{Pt}_{\text{LA}}\text{-TiO}_2$, confirming the rapid electron transfer to Pt in this sample. In the presence of methanol, its reaction with holes gives rise to the latter's disappearance and formation of a triplet signal of the $\cdot\text{CH}_2\text{OH}$ radical ⁶¹. Simultaneously, stronger signals of the trapped electrons were recorded, attributed to the current doubling

effect²⁰ caused by the injection of electrons of the $\bullet\text{CH}_2\text{OH}$ radical (Equations 6-23 and 6-26) into TiO_2 's conduction band. As a consequence of the greater number of electrons available from current doubling, the signal of trapped electrons increases in both samples in comparison with the experiments in the absence of methanol.

Furthermore, the analysis of the charge carrier dynamics of both platinumized TiO_2 materials employing TAS results in agreement with the EPR and the photocatalytic experiment results. In the N_2 atmosphere, a broad absorption maximum is observed around 520 nm for $\text{Pt}_{\text{PD}}\text{-TiO}_2$, whereas, $\text{Pt}_{\text{LA}}\text{-TiO}_2$ material exhibits a featureless, broad transient absorption (Figure 6-9 a and b). This suggests that $\text{Pt}_{\text{PD}}\text{-TiO}_2$ exhibits a higher number of surface trapped holes aided by the electron transfer to Pt than $\text{Pt}_{\text{LA}}\text{-TiO}_2$ ⁶². Indeed, the TAS measurements were performed in the wavelength range between 400 and 660 nm, where both trapped holes and electrons in the TiO_2 -based materials contribute signals to the transient absorption^{1, 62-64}. The photogenerated holes exhibit a transient absorption in the range of 430 – 550 nm, while trapped electrons do so at around 650 nm^{63, 64}. In particular, Bahnemann et al.¹³ reported that in the absence of any hole scavenger, Pt- TiO_2 sols reveal a broad absorption band with a maximum at 475 nm immediately after the laser pulse. The authors attributed this absorption to the positive holes that are trapped on the surface of the colloidal particles. The broadness of the band is related to the multiple possible electronic transitions from the valence band to the O^- trap and/or from the trap into the conduction band. The wide range of the detected holes signal in the presented study suggests that the holes are delocalized over different trapping sites, most likely near the surface, therefore, they are ready for participating in the reactions with the adsorbed organic compound. It is well reported that the valence band holes can be rapidly transported to the surface, where surface hole trap sites are formed on $\text{Ti-O}_s\text{H}$ and/or $\text{Ti-O}_s\text{-Ti}$. These surface trapped holes ($\text{Ti-O}_s\text{H}^{+\bullet}$ and/or $\text{Ti-O}_s^{+\bullet}\text{-Ti}$) are the main oxidants for any adsorbed electron donor.

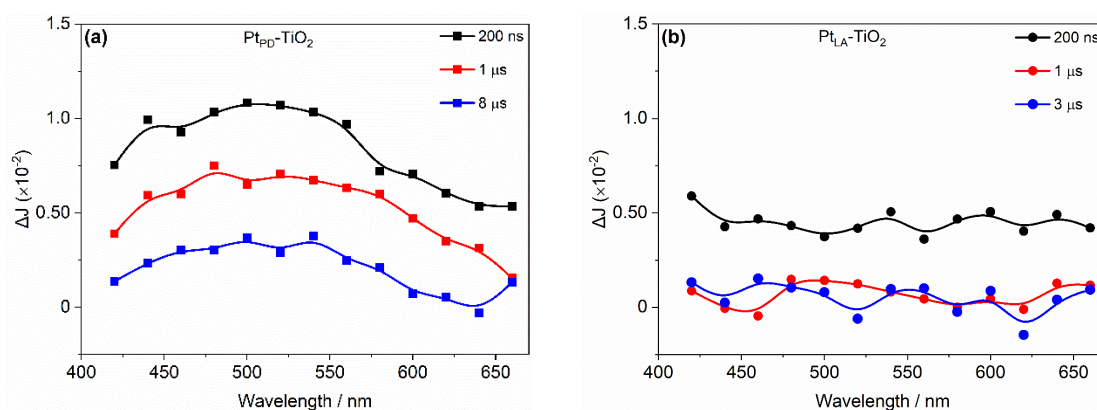


Figure 6-9: Transient absorption spectra measured for (a) $Pt_{PD}-TiO_2$ (■) and (b) $Pt_{LA}-TiO_2$ (●) under N_2 atmosphere at 200 ns (black line), 1 μs (red line), and 8 or 3 μs following the laser pulse.

Moreover, as shown in Chapter 4 (Figure 4-7), the initial intensity of the TA signals recorded at 520 nm upon excitation is significantly higher with a slower decay rate in $Pt_{PD}-TiO_2$. The lower rate constant (second-order reaction kinetic) displayed by $Pt_{PD}-TiO_2$ ($7.03 \times 10^5 \pm 0.23 \times 10^5 \text{ s}^{-1}$) comparing to $Pt_{LA}-TiO_2$ ($2.07 \times 10^7 \pm 0.76 \times 10^7 \text{ s}^{-1}$) indicates a slower recombination rate and increased lifespan of the electron-hole pairs^{63,64}. This can also be seen clearly in the TA spectra for both materials in Figure 6-9. While $Pt_{LA}-TiO_2$ displays the fast decay of the hole signal, the opposite is observed for $Pt_{PD}-TiO_2$. The signal of the trapped holes can be observed after 8 μs of $Pt_{PD}-TiO_2$ excitation, however, it was quenched within the first μs in $Pt_{LA}-TiO_2$. This again evidenced that the charge carrier recombination is slower in $Pt_{PD}-TiO_2$.

On the other hand, in presence of methanol (Figure 6-10), the $Pt_{PD}-TiO_2$ sample displays stronger absorption signals of electrons at 660 nm. Although it was expected to display smaller signals due to their migration to the Pt islands. This signal attributed to the formation of Ti^{+3} as a result of the reaction of Ti^{+4} ions with the photogenerated electrons formed by the laser excitation and also from the current doubling effect that occurs after the hole reaction with methanol to produce α -hydroxyl radicals (Equations 6-13 and 6-14), which in turn inject an electron into TiO_2 ^{45,59}. However, since the fractional ratio of Pt is very low on the surface of the TiO_2 , which is not enough to accept all the electrons, a part of these electrons will react with any available electron acceptor in the system like Ti^{+3} leading to such absorption signal. This indicates that (i) under conditions of a high density of photogenerated electrons (due to current doubling and due to the relatively high intensity of the laser pulse) a significant number of these electrons remain on the TiO_2 particles⁶⁵, and (ii) that even under these conditions, the $Pt_{PD}-TiO_2$ sample still seems to yield a lower recombination rate, as evidenced by the higher number of trapped electrons.

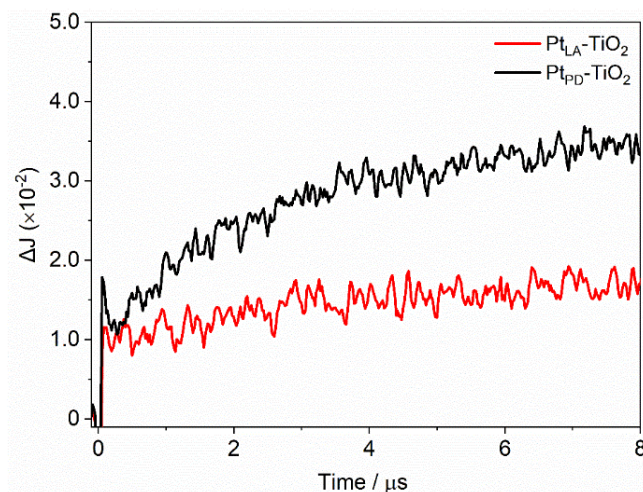


Figure 6-10: Transient absorption signals observed at 660 nm in N_2 – methanol atmosphere for Pt_{LA} - TiO_2 (●, red line) and Pt_{PD} - TiO_2 (■, black line) at 3.0 μs following the laser pulse.

A further aspect that is thought to influence the activity of Pt as a co-catalyst is the interaction between the Pt nanoparticles and the TiO_2 surface. In contrast with macroscopic crystals, nanocrystalline TiO_2 powders display a complex distribution of exposed facets. In particular, although often assumed to be composed mainly of (101) and (001) facets, surfaces of anatase nanoparticles have been shown to display large fractions of (100) or (111) facets⁶⁶. Besides, both computational modeling⁶⁷ and experimental studies⁶⁸ have shown that some surfaces are more adept than others for each hemi-reaction; in other words, while electrons seem to migrate to (101) facets, they avoid (001) facets, favoring reductions in the former and oxidation reactions in the latter. When preparing Pt_{LA} - TiO_2 , it is expected that the Pt NPs physically bind to TiO_2 homogeneously across all surfaces. Since Pt^0 in Pt_{LA} - TiO_2 is deposited non-specifically, a significant fraction of the islands may end up in contact with surfaces avoided by the photogenerated electrons, thus leading to an underutilization of the co-catalyst. A similar situation can be envisioned for the initial step of the photodeposition method, where the Pt precursor (here, H_2PtCl_6) may adsorb uniformly. However, once photodeposition starts, the precursor reduction (and Pt^0 deposition) will preferentially occur on those facets that facilitate electron transfer. This means that once formed, Pt islands will be in close contact with the surfaces that have a strong tendency to release electrons, thus, enhancing the charge carrier transfer and reducing the recombination rate.

6.5 Mechanism of Photocatalytic Reforming of Naphthalene

To this day, the trapped hole's nature is still controversial ^{27, 69-71}. According to Ohtani ⁷², the positive hole is defined as a defect of an electron. Considering that the surface of the photocatalyst is covered with water molecules (chemically or physically adsorbed), the hole is not only produced by a photoinduced band-to-band transition in solid materials, but also it can be a hydroxyl radical which is a one-electron deficient hydroxyl anion ². In the solution, this positive hole, thus, passing through this water layer into the solution as a hydroxyl radical or its protonated or deprotonated species (Figure 6-11) ⁷².

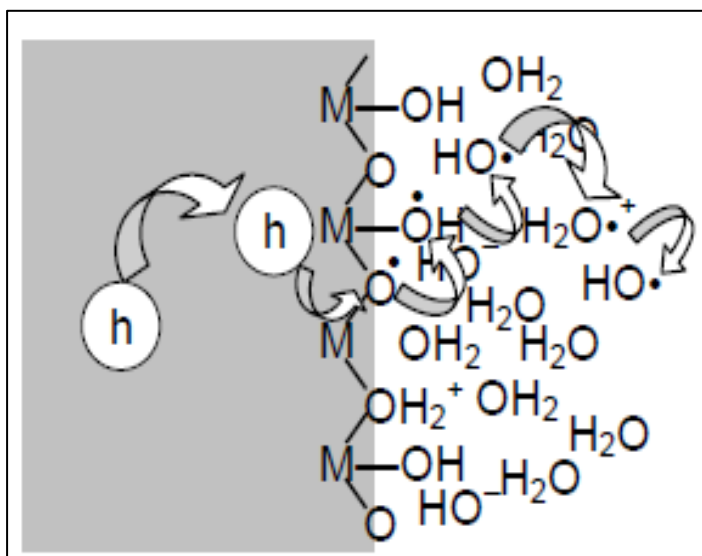


Figure 6-11: Transfer of positive holes from the bulk of a photocatalyst through the interface to an aqueous solution phase. Surface-adsorbed and free (hydrated) hydroxyl radicals and their derivatives can be a possible form of positive holes. Reprinted with permission from reference 72. Copyright 2013 Elsevier B.V.

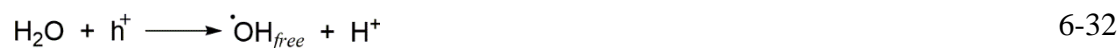
Turchi and Ollis ⁷³ proposed four possible mechanisms for the degradation of organic water pollutants (RH_2) on the TiO_2 photocatalyst. All of these mechanisms are based on the attack of the organic reactant, however, the reaction of free photogenerated holes with specifically adsorbed organic species was not considered. According to those authors: (1) the adsorbed $\text{OH}^{\bullet}_{\text{ads}}$ at terminal Ti^{+4} atoms react with adsorbed $\text{RH}_2(\text{ads})$; (2) the free $\text{OH}^{\bullet}_{\text{free}}$ (non-adsorbed) react with $\text{RH}_2(\text{ads})$; (3) the adsorbed $\text{OH}^{\bullet}_{\text{ads}}$ react with non-adsorbed RH_2 ; and (4) $\text{OH}^{\bullet}_{\text{free}}$ react with dissolved RH_2 .

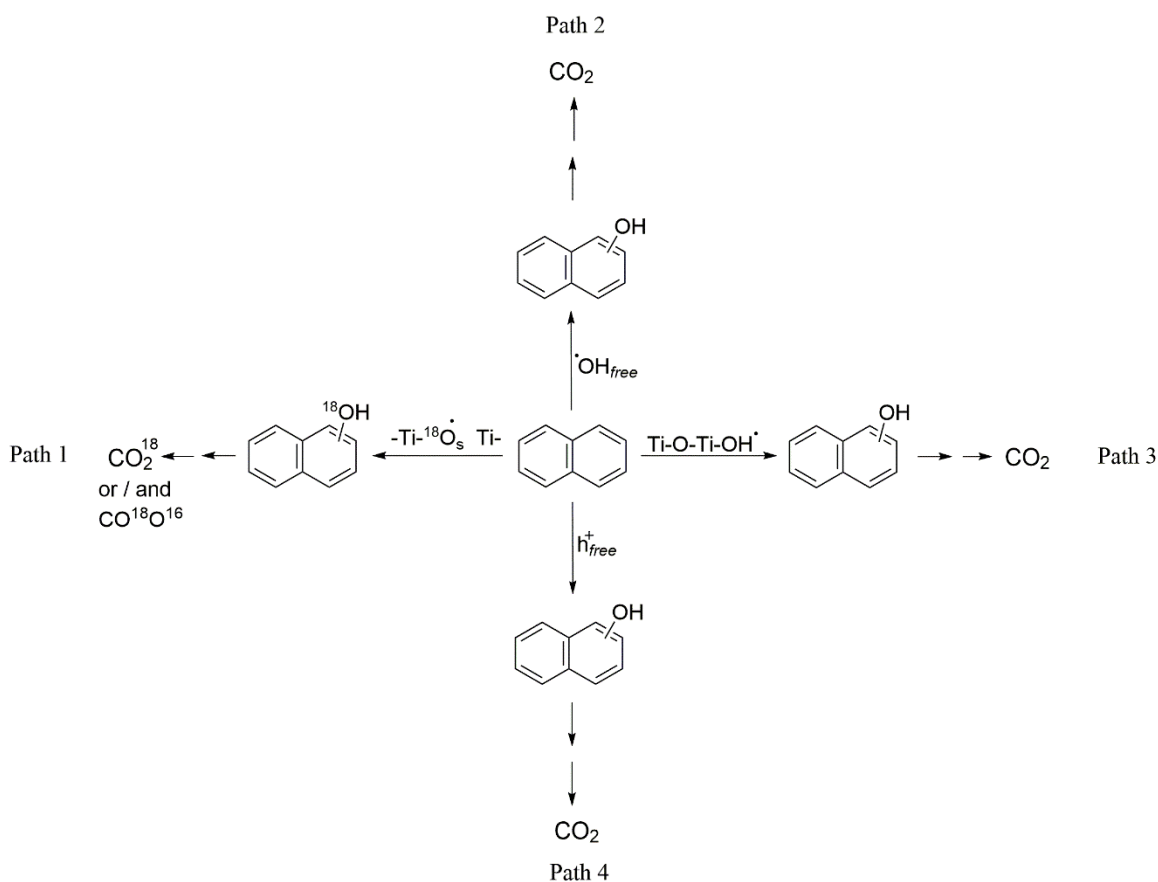
In the mechanism of the photocatalytic reaction, although OH^{\bullet} has been usually adopted as the most important active species in the oxidative half-reaction ^{69, 74}, other reports confirmed its limited contribution in the oxidation process ^{70, 71}. Indeed, most of the

investigations dealing with the $\cdot\text{OH}$ as the main oxidant in the photocatalytic reactions have assumed its involvement in the oxidation mechanism without any reported mechanistic evidence⁷⁴. However, the detection of hydroxylated reaction products and the kinetic isotope effects were considered as evidence to support one or another form of $\cdot\text{OH}$ as the main oxidative species⁷³. Recently, besides photogenerated holes and hydroxyl radicals as active species in photocatalytic processes, the role of bridging oxygen radicals at the TiO_2 surface (O_s) has been discussed^{28,75}. Holes could be trapped by bridging oxygen atoms on the TiO_2 surface ($\equiv\text{Ti}-\text{O}_s-\text{Ti}\equiv$) to produce the active species oxygen radical ($\equiv\text{Ti}-\text{O}_s\cdot-\text{Ti}\equiv$), which ultimately can be incorporated into the reaction products, creating oxygen vacancies that are subsequently healed by water. In fact, isotope labeling of the TiO_2 photocatalyst is a useful strategy to evaluate such a mechanism. Montoya et al.^{71, 75} observed $\text{C}^{16}\text{O}^{18}\text{O}$ evolution during the photocatalytic oxidation of benzene over Ti^{18}O_2 in anaerobic conditions. The authors considered the participation of surface-trapped holes ($-\text{O}_s\cdot / -\text{O}_s^-$) and the incorporation of surface oxygens into the oxidation products ($\text{C}^{16}\text{O}^{18}\text{O}$) as proof for the main role played by those species in TiO_2 -assisted photocatalytic processes.

In Chapter 5, the photocatalytic degradation of naphthalene coupled with the production of molecular hydrogen was presented. Applying a combination of chromatographic and mass spectroscopic techniques showed that the aromatic ring hydroxylation is the main reaction of phototransformation “photooxidation” of naphthalene. However, the pathway of naphthalene hydroxylation, and what is /are the oxidative species(es) responsible for its photooxidation are not clear.

Thus, many possible pathways for photoinduced reforming of naphthalene, involving different reactive species on the surface of photoexcited Pt/TiO_2 (Equations 6-1, and 6-32 to 6-34), have been tested to decide and determine the most likely path, by many different mechanistic techniques (Scheme 6-1).





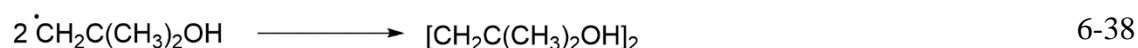
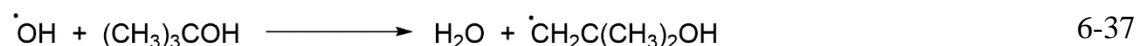
Scheme 6-1: Possible pathway for initiation of the photocatalytic oxidation of naphthalene.

As shown in Figure 4-4, Chapter 5, the use of Ti^{18}O_2 during the photocatalytic reforming of naphthalene did not result in a significant evolution of ^{18}O -enriched CO_2 (Scheme 6-1, path 1).

Civis and co-workers⁷⁶ studied the photocatalytic decomposition of formic acid on the surface of Ti^{18}O_2 by the means of Fourier-transform infrared absorption spectroscopy and found that the process does not lead to the evolution of either $\text{C}^{16}\text{O}^{18}\text{O}$ or C^{18}O_2 . On the contrary, Montoya and co-workers^{71, 75} did observe $\text{C}^{16}\text{O}^{18}\text{O}$ evolution during the photocatalytic oxidation of benzene over Ti^{18}O_2 in anaerobic conditions. Since benzene and naphthalene belong to the same kind of organic compounds, namely aromatic hydrocarbons, it could be deduced that both of them are photooxidized in the same manner. However, naphthalene seems to be photocatalytically oxidized by a different mechanism. This can be argued from several angles. First, a significant production of 1,1'-binaphthalene was observed (Equation 6-21), which cannot be accounted for by the bridging oxygen mechanism. Second, the one-electron standard redox potentials for the oxidation of benzene and naphthalene in acetonitrile are 2.65 and 1.85 V vs. NHE respectively⁷⁷. Thus,

neglecting the slight variation in aqueous solution, the one-electron oxidation of naphthalene by its direct reaction with holes (valence band potential: 2.68 V vs. NHE at pH 7) ⁷⁸ is thermodynamically favored with respect to the same reaction for benzene. Hence, as long as the reaction does not fall into the Marcus inverted region, it will be significantly faster. The observation by Fox et al. of increasing photocatalytic oxidation rates for substituted naphthalene's as the exergonicity increased supports this notion ⁷⁹. Accordingly, the abstraction of an electron from naphthalene by the valence band hole, which has a more positive potential, is likely to take place. And third, as shown in Figure 6-3, naphthalene adsorbed significantly on the TiO₂ surface, unlike benzene ⁸⁰. Indeed, temperature programmed desorption measurements over rutile single crystals have shown a significantly stronger binding by naphthalene ⁸¹. Notably, the direct-indirect hole transfer model (DT-IT) of Salvador et al ⁸², proposes that the specific pathway depends on the degree of electronic interaction of the dissolved molecules with the semiconductor surface. The relatively strong interaction of naphthalene with TiO₂ leads us to conjecture that, although both mechanisms may be operative, in contrast with benzene, the direct transfer of holes to naphthalene is favored with respect to the indirect, bridging oxygen mediated transfer ⁸⁰.

Furthermore, as shown in *Chapter 5*, the photocatalytic reforming of naphthalene was performed in the presence of the scavengers potassium iodide (KI), and 2-methylpropan-2-ol ((CH₃)₃COH, TBA). The iodide ion is an excellent hole scavenger. Once adsorbed on the TiO₂ it can act as an electron donor and easily capture the photogenerated hole (Equations 6-35 and 6-36). While the short aliphatic alcohols, such as TBA, are weakly adsorbed to the TiO₂ surface in aqueous media, therefore, they are usually used as hydroxyl radical ([•]OH) quenchers in the bulk (Equations 6-37 and 6-38) ^{83, 84}.



The complete inhibition of naphthalene conversion in the presence of KI, reflects the importance of the hole. On the other hand, the addition of TBA does not affect the photocatalytic process since it yields a virtually identical kinetic profile to naphthalene

conversion in the absence of any scavenger, highlighting the limitation role of $\cdot\text{OH}_{\text{free}}$ in the oxidation reaction. The results of these experiments showed that $\cdot\text{OH}_{\text{free}}$ radicals do not play an important role in the initial reaction of naphthalene (Scheme 6-1, path 2).

Complementarily, the kinetic profiles for the formation of naphthalen-1-ol and naphthalen-2-ol during the previous experiments are consistent with those of naphthalene degradation: while the addition of TBA does not significantly affect the formation of naphthalenols, the addition of KI hinders naphthalene degradation almost completely, confirming the limitation of the free hydroxyl radical in the process. Miller and Olejnik¹⁰, as well as Beltran et al.⁸⁵, showed that neither TBA nor bicarbonate ions, respectively, affect the degradation rate of different PAH compounds in the presence of hydroxyl radicals in homogeneous systems. Therefore, they concluded that the photooxidation of these compounds was initiated via the formation of a radical cation, without involving free hydroxyl radicals. Accordingly, the presented results in this study are in good agreement with their findings, despite the difference between both types of systems. Although, it is not feasible and scientifically insignificant to propose the mechanism of the photocatalytic reaction only based on such scavenger experiments, since the hydroxyl radical is involved in many forms of trapped holes. However, many previous reports have adopted that⁸⁶. Alam et al.⁸⁷ proposed the mechanism of the photocatalytic degradation of methylene blue (MB) dye by adding different scavengers during the photocatalytic process. They observed a strong inhibition in MB degradation in the presence of isopropyl alcohol, while, no effects were observed by the addition of the EDTA (as a hole quencher), and benzoquinone (BQ) (as a quencher of $\cdot\text{O}_2^-$). Accordingly, they proposed a photocatalytic reaction mechanism assuming that $\cdot\text{OH}$ is the main reactive species in the system.

The involvement of $\cdot\text{OH}_{\text{free}}$ in photocatalytic reactions is the subject of a long-standing debate. Recent work for Nosaka has challenged this idea, suggesting that the irradiation of anatase TiO_2 does lead to the formation of $\cdot\text{OH}_{\text{free}}$, although this is not the case for the rutile polymorph⁸⁸.

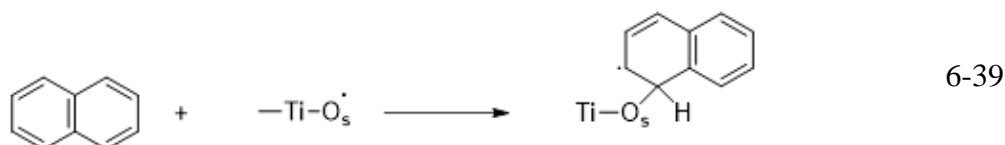
Usually, to obtain additional insights into the role of $\cdot\text{OH}_{\text{free}}$ in the aqueous photocatalytic process, the spin trapping reagents, such as DMPO (5,5-dimethyl-1-pyrroline-N-oxide) were used to detect OH radicals⁶. As shown in chapter 5, the employing of in-situ spin trapping - EPR spectroscopy during the naphthalene photoreforming experiments in the presence of either TBA or KI, and DMPO was helpful to obtain additional insights

regarding the role of $\cdot\text{OH}_{\text{free}}$ in our system. Upon irradiation of the tested samples under all conditions, a signal attributable to the DMPO-OH adduct was evolved. The production of the $\cdot\text{OH}$ adduct in the absence of molecular oxygen, providing evidence in favor of their formation from the oxidation of water⁸⁹. In the presence of TBA, however, the adduct signal shows a decrease of 35 % and vanished within 90 sec comparing to more than 240 sec in its absence (naphthalene and DMPO alone), confirming TBA's $\cdot\text{OH}$ scavenging properties. Nevertheless, this lower quantity of available $\cdot\text{OH}$ radicals does not impact naphthalene's degradation (*as mentioned previously*), providing proof against a degradation mechanism initiated by the attack of $\cdot\text{OH}_{\text{free}}$. The addition of KI to the system, on the other hand, practically nullifies the adduct formation, as could be expected from the efficient hole consumption by this scavenger. Regarding the role of holes, although these results confirm their importance, the direct hole (h^+) transfer to naphthalene or its indirect oxidation via surface-trapped holes ($-\text{OH}_s$) can't be distinguished.

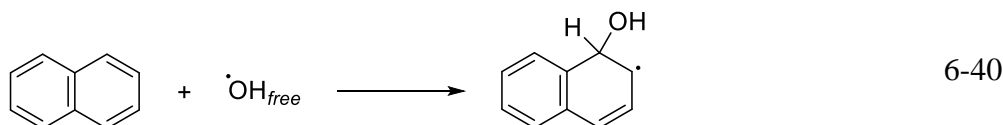
Moreover, utilizing an electrochemical degradation process, Li and Goel⁹⁰ showed that naphthalene degradation was not affected by the presence of acetone and methanol as an $\cdot\text{OH}$ competitor, suggesting that naphthalene degradation occurred as a result of direct electron transfer. Thus, they excluded the indirect oxidation via the $\cdot\text{OH}$. As presented in Chapter 5, the experimental data were combined with the computational theoretical calculations by applying the simple model of Luo et al.⁹¹ to determine the Gibbs free energy (ΔG°) for the single electron transfer reaction from benzene, naphthalene, and anthracene to $\cdot\text{OH}$ to produce the corresponding radical cation and hydroxide ions. The calculated values were +24.6, +1.7, and -21.5 kcal mol⁻¹, respectively. Thus, it is obvious that by increasing the number of aromatic rings in the organic compound the reaction becomes more spontaneous. Hence, naphthalene has a higher tendency to react with $\cdot\text{OH}$ forming a radical cation, rather than an adduct, as is the case for benzene.

To summarize the above discussion in this section, the following paths for the photooxidation of naphthalene can be excluded.

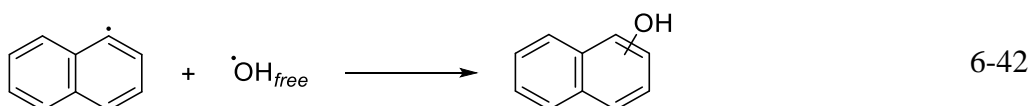
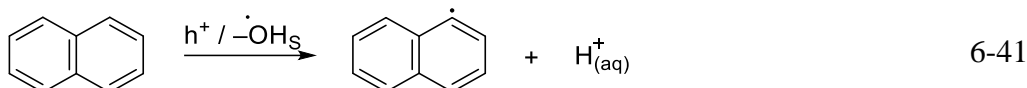
- 1- The photocatalytic reforming of naphthalene in the presence of Ti^{18}O_2 did not result in a significant evolution of ^{18}O -enriched CO_2 , suggesting that lattice oxygen atoms are not incorporated into the reaction (Equation 6-39).



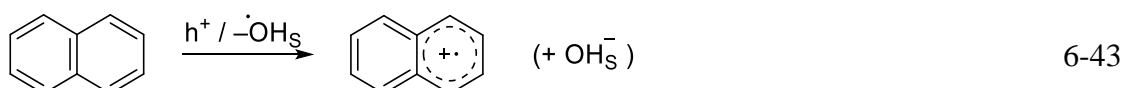
- 2- The EPR experiments and the associated photocatalytic runs in the presence of scavengers postulated that $\cdot\text{OH}_{\text{free}}$ radicals do not play an important role in the initial reaction of naphthalene (Equation 6-40).



- 3- Besides that, the generation of naphthyl radical through hydrogen abstracting reaction via indirect hole transfer by reaction of naphthalene with surface trapped holes ($-\text{OH}_\text{s}$) was excluded also. If this occurs, a strong effect from the presence of $\cdot\text{OH}_{\text{free}}$ should be expected, since they would promptly react with the naphthyl radicals to yield naphthalenol, however, the EPR experiment excluded this effect (Equation 6-41 and 6-42).



In consequence, the only possible path for naphthalene's degradation is initiated either by a direct hole transfer or indirectly via its reaction with the surface trapped holes ($-\text{OH}_\text{s}$) via a single electron transfer (SET) leading to the production of a radical cation (Equation 6-43).



Indeed, applying the transient absorption spectroscopy in the presented investigation in chapter 5 confirmed the formation of a naphthalene radical cation. Various methods were reported for the production of the radical cations of organic molecules in different media. Pulse radiolysis of naphthalene in different solvents produced a transient species which was assigned to naphthalene radical cation ($\text{NP}^{+\cdot}$) on the basis of its electronic spectrum⁹². Besides, different chemical or electrochemical attempts to prepare salts of naphthalene radical cation in inert media result exclusively in the formation of the dimer cation salts⁹³.

The three distinct bands that can be seen in the TA spectra, Figure 5-7, which was obtained after the laser excitation of anaerobic Pt-TiO₂ slurries (water/acetonitrile) in the presence

of naphthalene have been attributed to transient species related to naphthalene, as follows: (i) The absorption band at 685 nm has been assigned to the naphthalene radical cation in homogeneous photolysis experiments.⁹⁴ (ii) The absorption centered at 580 nm is related to dimer radical cation $(NP)_2^{\bullet+}$ formed after the reaction of $NP^{\bullet+}$ with a second naphthalene molecule, as reported by Gschwind et al.,⁹⁴ and Steenken⁹⁵. (iii) Additionally, the absorption band at 600 nm has been attributed to the electronic interactions between $NP^{\bullet+}$ polyaromatic radical cations and the TiO_2 surface, which was observed due to the red-shifted with respect to the free species⁹⁶.

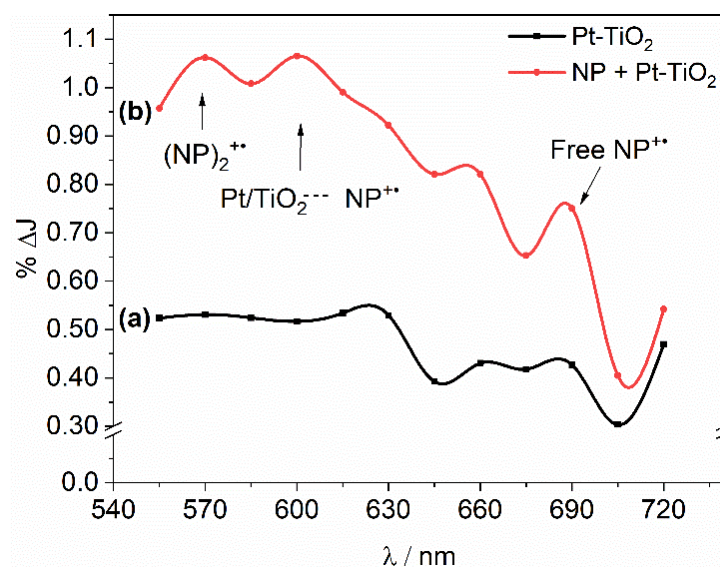
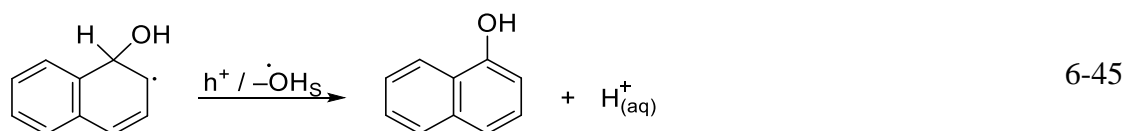
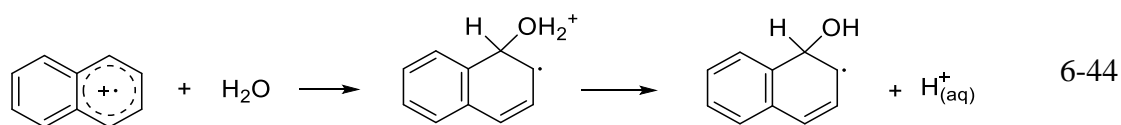


Figure 6-12. Diffuse reflectance transient absorption spectroscopy spectra obtained 300 ns after the laser excitation (355 nm , 6 mJ pulse^{-1}) of anaerobic $Pt-TiO_2$ slurries in the presence of (a) a (1:1) water/acetonitrile mixture and (b) naphthalene (NP) in the same solvent.

Moreover, in coincidence with the reported reactions of benzene with both persulfate and $Pt-TiO_2$ in aqueous media^{27, 97}, the formed naphthalene radical cation swiftly reacts with water to form an OH adduct (Equation 6-44)⁹⁸. The adduct itself reacts in a further oxidation step (Equation 6-45) to form (as exemplified) naphthalen-1-ol, or naphthalene-2-ol.



As exhibited previously in different parts of this thesis, the photogenerated electrons have a strong tendency to accumulate in the platinum particles. Once there, they can reduce protons to hydrogen atoms (Equation 6-29), which upon dimerization form H_2 (Equation 6-30).

However, a question arises: what is the origin of the reduced protons?

Photocatalytic reforming of naphthalene by using solvents with variable $H_2O - D_2O$ compositions and deuterated naphthalene led to an isotopic composition of the evolved hydrogen (H_2 , HD, and D_2) matching those of the solvent, and not that of naphthalene. While, analyzing the reaction rates revealed that water (but not naphthalene) is apparently to be involved in the rate-determining step of the reaction. The first evident effect of replacing H_2O with D_2O is a progressive decrease in the total amount of evolved gases (H_2 and HD) as the D_2O fraction increases (Figure 6-13).

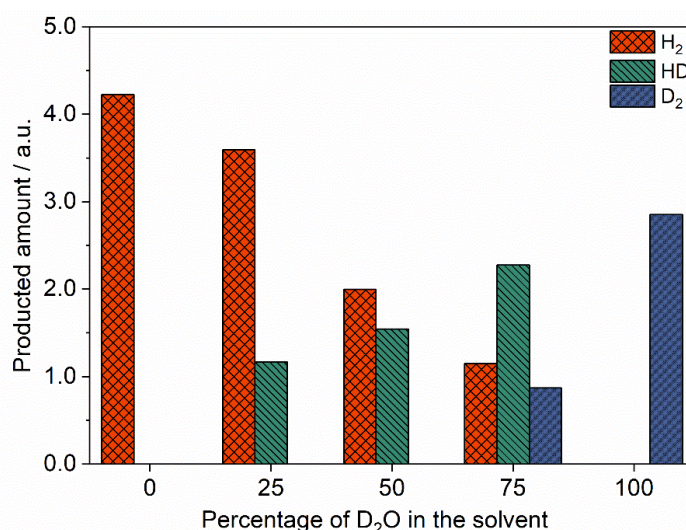


Figure 6-13: Isotopic distribution of the evolved gases (H_2 , HD, and D_2) from the photocatalytic reforming of aqueous naphthalene over Pt-UV100 a) employing different D_2O/H_2O compositions. Conditions: reaction volume, 15 mL; [Naphthalene] = $235 \mu\text{mol L}^{-1}$; [catalyst] = 1 g L^{-1} ; $T = 25 \text{ }^\circ\text{C}$; illumination with simulated solar light. Note: Since the setup was operated at the same sensitivity factor for all gases, the observed signals are directly comparable.

Remarkably, neither H_2 nor HD are detected when using 100% D_2O . Similar results have been previously interpreted as proof that water (and not the sacrificial electron donor) is the source of H_2 in the photocatalytic reforming of methanol⁵. However, proton exchange reactions in aqueous media are extremely fast, and thus it is also possible that the hydrogen atoms originate from the sacrificial donor. Since the solvent's isotopic species are present in an overwhelming majority, the exchange reaction could mask the real origin of the atoms.

On the other hand, recent reports have shown that in some photocatalytic systems the production of H₂ from sacrificial electron donors can be sufficiently fast and spatially localized to avoid proton exchange, leading to isotopic compositions of the gases matching those of the sacrificial donor⁹⁹. From our analysis, we can conclude that such effects are not operative in the present system.

Considering the two extreme cases, pure H₂O and pure D₂O, the ratio between the amounts of evolved gases after 4h is ~1.3. Similar behavior has been observed for the photocatalytic reforming of formaldehyde¹⁰⁰ and benzene²⁸ over platinized TiO₂ and interpreted on the basis of a hindered production of $\cdot OH$ radicals when using D₂O, which limits the rate of the reaction. In the presented case, however, the effect of these radicals was ruled out since they didn't play an important role in naphthalene's oxidation as demonstrated previously in this section. Post and Hiskey¹⁰¹, as well as other researchers¹⁰², have reported that the D₂ overvoltage in D₂O at 25 C° was found to be about 50 to 87 mV greater than the H₂ overvoltage in H₂O. Therefore, the observed kinetic isotope effect responds to a rate-determining step related to proton reduction. Additionally, a very close agreement between naphthalene and deuterated naphthalene in the ratio between the amounts of evolved gases, and the coincides of the total amount of evolved gases in both solvents was observed (Figure 6-14). This suggested that, in contrast with water, hydrogen abstraction from naphthalene is not involved in the rate-determining step of the reaction. Similar conclusions have been drawn for the photoreforming of aqueous benzene over platinized TiO₂²⁸.

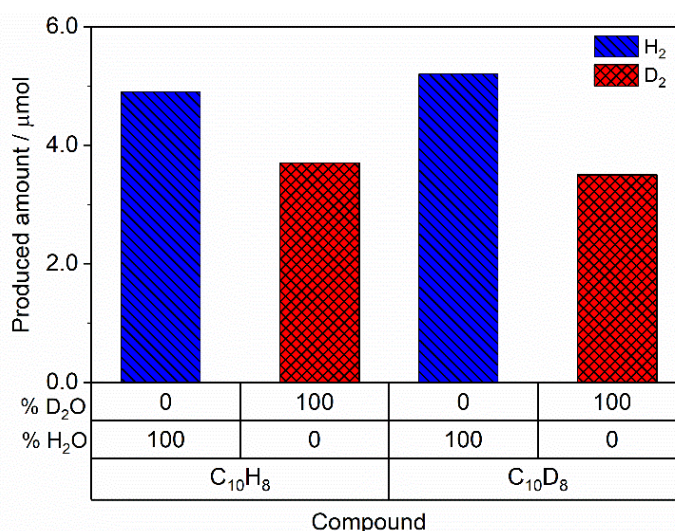


Figure 6-14. Isotopic distribution of the evolved gases (H₂, and D₂) from the photocatalytic reforming of aqueous naphthalene and deuterated naphthalene over Pt-UV100 employing D₂O and H₂O. Conditions: reaction volume, 15 mL; [Naphthalene] = 235 $\mu\text{mol L}^{-1}$; [catalyst] = 1 g L⁻¹; T = 25 °C; illumination with simulated solar light.

6.6 Conclusions

As a general conclusion, the results presented in this thesis provide a better understanding of the principle of the photocatalytic degradation of naphthalene, the most abundant polycyclic aromatic hydrocarbon in water, coupled with the production of molecular hydrogen. Although naphthalene can be slowly degraded (photolysis) in water under anaerobic conditions through the simulated sunlight irradiation, the presence of the photocatalyst TiO_2 enhances the rate of its degradation. However, the evolution of molecular hydrogen was not observed in both processes. The evolution of H_2 gas after platinization of the TiO_2 reveals the essential role of the Pt nanoparticles to decrease the overpotential of H_2 evolution. Despite the higher photocatalytic activity of the pristine P25 for removal of naphthalene, the 0.5wt.% Pt-UV100 exhibits a higher photocatalytic activity toward the H_2 formation and naphthalene conversion under solar radiation compared to all other pristine and platinized photocatalysts. It is shown in this study that, in the presence of the hole scavenger naphthalene, Pt nanoparticles on the surface of UV100 act as electron scavengers, which scavenge the photogenerated electrons, thereby retarding the electron-hole recombination and enhancing hydrogen production rates. On contrary, Pt nanoparticles on the surface of P25 act as recombination centers for the photogenerated charge carrier leads to decrease the photocatalytic activity.

Although this study has shown that naphthalene can be efficiently removed from the system and producing H_2 and CO_2 during its photoreforming, however, its hazardous effect was not completely eliminated, since it was converted to less harmful compounds, mainly to 1-naphthalenol, 2-naphthalenol, 1,4-naphthalendione, and other hydroxylated compounds. There are, indeed, several factors affecting the H_2 formation during the photoreforming of naphthalene. The combination of the photocatalytic experiments with chromatographic and mass spectroscopic techniques reveals that the inhibition of the H_2 formation and naphthalene conversion rates during the photocatalysis process is ascribed to the adsorption of the high stable photoformed products on the surface of the photocatalyst.

Electron paramagnetic resonance and transient absorption spectroscopy measurements evinced that the interfacial transfer and trapping of photogenerated charges carrier are influenced by the deposition of Pt and the method to do so. The deposition of a higher Pt content on the TiO_2 surface than the optimal ratio (0.5 wt.%) dramatically inhibits the H_2 formation and naphthalene conversion. Complementary, although the higher photocatalytic

activity of the Pt-UV100 that was prepared via the photodeposition method compared to the one prepared by the physical mixing method could be explained by the formation of smaller average Pt particle size that influences its properties. Based on the EPR and TAS experiments in the absence of electron or hole scavengers, it was shown in this study that the main factor governing the high activity is the formation of a strong interaction between the Pt nanoparticles and the TiO₂ surface during the photodeposition process. This could be aided by the selective photodeposition of Pt nanoparticles on crystalline facets with a high tendency for electron transfer.

Since there are different reactive species that can be formed on the surface of photoexcited Pt-TiO₂ and involved in the photoinduced reforming of naphthalene, this study elucidates a systematic method to get more insight into the most possible reaction mechanism of naphthalene reforming among several possible pathways. The use of Ti¹⁸O₂ did not lead to a significant evolution of ¹⁸O-enriched CO₂, suggesting that lattice oxygen atoms are not incorporated into this product. The performing of the photocatalytic and spin trapping experiments in the presence of the hole and hydroxyl radical scavengers evinced that free hydroxyl radical was not involved in the hydroxylation of naphthalene, whereas only the photogenerated holes play a significant role in this process. Moreover, experiments using solvents with variable H₂O - D₂O compositions and deuterated naphthalene led to evolved H₂ isotopologues which match those of the solvent and not that of naphthalene. The analysis of the reaction rates reveals that water (but not naphthalene) appears to be involved in the rate-determining step of the reaction. Ultimately, by employing the transient absorption spectroscopy, the radical cations of naphthalene and its dimer as short-lived species in the nanosecond time scale, in addition to their interaction with the Pt/TiO₂ surface was detected.

Based on the results presented in Chapter 5 of this thesis, the most probable reaction route is the formation of naphthalene radical cation via SET from naphthalene, scavenging the photogenerated hole in the Pt/TiO₂ surface. This carbocation radical swiftly reacts with water to form an OH adduct which is subsequently oxidized by another hole to produce the hydroxylated naphthalene. Concomitantly, the photogenerated electrons reduced the proton originating mainly from water to molecular hydrogen.

6.7 References

1. Schneider, J.; Matsuoka, M.; Takeuchi, M.; Zhang, J.; Horiuchi, Y.; Anpo, M.; Bahnemann, D. W., Understanding TiO₂ photocatalysis: Mechanisms and materials. *Chem. Rev.* **2014**, *114* (19), 9919-86.
2. Rabani, J.; Goldstein, S., Mechanisms of reactions induced by photocatalysis of titanium dioxide nanoparticles. In *Environmental Photochemistry Part III*, Bahnemann, D. W.; Robertson, P. K. J., Eds. Springer Berlin Heidelberg: Berlin, Heidelberg, 2013; pp 115-157.
3. Ohtani, B., Photocatalysis A to Z—What we know and what we do not know in a scientific sense. *J. Photochem. Photobiol., C* **2010**, *11* (4), 157-178.
4. Puga, A. V., Photocatalytic production of hydrogen from biomass-derived feedstocks. *Coord. Chem. Rev.* **2016**, *315*, 1-66.
5. Kandiel, T. A.; Ivanova, I.; Bahnemann, D. W., Long-term investigation of the photocatalytic hydrogen production on platinumized TiO₂: an isotopic study. *Energy Environ. Sci.* **2014**, *7* (4), 1420-1425.
6. AlSalka, Y.; Al-Madanat, O.; Curti, M.; Hakki, A.; Bahnemann, D. W., Photocatalytic H₂ evolution from oxalic acid: Effect of cocatalysts and carbon dioxide radical anion on the surface charge transfer mechanisms. *ACS Appl. Energy Mater.* **2020**, *3* (7), 6678-6691.
7. Kandiel, T. A.; Dillert, R.; Robben, L.; Bahnemann, D. W., Photonic efficiency and mechanism of photocatalytic molecular hydrogen production over platinumized titanium dioxide from aqueous methanol solutions. *Catal. Today* **2011**, *161* (1), 196-201.
8. Galińska, A.; Walendziewski, J., Photocatalytic water splitting over Pt-TiO₂ in the presence of sacrificial reagents. *Energy & Fuels* **2005**, *19* (3), 1143-1147.
9. Fasnacht, M. P.; Blough, N. V., Mechanisms of the aqueous photodegradation of polycyclic aromatic hydrocarbons. *Environ. Sci. Technol.* **2003**, *37* (24), 5767-72.
10. Miller, J. S.; Olejnik, D., Photolysis of polycyclic aromatic hydrocarbons in water. *Water Res.* **2001**, *35* (1), 233-243.
11. Vialaton, D.; Richard, C.; Baglio, D.; Paya-Perez, A.-B., Mechanism of the photochemical transformation of naphthalene in water. *J. Photochem. Photobiol., A* **1999**, *123* (1), 15-19.
12. Linsebigler, A. L.; Lu, G.; Yates Jr, J. T., Photocatalysis on TiO₂ surfaces: Principles, mechanisms, and selected results. *Chem. Rev.* **1995**, *95* (3), 735-758.
13. Bahnemann, D.; Henglein, A.; Lilie, J.; Spanhel, L., Flash photolysis observation of the absorption spectra of trapped positive holes and electrons in colloidal titanium dioxide. *J. Phys. Chem.* **1984**, *88* (4), 709-711.
14. Kozlova, E. A.; Lyubina, T. P.; Nasalevich, M. A.; Vorontsov, A. V.; Miller, A. V.; Kaichev, V. V.; Parmon, V. N., Influence of the method of platinum deposition on activity and stability of Pt/TiO₂ photocatalysts in the photocatalytic oxidation of dimethyl methylphosphonate. *Catal. Commun.* **2011**, *12* (7), 597-601.
15. Yamakata, A.; Ishibashi, T.-a.; Kato, H.; Kudo, A.; Onishi, H., Photodynamics of NaTaO₃ catalysts for efficient water splitting. *J. Phys. Chem. B* **2003**, *107* (51), 14383-14387.

16. Patsoura, A.; Kondarides, D. I.; Verykios, X. E., Enhancement of photoinduced hydrogen production from irradiated Pt/TiO₂ suspensions with simultaneous degradation of azo-dyes. *Appl. Catal., B* **2006**, *64* (3-4), 171-179.
17. Lakshminarasimhan, N.; Bae, E.; Choi, W., Enhanced photocatalytic production of H₂ on mesoporous TiO₂ prepared by template-free method: Role of interparticle charge transfer. *J. Phys. Chem. C* **2007**, *111* (42), 15244-15250.
18. Wang, D.; Liu, Z. P.; Yang, W. M., Revealing the size effect of platinum cocatalyst for photocatalytic hydrogen evolution on TiO₂ support: A DFT study. *ACS Catal.* **2018**, *8* (8), 7270-7278.
19. Lair, A.; Ferronato, C.; Chovelon, J.-M.; Herrmann, J.-M., Naphthalene degradation in water by heterogeneous photocatalysis: An investigation of the influence of inorganic anions. *J. Photochem. Photobiol., A* **2008**, *193* (2-3), 193-203.
20. Hurum, D. C.; Agrios, A. G.; Gray, K. A.; Rajh, T.; Thurnauer, M. C., Explaining the enhanced photocatalytic activity of Degussa P25 mixed-phase TiO₂ using EPR. *J. Phys. Chem. B* **2003**, *107* (19), 4545-4549.
21. Scanlon, D. O.; Dunnill, C. W.; Buckeridge, J.; Shevlin, S. A.; Logsdail, A. J.; Woodley, S. M.; Catlow, C. R.; Powell, M. J.; Palgrave, R. G.; Parkin, I. P.; Watson, G. W.; Keal, T. W.; Sherwood, P.; Walsh, A.; Sokol, A. A., Band alignment of rutile and anatase TiO₂. *Nat. Mater.* **2013**, *12* (9), 798-801.
22. Sun, B.; Vorontsov, A. V.; Smirniotis, P. G., Role of platinum deposited on TiO₂ in phenol photocatalytic oxidation. *Langmuir* **2003**, *19* (8), 3151-3156.
23. Lindner, M.; Theurich, J.; Bahnemann, D. W., Photocatalytic degradation of organic compounds: Accelerating the process efficiency. *Water Sci. Technol.* **1997**, *35* (4), 79-86.
24. Colon, G.; Hidalgo, M. C.; Navio, J. A., Photocatalytic deactivation of commercial TiO₂ samples during simultaneous photoreduction of Cr(VI) and photooxidation of salicylic acid. *J. Photochem. Photobiol., A* **2001**, *138* (1), 79-85.
25. Anpo, M.; Takeuchi, M., The design and development of highly reactive titanium oxide photocatalysts operating under visible light irradiation. *J. Catal.* **2003**, *216* (1-2), 505-516.
26. Yoshida, H.; Yuzawa, H.; Aoki, M.; Otake, K.; Itoh, H.; Hattori, T., Photocatalytic hydroxylation of aromatic ring by using water as an oxidant. *Chem. Commun.* **2008**, (38), 4634.
27. Hashimoto, K.; Kawai, T.; Sakata, T., Photocatalytic reactions of hydrocarbons and fossil fuels with water. Hydrogen production and oxidation. *J. Phys. Chem.* **1984**, *88* (18), 4083-4088.
28. Yuzawa, H.; Aoki, M.; Otake, K.; Hattori, T.; Itoh, H.; Yoshida, H., Reaction mechanism of aromatic ring hydroxylation by water over platinum-loaded titanium oxide photocatalyst. *J. Phys. Chem. C* **2012**, *116* (48), 25376-25387.
29. Ollis, D. F., Kinetics of photocatalyzed reactions: Five lessons learned. *Front. Chem.* **2018**, *6* (378).

30. Schneider, J. T.; Firak, D. S.; Ribeiro, R. R.; Peralta-Zamora, P., Use of scavenger agents in heterogeneous photocatalysis: Truths, half-truths, and misinterpretations. *PCCP* **2020**, *22* (27), 15723-15733.
31. Mahmoodi, V.; Sargolzaei, J., Optimization of photocatalytic degradation of naphthalene using nano-TiO₂/UV system: Statistical analysis by a response surface methodology. *Desalin. Water Treat.* **2014**, *52* (34-36), 6664-6672.
32. Nagao, M.; Suda, Y., Adsorption of benzene, toluene, and chlorobenzene on titanium-dioxide. *Langmuir* **1989**, *5* (1), 42-47.
33. Kim, J.; Monllor-Satoca, D.; Choi, W., Simultaneous production of hydrogen with the degradation of organic pollutants using TiO₂ photocatalyst modified with dual surface components. *Energy Environ. Sci.* **2012**, *5* (6), 7647-7656.
34. Kim, J.; Choi, W., Hydrogen producing water treatment through solar photocatalysis. *Energy Environ. Sci.* **2010**, *3* (8), 1042.
35. Hykrdová, L.; Jirkovský, J. r.; Mailhot, G.; Bolte, M., Fe(III) photoinduced and Q-TiO₂ photocatalysed degradation of naphthalene: Comparison of kinetics and proposal of mechanism. *J. Photochem. Photobiol., A* **2002**, *151* (1), 181-193.
36. King, S. M.; Leaf, P. A.; Olson, A. C.; Ray, P. Z.; Tarr, M. A., Photolytic and photocatalytic degradation of surface oil from the Deepwater Horizon spill. *Chemosphere* **2014**, *95*, 415-22.
37. Qourzal, S.; Assabbane, A.; Ait-Ichou, Y., Synthesis of TiO₂ via hydrolysis of titanium tetraisopropoxide and its photocatalytic activity on a suspended mixture with activated carbon in the degradation of 2-naphthol. *J. Photochem. Photobiol., A* **2004**, *163* (3), 317-321.
38. Al-Madanat, O.; Alsalka, Y.; Curti, M.; Dillert, R.; Bahnemann, D. W., Mechanistic insights into hydrogen evolution by photocatalytic reforming of naphthalene. *ACS Catal.* **2020**, *10* (13), 7398-7412.
39. Weon, S.; Choi, W., TiO₂ nanotubes with open channels as deactivation-resistant photocatalyst for the degradation of volatile organic compounds. *Environ. Sci. Technol.* **2016**, *50* (5), 2556-63.
40. Ajmal, A.; Majeed, I.; Malik, R. N.; Idriss, H.; Nadeem, M. A., Principles and mechanisms of photocatalytic dye degradation on TiO₂ based photocatalysts: A comparative overview. *RSC Adv.* **2014**, *4* (70), 37003-37026.
41. Qourzal, S.; Barka, N.; Tamimi, M.; Assabbane, A.; Ait-Ichou, Y., Photodegradation of 2-naphthol in water by artificial light illumination using TiO₂ photocatalyst: Identification of intermediates and the reaction pathway. *Appl. Catal., A* **2008**, *334* (1-2), 386-393.
42. Walenta, C. A.; Courtois, C.; Kollmannsberger, S. L.; Eder, M.; Tschurl, M.; Heiz, U., Surface species in photocatalytic methanol reforming on Pt/TiO₂(110): Learning from surface science experiments for catalytically relevant conditions. *ACS Catal.* **2020**, *10* (7), 4080-4091.
43. Das, T. N.; Neta, P., Reduction potentials of naphthoxyl and pyridoxyl radicals in aqueous solutions. *J. Phys. Chem. A* **1998**, *102* (35), 7081-7085.
44. Fuchigami, T.; Inagi, S.; Atobe, M., *Fundamentals and Applications of Organic Electrochemistry*. John Wiley & Sons: 2014.

45. Bahnemann, D.; Henglein, A.; Spanhel, L., Detection of the intermediates of colloidal TiO₂-catalysed photoreactions. *Faraday Discuss. Chem. Soc.* **1984**, *78* (0), 151-163.
46. Bamwenda, G. R.; Tsubota, S.; Nakamura, T.; Haruta, M., Photoassisted hydrogen production from a water-ethanol solution: A comparison of activities of Au-TiO₂ and Pt-TiO₂. *J. Photochem. Photobiol., A* **1995**, *89* (2), 177-189.
47. Wenderich, K.; Mul, G., Methods, mechanism, and applications of photodeposition in photocatalysis: A review. *Chem. Rev.* **2016**, *116* (23), 14587-14619.
48. Siuzdak, K.; Sawczak, M.; Klein, M.; Nowaczyk, G.; Jurga, S.; Cenian, A., Preparation of platinum modified titanium dioxide nanoparticles with the use of laser ablation in water. *PCCP* **2014**, *16* (29), 15199-206.
49. Benz, D.; Felter, K. M.; Koser, J.; Thoming, J.; Mul, G.; Grozema, F. C.; Hintzen, H. T.; Kreuzer, M. T.; van Ommen, J. R., Assessing the role of Pt clusters on TiO₂ (P25) on the photocatalytic degradation of Acid Blue 9 and Rhodamine B. *J. Phys. Chem. C* **2020**, *124* (15), 8269-8278.
50. Sakthivel, S.; Shankar, M. V.; Palanichamy, M.; Arabindoo, B.; Bahnemann, D. W.; Murugesan, V., Enhancement of photocatalytic activity by metal deposition: Characterisation and photonic efficiency of Pt, Au and Pd deposited on TiO₂ catalyst. *Water Res.* **2004**, *38* (13), 3001-8.
51. Fu, X.; Long, J.; Wang, X.; Leung, D. Y. C.; Ding, Z.; Wu, L.; Zhang, Z.; Li, Z.; Fu, X., Photocatalytic reforming of biomass: A systematic study of hydrogen evolution from glucose solution. *Int. J. Hydrog. Energy* **2008**, *33* (22), 6484-6491.
52. Naldoni, A.; D'Arienzo, M.; Altomare, M.; Marelli, M.; Scotti, R.; Morazzoni, F.; Selli, E.; Dal Santo, V., Pt and Au/TiO₂ photocatalysts for methanol reforming: Role of metal nanoparticles in tuning charge trapping properties and photoefficiency. *Appl. Catal., B* **2013**, *130-131*, 239-248.
53. Saravanan, R.; Gracia, F.; Stephen, A., Basic principles, mechanism, and challenges of photocatalysis. In *Nanocomposites for visible light-induced photocatalysis*, Khan, M. M.; Pradhan, D.; Sohn, Y., Eds. Springer International Publishing: Cham, 2017; pp 19-40.
54. Al-Azri, Z. H. N.; AlOufi, M.; Chan, A.; Waterhouse, G. I. N.; Idriss, H., Metal particle size effects on the photocatalytic hydrogen ion reduction. *ACS Catal.* **2019**, *9* (5), 3946-3958.
55. Li, F. B.; Li, X. Z., The enhancement of photodegradation efficiency using Pt-TiO₂ catalyst. *Chemosphere* **2002**, *48* (10), 1103-1111.
56. Wang, C. Y.; Pagel, R.; Bahnemann, D. W.; Dohrmann, J. K., Quantum yield of formaldehyde formation in the presence of colloidal TiO₂-based photocatalysts: Effect of intermittent illumination, platinization, and deoxygenation. *J. Phys. Chem. B* **2004**, *108* (37), 14082-14092.
57. Farsinezhad, S.; Sharma, H.; Shankar, K., Interfacial band alignment for photocatalytic charge separation in TiO₂ nanotube arrays coated with CuPt nanoparticles. *PCCP* **2015**, *17* (44), 29723-33.
58. Loeb, S. K.; Alvarez, P. J. J.; Brame, J. A.; Cates, E. L.; Choi, W.; Crittenden, J.; Dionysiou, D. D.; Li, Q.; Li-Puma, G.; Quan, X.; Sedlak, D. L.; David Waite, T.; Westerhoff, P.; Kim,

- J. H., The technology horizon for photocatalytic water treatment: Sunrise or sunset? *Environ. Sci. Technol.* **2019**, *53* (6), 2937-2947.
59. Schneider, J.; Bahnemann, D. W., Undesired role of sacrificial reagents in photocatalysis. *J. Phys. Chem. Lett.* **2013**, *4* (20), 3479-3483.
60. Kandiel, T. A.; Dillert, R.; Bahnemann, D. W., Enhanced photocatalytic production of molecular hydrogen on TiO₂ modified with Pt-polypyrrole nanocomposites. *Photochem. Photobiol. Sci.* **2009**, *8* (5), 683-690.
61. Micic, O. I.; Zhang, Y.; Cromack, K. R.; Trifunac, A. D.; Thurnauer, M. C., Trapped holes on titania colloids studied by electron paramagnetic resonance. *J. Phys. Chem.* **1993**, *97* (28), 7277-7283.
62. Bahnemann, D. W.; Hilgendorff, M.; Memming, R., Charge carrier dynamics at TiO₂ particles: Reactivity of free and trapped holes. *J. Phys. Chem. B* **1997**, *101* (21), 4265-4275.
63. Nunzi, F.; De Angelis, F.; Selloni, A., Ab Initio simulation of the absorption spectra of photoexcited carriers in TiO₂ nanoparticles. *J. Phys. Chem. Lett.* **2016**, *7* (18), 3597-602.
64. Yoshihara, T.; Katoh, R.; Furube, A.; Tamaki, Y.; Murai, M.; Hara, K.; Murata, S.; Arakawa, H.; Tachiya, M., Identification of reactive species in photoexcited nanocrystalline TiO₂ Films by wide-wavelength-range (400–2500 nm) transient absorption spectroscopy. *J. Phys. Chem. B* **2004**, *108* (12), 3817-3823.
65. Kowalska, E.; Remita, H.; Colbeau-Justin, C.; Hupka, J.; Belloni, J., Modification of titanium dioxide with platinum ions and clusters: Application in photocatalysis. *J. Phys. Chem. C* **2008**, *112* (4), 1124-1131.
66. Feldhoff, A.; Mendive, C.; Bredow, T.; Bahnemann, D., Direct measurement of size, three-dimensional shape, and specific surface area of anatase nanocrystals. *ChemPhysChem* **2007**, *8* (6), 805-9.
67. Selcuk, S.; Selloni, A., Facet-dependent trapping and dynamics of excess electrons at anatase TiO₂ surfaces and aqueous interfaces. *Nat. Mater.* **2016**, *15* (10), 1107-12.
68. Ohno, T.; Sarukawa, K.; Matsumura, M., Crystal faces of rutile and anatase TiO₂ particles and their roles in photocatalytic reactions. *New J. Chem.* **2002**, *26* (9), 1167-1170.
69. Andas, J.; Adam, F.; Rahman, I. A.; Taufiq-Yap, Y. H., Optimization and mechanistic study of the liquid-phase oxidation of naphthalene over biomass-derived iron catalyst. *Chem. Eng. J.* **2014**, *252*, 382-392.
70. Li, Y.; Wen, B.; Yu, C.; Chen, C.; Ji, H.; Ma, W.; Zhao, J., Pathway of oxygen incorporation from O₂ in TiO₂ photocatalytic hydroxylation of aromatics: Oxygen isotope labeling studies. *Chemistry* **2012**, *18* (7), 2030-9.
71. Montoya, J. F.; Ivanova, I.; Dillert, R.; Bahnemann, D. W.; Salvador, P.; Peral, J., Catalytic role of surface oxygens in TiO₂ photooxidation reactions: Aqueous benzene photooxidation with Ti¹⁸O₂ under anaerobic conditions. *J. Phys. Chem. Lett.* **2013**, *4* (9), 1415-22.
72. Ohtani, B., Chapter 5 - Principle of photocatalysis and design of active photocatalysts. In *New and Future Developments in Catalysis*, Suib, S. L., Ed. Elsevier: Amsterdam, 2013; pp 121-144.

73. Turchi, C. S.; Ollis, D. F., Photocatalytic degradation of organic water contaminants: Mechanisms involving hydroxyl radical attack. *J. Catal.* **1990**, *122* (1), 178-192.
74. Mohamed, R. M.; Ismail, A. A.; Kadi, M. W.; Bahnemann, D. W., A comparative study on mesoporous and commercial TiO₂ photocatalysts for photodegradation of organic pollutants. *J. Photochem. Photobiol., A* **2018**, *367*, 66-73.
75. Montoya, J. F.; Bahnemann, D. W.; Peral, J.; Salvador, P., Catalytic role of TiO₂ terminal oxygen atoms in liquid-phase photocatalytic reactions: oxidation of aromatic compounds in anhydrous acetonitrile. *ChemPhysChem* **2014**, *15* (11), 2311-20.
76. Civiš, S.; Ferus, M.; Zukalová, M.; Kubát, P.; Kavan, L., Photochemistry and gas-phase FTIR spectroscopy of formic acid interaction with anatase Ti¹⁸O₂ nanoparticles. *J. Phys. Chem. C* **2012**, *116* (20), 11200-11205.
77. Pysh, E. S.; Yang, N. C., Polarographic oxidation potentials of aromatic compounds. *J. Am. Chem. Soc.* **1963**, *85* (14), 2124-&.
78. Rothenberger, G.; Fitzmaurice, D.; Graetzel, M., Spectroscopy of conduction band electrons in transparent metal oxide semiconductor films: Optical determination of the flatband potential of colloidal titanium dioxide films. *J. Phys. Chem.* **1992**, *96* (14), 5983-5986.
79. Fox, M. A.; Chen, C. C.; Younathan, J. N. N., Oxidative cleavage of substituted naphthalenes induced by irradiated semiconductor powders. *J. Org. Chem.* **1984**, *49* (11), 1969-1974.
80. Montoya, J. F.; Atitar, M. F.; Bahnemann, D. W.; Peral, J.; Salvador, P., Comprehensive kinetic and mechanistic analysis of TiO₂ photocatalytic reactions according to the direct–indirect model: (II) Experimental validation. *J. Phys. Chem. C* **2014**, *118* (26), 14276-14290.
81. Reiß, S.; Krumm, H.; Niklewski, A.; Staemmler, V.; Wöll, C., The adsorption of acenes on rutile TiO₂(110): A multi-technique investigation. *J. Chem. Phys.* **2002**, *116* (17), 7704-7713.
82. Monllor-Satoca, D.; Gómez, R.; González-Hidalgo, M.; Salvador, P., The “Direct–Indirect” model: An alternative kinetic approach in heterogeneous photocatalysis based on the degree of interaction of dissolved pollutant species with the semiconductor surface. *Catal. Today* **2007**, *129* (1-2), 247-255.
83. Chen, Y.; Wang, Y. N.; Li, W. Z.; Yang, Q.; Hou, Q. D.; Wei, L. H.; Liu, L.; Huang, F.; Ju, M. T., Enhancement of photocatalytic performance with the use of noble-metal-decorated TiO₂ nanocrystals as highly active catalysts for aerobic oxidation under visible-light irradiation. *Appl. Catal., B* **2017**, *210*, 352-367.
84. Chen, Y.; Yang, S.; Wang, K.; Lou, L., Role of primary active species and TiO₂ surface characteristic in UV-illuminated photodegradation of Acid Orange 7. *J. Photochem. Photobiol., A* **2005**, *172* (1), 47-54.
85. Beltran, F. J.; Ovejero, G.; Garciaaraya, J. F.; Rivas, J., Oxidation of polynuclear aromatic hydrocarbons in water .2. UV-radiation and ozonation in the presence of UV-radiation. *Ind. Eng. Chem. Res.* **1995**, *34* (5), 1607-1615.
86. Hasan, I.; Shekhar, C.; Bin, S., II; Khan, R. A.; Alsalmeh, A., Ecofriendly green synthesis of the ZnO-doped CuO@Alg bionanocomposite for efficient oxidative degradation of p-nitrophenol. *ACS Omega* **2020**, *5* (49), 32011-32022.

87. Alam, U.; Fleisch, M.; Kretschmer, I.; Bahnemann, D.; Muneer, M., One-step hydrothermal synthesis of Bi-TiO₂ nanotube/graphene composites: An efficient photocatalyst for spectacular degradation of organic pollutants under visible light irradiation. *Appl. Catal., B* **2017**, *218*, 758-769.
88. Nosaka, Y.; Nosaka, A., Understanding hydroxyl radical (\bullet OH) generation processes in photocatalysis. *ACS Energy Lett.* **2016**, *1* (2), 356-359.
89. Shibata, H.; Ogura, Y.; Sawa, Y.; Kono, Y., Hydroxyl radical generation depending on O₂ or H₂O by a photocatalyzed reaction in an aqueous suspension of titanium dioxide. *Biosci. Biotechnol. Biochem.* **1998**, *62* (12), 2306-11.
90. Li, L.; Goel, R. K., Role of hydroxyl radical during electrolytic degradation of contaminants. *J. Hazard. Mater.* **2010**, *181* (1-3), 521-5.
91. Luo, S.; Wei, Z.; Spinney, R.; Villamena, F. A.; Dionysiou, D. D.; Chen, D.; Tang, C. J.; Chai, L.; Xiao, R., Quantitative structure-activity relationships for reactivities of sulfate and hydroxyl radicals with aromatic contaminants through single-electron transfer pathway. *J. Hazard. Mater.* **2018**, *344*, 1165-1173.
92. Rodgers, M. A. J., Nanosecond pulse radiolysis of acetone. Kinetic and thermodynamic properties of some aromatic radical cations. *J. Chem. Soc., Faraday Trans. 1 F* **1972**, *68* (0), 1278-1286.
93. Fritz, H. P.; Gebauer, H.; Friedrich, P.; Ecker, P.; Artes, R.; Schubert, U., Elektrochemische syntheses, XIV [1] Radikalkation-salze des naphthalins / electrochemical syntheses, XIV [1]. radical cation salts of naphthalene. *Z. Naturforsch., B* **1978**, *33* (5), 498-506.
94. Gschwind, R.; Haselbach, E., Laser flash-photolysis of the p-Chloranil/naphthalene system: Characterization of the naphthalene radical cation in a fluid medium. *Helv. Chim. Acta* **1979**, *62* (4), 941-955.
95. Steenken, S.; Warren, C. J.; Gilbert, B. C., Generation of radical-cations from naphthalene and some derivatives, both by photoionization and reaction with SO⁴⁻: Formation and reactions studied by laser flash photolysis. *J. Chem. Soc., Perkin Trans. 2* **1990**, (2), 335-342.
96. Tachikawa, T.; Tojo, S.; Fujitsuka, M.; Majima, T., Photocatalytic one-electron oxidation of biphenyl derivatives strongly coupled with the TiO₂ surface. *Langmuir* **2004**, *20* (7), 2753-9.
97. Eberhardt, M. K., Reaction of benzene radical cation with water. Evidence for the reversibility of hydroxyl radical addition to benzene. *J. Am. Chem. Soc.* **1981**, *103* (13), 3876-3878.
98. Jenks, W., Photocatalytic reaction pathways - effects of molecular structure, catalyst, and wavelength. In *Photocatalysis and Water Purification: From Fundamentals to Recent Applications*, Pichat, P., Ed. Wiley-VCH Verlag GmbH & Co.: 2013; pp 25-51.
99. Zhao, G.; Busser, G. W.; Froese, C.; Hu, B.; Bonke, S. A.; Schnegg, A.; Ai, Y.; Wei, D.; Wang, X.; Peng, B.; Muhler, M., Anaerobic alcohol conversion to carbonyl compounds over nanoscaled Rh-doped SrTiO₃ under visible light. *J. Phys. Chem. Lett.* **2019**, *10* (9), 2075-2080.
100. Belhadj, H.; Hamid, S.; Robertson, P. K. J.; Bahnemann, D. W., Mechanisms of simultaneous hydrogen production and formaldehyde oxidation in H₂O and D₂O over platinumized TiO₂. *ACS Catal.* **2017**, *7* (7), 4753-4758.

101. Post, B.; Hiskey, C. F., Electrokinetics of hydrogen evolution.1,2 II. Deuterium overvoltage on mercury. *J. Am. Chem. Soc.* **1951**, 73 (1), 161-164.
102. Yates, J. T.; McKee, D. W., Kinetic isotope effect in the heterogeneous reaction of graphite with H₂O (D₂O). *J. Chem. Phys.* **1981**, 75 (6), 2711-2714.

Curriculum Vitae

Personal Data

Name: Al-Madanat, Osama
Address: Am Queckenberg 30B, Braunschweig, Germany
E-mail: al-madanat@iftc.uni-hannover.de
madanat@mutah.edu.jo
Date & place of birth: 04.03.1977, Adir/ Jordan.
Nationality: Jordanian
Marital status: Married, three children.

Education

017 – present Ph.D. Student at Institute of Technical Chemistry, Leibniz University of Hannover, Hannover, Germany.
Ph.D. Thesis: “Photocatalytic Transformation of Water Pollutants into Fuels”
2011 – 2014 Master's degree in "Chemistry", Environmental Analytical Chemistry, Department of Chemistry, Faculty of Sciences, Mutah University, Jordan
1995 – 1999 Bachelor's Degree "Chemistry"
Department of Chemistry, Faculty of Sciences, Mutah University, Jordan
1977 High School, Adir Secondary School

Work Experience

08.2017 – present **Research and Teaching Assistant**
Institut für Technische Chemie, Leibniz Universität Hannover, Germany
07.2001 – 04.2017 **Lecturer and Teaching Assistant**
Department of Chemistry, Faculty of Sciences, Mutah University, Jordan
08.1999 – 07.2001 **Chemistry Teacher**
Ministry of Education Karak, Jordan

Awards

- 2020 Completion Grant from Graduate Academy of Leibniz Universität Hannover for 9 Months to the Completion of a PhD Study at Leibniz Universität Hannover, Germany.
- 2019 Travel Grant to Participate at Conferences, Graduate Academy of Leibniz Universität Hannover.
- 2019 DAAD Grant to Participate at German-Russian Workshop at Sant-Petersburg University, Russia
- 2017 KAAD scholarship (3.5 years) for the Completion of a PhD Study at Leibniz Universität Hannover, Germany.

Publications

- **Al-Madanat, O.**, AlSalka, Y., Ramadan, W., Bahnemann, D.W. 2021. TiO₂ photocatalysis for the transformation of aromatic water pollutants into fuels. *Catalysts*. 11(3): 317. <https://doi.org/10.3390/catal11030317>.
- **Al-Madanat, O.**, AlSalka, Y., Dillert, R., Bahnemann, D.W. 2021. Photocatalytic H₂ production from naphthalene by various TiO₂ photocatalysts: Impact of Pt loading and formation of intermediates. *Catalysts*. 11(1): 107. <https://doi.org/10.3390/catal11010107>.
- **Al-Madanat, O.**, AlSalka, Y., Curti, M., Dillert R., Bahnemann, W. D. 2020. Mechanistic Insights into hydrogen evolution by photocatalytic reforming of naphthalene. *ACS Catalysis*. 10: 7398–7412. <https://doi.org/10.1021/acscatal.0c01713>
- **Al-Madanat, O.**; Curti, M., Günemann, C., AlSalka, Y., Dillert, R., Bahnemann, D.W. 2021. TiO₂ photocatalysis: Impact of the platinum loading method on reductive and oxidative half-reactions. *Catalysis Today*. 380: 3-15. <https://doi.org/10.1016/j.cattod.2021.07.013>
- Al-Nasir, F. M., Jiries, A. G., Al-Rabadi, G. J., Alu'datt, M. H., Tranchant, C. C., Al-Dalain, S. A., Alrabadi, N., **Madanat, O. Y.**, Al-Dmour, R. S. 2020. Determination of pesticide residues in selected citrus fruits and vegetables cultivated in the Jordan Valley, *LWT - Food Science and Technology*. 123: 109005. <https://doi.org/10.1016/j.lwt.2019.109005>
- AlSalka, Y., **Al-Madanat, O.**, Curti, M., Hakki, A., Bahnemann, W. D. 2020. Photocatalytic H₂ evolution from oxalic acid: Effect of co-catalysts and carbon dioxide radical anion on the surface charge transfer mechanisms. *ACS Applied Energy Materials*. 3, 7, 6678–6691. <https://doi.org/10.1021/acsaem.0c00826>.
- Altarawneh, M., Alharazneh, G., **Al-Madanat, O.** 2018. Dielectric properties of single wall carbon nanotubes-based gelatin phantoms, *Journal of Advanced Dielectrics*. 08 (2): 1850010. <https://doi.org/10.1142/S2010135X18500108>
- AlRabadi, G., Al-Nasir, F., Jiries, A., Al-Dmour, R., **Al-Madanat, O.**, Al-Dalain, S. 2019. Polychlorinated biphenyls (PCBs) in citrus and vegetables in the Jordan Valley-jordan. *The Jordan Journal of Earth and Environmental Sciences*, 10 (4): 247-251.
- **Al-Madanat, O.**, Jiries, A., Batarseh, M., Al-Nasir, F. 2017. Indoor and Outdoor Pollution with Heavy Metals in Al-Karak City, Jordan. *J. Int. Environmental Application & Science*, 12(2): 131-139.
- Ombaka, L., McGettrick, J., Oseghe, E., **Al-Madanat, O.**, genannt-Best, F., Msagati, T., Lloyd Davies, M., Bredow, T., Bahnemann, W. D. 2021. Bridging the interface between Metallic Copper and TiO₂ via B/N-graphene for enhanced

Photocatalytic H₂ Production and 2-Chlorophenol Degradation: A DFT, experimental and mechanistic investigation. *ACS Catalysis*. (Under Review).

Oral Presentations

- **Al-Madanat**, O., Dillert, R., Bahnemann, W. D. “Hydrogen Production by Photocatalytic Reforming of Naphthalene “. 6th European Conference on Environmental Applications of Advanced Oxidation Processes, Portoroz, Slovenia, 26-30 June 2019.
- **Al-Madanat**, O., Dillert, R., Bahnemann, W. D. “Mechanistic Insights into Hydrogen Production by Pt/TiO₂ Anaerobic Photocatalytic Reforming of Aqueous Naphthalene”. 7th German-Russian Workshop,” Photoactive Nanocomposite Materials”, National University of St. Petersburg, October 2019, St. Petersburg, Russia.
- **Al-Madanat**, O., Dillert, R., Bahnemann, W. D. “Photocatalytic H₂ Production from Naphthalene by Various TiO₂ Photocatalysts: Impact of Pt Loading and Formation of Intermediates “. 5th International Conference on Catalysis and Chemical Engineering. February 22-26, 2021-Virtual

Poster Presentations

- **Al-Madanat**, O., Dillert, R., Bahnemann, W. D. Impact of the Platinum-Loading Method on the Reductive and Oxidative Photocatalytic Half-Reactions over TiO₂. Inaugural CataLight Young Scientist Symposium on Light-Driven Catalysis on November 24, 2020
- **Al-Madanat**, O. “Indoor and Outdoor Pollution with Polycyclic Aromatic Hydrocarbons (PAHs) and Heavy Metals in Karak Province / Jordan “. Conference: Humboldt Kolleg "Building International Networks for Enhancement of Research in Jordan " Princess Sumaya University Amman, April 3 - 5, 2014.